AD-A079 663 WESTINGHOUSE ELECTRIC CORP BALTIMORE MD F/G 17/7
FAR FIELD MONITOR FOR INSTRUMENT LANDING SYSTEMS.(U)
NOV 79 R MORE, J C BRADLEY, B NEWMAN DOT-FA75WA-3689
UNCLASSIFIED FAA-RD-79-70 NL

1 OF 4
AD
A079663

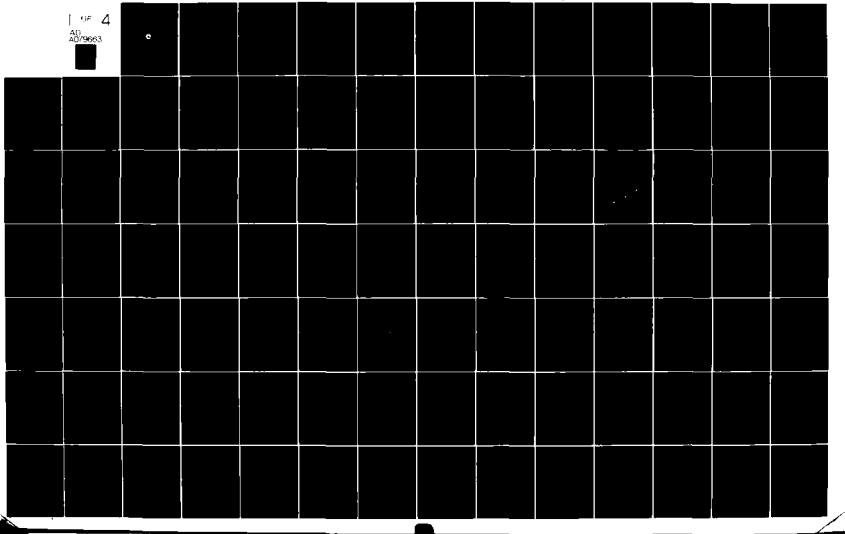

Report No. FAA-RD-79-70

FAR FIELD MONITOR FOR INSTRUMENT LANDING SYSTEMS

November 1979
Interim Report
Phases I & II

Prepared for

U.S. DEPARTMENT OF TRANSPORTATION
FEDERAL AVIATION ADMINISTRATION
Systems Research & Development Service
Washington, D.C. 20590

NOTICE

This document is disseminated under the sponsorship of the Department of Transportation in the interest of information exchange. The United States Government assumes no liability for its contents or use thereof.

Technical Report Documentation Page

1. Report No. FAA-RD-79-70	2. Government Accession No.	3. Recipient's Catalog No.
4. Title and Subtitle: NEAR FIELD MONITOR FOR INSTRUMENT LANDING SYSTEMS		5. Report Date: November 1979
		6. Performing Organization Code
7. Author's: R. More, J. C. Bradley, B. Newman		8. Performing Organization Report No.
9. Performing Organization Name and Address: Westinghouse Electric Corporation, P.O. Box 1897, Baltimore, Maryland 21203		10. Work Unit No. (TRAIS)
		11. Contract or Grant No.: DOT-FA75WA-3689
		13. Type of Report and Period Covered: Interim Report, Phases I & II
12. Sponsoring Agency Name and Address: Federal Aviation Administration, Systems Research & Development Service, Washington, D.C. 20590		14. Sponsoring Agency Code: FAA/ARD-320

15. Supplementary Notes

317

16. Abstract

This report describes a study performed to determine the nature of scattering of ILS radiated signals by objects on the airport property. These included both taxiing and overflying aircraft. The interaction of this scattered energy with the direct radiation was studied to determine the derogating effects of ILS guidance. This resulted in the development of four system level concepts for detecting glide path derogation. One technique, the Vector DDM, was selected as being most practical from a sensitivity, reliability, and cost point-of-view.

Interim rept. on Phases 1 and 2,

17. Key Words	18. Distribution Statement
Monitor, Localizer Monitor, ILS, Glide Slope Monitor, Far Field Monitor	Document is available to the U.S. public through the National Technical Information Service, Springfield, Virginia 22161.

19. Security Classif. (of this report)	20. Security Classif. (of this page)	21. No. of Pages	22. Price
Unclassified	Unclassified	314	

Form DOT F 1700.7 (8-72) Reproduction of completed page authorized

METRIC CONVERSION FACTORS

Approximate Conversions to Metric Measures

Symbol	When You Know	Multiply by	To Find	Symbol
		LENGTH		
in	inches	*2.5	centimeters	cm
ft	feet	30	centimeters	cm
yd	yards	0.9	meters	m
mi	miles	1.6	kilometers	km
		AREA		
in^2	square inches	6.5	square centimeters	cm^2
ft^2	square feet	0.09	square meters	m^2
yd^2	square yards	0.8	square meters	m^2
mi^2	square miles	2.6	square kilometers	km^2
	acres	0.4	hectares	ha
		MASS (weight)		
oz	ounces	28	grams	g
lb	pounds	0.45	kilograms	kg
	short tons (2000 lb)	0.9	tonnes	t
		VOLUME		
tsp	teaspoons	5	milliliters	ml
Tbsp	tablespoons	15	milliliters	ml
fl oz	fluid ounces	30	milliliters	ml
c	cups	0.24	liters	l
pt	pints	0.47	liters	l
qt	quarts	0.95	liters	l
gal	gallons	3.8	liters	l
ft^3	cubic feet	0.03	cubic meters	m^3
yd^3	cubic yards	0.76	cubic meters	m^3
		TEMPERATURE (exact)		
°F	Fahrenheit temperature	5.9 (after subtracting 32)	Celsius temperature	°C

*1 in = 2.54 (exactly). For other exact conversions and more detailed tables, see NBS Misc. Publ. 286, Units of Weights and Measures, Price $2.25, SD Catalog No. C13.10:286.

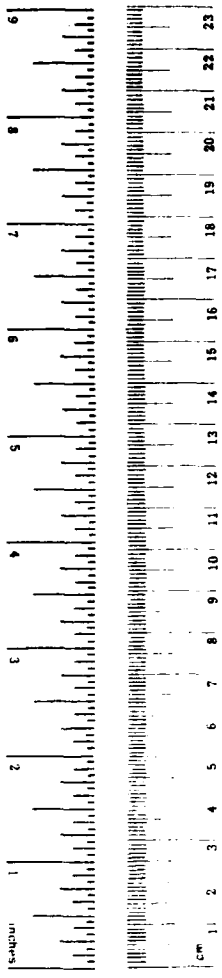

Approximate Conversions from Metric Measures

Symbol	When You Know	Multiply by	To Find	Symbol
		LENGTH		
mm	millimeters	0.04	inches	in
cm	centimeters	0.4	inches	in
m	meters	3.3	feet	ft
m	meters	1.1	yards	yd
km	kilometers	0.6	miles	mi
		AREA		
cm^2	square centimeters	0.16	square inches	in^2
m^2	square meters	1.2	square yards	yd^2
km^2	square kilometers	0.4	square miles	mi^2
ha	hectares (10,000 m^2)	2.5	acres	
		MASS (weight)		
g	grams	0.035	ounces	oz
kg	kilograms	2.2	pounds	lb
t	tonnes (1000 kg)	1.1	short tons	
		VOLUME		
ml	milliliters	0.03	fluid ounces	fl oz
l	liters	2.1	pints	pt
l	liters	1.06	quarts	qt
l	liters	0.26	gallons	gal
m^3	cubic meters	35	cubic feet	ft^3
m^3	cubic meters	1.3	cubic yards	yd^3
		TEMPERATURE (exact)		
°C	Celsius temperature	9/5 (then add 32)	Fahrenheit temperature	°F

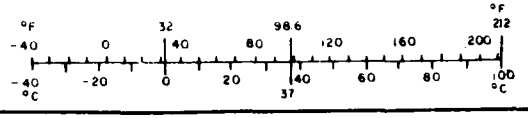

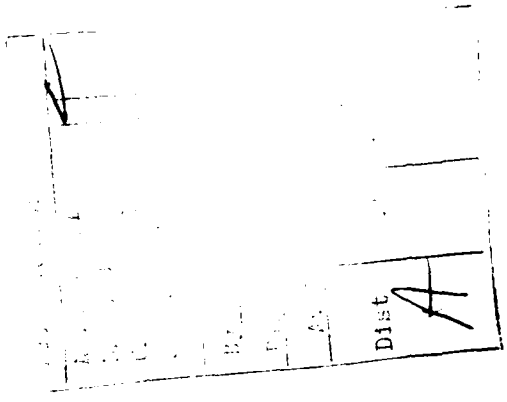

TABLE OF CONTENTS

LIST OF ILLUSTRATIONS

LIST OF ILLUSTRATIONS (CON'T.)

LIST OF ILLUSTRATIONS (CON'T.)

LIST OF ILLUSTRATIONS (CON'T.)

LIST OF ILLUSTRATIONS (CON'T.)

LIST OF ILLUSTRATIONS (CON'T.)

LIST OF ILLUSTRATIONS (CON'T.)

1.0 INTRODUCTION

The Far Field Monitor Program is divided into four phases, directed at developing an optimum design ILS monitor system. The scope of these phases is as follows:

I. A review and analysis of previous monitor approaches.

II. An analysis of the nature of ILS derogations and the development of system concepts for their detection.

III. Design, develop and furnish one set of prototype equipment for an executive type ILS Far Field Monitor.

IV. Provide equipment specifications for Phase III.

Only the first two phases were funded. The results are given in this Interim Report.

This study was directed at both the localizer and the glide slope. The greater emphasis was placed on the localizer since it has the greater susceptibility to derogation by aircraft in the immediate vicinity of the airport.

Present monitors can detect certain time varying disturbances but they cannot accurately determine the magnitude of the disturbance. An executive far field monitor must detect quasi-static derogation of a time duration long enough to cause an unsafe condition for approaching aircraft. This requires two pieces of information: (1) the maximum amplitude of the derogation, and (2) the time component of the derogation. In order to develop a system with this capability, the nature of the derogations to be measured must be determined. A variety of scatterers were analized in critical locations about the airport. This included simulating aircraft overflying the localizer antenna. In all cases it was found that the DDM on glide path cannot be deduced by measuring the DDM at any point near the ground. This is due to the fact that a knowledge of DDM does not uniquely define a field (CSB, SBO). The analysis did indicate that there is a unique relationship between the field structure on glide path and the field structure near the ground immediately below the glide path. It also showed that the maximum of the derogation on glide path can, in all cases, be calculated from a knowledge of the characteristics of the envelop of the interference pattern near the ground. This is the essence of the far field monitor.

The results of the analysis of the field structure produced by scattering from various derogation sources was confirmed by scale model range measurements performed under a subcontract by G.E.C. Marconi. The results were in excellent

agreement with the theoretical predictions, and hence, the analysis constitutes a reasonable starting point for the design of a detection system. Four different techniques were investigated for making ground level measurements indicative of glide path performance.

The first technique considered is a Statistical Multiprobe System. This consists of an array of sampling probes dense enough to insure that at least one probe will detect a derogation peak. After analysis, this systems was dismissed as being impractical since it would require a large number of probes and would be very sensitive to probe location.

The second technique investigated is a Curve Fitting System. This makes use of an analytical technique, developed on this contract, whereby the measurement of a few points of the interference pattern allows the mathematical construction of one full cycle of the interference pattern. Hence, the derogation peak could be determined even though no probe was actually located at a peak. The shortcoming of this approach lies in the fact that an extreme accuracy is required in these measurements followed by a very complex computational program to insure a correct determination of the derogation peak.

The remaining two techniques, the Interferometric and the Vector DDM, are both shown to be viable approaches, differing only in cost to implement and maintain, and in reliability. The Interferometric System would use four probes, mounted transverse to the runway centerline and unequally spaced. These probes are phased to cancel the direct localizer radiation and any fixed scattering from buildings, etc. Hence, only new derogations are seen, and their magnitude and angle of arrival will be immediately known. This is very similiar to linear array interferometers used by radio astronomers. Although it was beyond the scope of Phase II, a full scale system of this type was assembled at Stansted Airport, Essex, England. Measurements were made under a variety of conditions, and were shown to correlate very well with the on glide path condition. This work was performed by G.E. C. Marconi under a subcontract, and is fully discussed in Appendix B of this report. This type of system would be more difficult to implement for the glide slope.

The Vector DDM System appears to be the best choice from all points of view. It consists of a single sampling device the output of which is processed to determine both amplitude and phase modulation. The term Vector DDM refers to the fact that this systems measures both the total (scalar) DDM and any quadrature phase component:

$$\overrightarrow{DDM} = \qquad (DDM_{Tot}, \; Q \; DDM).$$

A microprocessor operating on this information can calculate the derogation peak independent of the location of the sampling probe. The simplicity of a single sampling device and routine signal processing enhances the reliability and cost effectiveness of this technique. However, one must be careful not to misinterpret this single sampling technique with the far field probes in present use. This system makes an exact measurement of the field structure and then calculates the derogation on glide path. It is not a simple DDM detector. Furthermore, it measures the time signature of the derogation, allowing it to accurately

differentiate overflights and not to depend on a simple built-in time delay.

The combined results of analysis and scale modeling have indicated that a ground level system for detecting an out of tolerance glide path is feasible. A comprehensive system analysis of potential detection techniques has resulted in a conceptual design of a system, simple in implementation and operation, but sophisticated enough to be truly an executive far field monitor.

2.0 BACKGROUND AND REQUIREMENTS

Monitors now exist that can sense, in a limited way, the presence of certain time varying diffractions or reflections. These monitors cannot, however, quantitatively evaluate the magnitude of the resulting guidance perturbation on the approach path, because there is no simple relationship between the electromagnetic field at a ground location and the field on the approach path. To accurately represent the approach path guidance due to time varying, diffractions or reflectors, a comprehensive far field monitor is required.

Most investigations of far field monitor parameters and techniques have been limited to consideration of very simple monitors[1,2] but one significant investigation of a particular geometry has been monitoring the localizer derogation due to taxiing aircraft in the runway environment of Heathrow Airport (London).

The utilization and requirements for far field monitoring can best be understood by considering them in combination with present monitors to provide complete monitoring protection. For any installation, the far field monitor can be used in combination with present monitors. The primary deficiency of present monitor systems is the lack of information about events that occur on and beyond the runway, that can substantially derogate guidance, and can be detected only by a far field monitor. A far field monitor, to provide complete monitoring, would be very costly, but in combination with one or more present monitors it could vastly extend at a modest cost the ability to measure events that significantly derogate guidance.

ILS monitor systems are of three basic types: integral/aperture, near field and far field, which attempt to predict localizer and glide slope guidance quality on the glide path. A full fledged far field monitor provides the most complete response of the ILS system to effects which cause derogation to the glide path guidance.

The diagram shows the region of coverage for each type of monitor. In each case, the more comprehensive monitor provides information on all quantities detected by the less comprehensive monitor. Thus, in principle, the far field monitor could detect all sources of derogation, while the integral system monitors only transmitter and feedline performance. Because the far field monitor must contend with very difficult geometries, it is desirable to use it in combination with one of the "close in" (integral, aperture or near field) monitors so it must only contend with events beyond the transmitter and radiation system. The monitor types briefly characterized below are described in greater detail in Appendix C.

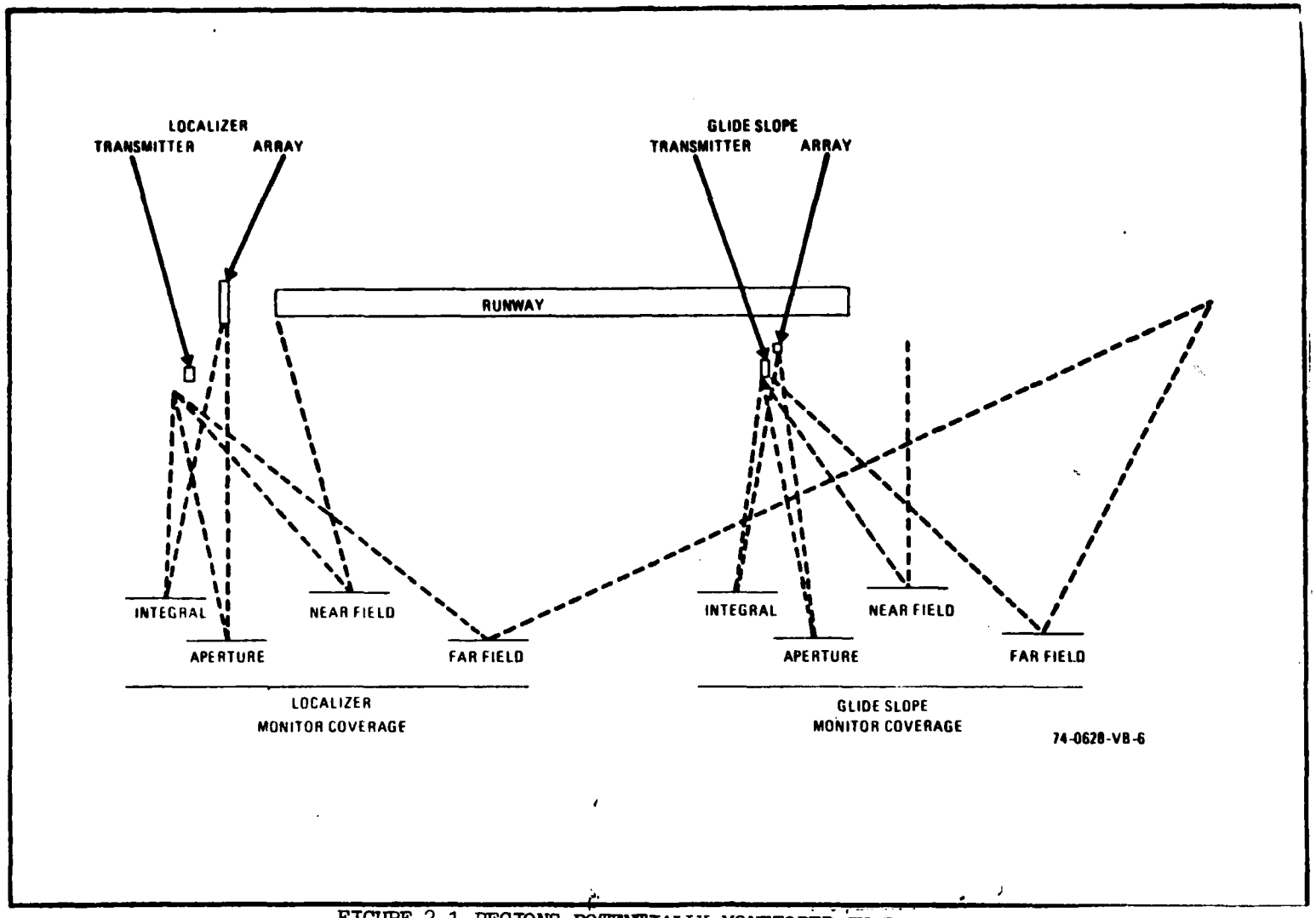

FIGURE 2-1 REGIONS POTENTIALLY MONITORED BY EACH TYPE MONITOR SYSTEM FOR BOTH LOCALIZER AND GLIDE SLOPE

- Integral Monitor - The integral monitor couples directly to the transmitter system and monitors the integrity of the system electronics, and in some cases, the transmission to the antenna.

- Aperture Monitor - The aperture monitor provides pickups in the aperture of the antenna. It monitors integrity of the antenna operation as well as the transmitter electronics.

- Near Field Monitor - The near field monitor pickup is placed on separate mountings in the near field of the transmitting antennas, normally within a few hundred feet. The near field monitor can identify unsafe conditions due to any cause at the transmitter electronics and antennas. It is superior to the aperture monitor in that it monitors the structural integrity of the antenna. It cannot provide information due to runway and taxiway activity.

- Far Field Monitor - The far field monitor provides information on unsafe derogation of ILS due to reflections in and near the field. The far field monitor is the most comprehensive of those under consideration and is the only type with the potential for comprehensive evaluation of guidance derogation due to all causes.

2.1 Requirements and Considerations for Far Field Monitors

Within the context of this program, the far field monitor, in combination with one or more present monitors, is required to provide monitoring capabilities as specified in ICAO, Annex 10, Part 1, and the U.S. Flight Inspection Manual, FAA Handbook C.P. 82001. The specification requires that the far field monitor sense guidance deviations that are beyond the scope of present monitor systems.

Briefly, the far field monitor must identify and evaluate alarm level derogation due to all causes beyond the immediate vicinity of the transmitter. Much of this derogation is either dynamic or quasi-static. The former category includes derogations due to overflight and actively taxiing aircraft. The latter includes parked aircraft and changes such as opening and closing of hangar doors.

It is the presence of quasi-static derogation above specified levels that is most likely to cause unsafe conditions and require alarm. Because quasi-static derogation may be at an unsafe level for significant periods of time, the aircraft guidance instrumentation has sufficient time to respond to the perturbed guidance. An alarm must occur quickly. By contrast, derogation due to fast moving disturbances may considerably exceed specified limits for static derogation and yet be completely safe because of the very brief time period of occurence. For example, unless a derogation peak exceeds guidance specified limits sufficiently to register on a meter measurement with a 0.4 second time control, it is not considered out of specification on ILS guidance.

Further, the present centerline far field monitor must provide significant delays of up to 60 seconds after experiencing alarm conditions before going into alarm in the presence of dynamic derogation.

These requirements are the first order points of comparison of the far field monitor investigated on this program.

2.2 Nature of Derogation

Experience and computation, both ours and others[4], have shown that the presence of large reflecting objects in certain areas cause unacceptable derogation of approach guidance. Also, other changes occur which affect guidance in certain wet and snowy weather conditions. Some of these effects, such as reflections from ground taxiing objects, lead to real derogation of the magnitude measured by present monitors. Some, particularly over flying aircraft and wet and snowy weather, lead to large exaggerations of the active derogation as measured in present near field monitors. Thus alarm occurs much more frequently than necessary with the accompanying economic losses of personnel, time and inconvenience.

Figure 2-2 illustrates approximate critical areas for both overflying and ground taxiing aircraft. (It illustrates the fact that scattered energy is more serious when scatterers are close to the radiating and receiving antennas.) The operationally critical areas shown by the dotted lines both vertically and horizontally suggest regions in which aircraft are likely to penetrate in normal operations. Though it is possible to minimize the time duration of these penetrations, they cannot be prevented. A useful far field monitor must evaluate the magnitude of localizer derogation to guidance when these regions are penetrated. Since these regions are penetrated regularly and since this derogation is occurring it would appear desirable to provide such information to appropriate operation-coordinating-activities with an appropriately designed strategy for dealing with these disturbances. For these reasons, greatest concentration has been given to scatterers in the rollout regions.

The geometry for the glide slope also suggests the greater sensitivity to weather and snow. Considerable attention has been given to this by the FAA, and it has been found that both wet weather and snow outages are frequently due more to the monitor than to the actual guidance[5]. An attempt has been made to justify a lower susceptability of a far field monitor to these false disturbances in comparison to near field monitors.

A large catalog of data is available from experiences with derogations of approach guidance, both with localizers and glide slope. Measurements are regularly made both on the ground and by approaching aircraft. Typically, derogation takes the form of long gradual bends and quasi-oscillatory variations in the guidance. The form depends on the locations of the scatterers and the magnitude on size of the scatterer. The source of these disturbances can be visualized with the geometry of Figure 2-3.

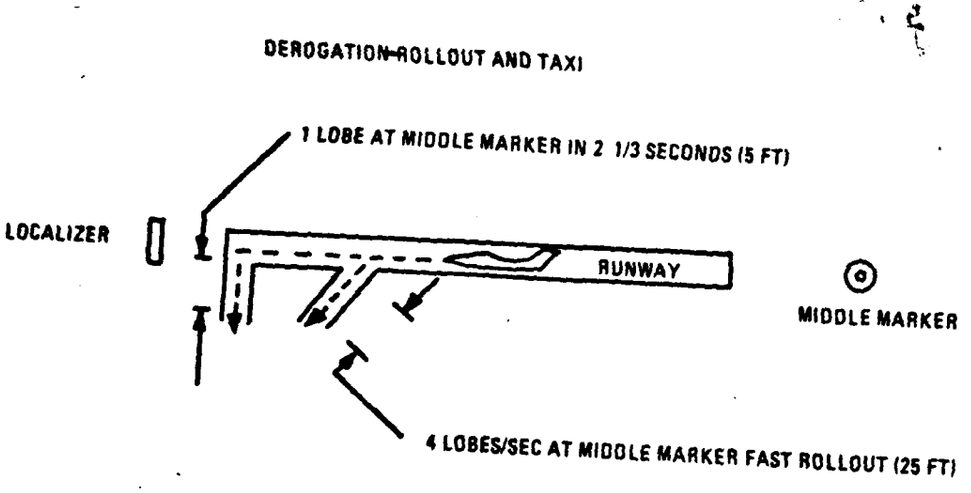

Figure 2-2. Operationally critical areas the penetration of which cause excessive localizer derogation for approaching aircraft.

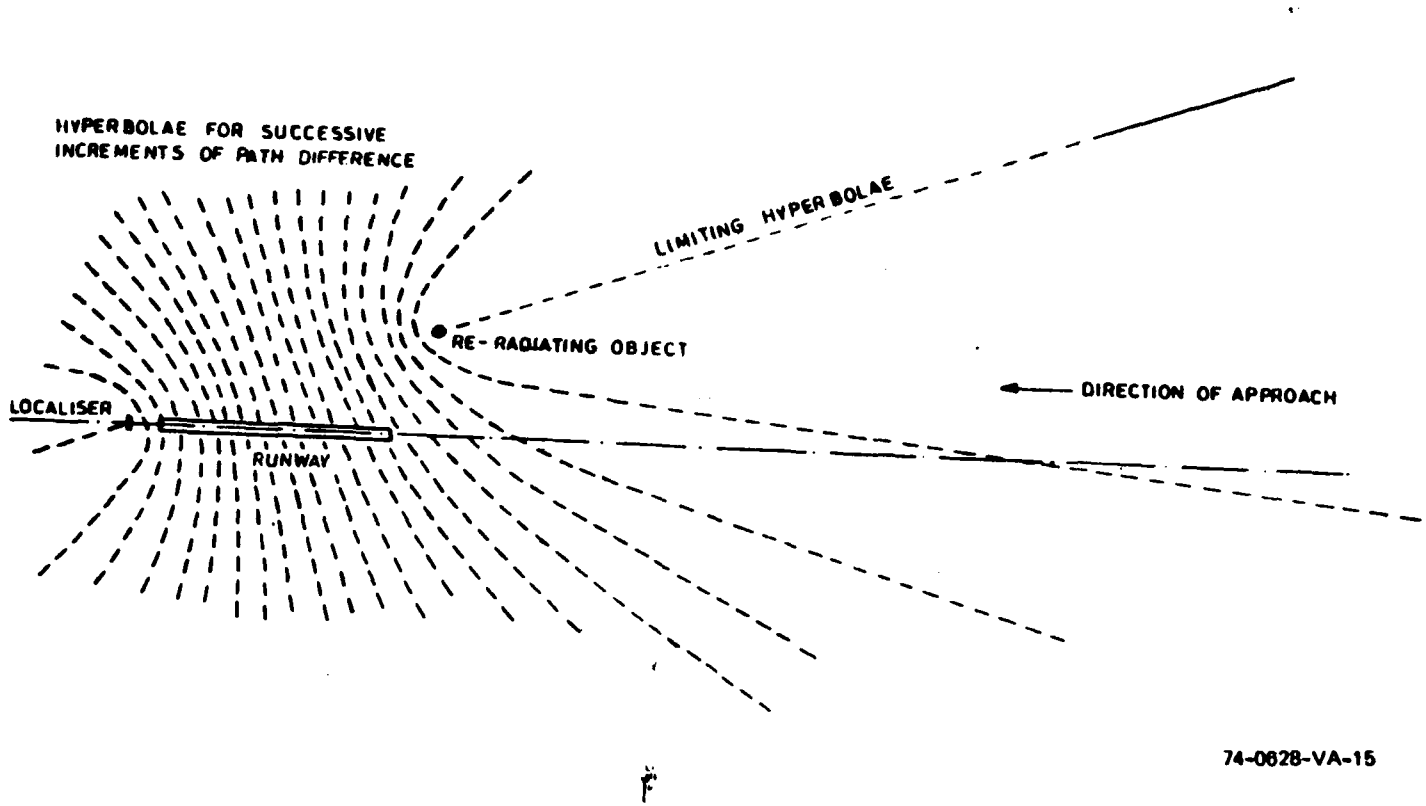

FIGURE 2-3 HYPERBOLA OF COHERENT INTERFERENCE

2.2.1 Ground Based Sources of Scattering

The ILS system and the scattering object may be regarded initially as two coherent sources, having an amplitude ratio and constant time (phase) difference. Such a system generates a family of hyperbolae, with each hyperbola representing a locus of two points having a constant path difference between the two foci, as seen in Figure 2-3. This diagram illustrates a localizer; however, a similar diagram can be constructed for a glide slope array. Successive hyperbolae, drawn at equal increments of path difference, have increasingly spaced intercepts with the course center line as distance increases from the transmitter. If these increments are each one wavelength at the carrier frequency, then the separation of the intercepts is the "wavelength" of a complete cycle of course-line disturbance, during which the guidance signal is unbalanced to one side and then the other. The longest "wavelengths" are caused by objects which are closest to the transmitter.

As illustrated in Figure 2-3, the interference patterns of a re-radiating object can be illustrated as both beam bend and noise (the derogation wavelength is very short) in between the transmitter and diffracting reflector. Near the approach direction the wavelength is very long. This is shown quantitatively in Figure 2-4, where the interference pattern frequency is shown as a function of the incidence angle between the direct and derogating radiation with plane approach speed as a parameter.

Beam bends can result from reflected or diffracted energy and can have interference envelopes of many thousands of feet. Noise - like derogation occurs in regions where reflected energy crosses the approach path close to 90 degrees. If only one reflector is involved, the effect would be a sine wave with frequencies as high as 20 to 40 Hz, as can be seen by extending the curves in Figure 2-4 to 90 degrees. Typically, since several diffracting reflectors or terrain elements are involved in the signal propagation path to a specific location, there will be several scattered signals crossing the glide path at each point.

Time variations in the derogation experienced by an approaching aircraft is also caused by movement of the scatterer causing the derogation. A key example of this happening while the scatterer is in the critical areas defined in Figure 2-2 is illustrated in Figure 2-5. Here the scatterer is in the process of rollout and turn off. Due to the motion of the disturbing aircraft, the frequencies suggested by this figure must be combined with the variations due to the motions of the approaching aircraft to determine the dynamic character of the guidance seen by the approaching aircraft.

2.2.2 Effect of Elevated Sources of Reflection

The effect of scattering on ILS monitoring is particularly serious because of the great variety of vertical interference patterns which can be generated. Elevated sources can be the result of reflection or diffraction from the vertical fin of large aircraft on the ground or from aircraft in takeoff or landing maneuvers, as illustrated in the next sequence of figures.

Figure C4 (Appendix C) shows the outline drawing of a 747. On the ground, the most prominent source of scattering is the tail because of its height. The effect on the monitor is illustrated on Figure 2-6. The broad lobe is the radiation pattern of a localizer at a height of 9 feet. The lower lobe is the result of diffraction/reflection from a 747 tail. Clearly, if the lobe peak amplitudes were equal, the reflected signal would dominate the direct signal both at a ground monitor location and on the glide path. For this reason, even moderate reflections can derogate guidance and seriously affect the integrity of the monitor.

The effect on the monitor of overflying aircraft on take off maneuvers is potentially much greater. Because of the different aspect the wings become reflectors while on the ground, the tail is the dominant reflector. Flight profile for the KC 135/707 type aircraft is shown in Figure 2-7. The localizer is usually between the 11,000 and 13,000 feet points. Thus, a lightly loaded aircraft might be high enough when it crosses the localizer antenna to cause little effect, while a heavily loaded aircraft might be low enough to cause appreciable localizer derogation. The times shown are for the aircraft to maneuver through the climb out portions of the profile. Figure 2-8 shows the lobing which would be experienced by an approaching aircraft for the taking off plane at three positions along the profile. The points are identified by: (1) interfering lobe (90 feet), about midway up the climb out profile (360 ft.) and for six interfering lobes at 540 feet.

The crowding of the lobes toward the ground and into the flight path causes an overpowering level of derogation to be experienced at a ground based monitor.

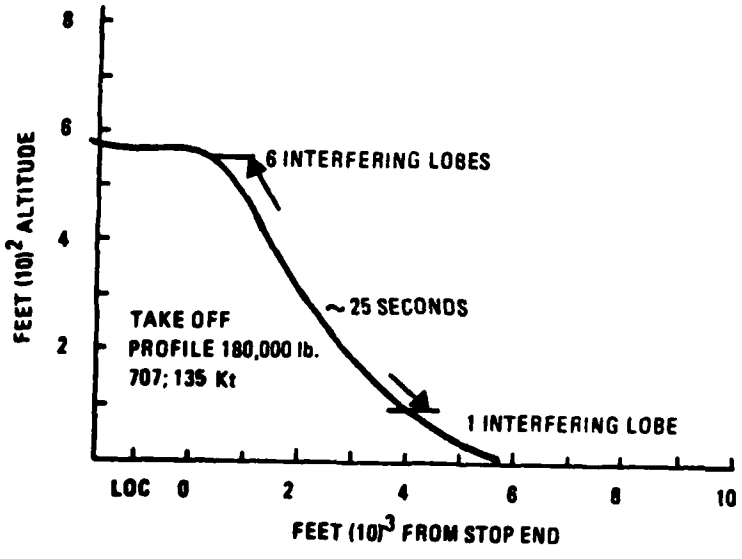

FIGURE 2-7. TAKE-OFF PROFILE FOR A KC135/707 TYPE AIRCRAFT.

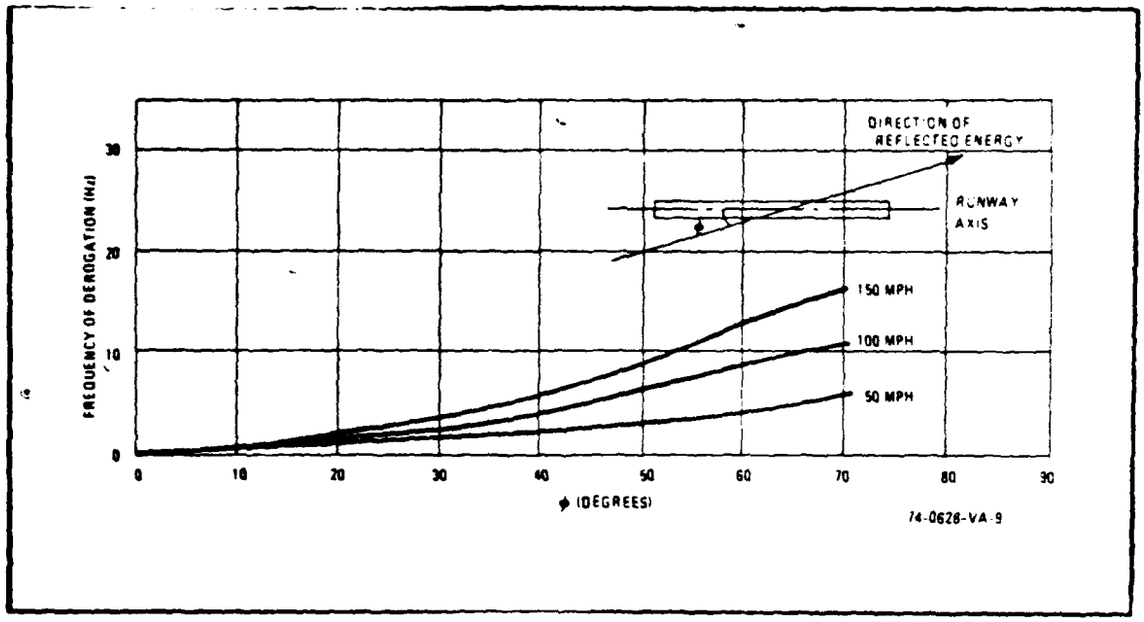

FIGURE 2-4. OSCILLATORY FREQUENCIES OF LOCALIZER DEROGATION VS. AIRCRAFT LANDING SPEED AND INCIDENCE ANGLE

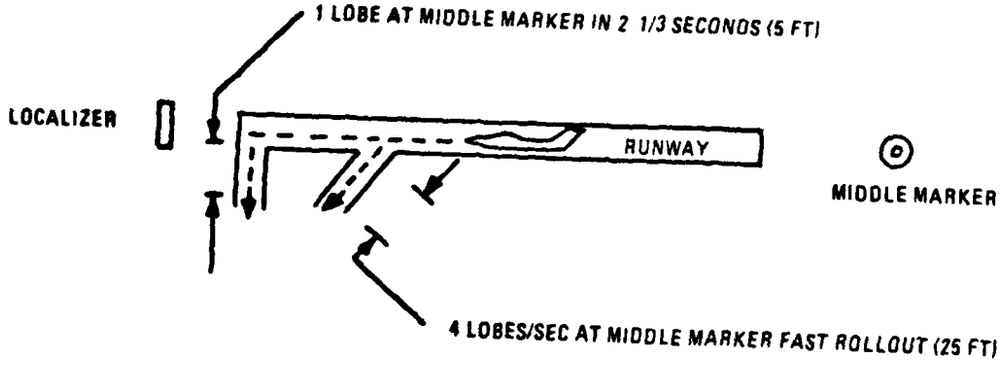

FIGURE 2-5. TYPICAL ROLL OUT AND TURN OFF GEOMETRY. CABLE SUPPORT EFFECT ON FREQUENCY AND MAGNITUDE OF DEROGATION.

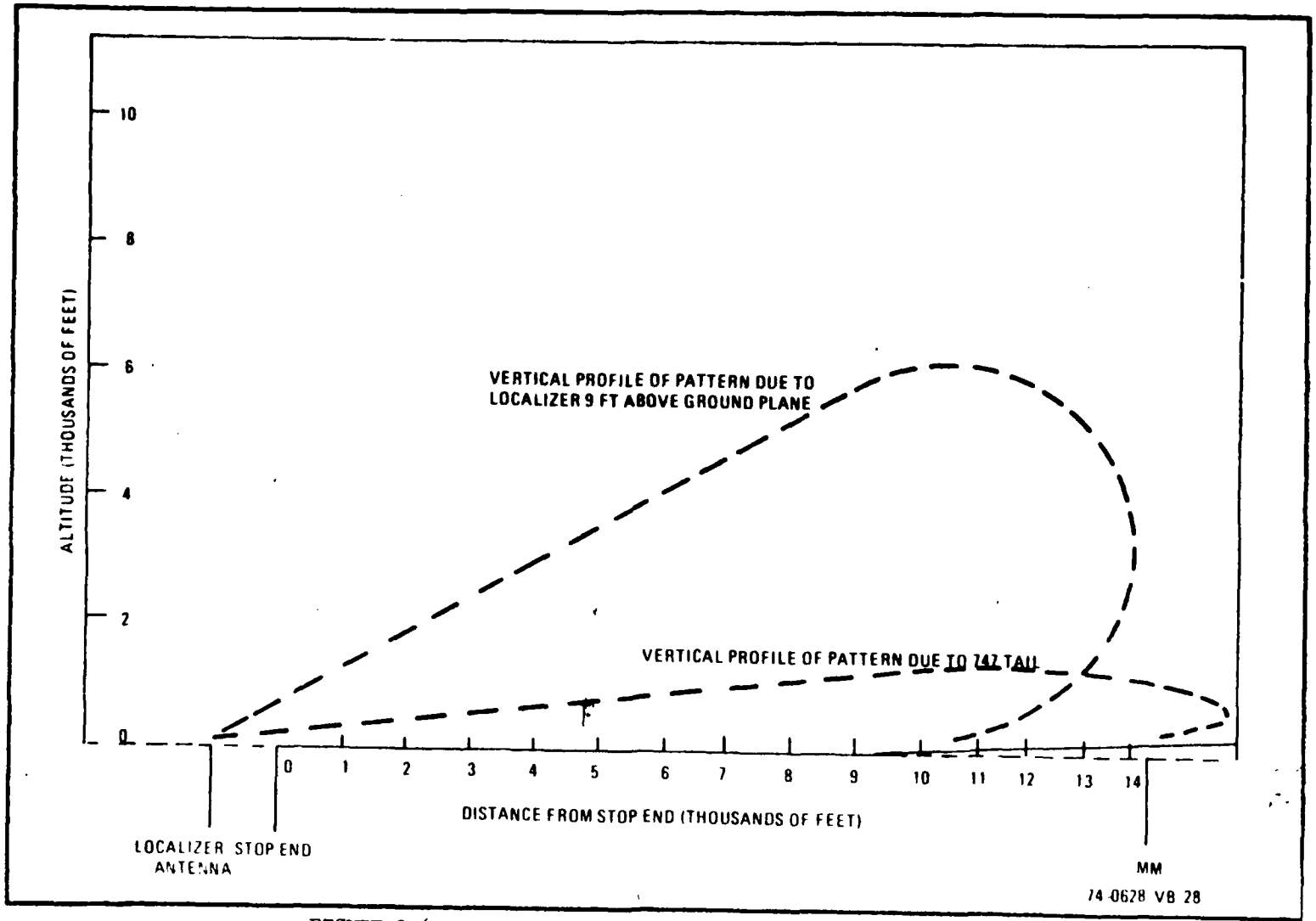

FIGURE 2-6. VERTICAL PROFILE OF GUIDANCE LOBE OF LOCALIZER SIGNAL AND REFLECTIVE LOBE OF 747 TAIL CLOSE TO THE LOCALIZER ANTENNA.

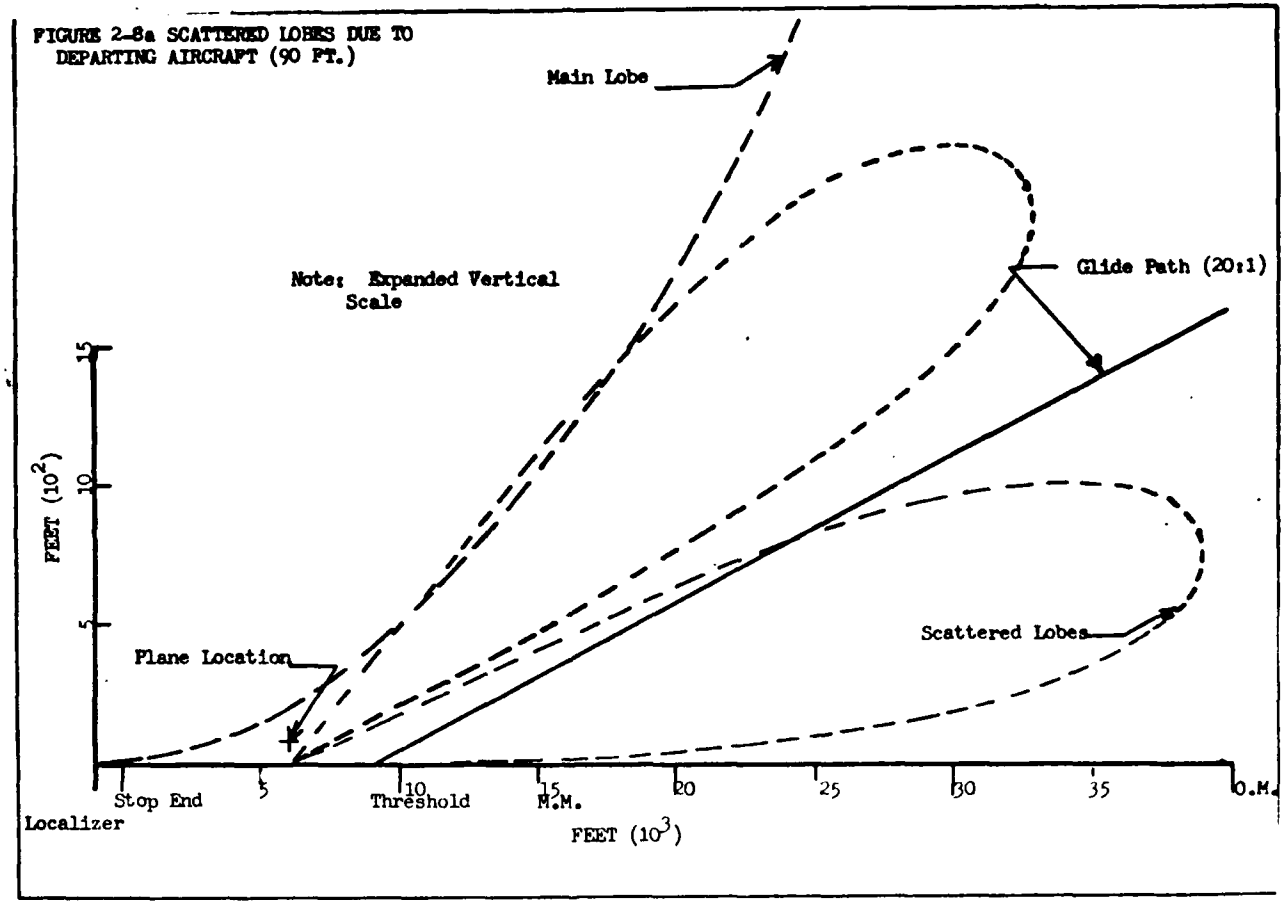

FIGURE 2-8a VERTICAL LOBING STRUCTURE OF LOCALIZER GUIDANCE DUE TO AIRCRAFT TAKING OFF ALONG THE PROFILE SHOWN IN FIGURE 2-7 FOR THE AIRCRAFT AT 90 FEET.

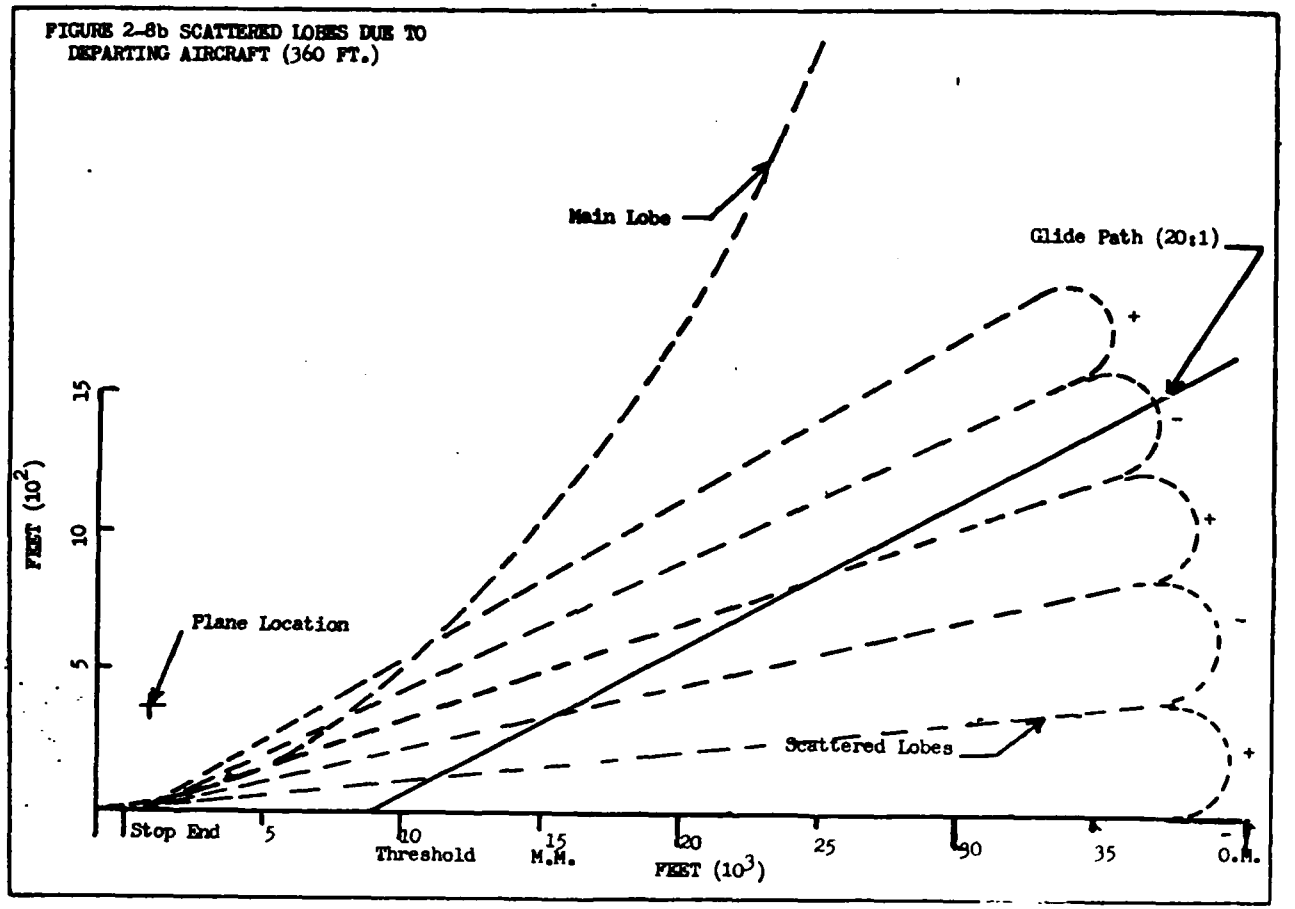

FIGURE 2-8b VERTICAL LOBING STRUCTURE OF LOCALIZER GUIDANCE DUE TO AIRCRAFT TAKING OFF ALONG THE PROFILE SHOWN IN FIGURE 2-7 FOR THE AIRCRAFT AT 360 FEET.

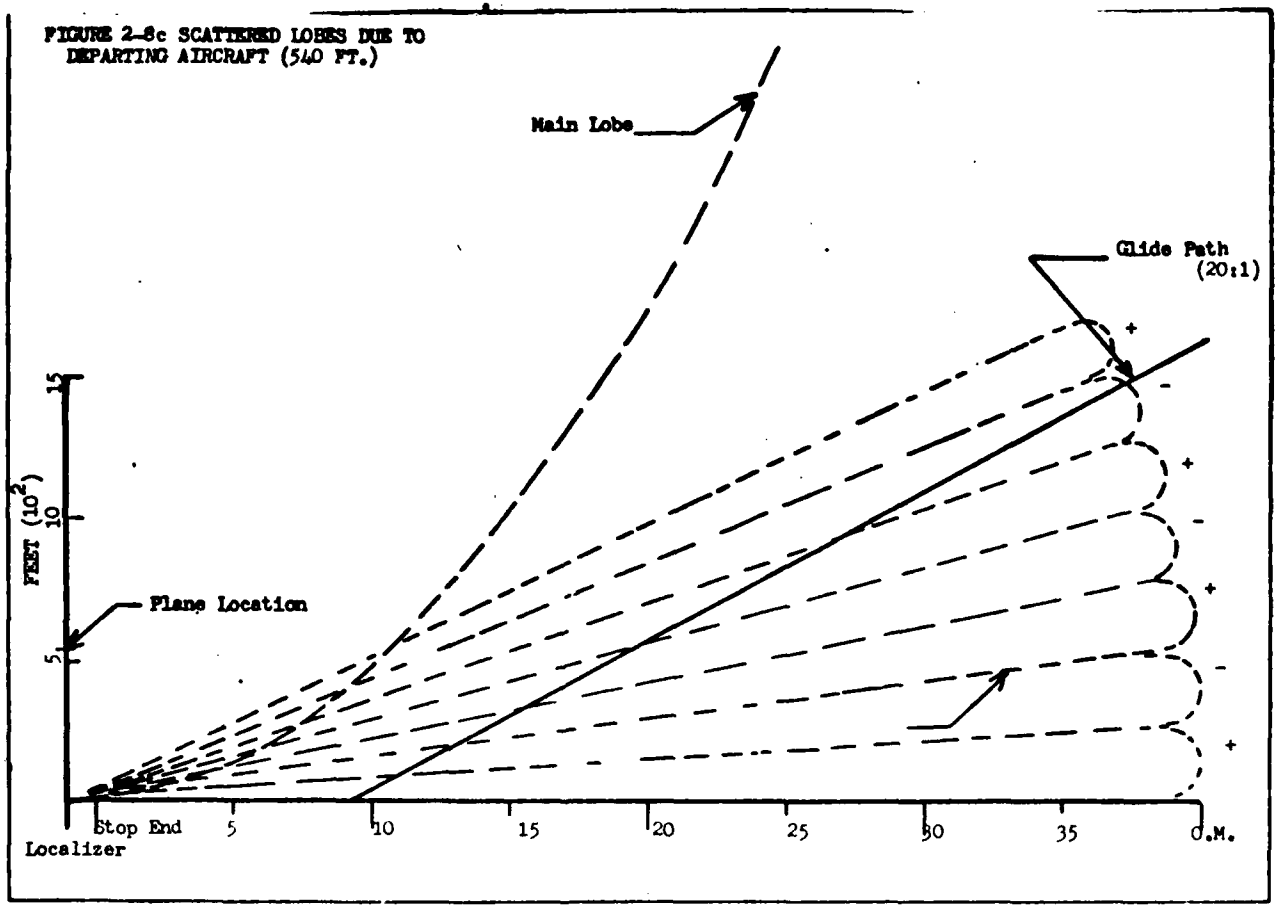

FIGURE 2-8c VERTICAL LOBING STRUCTURE OF LOCALIZER GUIDANCE DUE TO AIRCRAFT TAKING OFF ALONG THE PROFILE SHOWN IN FIGURE 2-7 FOR THE AIRCRAFT AT 540 FEET.

For an aircraft flying low over the localizer this may be as much as an order of magnitude greater than alarm. Because, however, the overpowering level of derogation measured at the ground does not project to the approach path, the ground based far field monitor must be capable of projecting the actual flight path derogation with reasonable accuracy.

The overpowering nature of derogation due to the low lobe position for diffraction/reflection from aircraft taking off is illustrated in measurements made by Marconi[3]. Figure C-8 (Appendix C) shows the trace of derogation in guidance and flag current. This is one of a series of overflight measurements taken by Marconi at Andrews Airfield, Saling and Stansted Airport. This trace for a 707 aircraft on take off illustrates the overpowering effect of overflight derogation on ground based monitors. Other traces taken for smaller aircraft on take off and missed approach maneuvers show varying degrees of derogation, although all are overpowering.

2.2.3 Calculation of Derogation

The mathematics of the calculation of the ILS guidance in the presence of scatterers is in Appendix A. These calculations show that the disturbed field structure is very sensitive to the detailed antenna characterization.

Kirchhoff's theory of diffraction has been used to determine the scalar field emanating from a set of spherical radiators representing the localizer antenna and scattered by a set of independent (one or more) rectangular screens. The rectangular screens are used to represent taxiing and overflying aircraft. The formulation is carried out in detail in Appendix A. Experimental verification of the formulation is described in Appendix B.

The coordinates used for calculation of localizer derogation are illustrated in Figure 2-9. The origin of the angular deviation from the centerline is at the localizer antenna. The derogation is computed for a flat screen representation of a 747 tail.

Examples of the computation of derogations due to scatterers are illustrated in Figure 2-10, 2-11, and 2-12. The static localizer field has been subtracted from the total localizer field; the difference is the deviation from the static guidance that an aircraft would observe on an approach when it is flying in the area represented by the graph.

One of the most striking features of the derogation is its oscillatory nature as a function of position. This can be understood through the geometry of Figure 2-3, which shows the hyperbolae of constant differences in distance between the antennas and the scatterer. If each hyperbola represents a wavelength increment in distance, then the derogation is quasi-periodic with periods equal to the separation between the lines. Thus, the frequency of the derogation clearly depends upon the relative position of the antenna, scatterer and the viewer.

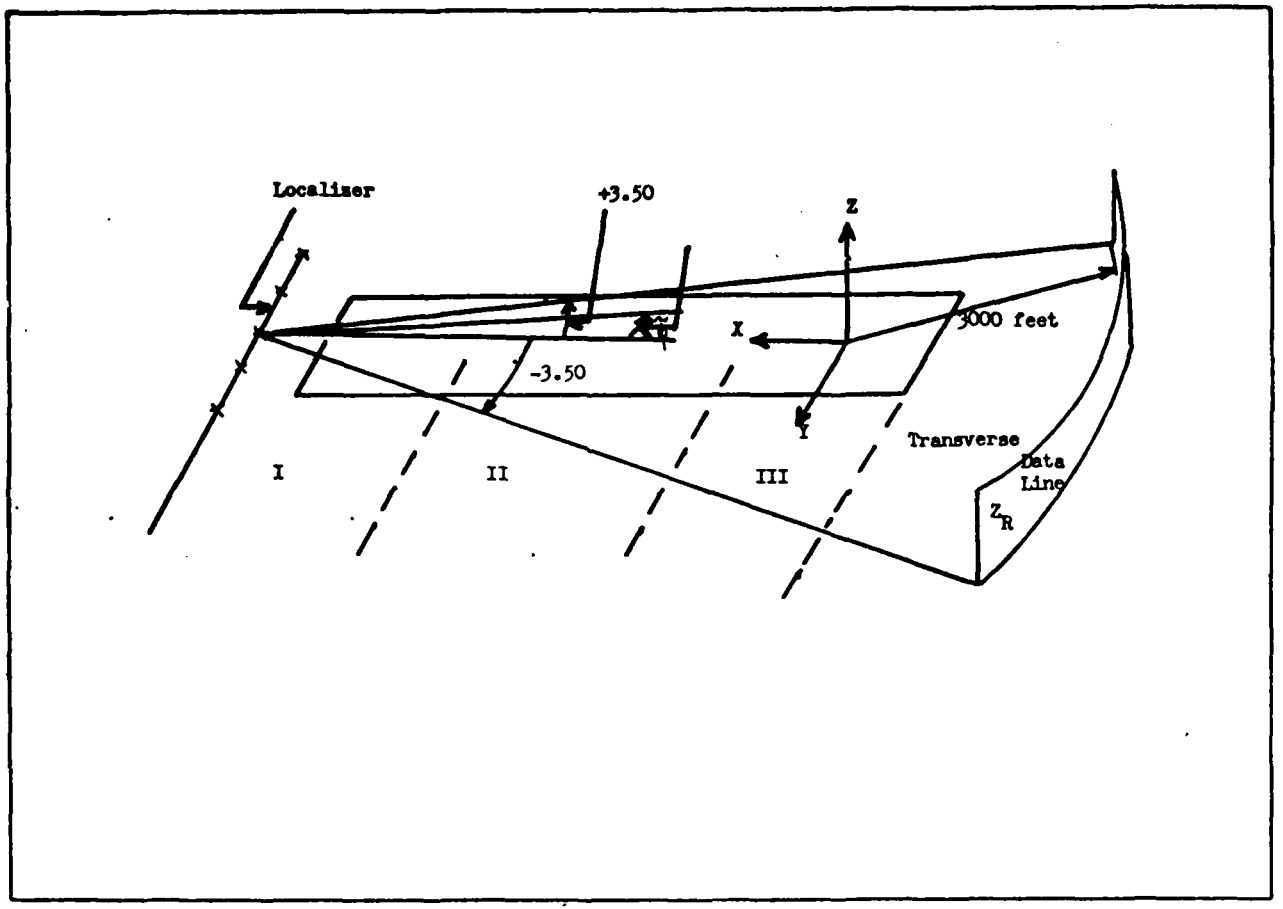

FIGURE 2-9. ILLUSTRATION OF TRANSVERSE DATA FIELD FOR LOCALIZER

Key:

Localizer

X = 8500'

Y = 250'

Z = 36'

Y = 90°

A = 24' } tail

B = 72' } approx.

Z_R = 25'

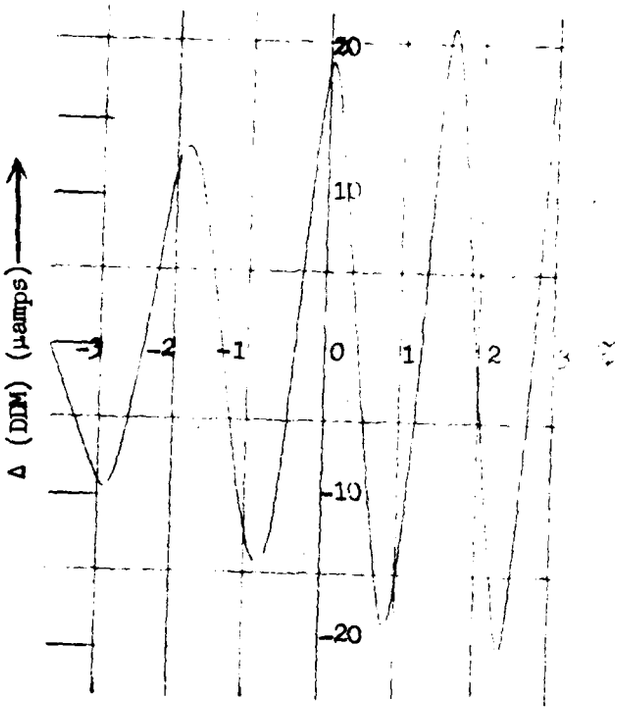

FIGURE 2-10. TRANSVERSE VARIATION OF Δ (DDM)

Key:

Localizer

X = 5000'

Y = 250'

Z = 36'

Φ = 90°

A = 24' } tail approx.

B = 72' }

Z_R = 25'

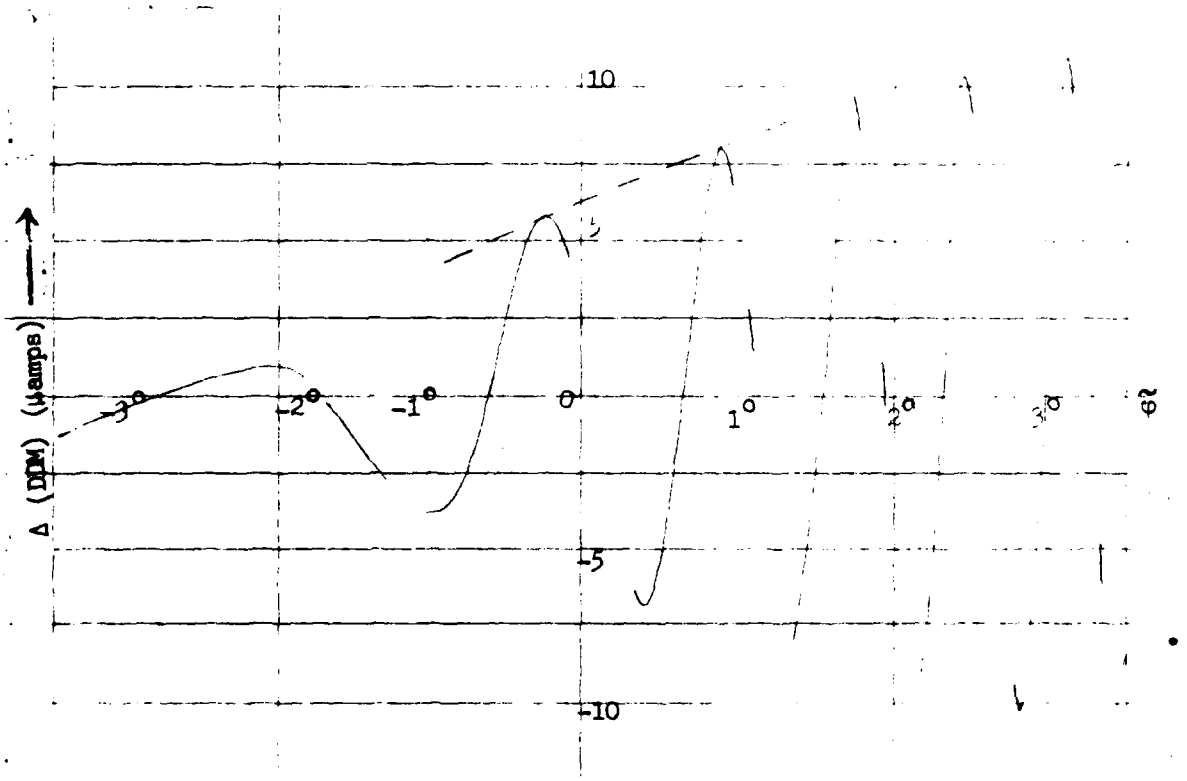

FIGURE 2-11. TRANSVERSE VARIATION OF Δ (DDM)

Key:

Localizer

X = 1500'

Y = 250'

Z = 36'

φ = 90°

A = 24' } tail approx.

B = 72' }

Z_R = 25'

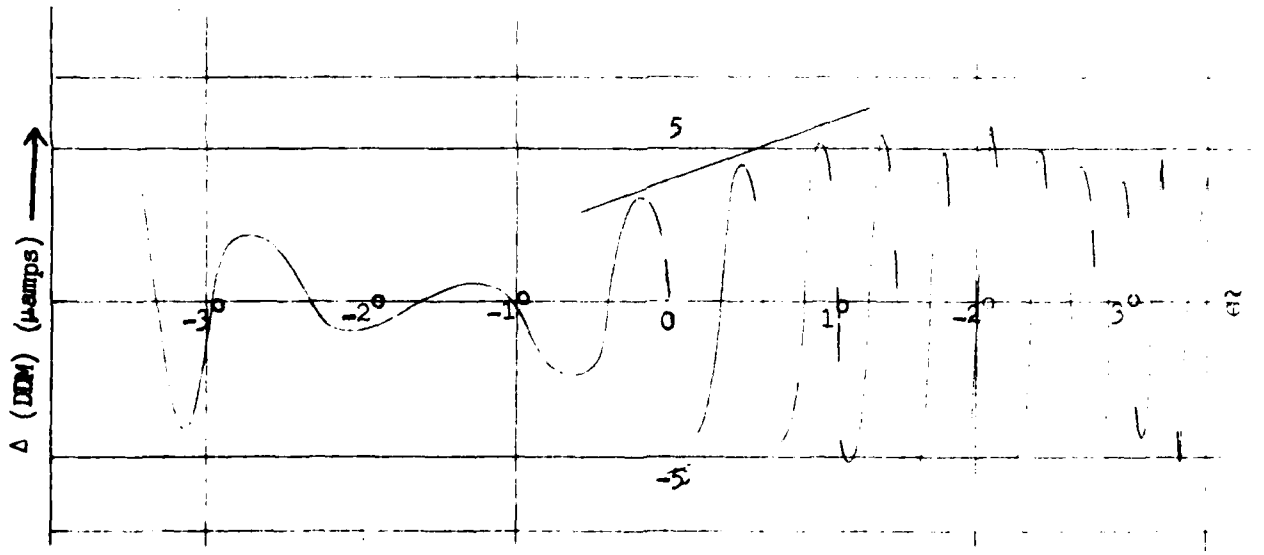

FIGURE 2-12. TRANSVERSE VARIATION OF Δ (DDM)

Key:

Localizer

X = 1500'

Y = 250'

Z = 36'

$\varphi = 90^{\circ}$

A = 24' } tail approx.

B = 72' }

Z_R = 25'

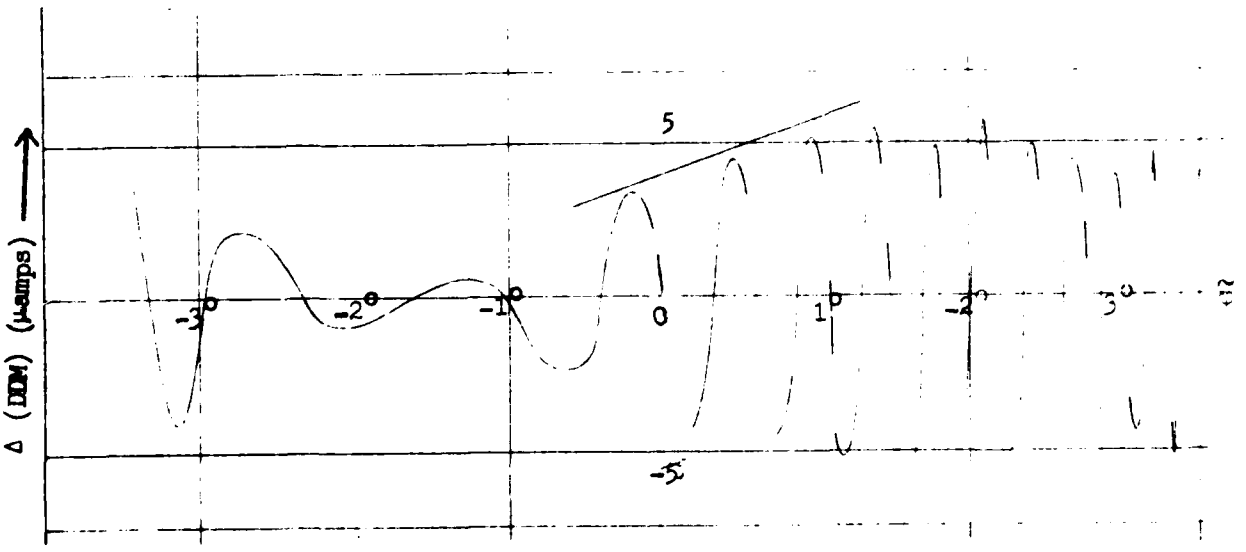

FIGURE 2-12. TRANSVERSE VARIATION OF Δ (DDM)

2.3 Concept of Envelope Monitoring

Another striking feature of the derogation is that the position of the maximum and minimum are very sensitive to the scatterer position. Thus, as the scatterer moves in rollout off the runway and into a taxiway, the position of the derogation maxima will also move. They will, in fact, pass through the approach path quasi-periodically.

It is clear from the foregoing that the mere absence of major derogation along the runway centerline is an insufficient test of safe guidance. It is also clear that low derogation on the centerline at the point of a monitor does not guarantee acceptable guidance even along the computed centerline. The peak derogation must be detected by the monitor. The magnitudes of the derogation peaks in the vicinity of the centerline are a reasonable measure of derogation level evaluation. The value of these peaks must be monitored, whether or not they fall directly on the centerline.

Figure 2-13 illustrates a plane in a sequence of three positions for which derogation was computed. They illustrate three different geometric conditions and the general relationship of the derogation patterns, both transverse and longitudinally for these conditions. Note that the closer the scattering object is to the approach end of the runway, the more extreme are the patterns. The closer the localizer, the more gradual the change in the patterns. In all cases, however, the derogation patterns are the largest close to the approach end of the runway, where it is most critical that the guidance be good, and where the highest specifications of the guidance exist. Two key points are (1) if alarm derogation conditions exist close to the approach end of the runway, the guidance is in alarm, and (2) it is sufficient to determine the derogation envelope. The derogation envelope correlates extremely well with the peak derogation along the glide path. These two considerations have been used to set the strategy for developing the technical aspects of a comprehensive far field monitor. The requirement is that the far field monitor be capable of determining the derogation envelope in the general region of the end of the runway and the middle marker.

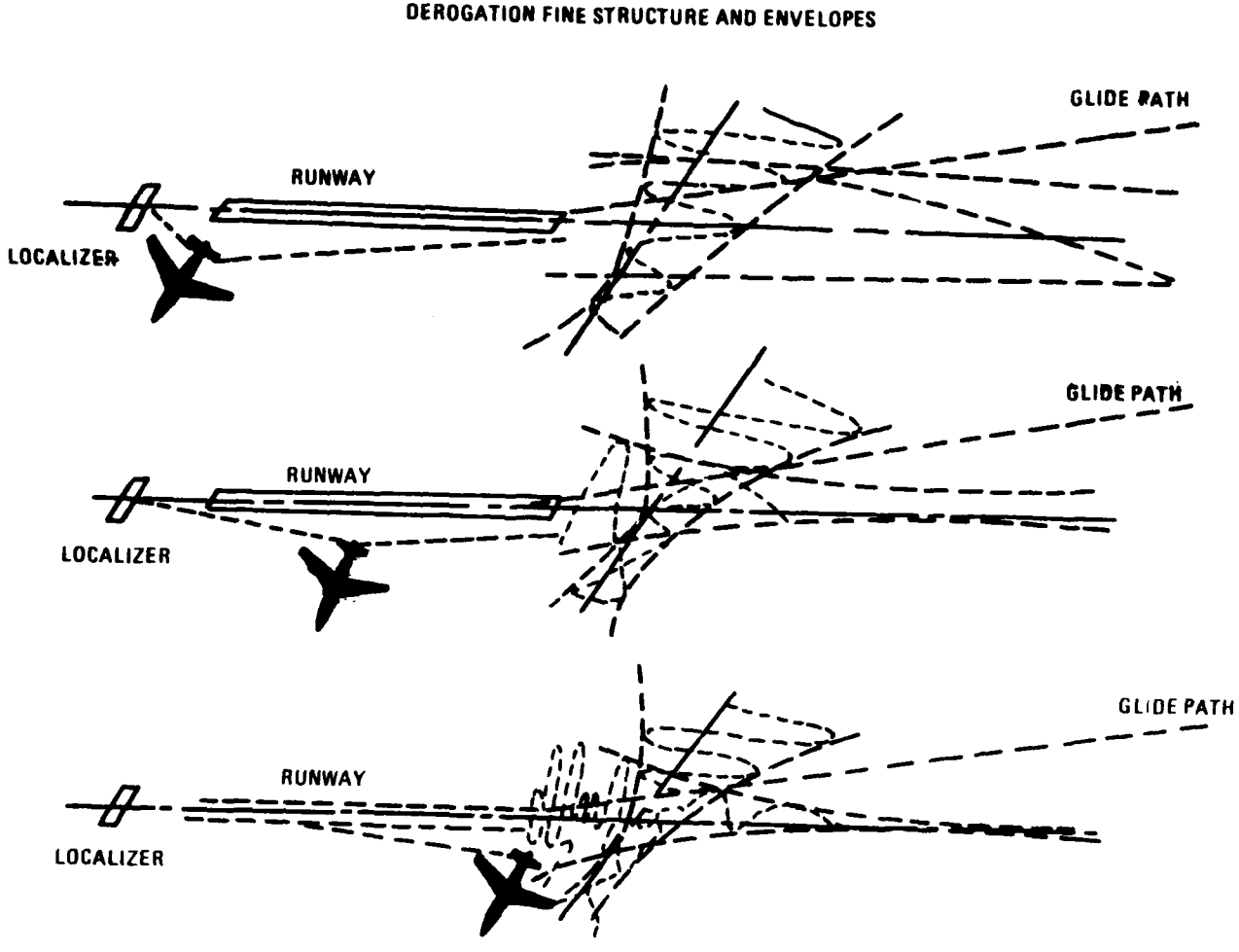

FIGURE 2-13. DEROGATION FOR PLANES IN THE SAME RELATIVE POSITION AS COMPUTED IN FIGURE 2-10.

3.0 MONITOR CONCEPTS DEVELOPED

The key to a successful monitor is the envelope concept which was identified in the previous chapter. In the vicinity of the glide path, scattering causes oscillatory or quasi-periodic changes in the envelope of the peaks of derogation. A further characteristic of the derogation is that due to moving scatterers, the peaks of the derogation move with the scatterer, and the peaks of the derogation can occur at various points along the glide path or within the guidance region. The envelope rather than the mere peaks must be identified since placement of the peaks is not of consequence as long as they occur within the glide path region and cause the guidance to fail to meet specification. The objective of all of the monitor concepts developed in this section is to detect the envelope of the derogation.

An additional requirement of all monitors is the projection of the value of the derogation into the glide path. It has been noted that some types of derogation, particularly from overflying aircraft, overpowered ground level monitors, whereas in the glide path the derogation may be considerably less. Time variation of some of this derogation may be very helpful in its evaluation. Virtually all such derogation that is overpowering also varies so rapidly that it causes little real disturbance in the aircraft landing guidance. This is an area where a mini computer may be useful in combination with the optimum detector in establishing an overall high performance monitor.

Four systems were chosen as candidates to be analyzed; two were acceptable of which one is considered superior in performance. The unit which is projected to provide the best performance also requires less hardware than the other acceptable system, thus implying the best cost trade off.

3.1 Monitors Considered, Summary

Four monitor concepts have been extensively analyzed mathematically. Each of the monitors offered the possibility of meeting the criteria for this program, and it was desirable but not mandatory if the monitor evolved logically from the present monitor.

Each of the monitors was evaluated for (1) its ability to measure the derogation envelope. Derogation has been shown to have fine structure as well as envelope. The fine structure is of immediate concern to the guidance though the envelope provides total evaluation of the propagation, and (2) Each was also evaluated for accuracy and susceptability to either false alarms or missed alarms.

Each of the far field monitors is positioned between the approach end of the runway and the middle marker. The following four subsections briefly identify the four monitors considered. Each section provides a brief description of the monitor and the derivation and analysis of the monitor. The interferometric monitor and the vector monitor require the least amount of hardware.

3.1.1 Multiprobe Monitor

The multiprobe far field monitor is an extension of the centerline monitor in which a series of probes of the same type is displaced across the approach path between the end of the runway and the middle marker. Sufficient probes are distributed in this manner to provide a high probability of defining the fine structure maxima of the derogation. With sufficient individual probes there is a minimum probability of unsafe derogation occurring, without being detected by at least one monitor probe. The derogation identified is the maximum derogation measured at any one of the individual pickup probes.

3.1.2 Curve-Fitting Monitor

The curve fitting monitor is the next order evolution of the present centerline monitor beyond the multiprobe monitor. It consists of a series of individual receivers displaced in a line transverse to the runway centerline. As opposed to the multiprobe monitor in which the maximum measured derogation is identified as the derogation, this monitor uses a minicomputer to process the individual probe outputs. The approach is then to fit a curve of the fine structure between the measure points. To do this the monitor points are more closely spaced than for the multiprobe monitor, but will use the same type receiver.

3.1.3 Interferometric Monitor

The interferometric monitor makes use of the fact that the magnitude of any wave front, either from the localizer antenna or a scattering object, can be measured at any point in the vicinity of the approach to the airport. This monitor consists of a series of pickups separated in varying amounts and can be placed anywhere in the airport. A logical choice is close to the centerline at the opposite end of the runway. The variation in separations of the pickups provides a variation in rate of phase change relative to sets of pickups as the positions of a scatterer change. The maximum derogation measured for all such interferometric comparisons is the indicated derogation. During setup the interferometric monitor is adjusted so that, between all pickups compared, the localizer signal is completely nulled. With sufficient monitors the analysis shows that the derogation from a scatterer is measured in any direction from the monitor. This then measures the envelope of the fine structure of the derogation passing the monitor.

3.1.4 Vector Monitor

In the presence of derogation the modulation of the signal passing the monitor is either in phase, out of phase, or at some intermediate phase

relationship to the carrier. As the derogation progresses across the path of the direct signal the phase relationship between the modulation and the carrier varies quasi-periodically. This is the reason for the quasi-periodic derogation. The derogation peaks occur when the modulation is in phase or 180° out of phase with the carrier. By providing both quadrature and in-phase modulation detection, the vector sum of these two modulations provides the envelope of the derogation. Thus a single vector DDM detector along the centerline can measure the envelope of the DDM and project the derogation along the centerline.

3.2 Multiprobe Monitor

This most straight forward extension of the present centerline monitor is illustrated diagramatically in Figure 3-1. Each of the receivers is set to provide an output of deviation from the normal DDM at the monitor point.

The multiprobe monitor is analyzed in the following subsection in which various probe placements are used to evaluate the ability of the monitor to accurately predict unsafe conditions. The result of this evaluation is illustrated in Figure 3-2 which is a plotted diagram of a suitable number of scatterers. The vertical and horizontal coordinates are, respectively, the actual and computed (DDM's) on the glide path and at the monitor probe points. For these examples nine probe points were used. It is clear that the evaluation is not sufficient to justify the multiprobe elements as a practical monitor.

3.2.1 Analysis

The multiprobe monitor assumes an isotropic scatterer and a DDM deviation of each probe of A cos φ where A is a constant amplitude determined by the position and size of the scatterer, and φ is the phase angle between the carriers of the direct and scattered signals arriving at the probe.

Two signals are generated by the localizer transmitter. They have a common carrier frequency and are amplitude modulated to a depth of 40% at 90 and 150 Hz, respectively, and they are radiated in such a way as to give two main beams offset symmetrically on each side of the centerline. If the two radiation patterns are $P_1(\tilde{\varphi})$ and $P_2(\tilde{\varphi})$, where $P_1(\tilde{\varphi}) = P_2(-\tilde{\varphi})$ then the sum pattern

$$C(\tilde{\varphi}) = P_1 + P_2(\tilde{\varphi})$$

is known as the carrier plus sidebands pattern (CSB), and the difference pattern

$$S(\tilde{\varphi}) = P_1(\tilde{\varphi}) - P_2(\tilde{\varphi})$$

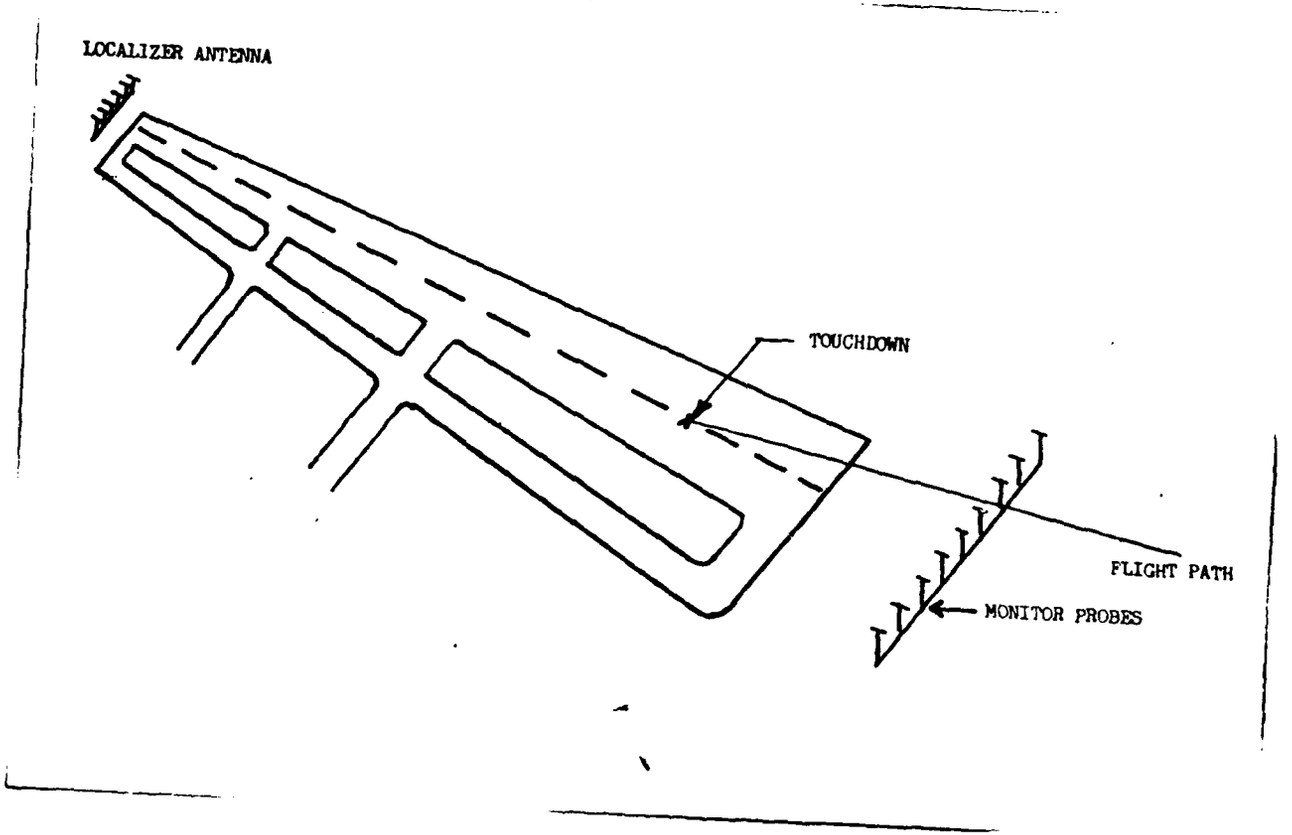

FIGURE 3-1. ILLUSTRATION OF TYPICAL ARRANGEMENTS OF RECEIVERS FOR MULTIPROBE FAR FIELD MONITORS

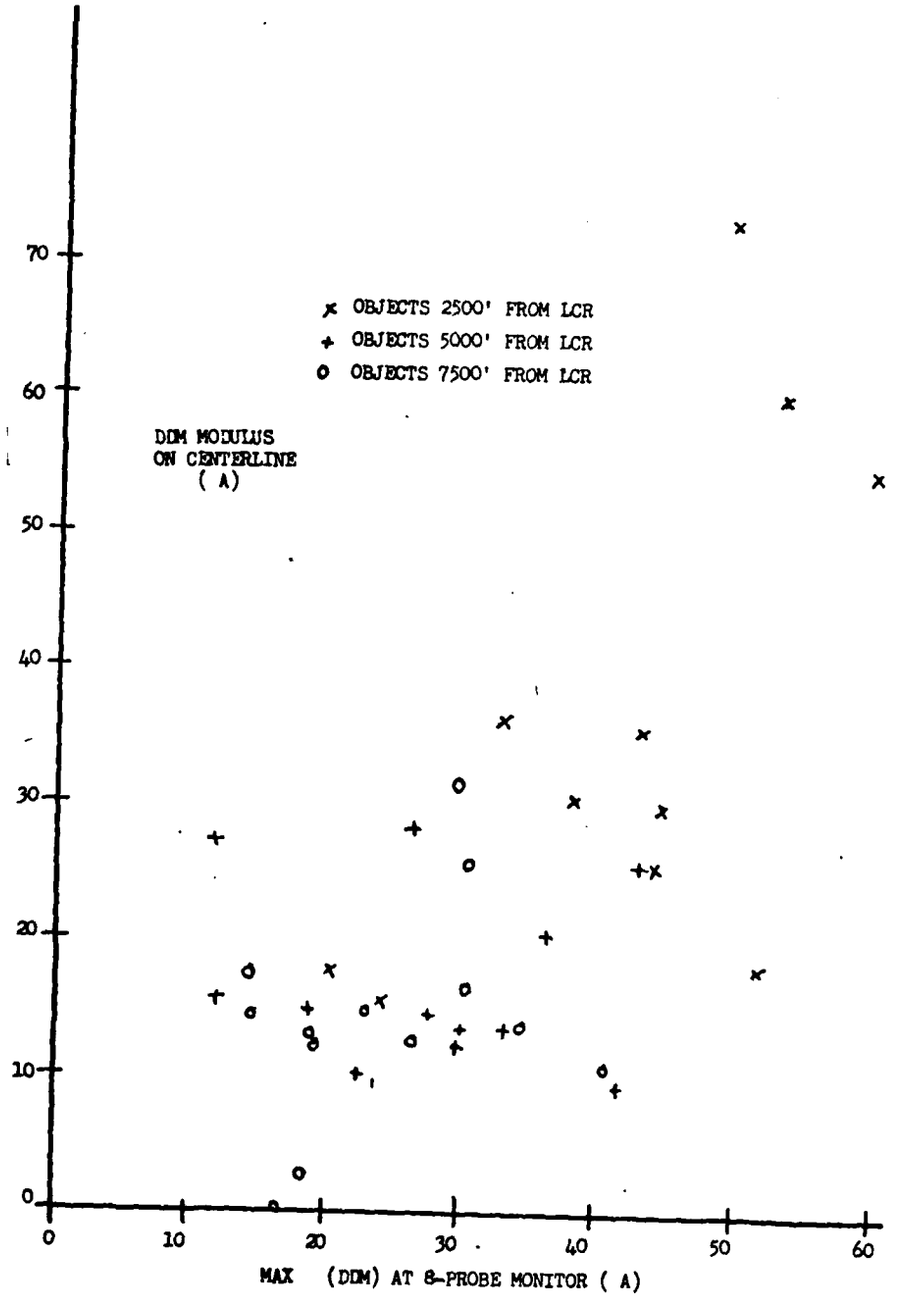

FIGURE 3-2. SCATTER DIAGRAM

is the sideband only pattern (SBO). At any azimuthal angle $\tilde{\Phi}$, measured from the centerline, the radiated carrier aplitude is therefore

$$P_1\ (\tilde{\varphi})\ (1 + 0.4\ \cos\omega_1 t) + P_2\ (\tilde{\varphi})\ (1 + 0.4\ \cos\omega_2 t)$$

where $\omega_1 = 2\pi \times 90$ Hz and $\omega_2 = 2\pi \times 150$ Hz

The depth of modulation at the two tone frequencies are $0.4\ P_1/C$ and $0.4\ P_2/C$, respectively, and it follows that the difference in depth of modulation (DDM) is given by

$$DDM\ (\tilde{\varphi}) = 0.4\ S\ (\tilde{\varphi})/C\ (\tilde{\varphi}).$$

In the presence of multipath interference from some scattering object, the reflection coefficient $k\ e^{j\phi}$ is defined as the ratio of the scattered carrier to the direct carrier arriving at the receiver, calculated on the assumption of an isotropic CW transmitter situated in place of the localizer transmitter. The signal received from the localizer with one scatterer present is then

$$P_1\ (\tilde{\varphi}_R)\ (1 + 0.4\ \cos\omega_1 t) + P_2\ (\tilde{\varphi})\ (1 + 0.4\ \cos\omega_2 t)$$

$$+ k\cos\phi \left\{ P_1\ (\tilde{\varphi}_S)\ (1 + 0.4\ \cos\omega_1 t) + P_2\ (\tilde{\varphi}_S)\ (1 + 0.4\ \cos\omega_2 t) \right\}$$

where $\tilde{\varphi}_S$ = Azimuth angle of receiver

$\tilde{\varphi}_R$ = Azimuth angle of scatterer

The DDM at the receiver is therefore

$$DDM\ (\tilde{\varphi}) = 0.4 \left[S\ (\tilde{\varphi}_R) + k\cos\phi\ S(\tilde{\varphi}_S) \right] / \left[C(\tilde{\varphi}_R) + k\cos o\ C\ (\tilde{\varphi}_S) \right]$$

$$\frac{0.4\left\{S(\tilde{\varphi}_R) + k\cos\phi\ \ S(\tilde{\varphi}_S)\right\}\left\{1 - k\cos\ \frac{C(\tilde{\varphi}_S)}{C(\tilde{\varphi}_R)}\right\}}{C(\tilde{\varphi}_R)}$$

Ignoring terms of order k^2 or greater we obtain the result

$$DDM = DDM\ (\tilde{\varphi}) + k\cos\phi \left\{ DDM\ (\tilde{\varphi}_S) - DDM\ (\tilde{\varphi}_R) \right\} \frac{C(\tilde{\varphi}_S)}{C(\tilde{\varphi}_R)}$$

i.e.,

$$\Delta\ (DDM) = k\cos\phi \left\{ DDM\ (\tilde{\varphi}_S) - DDM\ (\tilde{\varphi}_R) \right\} \frac{C(\tilde{\varphi}_S)}{C(\tilde{\varphi}_R)} \qquad (3.1)$$

This result gives the DDM deviation at the receiver (i.e., the actual DDM minus the DDM that would be obtained in the absence of the multipath contribution) as equal to the product of the reflection coefficient, the cosine of its phase, the difference between the direct DDM's obtained at the receiver and the scatterer, and the carrier ratio between the scattered and direct signals. Thus an additional variation of Δ(DDM) other than that introduced by path length variation of the relative phases is present when the receiver is off the centerline. The simplest representation of Δ(DDM) is therefore

$$(DDM) = A\ (\tilde{\varphi}_S - \tilde{\varphi}_R)\ \cos\phi \qquad (3.2)$$

where A is a constant. This assumes that DDM varies linearly with azimuth and is true only in the vicinity of the centerline.

With the receiver at position $\underline{r}_R$ and the scatterer at $\underline{r}_S$ the direct and scattered signals arriving at the receiver assuming an isotropic CW transmitter are given by E_D and E_S where

$$E_D = E_D\ (\underline{r}_R)$$

$$E_S = E_S\ (\underline{r}_R, \underline{r}_S).$$

With the modulation tones present, the received signal comprises two components arising from the CSB and SBO transmitted patterns. The received CSB component is

$$E_D\ C\ (\tilde{\varphi}_R) + E_S\ C\ (\tilde{\varphi}_S)$$

and the received SBO component is

$$E_D\ S\ (\tilde{\varphi}_R) + E_S\ S\ (\tilde{\varphi}_S).$$

The complex DDM at the receiver is therefore

$$0.4\ \frac{E_D\ S\ (\tilde{\varphi}_R) + E_S\ S\ (\tilde{\varphi}_S)}{E_D\ C\ (\tilde{\varphi}_R) + E_S\ C\ (\tilde{\varphi}_S)}$$

The actual DDM registered by an ordinary ILS receiver is the real part of this expression.

In the present exercise the localizer was modelled as a point source with the following radiation patterns:

$$P_1\ (\tilde{\varphi}) = \sin X_1/X_1,\ X_1 = \pi a\ \sin(\tilde{\varphi} - \tilde{\varphi}_o)$$

$$P_2\ (\tilde{\varphi}) = \sin X_2/X_2,\ X_2 = \pi a\ \sin\ (\tilde{\varphi} - \tilde{\varphi}_o)$$

$$C\ (\tilde{\varphi}) = P_1 + P_2$$

$$S\ (\tilde{\varphi}) = P_1 - P_2$$

$$a = 8$$

$$\tilde{\varphi} = 3^o$$

This model gives a sensitivity of 0.0878 DDM per degree and a maximum bend potential of 0 265 at azimuth angles of $\pm 5^{\circ}$. It is therefore a representative model for the main lobe region of a STAN-37 localizer with a 65 ft. aperture, installed at a 10000 ft. runway

To calculate the received DDM in the presence of more than one scatterer the following expression was used:

$$DDM = 0.4 \, Re \left\{ \frac{E_D \, S(\tilde{\varphi}_R) + \sum_i E_{si} \, S(\tilde{\varphi}_{si})}{E_D \, C(\tilde{\varphi}_R) + \sum_i E_{si} \, C(\tilde{\varphi}_{si})} \right\}, \qquad (3.3)$$

where the summation covers all the scattered signals. The DDM at each probe in the absence of interference was calculated as

$$DDM_o = 0.4 \, \frac{S(\tilde{\varphi}_R)}{C(\tilde{\varphi}_R)}$$

and the DDM deviation was therefore

$$\Delta(DDM) = DDM - DDM_o \qquad (3.4)$$

One further quantity was computed: this was the DDM modulus on the center line, i.e., the DDM observed by an approaching aircraft at the same distance, calculated on the assumption that the relative phases of all the signals had their worst possible values. This quantity was calculated as the modulus of the expression given in Eq. (3.3).

3.2.2 Properties of Multiprobe Monitors

The multipath situations computed involved four rectangular scatterers A, B, C and D placed 0, 100, 200 and 300 ft., respectively, from the centerline. All scatterers were 36 ft. wide by 72 ft. high, and oriented at 90° to the centerline. They were placed on a line cutting the centerline at right angles at a distance of 2500 ft. from the transmitter. The four scatterers were considered singly, in pairs, in triples and all together, and in each case the receiver probe was moved laterally along a line cutting the centerline 10,000 ft. from the transmitter. The exercise was then repeated with the four objects placed on similar lines 5000 ft. and 7500 ft. from the transmitter. The total number of runs carried out was 39.

The curves of Δ(DDM) plotted against lateral receiver position are given in Figures 3-3 through 3-12. Tables 3-I, 3-II and 3-III give the results in summarized form by listing the DDM modulus on the centerline and the maximum DDM deviation occurring at eight probes at $\pm$150, $\pm$200, $\pm$250 and $\pm$300 feet from the centerline. The tabulated results are also plotted on a scatter diagram which is given in Figure 3-2. In the scatter diagram each point represents a particular scattering situation and its coordinates are the DDM modulus observed on the centerline at 10,000 feet from the transmitter, and the maximum DDM deviation at the eight probes.

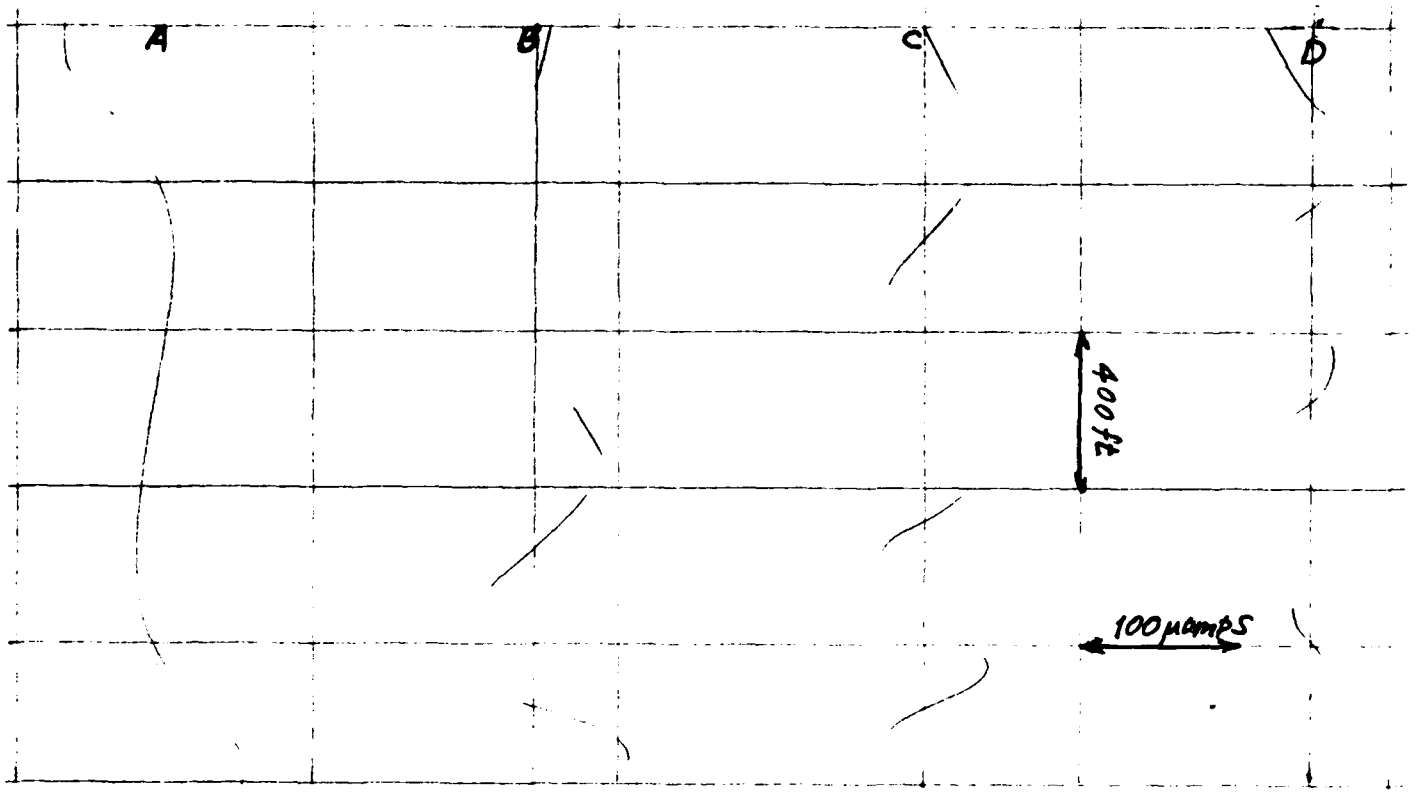

FIGURE 3-3 Δ (DDM) ALONG A TRANSVERSE LINE 10000 FT. FROM LOCALIZER.
OBJECTS 2500 FT. FROM LOCALIZER

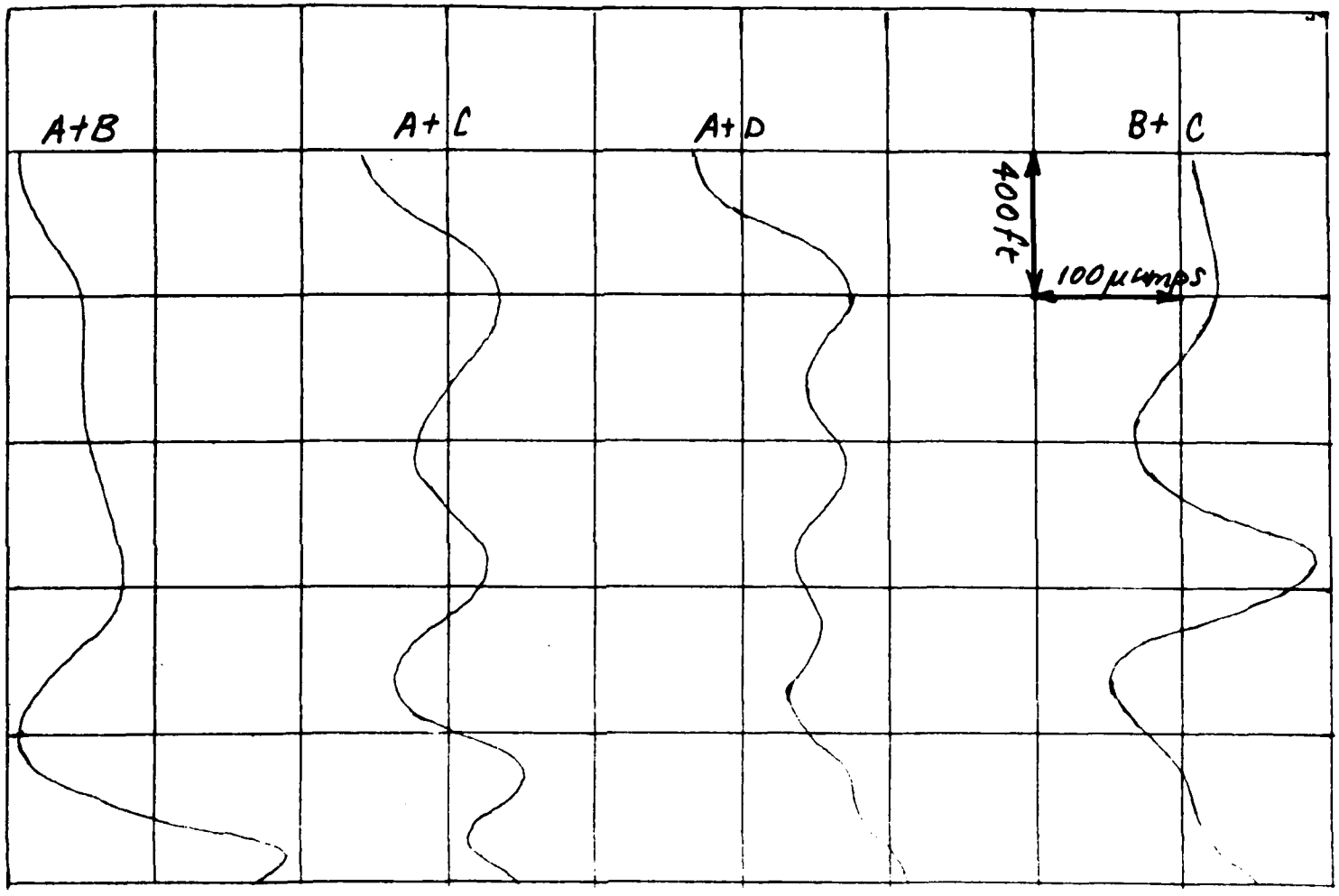

FIGURE 3-4 Δ(DDM) ALONG A TRANSVERSE LINE 10000 FT. FROM LOCALIZER.
OBJECTS 2500 FT. FROM LOCALIZER

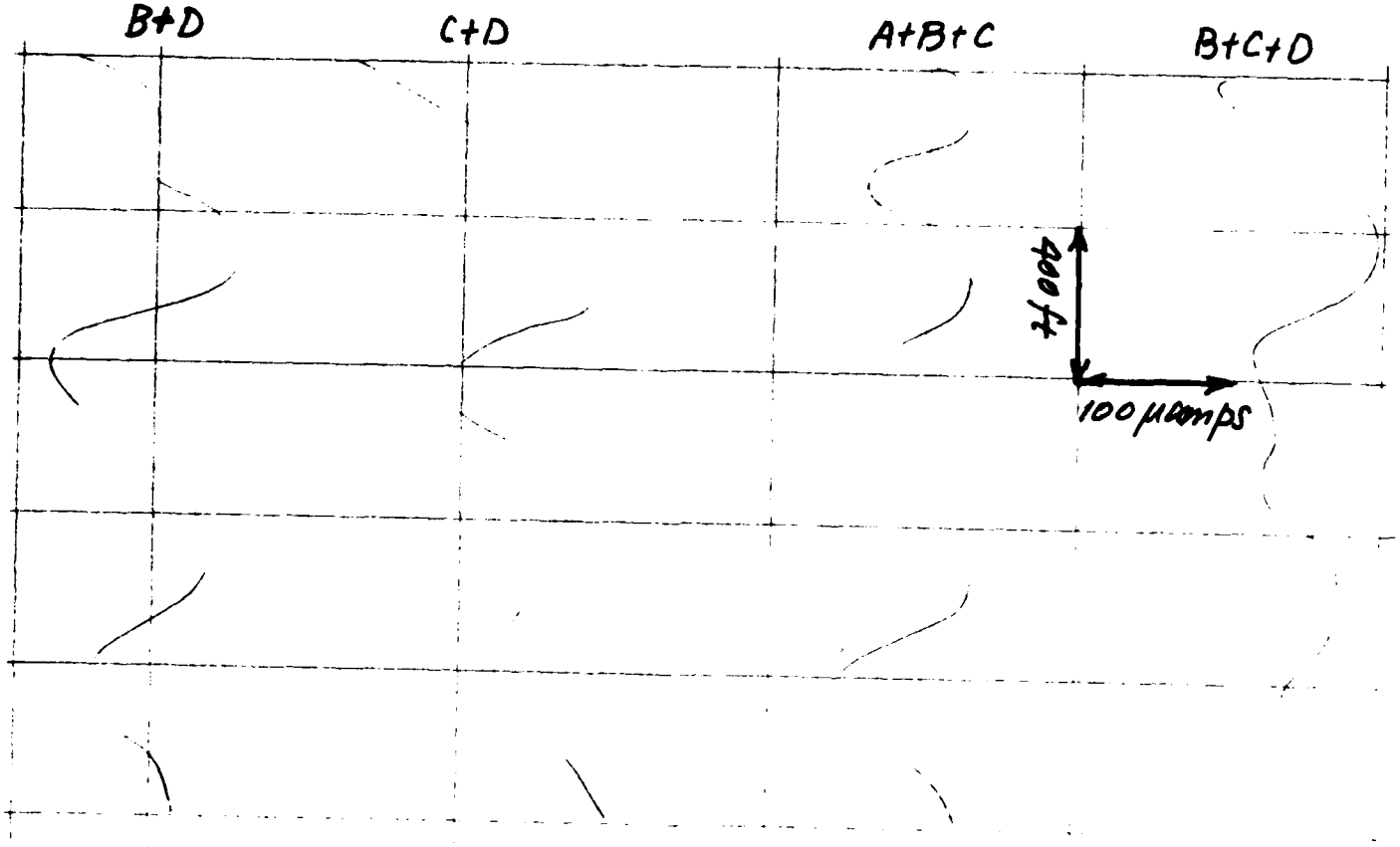

FIGURE 3-5 Δ (DDM) ALONG A TRANSVERSE LINE 10000 FT. FROM LOCALIZER.
OBJECTS 2500 FT. FROM LOCALIZER

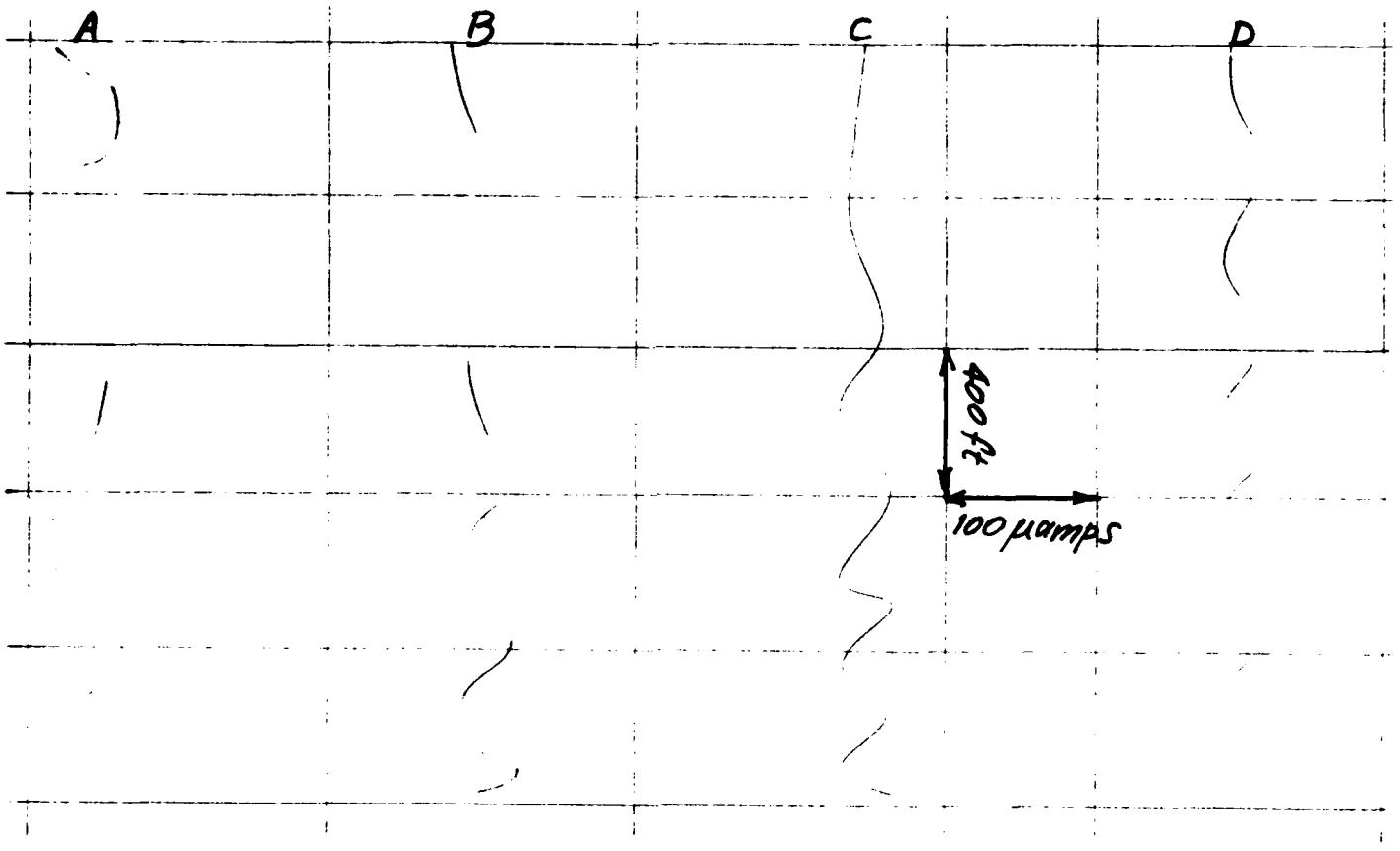

FIGURE 3-6 Δ (DDM) ALONG A TRANSVERSE LINE 10000 FT. FROM LOCALIZER.
OBJECTS 5000 FT. FROM LOCALIZER

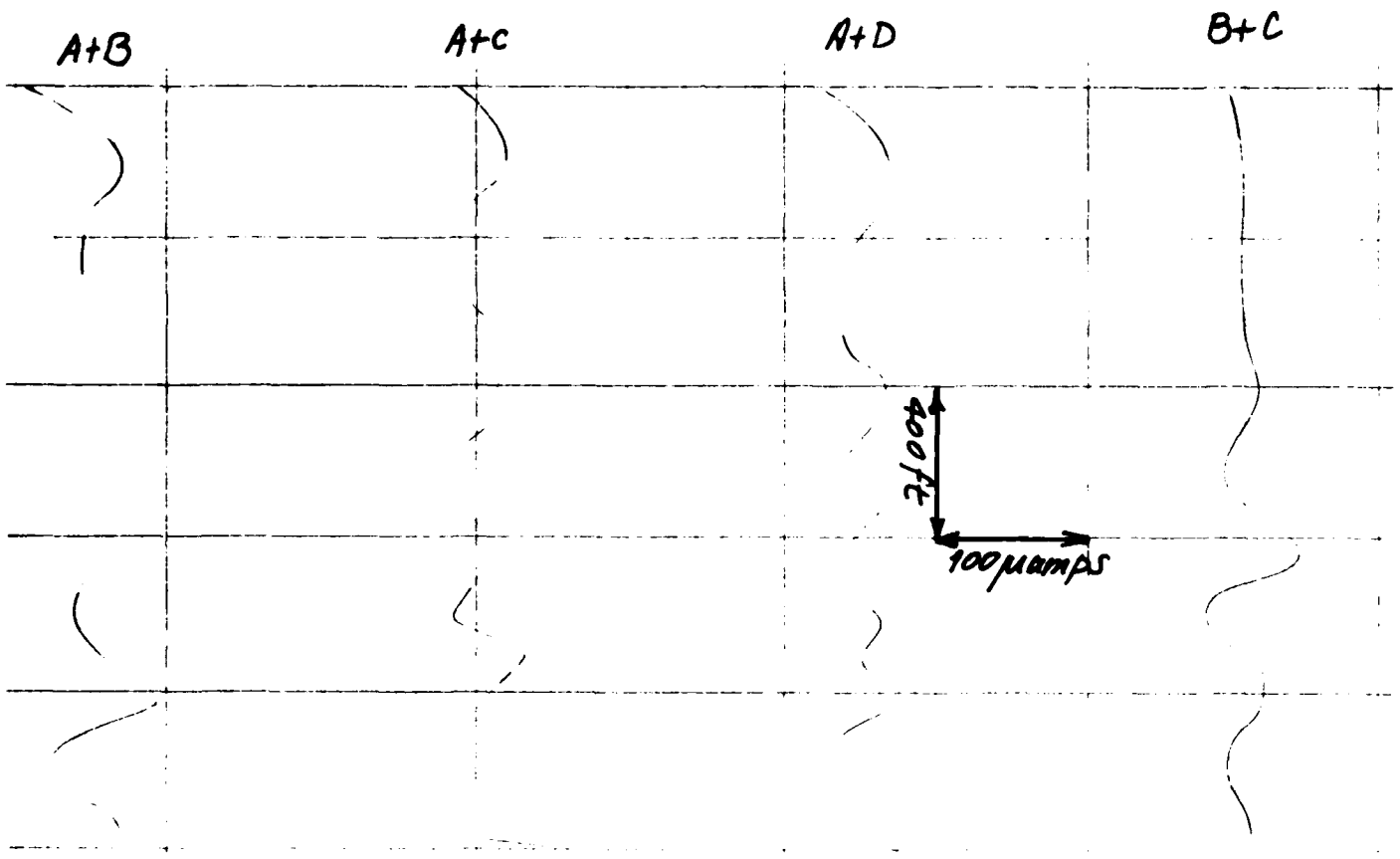

FIGURE 3-7 Δ (DDM) ALONG A TRANSVERSE LINE 10000 FT. FROM LOCALIZER.
OBJECTS 5000 FT. FROM LOCALIZER

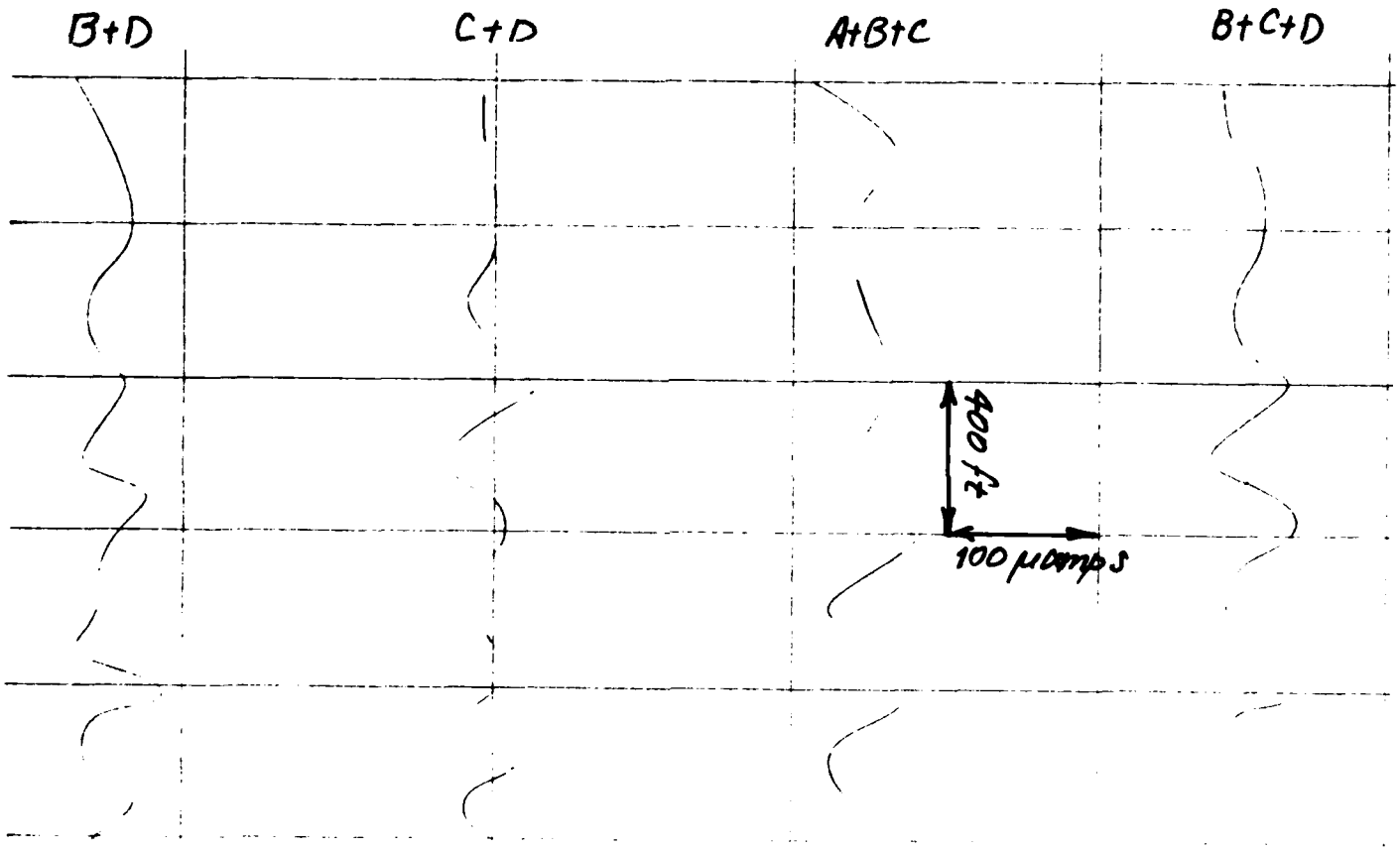

FIGURE 3-8 Δ (DDM) ALONG A TRANSVERSE LINE 10000 FT. FROM LOCALIZER.
OBJECTS 5000 FT. FROM LOCALIZER

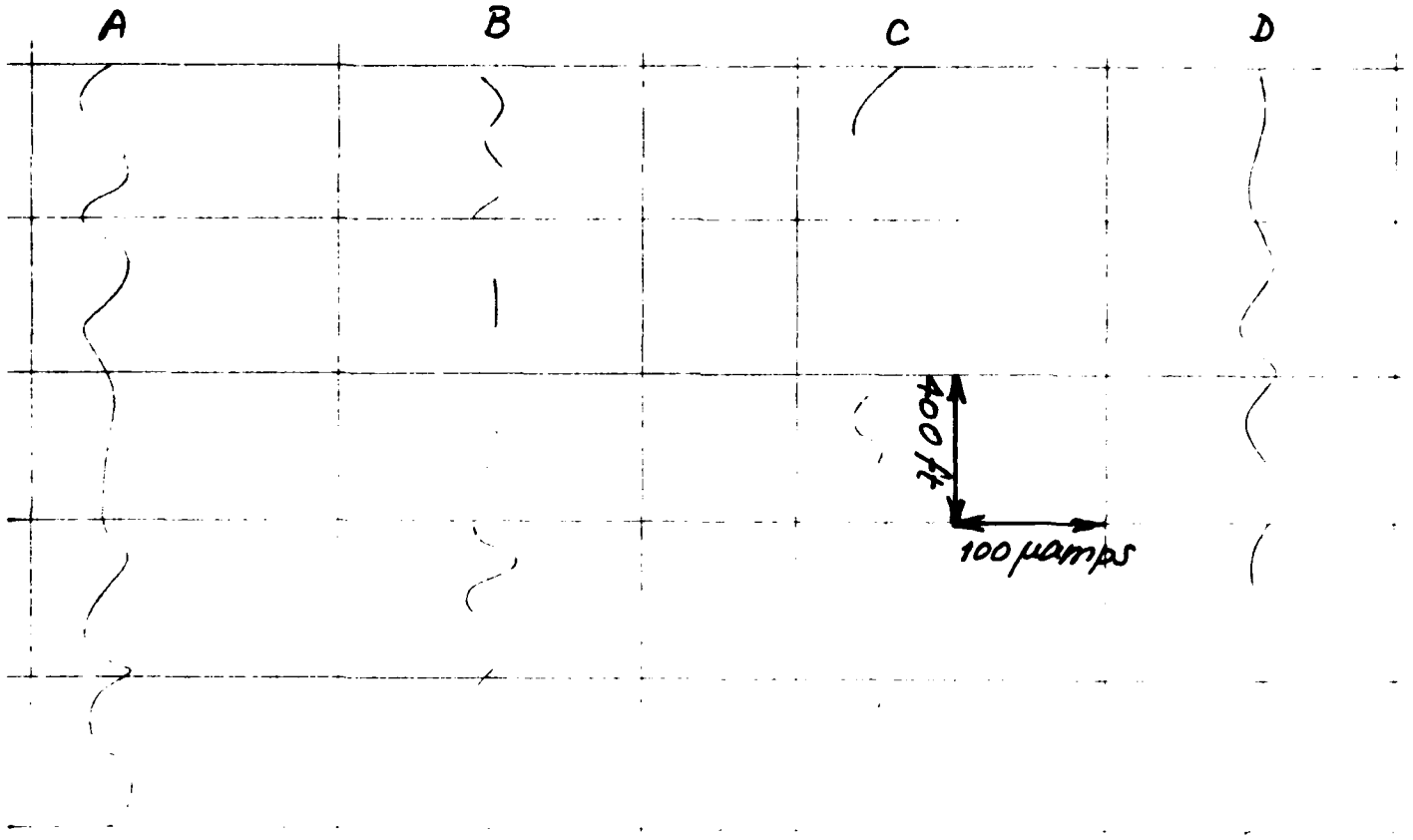

FIGURE 3-9 Δ (DDM) ALONG A TRANSVERSE LINE 1 000 FT. FROM LOCALIZER. OBJECTS 7500 FT. FROM LOCALIZER

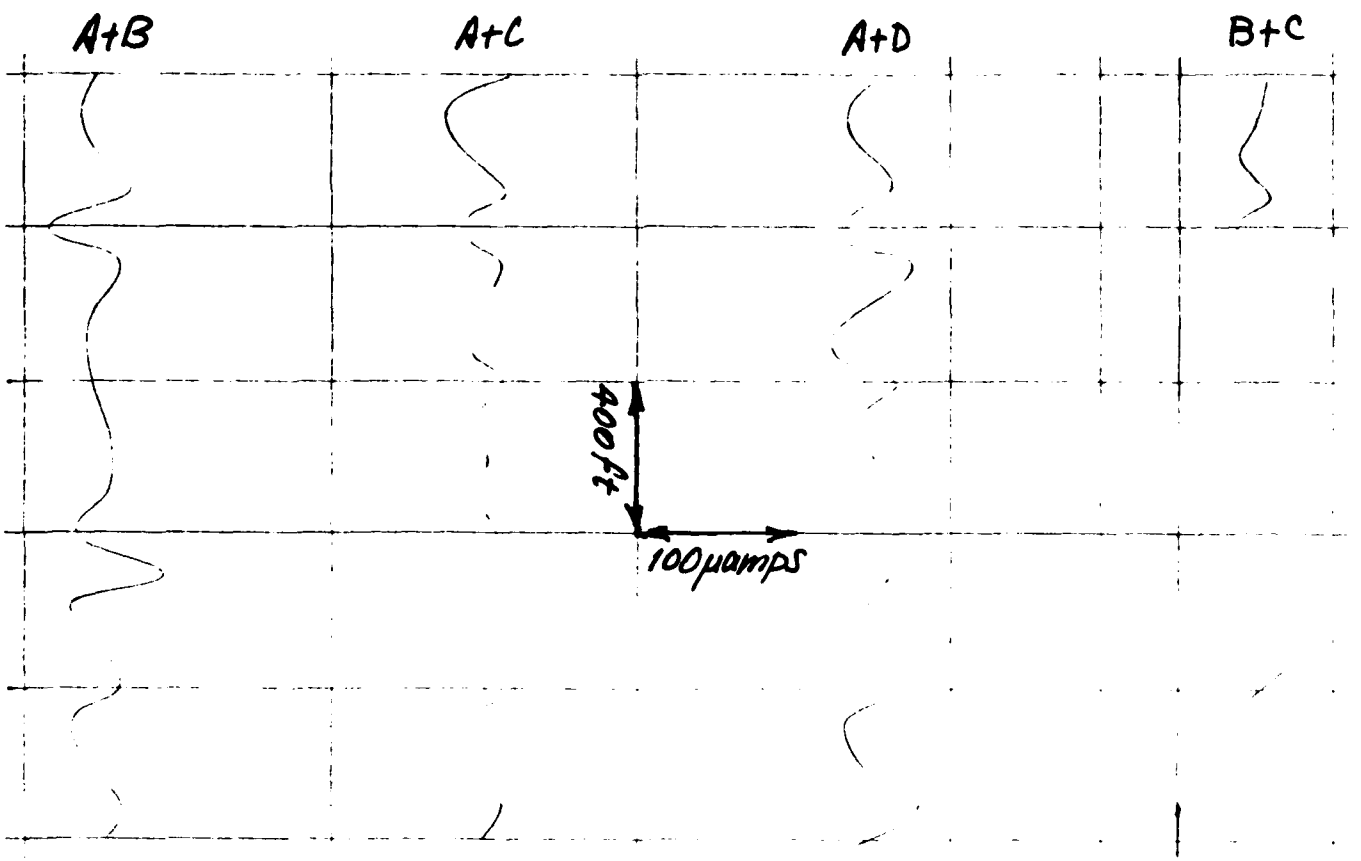

FIGURE 3-10 Δ(DDM) ALONG A TRANSVERSE LINE 10000 FT. FROM LOCALIZER.
OBJECTS 7500 FT. FROM LOCALIZER

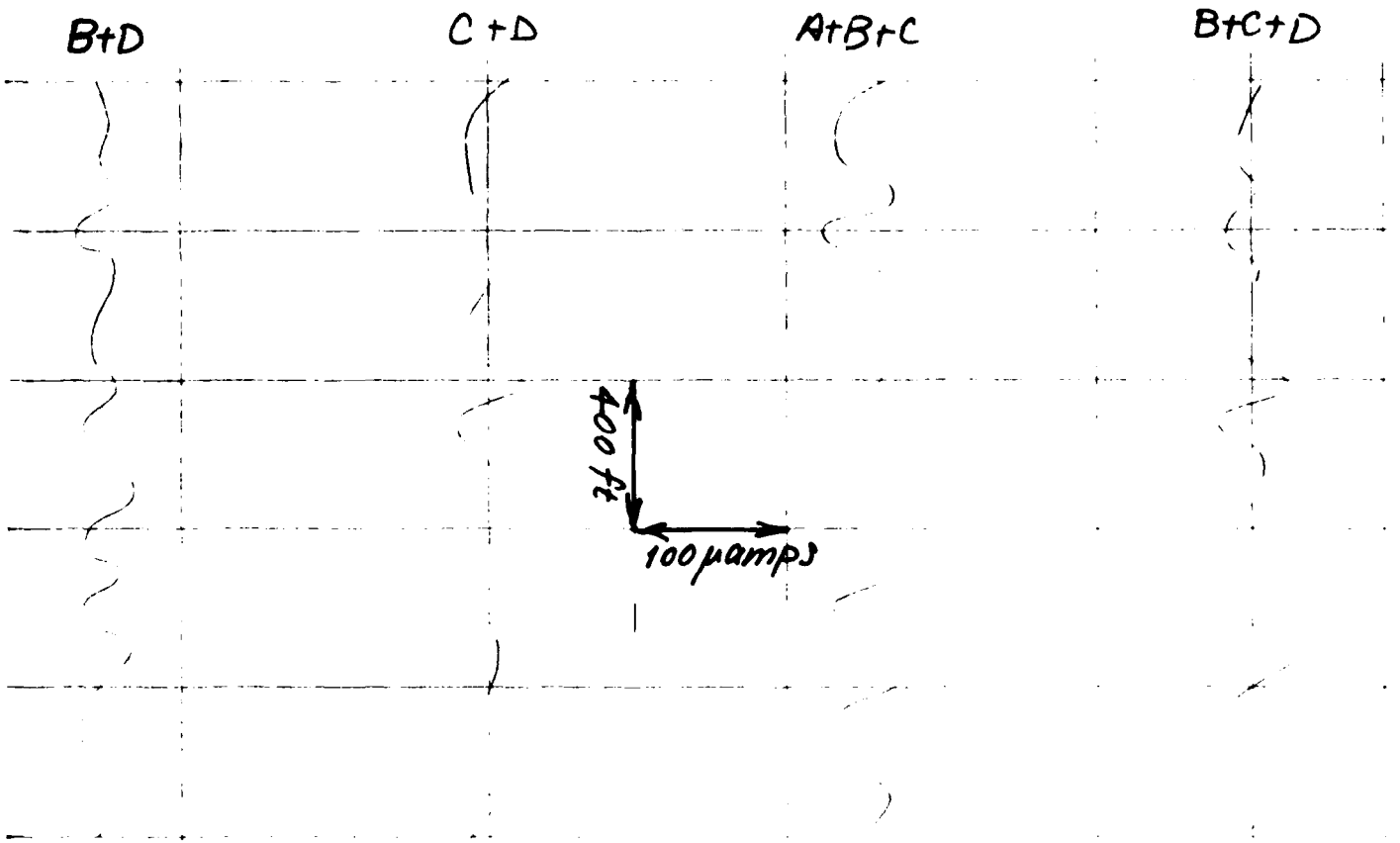

FIGURE 3-11 Δ(DDM) ALONG A TRANSVERSE LINE 3,000 FT. FROM LOCALIZER. OBJECTS 7500 FT. FROM LOCALIZER

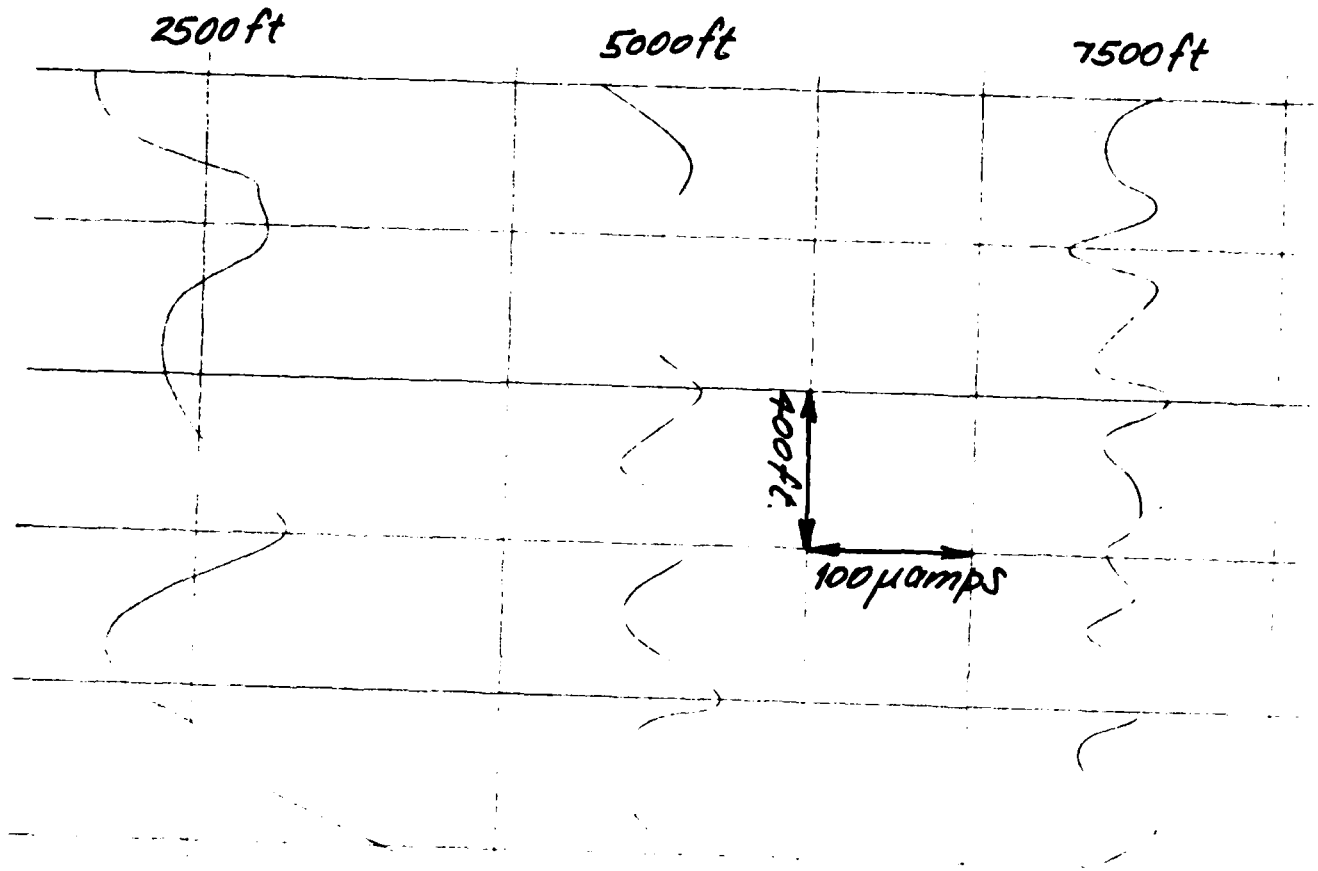

FIGURE 3-12 Δ (DDM) ALONG A TRANSVERSE LINE 10000 FT. FROM LOCALIZER. PRODUCED BY ALL FOUR OBJECTS PRESENT SIMULTANEOUSLY

Object	C/L Modulus	Max.Δ (DDM) at 8-probe monitor
A	0	10.3
B	35.5	43.1
C	36.1	33.2
D	17.9	20.2
A+B	29.7	44.9
A+C	30.8	38.3
A+D	15.4	24.2
B+C	72.2	49.2
B+D	25.5	44.5
C+D	18.0	51.8
A+B+C	59.9	53.3
B+C+D	54.2	59.7
A+B+C+D	45.0	63.2

Table 3-I. DDM in Microamps Obtained with Objects on a Line 2500 ft. from Localizer.

Object	C/L Modulus	Max.Δ (DDM) at 8-probe monitor
A	0	10.3
B	35.5	43.1
C	36.1	33.2
D	17.9	20.2
A+B	29.7	44.9
A+C	30.8	38.3
A+D	15.4	24.2
B+C	72.2	49.2
B+D	25.5	44.5
C+D	18.0	51.8
A+B+C	59.9	53.3
B+C+D	54.2	59.7
A+B+C+D	45.0	63.2

Table 3-I. DDM in Microamps Obtained with Objects on a Line 2500 ft. from Localizer.

Object	C/L Modulus	Max. Δ (DDM) at 8 probe monitor
A	0	14.9
B	10.2	22.4
C	15.0	18.7
D	15.9	12.0
A+B	9.3	41.9
A+C	13.7	33.1
A+D	14.5	27.7
B+C	13.6	30.1
B+D	20.8	36.2
C+D	27.2	11.7
A+B+C	12.4	30.0
B+C+D	28.2	26.5
A+B+C+D	25.7	43.2

Table 3-II. DDM in Microamps Obtained with Objects on a Line 5000 ft. from Localizer.

Object	C/L Modulus	Max. Δ (DDM) at 8-probe monitor
A	0	16.5
B	13.1	18.9
C	17.5	14.2
D	14.6	14.4
A+B	10.9	40.7
A+C	14.9	23.0
A+D	12.7	26.6
B+C	31.3	29.8
B+D	12.1	19.1
C+D	2.9	18.1
A+B+C	25.8	30.7
B+C+D	16.6	30.5
A+B+C+D	13.7	34.6

Table 3-III. DDM in Microamps Obtained with Objects on a Line 7500 ft. from Localizer.

The DDM deviation curves for object A at the three distances (Figs. 3-3, 3-6 and 3-9) show that an object placed on the centerline produces a detectable disturbance at an offset receiver. Furthermore the curves for objects B, C and D, considered singly, show that no disturbance is detected when the object lies on the line joining the transmitter and the offset receiver. Both these phenomena confirm the system's behavior as predicted by Eq. (3.1). In the first case the disturbance is produced by the object on the centerline re-radiating an excess carrier signal, and in the second case, with transmitter, object and receiver collinear, the scattered signal contains the same modulation as the direct signal and the guidance remains unpolluted.

The effectiveness of the multiprobe monitor may be judged from the scatter diagram Figure 3-2. For a perfect monitor all points lie on a line passing through the origin at 45^{o} to the axes. In the scatter diagram the spread of points indicates little correlation between the DDM detected by the monitor and that observed in an approaching aircraft. This is to be expected from Eq. (3.2) since a receiving probe at a similar azimuthal angle to that of a scatterer sees less Δ(DDM) than the DDM modulus on the centerline, even when the phase is optimum. When the receiving probe lies on the opposite side of the centerline from the scatterer, however, it may under certain conditions of phase see a greater Δ(DDM) than the modulus on the centerline.

3.3 Curve-Fitting Monitor

This monitor is based on the fact that mathematically with a certain limited number of points a curve can be constructed. A series of monitors is displaced, for instance, transverse to the centerline on an individual support. The derogation over the span of the monitors is evaluated and used to determine the derogation envelope.

Recalling quasi-periodic nature of derogation the strategy used with the curve fitting monitor is placement of the monitor points to allow mathematical construction of a "cycle" of the fine structure close to the centerline. Since the probes of the fine structure define the envelope, the identification of the two fine structure peaks on either side of the monitor probe sequence defines the derogation envelope.

Figure 3-13 illustrates a single cycle of derogation fine structure. The heavy horizontal line indicates the span of the probe sequence or data field. Note that the monitor projects the first derogation peak on each side of the monitor position with good accuracy. Since this represents the envelope at this point, it complies with the objective set out for the far field monitor. The problem, however, with this monitor is that to achieve these results, an unrealistic accuracy has to be assumed for the measurements of each of the probes. The results of the analysis shows the effect of realistic data accuracies.

3.3.1 Analysis

One method of realizing the maximum of an envelope function in a small azimuthal sector is to curve-fit a polynominal in $\tilde{\varphi}$ over this limited transverse segment and extrapolate the fitted curve to an extremum whose modulus was taken as the envelope of Δ(DDM) (see the dashed curve in Figure 2-11).

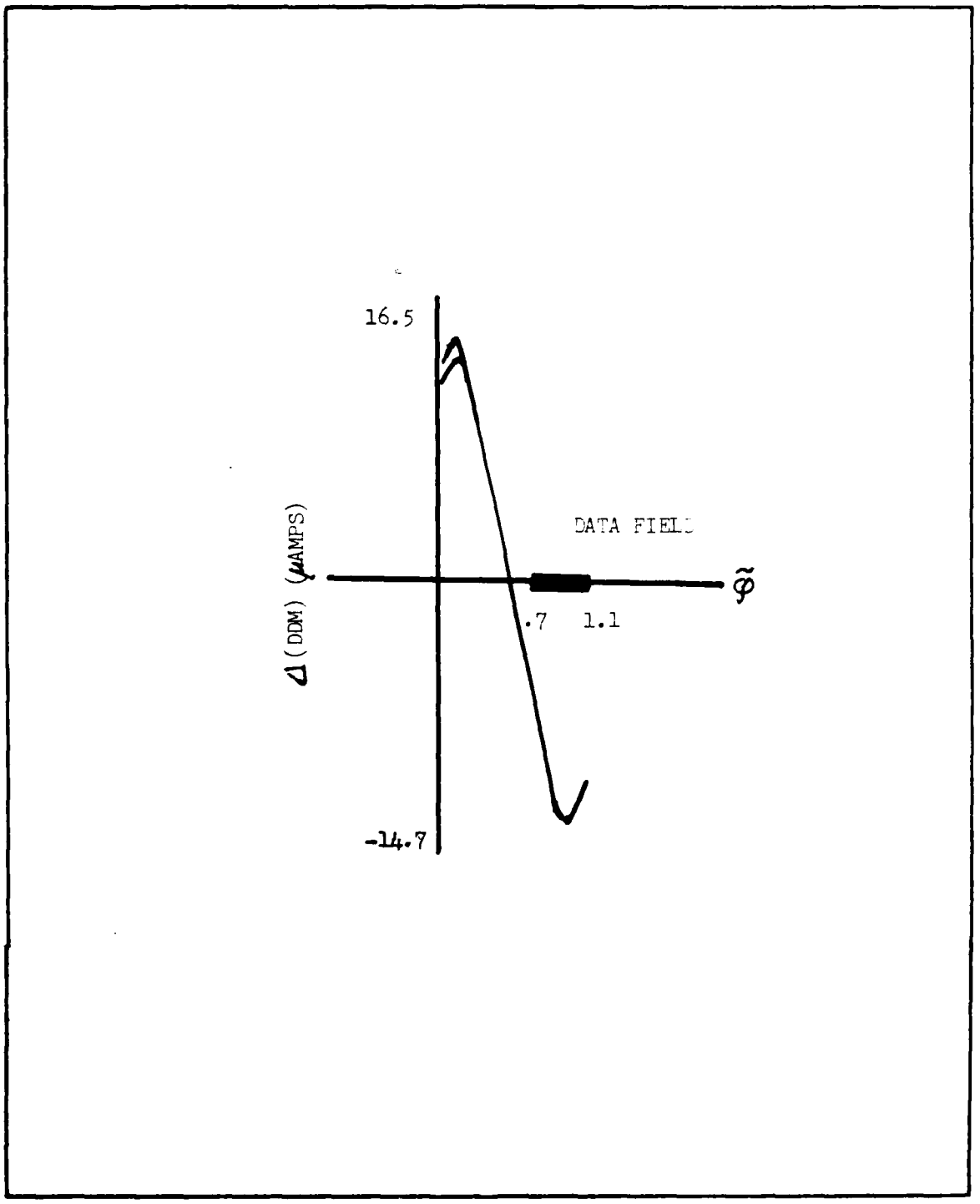

FIGURE 3-13 TRANSVERSE VARIATION OF Δ(DDM)

Thic calculation was carried out using a 4th degree polynominal in $\tilde{\varphi}$ and 8 transversely situated DDM probes for collecting data. Thus

$$\Delta\ (\mathrm{DDM})\ (\tilde{\varphi}) \doteq \sum_j d_j\ \ \Phi_j\ (\tilde{\varphi}) \qquad (3.5)$$

where $\Phi_j\ (\tilde{\varphi}) = \tilde{\varphi}^{j-1}$.

This procedure worked rather well so long as the noise in each DDM probe was negligible. Unfortunately, this was not the case, and on this basis, the remaining portion of this subsection is used to illustrate the sensitivity of the curve fitting monitor to probe noise or error. Because of this sensitivity, the curve-fitting probes are not viable as a far field monitor system.

If $B = A^{-1}$ where A is the matrix whose $(j,k)^{\underline{th}}$ element is

$$A_{jk} = \sum_i\ \Phi_j\ (\tilde{\varphi}_i)\ \Phi_k\ (\tilde{\varphi}_i)$$

with this sume extending over the data points, then each

$$\cdot_j = \Sigma_j\ \Sigma_i\ B_{jj},\ \Phi_j,\ (\tilde{\varphi}_i)\ \Delta\ (\mathrm{DDM})\ (\tilde{\varphi}_i).$$

Eq. (3.5) can now be expressed as

$$\Delta\ (\mathrm{DDM})\ \ (\tilde{\varphi}) \doteq \Sigma_i\ \gamma_i\ (\tilde{\varphi})\ \Delta\ (\mathrm{DDM})\ (\tilde{\varphi}_i) \qquad (3.5')$$

where

$$\gamma_i\ (\tilde{\varphi}) = \Sigma_j\ \Sigma_j,\ \ \ B_{jj},\ \Phi_j,\ (\tilde{\varphi}_i)\Phi_j\ (\tilde{\varphi}). \qquad (3.6)$$

Consider a fixed azimth $\tilde{\varphi}$. Then $\gamma_i(\tilde{\varphi})$ represents fixed values for each i that are either "hard wired" in a processor or constitute a combination of this with values obtained by the processor. Thus, no fluctuations occur in the $\gamma_i\ (\tilde{\varphi})$'s. It is concluded that fluctatuations in Δ (DDM) $(\tilde{\varphi})$ occur as a result of those present in each measured value Δ (DDM) $(\tilde{\varphi}_i)$.

The Δ (DDM) $(\tilde{\varphi})$'s are stochastically independent random variables (one for each i) and each has a standard deviation of, say, σ. Likewise the $\gamma_i(\tilde{\varphi})$ Δ (DDM) $(\tilde{\varphi}_i)$'s are independent random variables each with standard deviation $\gamma_i(\tilde{\varphi})\,\sigma$.

Finally it is concluded that Δ (DDM) (φ) has a standard deviation

$$\sigma_D(\tilde{\varphi}) = \sigma\cdot(\Sigma_i \gamma_i^{\,2}\ (\tilde{\varphi}))^{\frac{1}{2}}, \qquad (3.7)$$

and once the deterministic quanitity $\Sigma_i \gamma_i^2(\tilde{\varphi})$ for a given $\tilde{\varphi}$ and the value of σ are known, the standard deviation for Δ (DDM) is known at $\tilde{\varphi}$.

3.3.2 Properties

Numerical results of this procedure are indcated in Figutes 3-13 and 3-14 where the azimuthal data are taken on one side of the runway ($0.7^\circ \le \tilde{\varphi} \le 1.3^\circ$).

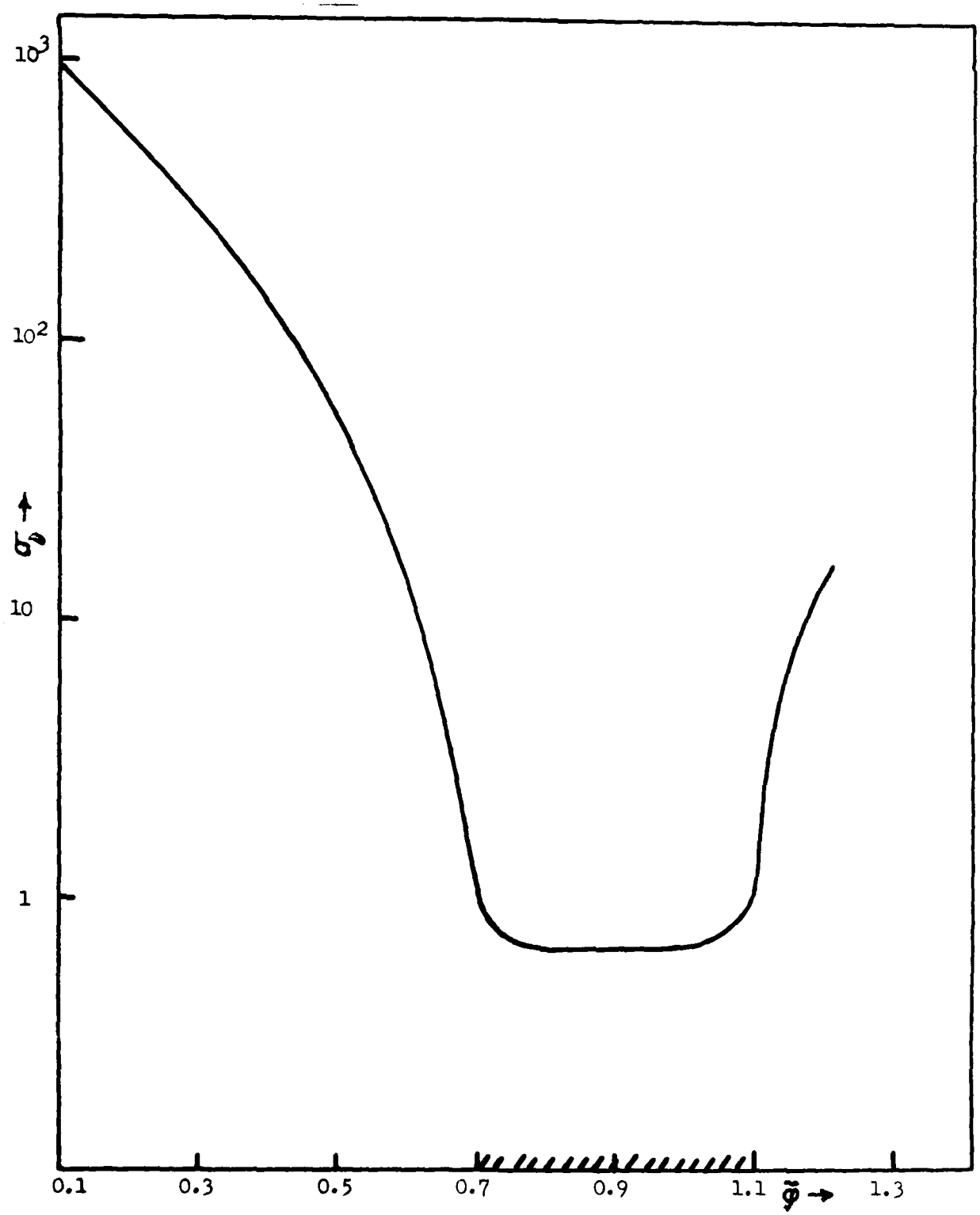

FIGURE 3-14 VARIATION OF σ_D WITH AZIMUTH $\tilde{\varphi}$

The extrapolated curve gives a reasonable estimate for the envelope, but the curve in Figure 3-14 illustrates an unfortunate circumstance when noise of measuring device is taken into account. On the basis of this example, a limitation in the uncertainty of the extrapolated Δ(DDM) to a few microamps requires an uncertainty of less than 1% that of DDM box in the individual probles. These large uncertainties depends on the distance over which the extrapolation extends and not on the particular data field.

3.4 Interferometric Monitor

The basic element of the interferometric monitor as shown in Figure 3-15 is a pair of aeri ls located at, or near, right angles to the centerline. The incoming signals are split or time shared at each aerial and the tones are cancelled separately between aerials using cables differing in electrical length by about half a wavelength and an amplitude and fine phase weighting circuit. Each cancelled tone signal is fed to the appropriate part of a normal ILS receiver. Weighting and carrier level correction factors are applied to the detected tone output and the two tone outputs are subtracted to give the DDM. There is sufficient carrier residue from the cancellers set for tone cancellation to operate the receivers but the separate carrier signal shown will be necessary to obtain the factors required to correctly scale the output to DDM.

The system has the advantage that the normal localizer signal and any permanent site multipath is nulled on setting up so the detected DDM is due solely to a new scatterer. The answer is, therefore, not affected by the phase in which a new scatterer and permanent site multipaths combine.

Another attribute of the system is the high sensitivity obtained in many situations relative to an ordinary DDM receiver using simple equipment. Scatterers in positions of low beam bend potential which give small or undetectable disturbance in a normal DDM receiver are clearly visible.

In terms of a localizer monitor, if the DDM disturbance is not above the allowed threshold in an ordinary receiver itcan be argued that it is not of interest. However, the ability to assess and disregard an object rather than state the guidance is not disturbed either because there is no object or not one re-radiating sufficient DDM is a definite advantage. Secondly, the increased information available about scatterers in areas of low DDM (i.e., near the centerline) could well be of great value in other operational areas.

3.4.1 Analysis

If a new scatterer occurs the DDM received by an ILS receiver on the centerline is:

$$DDM = \frac{D_o + K D_s}{C_o + K C_s} \quad \text{(neglecting scaling constants)}$$

D_o and C_o are the normal sideband difference and carrier signals on the course line and C_s and D_s are those from the scatterer.

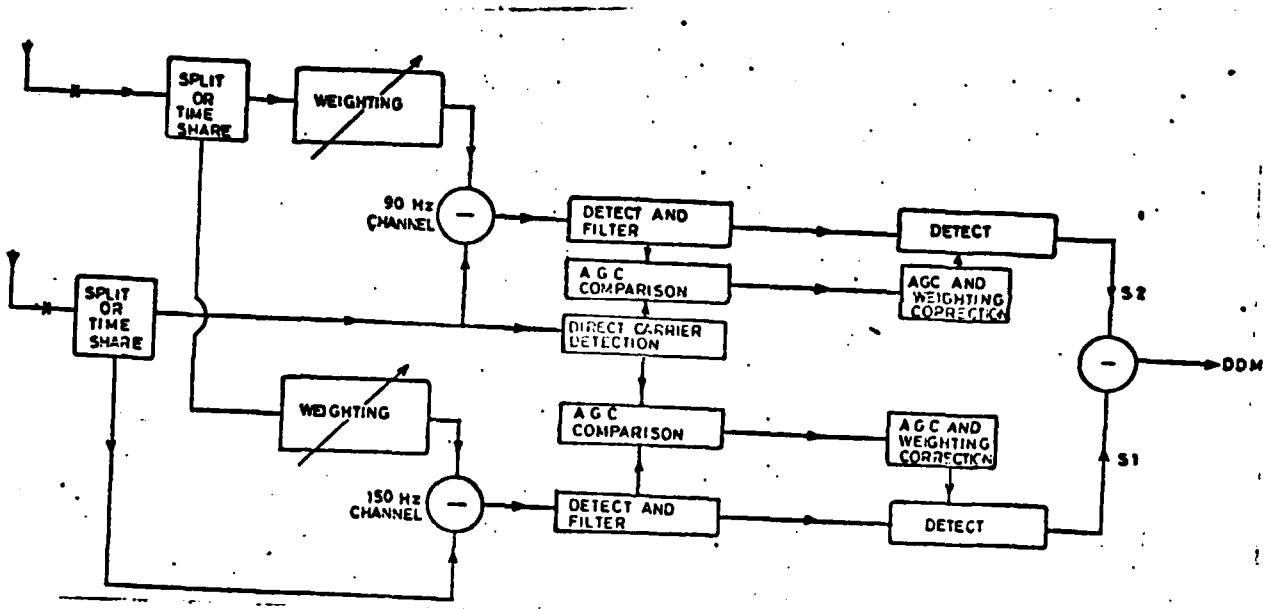

FIGURE 3-15. BASIC MONITOR PAIR

$\vec{K}$ is a complex vector incorporating the reflection coefficient of the scatterer and the phase difference between normal and new signals. D_o is, ideally, zero but may have a value due to permanent reflectors on the airfield.

A typical maximum value of $\|\vec{K}\|$ is 0.1 so K^2 terms can be neglected giving

$$DDM \simeq \frac{D_o + \vec{K} D_s}{C_o}$$

The worst possible case is if $\vec{K}$ D_s and D_o add in phase. The monitor obtains $\|\vec{K}\| D_s$ independently so that it may be added to D_o (previously measured) to obtain the worst combination of new disturbance and permanent site.

The single tone outputs S_1 and S_2 in Figure 3-15 are:

$$S_1 = \frac{2K\sqrt{W_1}\, S_{150}}{C_{R1}} \text{ Sin } (\frac{2\pi d}{\lambda} \sin x)$$

$$S_2 = \frac{2K\sqrt{W_2}\, S_{90}}{C_{R2}} \text{ Sin } (\frac{2\pi d}{\lambda} \sin x)$$

where

K = Modulus of the reflection coefficient
W_1 = 150 Hz tone weighting factor
W_2 = 90 Hz tone weighting factor
C_{R1} = 150 Hz tone canceller carrier residual
C_{R2} = 90 Hz tone caneller carrier residual
S_{150} = 150 Hz tone amplitude at the scatterer
S_{90} = 90 Hz tone amplitude at the scatterer
d = Half the aerial separation
x = Angle between scatterer and monitor - localizer line

The carrier levels C_{R1} and C_{R2} are the residual levels after the canceller, not the total carrier. These residuals depend upon the position of the monitor and are typically 5% to 10% of the uncancelled levels.

W_1 and W_2 are obtained when the canceller is set up and the ratio of cancelled and direct carriers is obtained using a separate comparison circuit.

After applying corrections for these factors as indicated in Figure 3-15 the DDM output of the monitor pair is

$$\frac{K(S_{150} - S_{90})}{C_o} \text{ Sin } (\frac{2\pi d}{\lambda} \text{ Sin } x)$$

which is the required quantity modified by Sin $(\frac{2\pi d}{\lambda}$ Sin x).

3.4.2 Characteristics

3.4.2.1 Complete Monitor Configuration

A single interferometer pair has nulls where $\frac{2\pi d}{\lambda}$ Sin x = $n\pi$ so, to obtain adequate cover, pairs of aerials with different spacing are required to cover each others null lines. The DDM due to the new scatterer is taken to be the maximum registered by any pair. While for economy different pairs will share an aerial and with time sharing pairs might share receivers the basic building block of a full monitor is the single pair described. The number of pairs and their separations can be tailored to suit a particular airfield configuration and its available monitor sites.

Figure 3-16 shows a block diagram for a four aerial monitor. The splitting boxes and multiple receivers may be replaceable by a time sharing switch and a single receiver. Figure 3-17 shows the response obtained with aerial spacings such that the response does not fall below 0.866 of the peak except along the localizer - monitor line. The maximum aperture of this monitor is 82' (or 150' if a minimum .707 of the peak is allowable). Observations have shown that adequate signal/noise is obtained with aerials 20' high 1500' from threshold which indicates that aerials may be placed near the centerline without infringing obstacle clearance. This leads to an alternative configuration of a five or six aerial monitor arranged as in Figure 3-18. The coverage of a six aerial monitor is as shown in Figure 3-19.

For the six aerial monitor the widest pair separation is 358'. In our experiments one of our pairs had cable lengths of over 150' in each limb and no special precautions were taken in terms of temperature stabilization, etc., which implies that such a separation is feasible. The five-element monitor would use a maximum separation of 174' with consequent lesser performance in the null. If a response minimum 0.707 of the peak is designed for these a null performance equivalent to the previous six aerial monitor can be obtained with five aerials.

The six aerial monitor response rises to 0.866 of the peak 0.48° off the monitor - localizer line which corredponds to $\pm$ 92' off the centerline at the localizer for the airfield of Figure 3-18. Thus, the reduced response area shown shaded in Figure 3-19 is totally along the main runway.

Aircraft on the main runway do not generate DDM distortion over much of the runway length since towards the touchdown end they are at small angles to the localizer and therefore illuminated with low DDM.

Thus, aircraft on much of the main runway will not cause DDM distortion, although they are still clearly a hazard to other landing aircraft which is monitored by ATC. It would seem reasonable, therefore, to postulate that

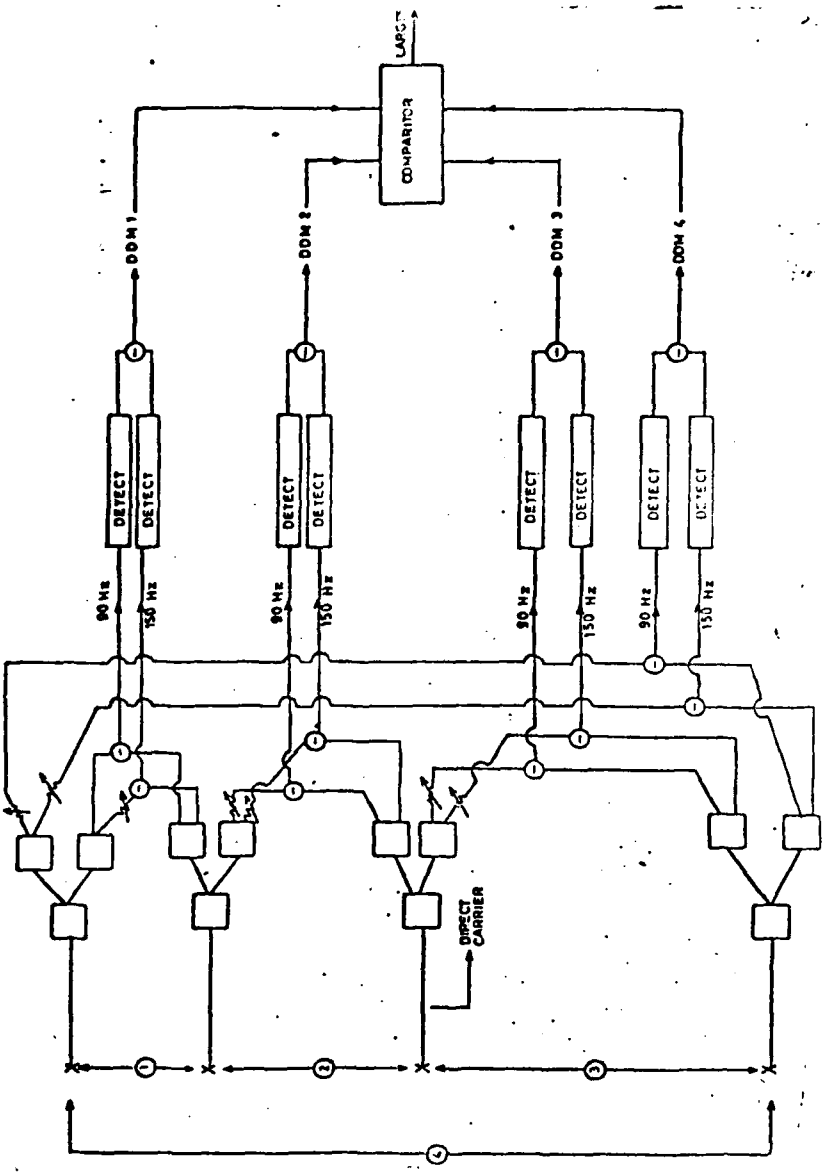

FIGURE 3-16. OUTLINE RECEIVER

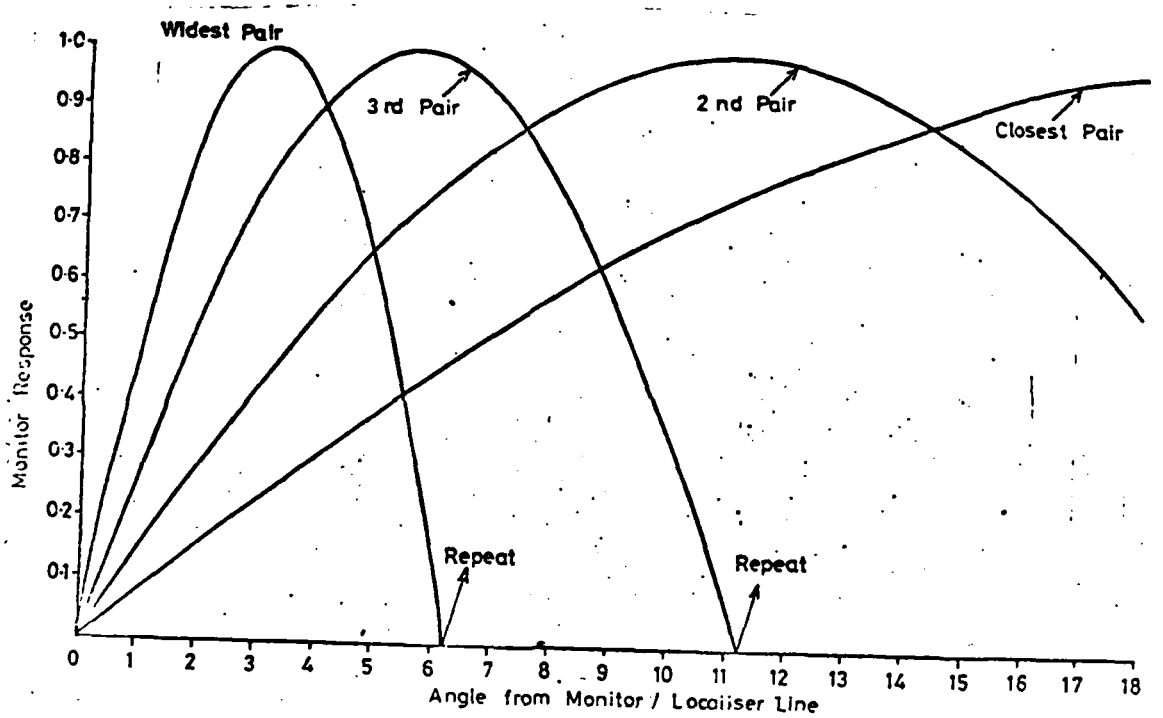

FIGURE 3-17. RESPONSE WITH OVERLAP AT 0.866 OF MAX.

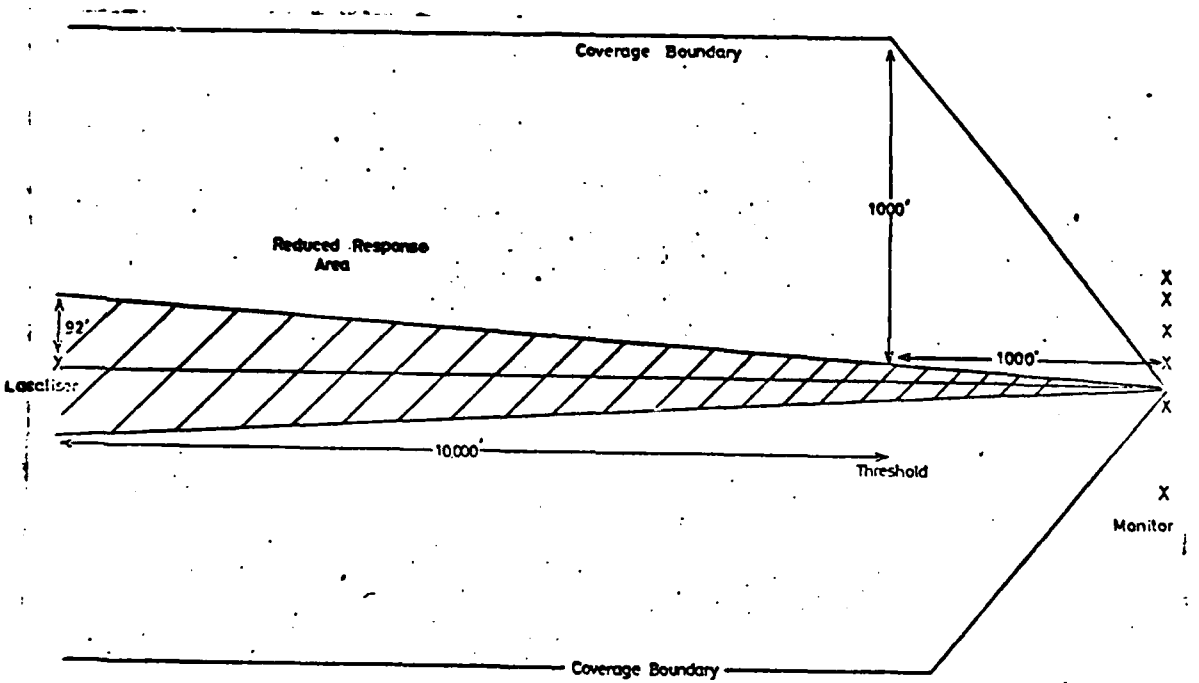

FIGURE 3-18. AIRFIELD DIMENSIONS

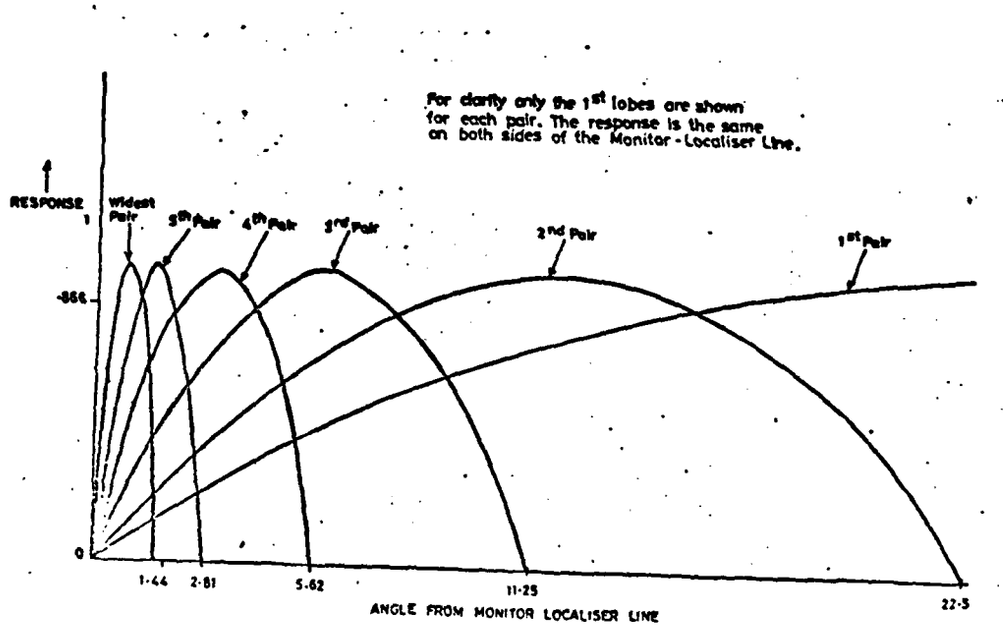

FIGURE 3-19. 6 AERIAL MONITOR RESPONSE

the procedures which give alarm if the main runway is not clear the touchdown end also operate if it is not clear at the localizer end. Thus, reduced response of the monitor to objects on the main runway is of no real concern since alarm will already have been generated for reasons of runway obstruction.

The minimum-response figure of .866 is chosen to keep the theoretical maximum DDM error to ±7% after scaling but scatterers will be detected much closer to the centerline than this; for example, the response is still 0.5 of the peak .24° from the centerline, i.e., ±46' from the centerline at the localizer. This is verified by the measurement plots shown where turns onto the centerline and turns on the runway are clearly detected with our aperture of 100'. Thus, the additional aircraft ground movements use for the monitor is not constrained by the null line to ±.48° but to considerably less.

3.4.2.2 Cancellation Residue and Stability

To estimate the order of cancellation required assume the aerials are near the centerline where the modulation amplitude is 0.2 relative to unity carrier. For a maximum error of 1 amp 0.1% DDM this must be cancelled to .001, that is, by .2/.001 = 200 46 dB. With the basic experimental equipment used a null of 41 dB with the separate tone was achieved in tone cancellation on site measured with one localizer tone off although this was swamped in our live aircraft measurements by breakthrough from the other tone due to inadequate filters. In bench tests figures of the order of 50 dB were achieved. A null of 41 dB would result in a worst case error of 1.8 amp. This is a worst case error of the reconstructed DDM. The high sensitivity of the individual tone measurements means that the presence of an object in the localizer beam will be strongly detected even when the DDM due to it is very small.

3.5 Vector Monitor

Of the four concepts herein detailed, the vector monitor appears to hold the greatest promise with respect to a cost-effective, accurate solution to the far field monitoring problem for a localizer array. It also appears to hold the greatest promise for providing a glide slope far field monitor. In order to facilitate an understanding of this concept, envelope functions and vector DDM will be discussed.

The vector involves detailed use of the field structure as time interfering signals overlap. Figure 2-3 illustrates the quasi-periodic nature of interference in the presence of the direct and a scattered signal in the vicinity of the runway approach path. Unless propagation of the two signals is in the same direction, their phase progression leads to the quasi-periodic support and interference along equidistance line as illustrated in Figure 2-3. Quadrature components of modulations relative to the carrier exist between the points of maximum support and cancellation. By measurement of these quadrature components, as evidenced by phase modulation, it is possible to reconstruct the complete derogation signal, independently of its relative phase to the guidance signal and thus identify the level of derogation from a single receiver.

The vector relationships are illustrated in Figure 3-20 which shows a scattered signal with significant quadrature component. The scattered modulation arrow being reversed relative to the carrier from that of the direct signal, suggests it was scattered from the opposite side of the runway from which it is being viewed. The remaining phase vector diagrams illustrate the component carrier and modulation relatiosnips and the in-phase and quadrature components of modulation relative to the composite carrier.

3.5.1 Theoretical Summary

3.5.1.1 Envelope Functions and Vector DDM

The envelope of DDM (or Δ (DDM)) is, roughly speaking, a smooth curve passing through the peaks of DDM (or Δ (DDM)). It is this concept that has proven useful in correlating the transverse monitor data with data along the flight path. In this section we present analytical definitions of the notions of "envelope" and "vector DDM", and discuss their relationship.

The definition of DDM may be expressed as

$$\mathrm{DDM} = N\,\mathrm{Re}\left(\frac{\mathrm{SBO}_{\mathrm{TOT}}}{\mathrm{CSB}_{\mathrm{TOT}}}\right)$$

$$= N\,\frac{\overrightarrow{\mathrm{SBO}}_{\mathrm{TOT}} \cdot \overrightarrow{\mathrm{CSB}}_{\mathrm{TOT}}}{\mathrm{CSB}^2_{\mathrm{TOT}}} \tag{3.8}$$

where $\overrightarrow{\mathrm{SBO}}_{\mathrm{TOT}}$ and $\overrightarrow{\mathrm{CSB}}_{\mathrm{TOT}}$ are the real components of the complex waveforms. For brevity we express this equation as

$$\mathrm{DDM} = N\,\frac{(\vec{A} - \vec{a}) \cdot (\vec{B} - \vec{b})}{B - b^2} \tag{3.9}$$

$$= N\,\frac{\vec{S} \cdot \vec{C}}{C^2},$$

where $\vec{S}$ and $\vec{C}$ represent total SBO and CSB signals.

Clearly

$$\mathrm{DDM} = NCS\cos(\vec{S},\vec{C})/C^2$$

$$= \frac{NS}{C}\cos(\vec{S},\vec{C})$$

and the envelope function of DDM is

$$\mathcal{E} \equiv \frac{NS}{C}\,(-1 \le \cos(S,C) \le +1)\,\max\left|\cos(\vec{S},\vec{C})\right| = N\frac{S}{C}. \tag{3.10}$$

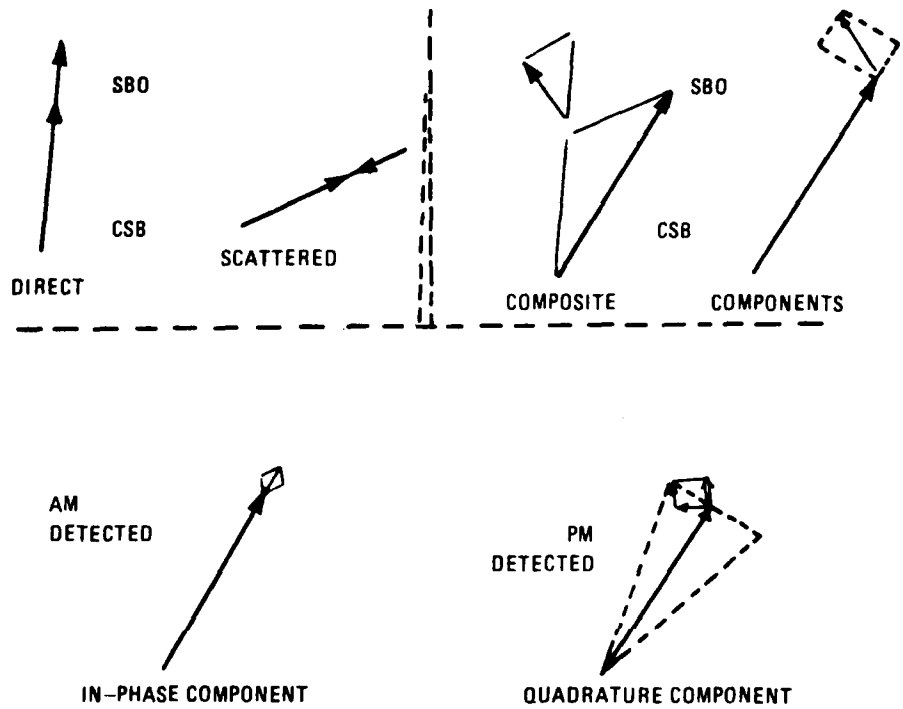

The vector derogation detector makes use of phase modulation detection as well as amplitude modulation detection to measure the derogation envelope.

FIGURE 3-20 VECTOR DDM DEROGATION DETECTION

It should be remarked that $\mathcal{E}$ is very accurately represented by

$$\mathcal{E} \approx Na/B \tag{3.11}$$

in a neighborhood of $\varphi = 0$.

One of the most promising approaches to correlating monitor data to flight path data is to relate $\mathcal{E}$ to a quantity we call "vector DDM." Vector DDM is a two-component vector with total DDM as its first component and the quadrature component of DDM as its second component. Specifically, it is defined as

$$\overrightarrow{DDM} \equiv N\left(\frac{\vec{S}\cdot\vec{C}}{C^2}, \frac{(\vec{S}\times\vec{C})_3}{C^2}\right) \tag{3.12}$$

where $(\vec{S}\times\vec{C})_3$ is the third and only non-zero component of the cross product $\vec{S}\times\vec{C}$. Expressing $\overrightarrow{DDM}$ as

$$\overrightarrow{DDM} = \frac{N}{C}\left(\frac{\vec{S}\cdot\vec{C}}{C}, \frac{(\vec{S}\times\vec{C})_3}{C}\right) \tag{3.12}$$

we obtain the geometrical relations:

$$\frac{\vec{S}\cdot\vec{C}}{C} = \text{scalar projection of } \vec{S} \text{ along } \vec{C}, \tag{3.13}$$

and

$$\frac{(\vec{S}\times\vec{C})_3}{C} = \text{scalar projection of } \vec{S} \text{ and normal to } \vec{C} \tag{3.14}$$

The vector $\overrightarrow{DDM}$ is sometimes expressed as

$$\overrightarrow{DDM} = (DDM_{TOT}, QDDM), \tag{3.15}$$

where the second component is called quadrature DDM. An illustration of the vector components in Eqs. (3.13) and (3.14) are given in Figure 3-21. One should realize that in a reasonably large neighborhood of (say $-3.5^\circ \leq \varphi \approx 3.5^\circ$) the components in Eq. (3.15) are simply those in the previous two equations multiplied by the slowly varying amplitude N/C.

A simple relationship between $\overrightarrow{DDM}$ and $\mathcal{E}$ exists which allows us to relate the desired quantity $\mathcal{E}$ (for correlation studies) with the measurable quantity DDM. Suppose the real components of the complex waveforms C and S are $\vec{C} = (C_1, C_2)$ and $\vec{S} = (S_1, S_2)$.

$$DDM = N \left\| \left(\frac{\vec{S} \cdot \vec{C}}{C^2}, \frac{(\vec{S} \times \vec{C})_3}{C^2} \right) \right\|$$

$$= \frac{N}{C^2} \left[(S_1 C_1 + S_2 C_2)^2 + (S_1 C_2 - S_2 C_1)^2 \right]^{1/2}$$

$$= \frac{N}{C^2} \left[(S_1^2 + S_2^2)(C_1^2 + C_2^2) \right]^{1/2}$$

$$= NS/C, \qquad (3.16)$$

and on comparison with Eq. (3.10) we have

$$= \| \overrightarrow{DDM} \| \qquad (3.17)$$

A more appropriate quantity than vector DDM is the perturbation on vector DDM caused by scatterers. Such a quantity can be defined by

$$\overrightarrow{\Delta (DDM)} = \left(\Delta (DDM), \frac{(\vec{S} \times \vec{C})_3}{C^2} \right) \qquad (3.18)$$

where Δ (DDM) is defined by Eq. (3.15) and its second component is the same quadrature component given in Eq. (3.12). Related to Δ (DDM) is an envelope function ξ. $\| (DDM) \|$ corresponds to the envelope of Δ (DDM) such as that given by the dashed line in Figure 2-11. So long as we are concerned with vector DDM near $\varphi = 0$ it is sufficient to use either formulation of the vector concept because

$$\| \Delta \overrightarrow{(DDM)} \|_{\tilde{\varphi} = 0} = \| \overrightarrow{DDM} \|_{\tilde{\varphi} = 0} \qquad (3.19)$$

3.5.2 Vector DDM with Multiple Probes: Toward A Glide Slope Monitor System

The application of this concept to the Glide slope obviously demands the placement of probes outside the glide path cone. This prompted the examination of vector DDM with multiple probes placed beyond the glide path; however, it is instructive to initiate the development of using a single probe. Let K be the (complex 2-) vector such that the re-radiated signal at the receiver is K times the illuminating signal at the scatterer; viz. the illustration below.

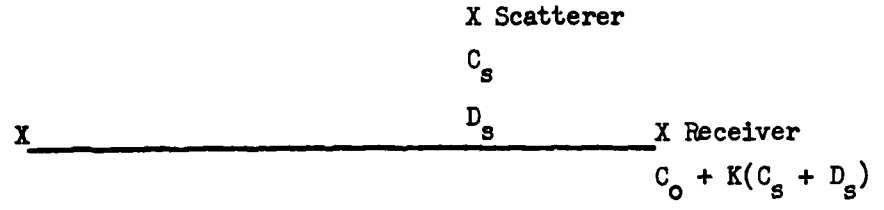

$\vec{K}$ includes the relative phase between the scatterer and the direct signal and the relative amplitudes.

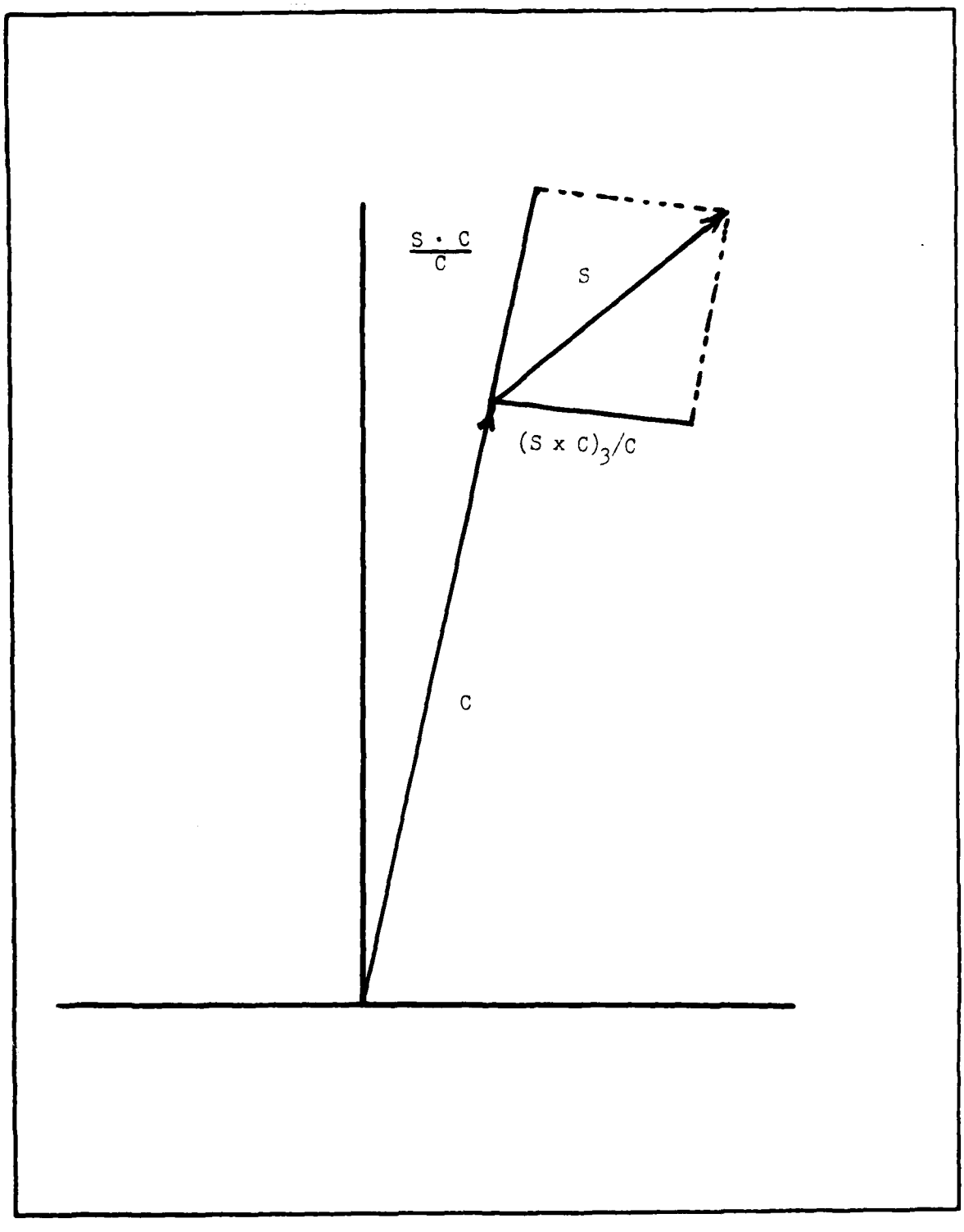

FIGURE 3-21 COMPONENTS OF VECTOR DDM

If the scatterer has a significant azimuth extent C_s and D_s will be a composite of the illumination over the scatterer but this will not affect the arguments below.

For the case of a receiver on the centerline, let the direct carrier be C_o. The sideband difference signal is zero.

The worst case DDM at the receiver is if $\vec{K}$ is such that the scattered signal is antiphase with the direct.

Then Centerline $DDM_{max} = \dfrac{-\|\vec{K}\| D_s}{C_o \|\vec{K}\| C_s} \quad \alpha \quad \dfrac{\|\vec{K}\| D_s}{C_o}$ for small K

Thus to calculate the worst case centerline DDM a monitor should provide $\|\vec{K}\| D_s/C_o$ or, ideally, $\|\vec{K}\| D_s$ and $\|\vec{K}\| C_s$ at the point on the flight path where K is a maximum. The maximum value of K occurs at close range so if the modulus of K is detected by a monitor near threshold this will correspond well with the maximum value on the flight path. $\|\vec{K} D_s\|$ is what the interferometric monitor measures.

Let C_p = Direct Carrier at probe

C_s = Carrier at the scatterer

D_p = Direct Sideband difference at probe

D_s = Sideband difference at scatterer

$\vec{K}$ = Reradiation vector as defined above

DDM_p = Direct DDM at probe

DDM_s = DDM at scatterer

Received Carrier = $C_p + \vec{K} C_s$

REceived Sideband difference = $D_p + \vec{K} D_s$

$$\frac{\text{Sideband difference}}{\text{Carrier}} = \frac{D_p + \vec{K} D_s}{C_p + \vec{K} C_s} = R \text{ (say)}$$

$$= \frac{D_p + \vec{K} D_s}{C_p\left(1+\vec{K}\dfrac{C_s}{C_p}\right)}$$

$$\approx \frac{(D_p + \vec{K}\, D_s)(1 - \vec{K}\, \frac{C_s}{C_p}}{C_p} \qquad \text{if } K^2 \text{ terms are neglectable}$$

$$\approx \frac{D_p + \vec{K}\,(D_s - \frac{C_s}{C_p} D_p)}{C_p} \qquad \text{if } K^2 \text{ terms are neglectable}$$

$$= \frac{D_p}{C_p} + \vec{K}\, \frac{C_s}{C_p} (\frac{D_s}{C_s} - \frac{D_p}{C_p})$$

$$= DDM_p + \vec{K}\, \frac{C_s}{C_p} (DDM_s - DDM_p)$$

Also

$$R = DDM_p + \Delta(DDM) + \vec{j}\, QDDM$$

where $\Delta(DDM)$ is the change in measured DDM at the probe and QDDM is the phase modulation DDM.

Equating expressions for R gives

$$\Delta(DDM) = \text{Real Part } \vec{K}\, \frac{C_s}{C_p} (DDM_s - DDM_p)$$

QDDM = Quadrature part

as vector DDM with norm (or modulus)

$$VDDM = \left\| K\, \frac{C_s}{C_p} (DDM_s - DDM_p) \right\|$$

Thus, vector DDM does not yield $\|K\| D_s/C_o$ unless $DDM_p = 0$ and $C_p = C_o$; i.e., unless the monitor probe is on the centerline.

If there are permanent scatterers on the site there is a permanent site quadrature component of DDM. This must be subtracted from the measured QDDM before calculation of VDDM.

If the vector DDM is measured at two probes

$$V_1 = \left\| \vec{K}\, \frac{C_s}{C_{p1}} (DDM_s - DDM_{p1}) \right\|$$

$$V_2 = \left\| \vec{K}\, \frac{C_s}{C_{p2}} (DDM_s - DDM_{p2}) \right\|$$

If $DDM_s - DDM_{p1}$ has the same sign as

$DDM_s - DDM_{p2}$ (positive say)

$$V_1 = \|\vec{K}\| \frac{C_s}{C_{p1}} (DDM_s - DDM_{p1})$$

$$V_2 = \|\vec{K}\| \frac{C_s}{C_{p2}} (DDM_s - DDM_{p2})$$

Let $\|\vec{K}\| = K$

Solving gives

$$K \quad C_s = \frac{C_{p1} V_1 - C_{p2} V_2}{DDM_{p2} - DDM_{p1}} \tag{3.20}$$

and

$$K \quad C_s \quad DDM_s = K \; D_s = C_{p1} V_1 + DDM_{p1} \left(\frac{C_{p1} V_1 - C_{p2} V_2}{DDM_{p2} - DDM_{p1}} \right) \tag{3.21}$$

$C_{p1}, V_1, C_{p2}, V_2, DDM_{p1}$ and DDM_{p2} are all measurable so $K C_s$ and $K D_s$, which are the quantities required in Eq. (3.2) for the calculation of the worst derogation can be calculated. Calculations performed for typical configurations on the computer conform these forumlae.

The above assumes $DDM_s - DDM_{p1}$ and $DDM_s - DDM_{p2}$ to be both positive. If they are both negative, using the equations above gives the negative of the correct values. This is unimportant since one is only concerned with the modulii of $K C_s$ and $K D_s$.

However, if $DDM_s - DDM_{p1}$ and $DDM_s - DDM_{p2}$ have different signs, i.e., the scatterer lies between the localizer to probe lines, then the correct formulae are

$$K C_s = \frac{C_{p1} V_1 + C_{p2} V_2}{DDM_{p2} - DDM_{p1}} \tag{3.22}$$

$$K D_s = C_{p1} V_1 + DDM_{p1} \left(\frac{C_{p1} V_1 + C_{p2} V_2}{DDM_{p2} - DDM_{p1}} \right) \tag{3.23}$$

or the negative of these.

One or two probes are required to resolve the ambiguity. Three probes can be used as follows:

The vector DDMs at the probes are measured and K C_s and K D_s are calculated using probes P1 P_2, and P_2 P_3 and Eqs. (3.20) and (3.21). If the answers differ then Eqs. (3.22) and (3.23) are used and the two pairs of answers which agree out of the four pairs obtained are tken as correct.

A method which would give greater confidence at the expense of another probe is

Use Eqs. (3.20) and (3.21) and probes P_1 P_2, P_3 P_4 and if they differ use P_2 P_3 and taken the answers which agree with the latter as correct. This would give some redundancy and also resolve any difficulties due to measurement errors, the approximation errors detailed in section 3.4.3 below, or any difficulties caused by the fact that a non-point scatterer is not illuminated with a uniform DDM.

3.5.3 Vector DDM Applied to the Glide Slope

The single probe VDDM monitor cannot be used since it is not permissible to erect it on the course line or on the course line angle separated in azimuth due to the aerial height required and consequent obstruction.

The multiprobe VDDM monitor has a problem not experienced by the localizer equivalent in that due to the ground reflections the scatterer cannot be considered omnidirectional and the magnitude of K as defined for the previous calculations varies for probes at different elevations.

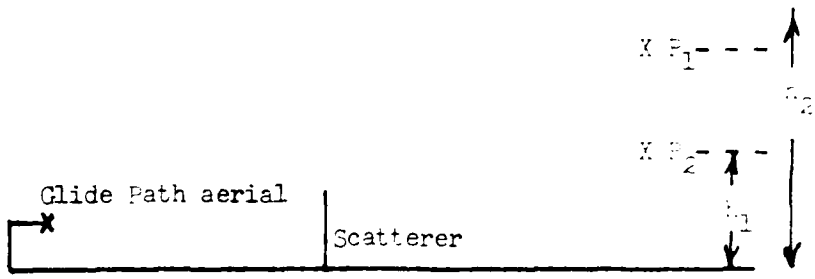

The equations are

$$V_1 = K_1 \frac{C_s}{C_{p1}} (DDM_s - DDM_{p1}) \qquad (3.24)$$

$$V_2 = L_2 \frac{C_s}{C_{p2}} (DDM_s - DDM_{p2}) \qquad (3.25)$$

and there is one unknown too many.

These equations can be solved if the ratio K_2/K_1 (= r say) is known.

Then Eq. (3.25) becomes

$V_2 = r K_1 \frac{C_s}{C_{p2}} (DDM_s - DDM_{p2})$ and we can solve as before.

A reasonable assumption about r can probably be made since the objects of interest are all ground-based scatterers with similar elevation polar diagrams.

There is a second problem in that due to height limitations the elevation separation of P_1 and P_2 will be small. A maximum will be of the order h_2 = 50', h_1 = 10'. Under these circumstances a scatterer will fill all the elevation angles between P_1 and P_2 (a 747 fin top is 64' above ground level) which pair of formulae to use and if eigher pair give the correct answer requires further investigation.

3.5.4 Effect of Neglecting K^2 Terms

If K^2 terms are included the expression for $\frac{\text{Sideband difference}}{\text{carrier}}$ becomes

$$R = DDM_p + \vec{K} \frac{C_s}{C_p} (DDM_s - DDM_p) + (\vec{K} \frac{C_s}{C_p})^2 (DDM_s - DDM_p)$$

and

$$VDDM = \left\| \vec{K} \frac{C_s}{C_p} (DDM_s - DDM_p) + (\vec{K} \frac{C_s}{C_p})^2 (DDM_s - DDM_p) \right\|$$

$\frac{C_s}{C_p} \approx 1$ so the K^2 term introduces an error in VDDM of the order K.

This can be significant if the probes are fairly close together since

$$K\ C_s = \frac{C_{p1}\ V_1 - C_{p2}\ V_2}{DDM_{p1} - DDM_{p2}}$$

$C_{p1}\ V_1 - C_{p2}\ V_2$ is a difference and if it is small the K^2 term which should be added to V_1 and V_2 can be significant.

For a pessimistic example typical figures taken from one of our computer runs are

$DDM_{p1} = -72.1$ $\qquad$ $DDM_{p2} = -95.8$

$C_{p1}\ V_1 = 4.04$ $\qquad$ $C_{p2}\ V_2 = 4.62$

$K = 0.02$

Then $K\ C_s = 0.58/23.7 = 0.0245$

$K\ D_s = 4.04 - 1.77 = 2.27$

Assume these figures are best case for illustration. The worst case will change $C_{p1}\ V_1$ and $C_{p2}\ V_2$ by 2%.

Then

$$K\ C_s = \frac{0.75}{23.7} = 0.0316 \text{ (30\% error)}$$

$$K\ D_s = 4.12 - 2.27 = 1.85 \text{ (20\% error).}$$

So the approximation can give a significant error (the case quoted is extreme) if the probes are not reasonably spaced. A four probe arrangement as suggested would provide sufficient redundancy to almost eliminate this error.

3.5.5 Implementation of the Monitor

A possible hardware embodiment of the vector DDM monitor is given below. The quadrature component of DDM (QDDM) is measured using the circuit of Figure 3-22. The quotient, $|SBO| / |CSB|$ is input to the module and immediately divided by four. This division serves two purposes. First, it allows one to use packaged phase locked loops (PLL) with typical maximum VCO frequencies of ≈30 MHz. Second, the frequency division places the modulating frequencies of 90 and 150 Hz closer to the carrier frequency and reduces their magnitude relative to it. This is quite important since the locked VCO output is then multiplied and used in the AM module for synchronous detection, a measure that provide distinct improvements in noise performance over that available current receivers. The demodulated output is then passed through an filter to separate the two audio tones and take their difference resulting output.

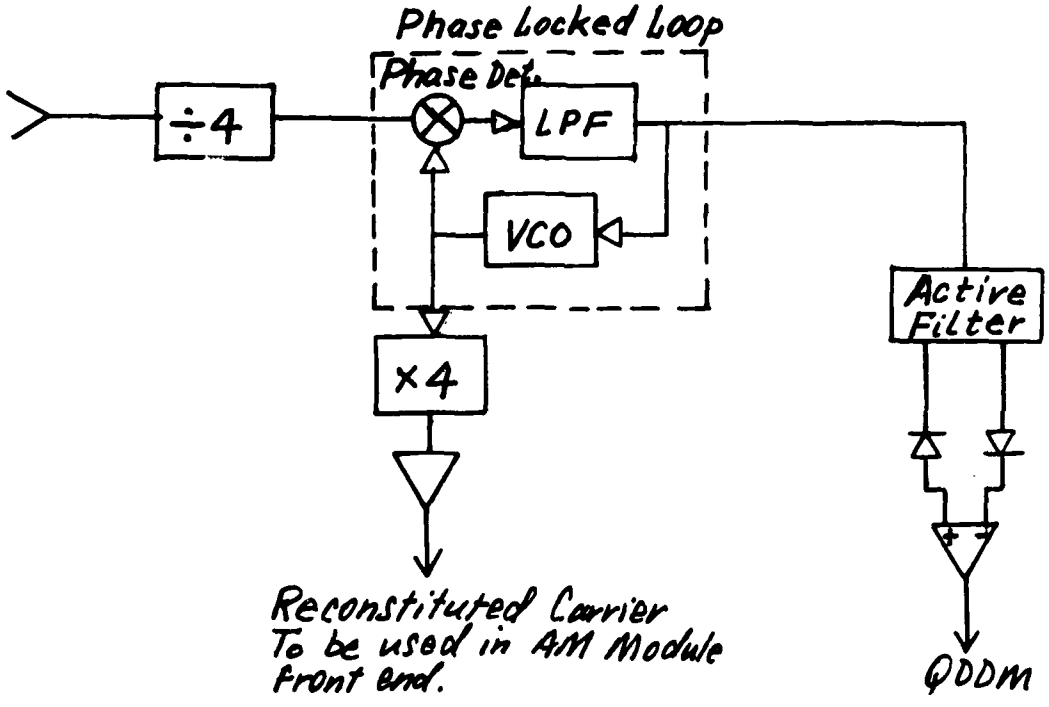

FIGURE 3-22a QUADRATURE DDM (QDDM) MODULE

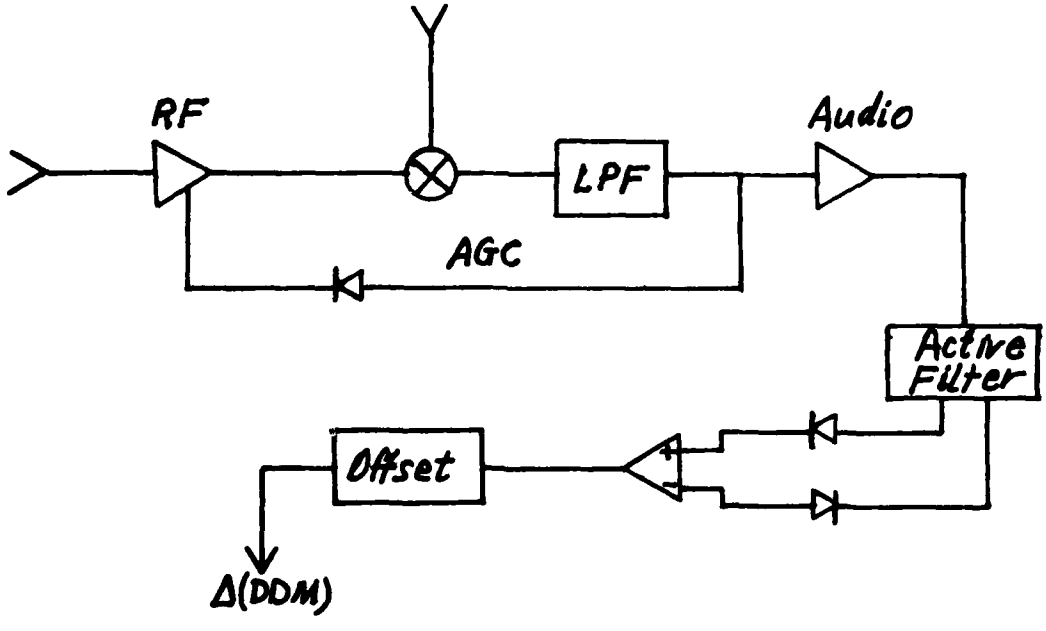

FIGURE 3-22b AM MODULE

The AM module pictured in Figure 3-22b yields Δ(DDM) by synchronous detection using the reconstituted carrier generated in the QDDM module. The audio tones are separated and their difference is taken resulting in Δ(DDM) after a DC offset. Figure 3-23 illustrates the use of the two modules and their subsequent reduction to a vector sum, VDDM.

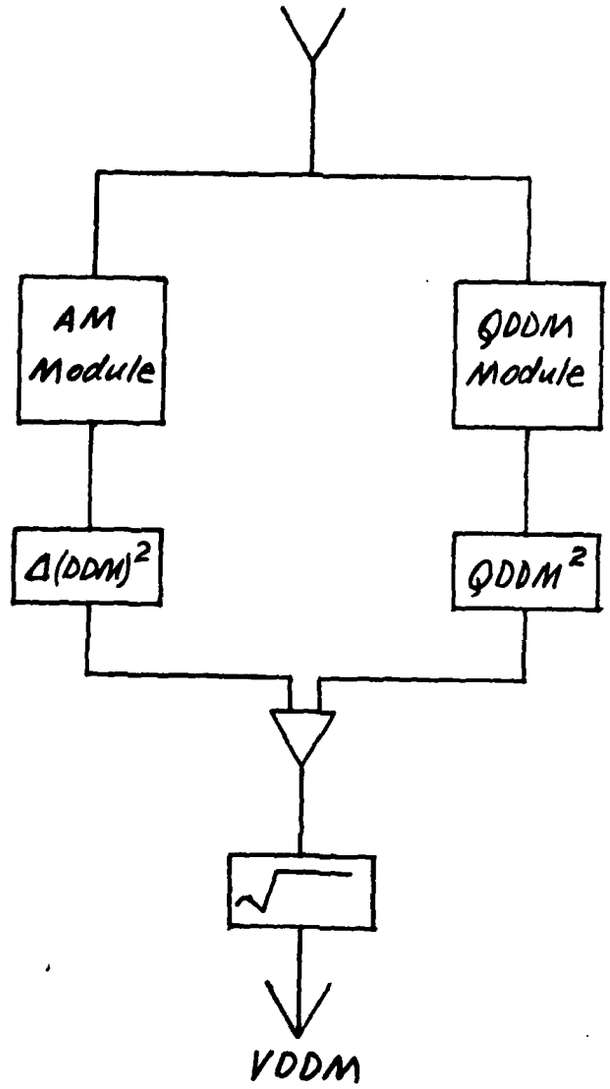

FIGURE 3-23 BLOCK DIAGRAM OF VECTOR DDM RECEIVER

4.0 OPERATIONAL USE OF A FAR FIELD MONITOR

Simply the detection of interference to the ILS radiated signals does not constitute a far field monitor. Once a derogation has been detected, the use of this information requires the establishment of an operational philosophy. The Recommendations Section of this report will outline the need for a close liaison with the FAA-ATC for the purpose of establishing an operational strategy. Some considerations critical to the determination of this strategy are discussed in this Section.

It has been established that take-offs, landings, and overflights produce disturbances to the glide path that greatly exceed those produced by aircraft parked on taxiways. However, the short time duration of these disturbances tends to make them less important in terms of the safety of a landing aircraft. In general, it is undesirable to alarm on this type of disturbance. The Vector DDM far field monitor can differentiate this class of disturbances from the more serious persistent type by a measurement of the frequency of the interference pattern. Frequency will be an adjustable alarm limit setting which will allow the large amplitude, short time duration disturbances to be rejected. This is a considerably more efficient and safer technique than the built-in time delay since it provides continuous monitor operation even during the occurrence of any of these short term disturbances.

During landing, aircraft are protected from these short term disturbances by a separation criteria. There is a possibility that in some instances these separations may not be properly maintained. This could result in an aircraft experiencing a short term derogation during a critical stage of its approach and landing. The most practical way to protect against this situation is to have the occurrence of a short term disturbance displayed to an air traffic controller. It would be his option to either accept or reject the alarm based on his knowledge of the traffic patterns. To automate the system to the level required to protect against this type of remote possibility would require a level of complexity beyond the scope of a practical far field monitor. A continuous update on all aircraft movements would be required by a decision making computer operating as an integral part of the monitor system.

Stationary or long term disturbances are produced by stopped aircraft, hanger doors, etc. This type of derogation produces beam bends in the ILS. The Vector DDM monitor system easily detects this type of fault. It can be automated to respond as a true executive monitor to any level desired by the FAA. This could include the cycling of the transmitter followed by shutdown if the fault persists.

The analysis of the Vector DDM monitor has determined that it has the ability to differeniate between the very large-short term derogations and true faults which are quasi-stationary and produce glide path bends. This is the fundamental determining factor which makes this system a true executive far field monitor as opposed to existing simple systems. The final decision for the operational use of this information must rest with the FAA.

5.0 CONCLUSTIONS AND RECOMMENDATIONS

Phase I of this program examined previous attempts at ILS far field monitoring. None of these were successful within the scope of the FAA definition of an executive monitor system. The majority of the existing systems are simple single point DDM detectors. It was demonstrated in the present analysis that there is no correlation between the DDM at ground level and the DDM in the glide path. A few of the systems studied were based on a distribution of detectors. These techniques failed to recognize that an accurate measurement of field structure is needed to determine the magnitude of the derogation, and that a time signature must be measured to determine the persistance of the derogation. Collectively, all existing systems would require a very complex operational strategy to be of any use as far field monitors, and in addition, they will always have a very high probability of both false and missed alarms.

The approach on this program was to first perform a precise analysis to determine the nature of the interaction between direct and scattered ILS signals. The results of this analysis are given in Appendix A. The most significant findings from a monitor design point-of-view are:

(1) There is an absolute correlation between the glide path deviations produced by scattered signals and the peak of the interference pattern produced by these same signals at ground level,

(2) The peak of the interference pattern can be accurately calculated from a measurement of the envelop of the interference pattern,

(3) The envelop of the interference pattern can be determined by a single point measurement,

(4) The time variation of the interference pattern at ground level is identical to that occurring on the glide path.

The significant conclusion from this analysis is that, with proper signal processing, a ground level far field monitor is technically feasible.

If an analysis is to be used as a basis for the system design, there must be some experimental confirmation to validate the correctness of the analytical approach. This was accomplished through a subcontract with G.E. C. Marconi, which provided both scale model range measurements and some full scale experiments. These results, given in Appendix B, are in excellent agreement with the theoretical predictions. They confirm that computer modeling is, not only a legitimate tool, but in fact, an excellent approach for designing a monitor system.

This report describes four system configurations that were studied in depth. These results indicated that the most promising approach is a measurement of the Vector DDM. In this system a phase sensitive receiver is used to measure both the scalar (magnitude) DDM and any quadrature component of the DDM. The circuit techniques described are well understood, and in fact, are in common practice in many military systems. The output of the phase sensitive receiver is fed to a microprocessor which computes the effective deviation of the glide path due to the measured derogation. The microprocessor will also examine the time component of the derogation and determine if an alarm is appropriate.

The results presented in this report indicate that it is feasible to develop a far field ILS monitor which truly functions as an executive monitor. The thrust of the program thus far has been directed to the localizer. However, many of the techniques are directly applicable to the glide slope. Based on the results of these first two phases, some recommendations are in order for the direction of effort for the remainder of the program.

(1) Construct a breadboard version of the phase sensitive receiver and perform tests in a real airport environment.

(2) Through close liaison with the FAA-Air Traffic Control, develop a strategy for the use of a far field monitor.

(3) Based on the operational decision of the FAA in item (#2), construct the breadboard version of the microprocessor and incorporate it into the field testing program.

(4) Extend the above techniques, developed for the localizer, to include the glide slope.

Item (1), the construction of the breadboard version of the receiver portion of the localizer monitor system, could be implemented immediately. This would not include the processor or the system display. Their design will depend on the choice of the operational technique. The output of the receiver will be the vector DDM. Measurements will be taken at an operational site for a variety of derogation conditions. Flight check will be used to correlate both the monitor response to the actual glide path deviations, and the measured monitor response to the computer predicted response. This experimental program will provide several significant results: (1) it will experimentally evaluate the feasibility of an executive far field monitor (2) it will determine the optimum monitor system configuration, (3) the nature of the data measured will strongly influence the operational strategy, and (4) the data can be used immediately by ATC to upgrade its knowledge of the effects of the ground movement of aircraft on ILS systems. This later consideration, although it is a spin-off of the present program, is a strong reason to pursue the breadboard development. The substantial increase in ground traffic at all major airports requires the maximum use of available taxiways that is consistent with ILS safety. The breadboard system, even without a processor or display, can be used as a tool to measure the effect of taxying aircraft at particular sites. Its portability will allow for convenient movement from site to site. Hence, each particular site could establish ground traffic patterns that are consis-

tent with safety and maximum ground use.

Concurrent with the testing program of item (1), a strategy will be developed for the operational use of the far field monitor. This will depend strongly on the nature of the measured data. Since it is an operational aspect, a very close relationship with the FAA will be required. The most important questions will be (1) how much of the system should be automated, (2) what role, if any, should personnel play in the monitor decision process, (3) what condition should constitute an alarm, and (4) what is the most desirable technique to monitor the monitor?

Once the operating mode is established, the processor and display subsystems will be breadboarded and incorporated into the field tests. At this stage, the system will function as a true executive far field monitor of the localizer. The glide slope monitor will be essentially a frequency scaled version of the localizer monitor, but having its own peculiar operating strategy.

The work described in this recommendation for the continued direction of the program would require an additional contract period of approximately 18 months. At the conclusion of this program, all drawings and specifications would be available for the production of the far field monitor system.

6.0 REFERENCES

1. FAA-E-21586, "Localizer Monitor Dipole Antenna," Aug. 28, 1970.

2. "Preliminary Instruction Book Monitor, Radio Frequency - (Type MX-9026/GRN-27CV)."

3. The Marconi Company, Research Division, "Investigation into the Effectiveness of a Far Field Monitor," Contract No. KJ/G/7293?CB66(a)2, Final Report, Jan. 1972.

4. Instrument Landing System Improvement Program, p. 11, Rept. FAA-RD-74214, Avionics Engineering Group, Department of Electrical Engineering, Ohio University, Ohio 45701. Dec. 1974.

5. Marehart, J.B. McFarland, R.M., Hildebrand, D.C., "Snow Effects on Image Glide Path Systems," Report No. FAA-RF-72-85, Contract FA 69 WA-2061, Mod 6, SRDS, FAA, DOT, by Alumni Buying Center, Dept. of E.E., Ohio University, Athens, Ohio, July 1972.

APPENDIX A

THEORETICAL STUDY OF DEROGATION

This appendix contains a summary of the theory and a number of calculations that were carried out to study the diffraction and reflection of localizer and glide slope antenna fields by rectangular screens of arbitrary size, position and orientation in space. This work is a first step in a more expansive program that involves (1) the determination of scattered ILS antenna fields in an aircraft landing path by moving targets in the vicinity of an airport such as trucks and taxiing, parked and overflying aircraft, and (2) the design of a ground based far field monitor that is capable of predicting the magnitude of perturbed antenna fields in the vicinity of the glide path. A typical airport runway environment and a possible monitor deployment is sketched in Figure A-1.

All scatterers are approximated by flat rectangular screens of various orientations. This approach is justified for scattering from ground based aircraft because, in such cases, the principal scattering centers are the planes' vertical tail sections, and tail sections are viewed as rectangular screens of roughly the same size. The Kirchhoff theory of diffraction has been used throughout this analysis to compute diffracted and reflected radiation from screens.

Investigations of various limitations of the scattering theory have been carried out and a formulation of the difference in depth of modulation (DDM) has been presented in a fashion that allows us to understand its general behavior.

A FORTRAN computer code was written and used to carry out the various calculations of scalar fields, DDM and DDM envelopes that were used in arriving at design criteria for far field monitors.

A.1 Kirchhoff Theory

The field originating from a spherical radiator located at $\vec{r}$ and passing through an aperture S in a plane screen gives rise to a diffracted field at $\vec{r}_R$ given by the Kirchhoff integral

$$E_{AP}(\vec{r}_R) = \frac{j}{2\lambda} \frac{\cos\alpha_1 - \cos\alpha_2}{r_R r_T} \int_S e^{jk(r_R r_T)} d\xi d\eta \qquad (A.1)$$

where the approximation of a "small aperture" has been used to remove the factor $(\cos\alpha_1 - \cos\alpha_2)/r_R r_T$ from the integrand. The quantities λ and k represent the wavelength and wave number ($k = 2\pi/\lambda$) for monochromatic radiation. All other quantities are identified in Figures A-2 and A-3. The magnitude of a vector $\vec{r}$ is denoted by r (as it is above) and sometimes by $\|\vec{r}\|$. Our main interest is to determine the diffracted field for the complement of the screen illustrated in Figure A-2 (i.e., for a screen occupying the region S). To accomplish this task we use Babinet's principle and write

$$E_D = E + E_{AP} \qquad (A.2)$$

where E_D is the field at $\vec{r}_R$ arising from radiation directly from $\vec{r}_T$, and E is the diffracted field at $\vec{r}_R$ resulting from the presence of screen S. On combining Eqs. (A.1) and (A.2) we obtain

$$E = E_D - \frac{j}{2\lambda} \frac{\cos\alpha_1 - \cos\alpha_2}{r_T r_R} \int_S e^{jk(r_R + r_T)} d\xi d\eta \qquad (A.3)$$

Next we note that the field reflected by a screen S is the same as that diffracted by an aperture S where the image of the source with respect to the plane of S is used in the equivalent diffraction problem and we account for the phase change in the field caused by reflection at the screen. This situation leads to the equation above where the convention of placing the normal to the aperture on the same side as the transmitter is used, and, for convenience, we may express the diffracted and reflected fields by the formula

$$E = E_D - \frac{j}{2\lambda} \frac{|\cos \alpha_1| + |\cos \alpha_2|}{r_T r_R} \int_S e^{jk (r_R + r_T)} \, d\xi d\eta. \qquad (A.4)$$

We use the terminology that the resulting diffracted and reflected field is a "scattered" or "perturbed" field.

A.2 Fields Perturbed by Rectangular Screens

Here we extend the formulation in section A.1 to obtain the field originating from a set of independent spherical radiators after it has been scattered by a finite collection of rectangular screens, each with possibly different dimensions, orientation and position in space. We assume that the scatterers are independent in the sense that the perturbation on the field arising from many scatterers is a superposition of the perturbations from the individual scatterers.

Most of the symbols and geometric configurations relating to this discussion are illustrated in Figure A-3 where the radiators are assumed to comprise a localizer antenna (the formulation is a general one, however, and does not depend on the characteristics of a localizer). The reference coordinate system is located at touch down and the sets $\{1,\ldots,l_{max}\}$ and

$\{1, \ldots, j_{max}\}$ are used to index screens and radiators, respectively. $\vec{X}_T$ locates the reference for the system of radiators, and $\vec{r}_j$ is the position of the j^{th} radiator relative to this reference. The direct (or unscattered) field at $\vec{X}_R$ due to the j^{th} radiator with amplitude A_j and phase φ_j is

$$E(\vec{r}, \vec{X}_R) = A_j e^{j(\varphi_j + kR_j)}/R_j \tag{A.5}$$

where

$$\vec{R}_j = \vec{X}_R - (\vec{r}_j + \vec{X}_T). \tag{A.6}$$

If the z-component of $\vec{X}_T$ is 0, the direct field due to the image of the j^{th} radiator in the ground plane is

$$E(\vec{r}_j^*, \vec{X}_R) = A_j e^{j(\varphi_j + kR_j^*)}/R_j^* \tag{A.7}$$

where

$$\vec{r}_j = (x_j, y_j, z_j)$$

is replaced by

$$\vec{r}_j^* = (x_j, y_j, -z_j)$$

in eqs. (A.5) and (A.6) to obtain Eq. (A.7). Accounting for the effect of the ground plane, the direct radiation at $\vec{X}_R$ due to the system of radiators is

$$E_D(\vec{X}_R) = \sum_j (E(\vec{r}_j, \vec{X}_R) - E(\vec{r}_j^*, \vec{X}_R)). \tag{A.8}$$

The field at $\vec{X}_R$, once it has been scattered by ℓ_{max} screens is

$$E_{TOT}(\vec{X}_R) = E_D(\vec{X}_R) - \sum_\ell E_\ell(\vec{X}_R) \tag{A.9}$$

where the perturbed field caused by the ℓ^{th} screen is

AD-A079 663 WESTINGHOUSE ELECTRIC CORP BALTIMORE MD F/G 17/7
FAR FIELD MONITOR FOR INSTRUMENT LANDING SYSTEMS.(U)
NOV 79 R MORE, J C BRADLEY, B NEWMAN DOT-FA75WA-3689
UNCLASSIFIED FAA-RD-79-78 NL

2 OF 4
AD
A079663

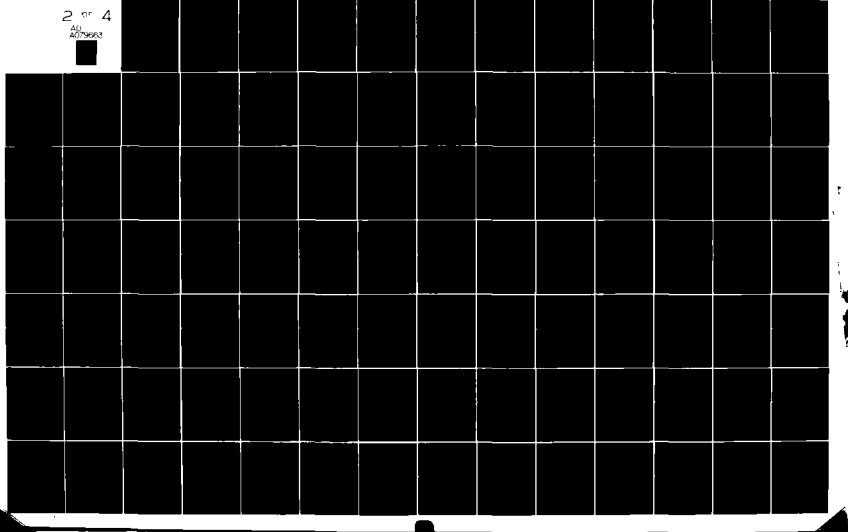

$$E_\ell(\vec{X}_R) = \frac{j}{2\lambda\rho_R^\ell} \sum_j (\rho_j^\ell)^{-1} \{|\cos\alpha_1(\rho_j^\ell)| + |\cos\alpha_2(\rho_R^\ell)|\}$$
$$\times A_j e^{i\varphi_j} \int_{S_\ell} e^{jk(R_j^\ell + r_R^\ell)} \, dS d\eta \qquad (A.10)$$

The contribution due to the image radiators is included later in this development

Euler angles are used to specify the orientation of a screen. These angles and the rotational operators they define are illustrated in Figure A-4 (see Goldstein[1]). Suppose a screen lying in the frame $\mathbf{V}_\ell$ (see Figure A-4) is oriented in the x-z plane with its center at the origin and with the unit normal vector (0, 1, 0); then any coordinate point on the screen has the form (ξ, 0, η). After the screen undergoes a rotation defined by the Euler angles φ, ϵ, Ψ, its coordinates in the $\mathbf{V}_\ell$ frame become

$$\begin{pmatrix} a_{11}^\ell & a_{12}^\ell & a_{13}^\ell \\ a_{21}^\ell & a_{22}^\ell & a_{23}^\ell \\ a_{31}^\ell & a_{32}^\ell & a_{33}^\ell \end{pmatrix} \begin{pmatrix} \xi \\ o \\ \eta \end{pmatrix} = \begin{pmatrix} a_{11}^\ell \xi + a_{13}^\ell \\ a_{21}^\ell \xi + a_{23}^\ell \\ a_{31}^\ell \xi + a_{33}^\ell \end{pmatrix} \qquad (A.11)$$

where the matrix (a_{ij}^ℓ) is the product $B_1^{-1}B_2^{-1}B_3^{-1}$ and is given by

$$\begin{pmatrix} \cos\Psi\cos\varphi - \cos\epsilon\cos\varphi\sin\Psi & -\sin\Psi\cos\varphi - \cos\epsilon\sin\varphi\cos\Psi & \sin\epsilon\sin\varphi \\ \cos\Psi\sin\varphi + \cos\epsilon\cos\varphi\sin\Psi & -\sin\Psi\sin\varphi + \cos\epsilon\cos\varphi\cos\Psi & -\sin\epsilon\cos\varphi \\ \sin\epsilon\sin\Psi & \sin\epsilon\cos\Psi & \cos\epsilon \end{pmatrix} \qquad (A.12)$$

Under this arbitrary rotation, the unit normal vector $\vec{n}^\ell$ has components a_{12}^ℓ, a_{22}^ℓ, a_{32}^ℓ). This information allows us to express $\cos(\alpha_1(\vec{\varphi}_j^{\,\ell}))$ and $\cos(\alpha_2(\vec{\varphi}_j^{\,\ell}))$ by

$$\cos\alpha_1(\vec{\rho}_j^{\,\ell}) = \vec{\rho}_j^{\,\ell} \cdot \vec{n}^\ell / \rho_j^\ell \qquad (A.13)$$

and

$$\cos \alpha_2(\vec{\rho}_R^{\,\ell}) = \vec{\rho}_R^{\,\ell} \cdot \vec{\pi}^{\ell}/\rho_R^{\,\ell} \tag{A.14}$$

with

$$\vec{\rho}_j^{\,\ell} = \vec{X}_T + \vec{r}_j - \vec{t}^{\,\ell} \tag{A.15}$$

and

$$\vec{\rho}_R^{\,\ell} = \vec{X}_R - \vec{t}^{\,\ell}, \tag{A.16}$$

and, using Figure A-5, we can see that the distance from a point on the screen indicated by $\vec{\nu}$ (relative to the frame $\mathbf{V}_\ell$) to the j^{th} radiator is the magnitude of the vector

$$\begin{aligned}\vec{R}_j^{\,\ell} &= \vec{X}_T - \vec{t}^{\,\ell} + \vec{r}_j - \vec{\nu} \\ &= \vec{\rho}_j^{\,\ell} - \vec{\nu}.\end{aligned} \tag{A.17}$$

An analogous consideration (see Figure A-3) gives

$$\vec{r}_R^{\,\ell} = \vec{\rho}_R^{\,\ell} - \vec{\nu}. \tag{A.18}$$

The integrand in Eq. (A.10) involves

$$R_j^{\,\ell} + r_R^{\ell} = \|\vec{\rho}_j^{\,\ell} - \vec{\nu}\| + \|\vec{\rho}_R^{\,\ell} - \vec{\nu}\|; \tag{A.19}$$

we evaluate the integrals in Eq. (A.10) using the expansion of Eq. (A.19) in terms of ξ and η up to quadratic terms with the assumption that powers of these coordinate values are small relative to $\rho_j^{\,\ell}$ and $\rho_R^{\,\ell}$; this assumption is justified for the parameters we have used in this problem. It gives

$$R_j^{\,\ell} + r_R^{\ell} = \rho_j^{\ell} + \rho_R^{\ell} + A_j^{\ell}\xi + B_j^{\ell}\xi^2 + C_j^{\ell}\eta + D_j^{\ell}\eta^2 + E_j^{\ell}\xi\eta \tag{A.20}$$

where

$$\vec{\rho}_j^{\,\ell} = (x_j^{\ell}, y_j^{\ell}, z_j^{\ell}), \tag{A.21}$$

$$\vec{\rho}_R^{\,\ell} = (x_R^{\ell}, y_R^{\ell}, z_R^{\ell}), \tag{A.21}$$

$$A_j^{\ell} = - \frac{x_j^{\ell} a_{11}^{\ell} + y_j a_{21}^{\ell} + z_j a_{31}^{\ell}}{\rho_j^{\ell}} - \frac{x_R^{\ell} a_{11}^{\ell} + y_R a_{21}^{\ell} + z_R a_{31}^{\ell}}{\rho_R^{\ell}} , \tag{A.22}$$

$$B_j^{\ell} = \frac{(a_{11}^{\ell})^2 + (a_{21}^{\ell})^2 + (a_{31}^{\ell})^2}{2} \left(\frac{1}{\rho_j^{\ell}} + \frac{1}{\rho_R^{\ell}} \right) - \left[\frac{(x_j^{\ell} a_{11}^{\ell} + y_j^{\ell} a_{21}^{\ell} + z_j^{\ell} a_{31}^{\ell})^2}{2(\rho_j^{\ell})^3} + \frac{(x_R^{\ell} a_{11}^{\ell} + y_R^{\ell} a_{21}^{\ell} + z_R^{\ell} a_{31}^{\ell})^2}{2(\rho_R^{\ell})^3} \right] , \tag{A.23}$$

$$C_j^{\ell} = - \frac{x_j^{\ell} a_{13}^{\ell} + y_j^{\ell} a_{23}^{\ell} + z_j^{\ell} a_{33}^{\ell}}{\rho_j^{\ell}} - \frac{x_R^{\ell} a_{13}^{\ell} + y_R^{\ell} a_{23}^{\ell} + z_R^{\ell} a_{33}^{\ell}}{\rho_R^{\ell}} , \tag{A.24}$$

$$D_j^{\ell} = \frac{(a_{13}^{\ell})^2 + (a_{23}^{\ell})^2 + (a_{33}^{\ell})^2}{2} \left(\frac{1}{\rho_j^{\ell}} + \frac{1}{\rho_R^{\ell}} \right) - \left[\frac{(x_j^{\ell} a_{13}^{\ell} + y_j^{\ell} a_{23}^{\ell} + z_j^{\ell} a_{33}^{\ell})^2}{2(\rho_j^{\ell})^3} + \frac{(x_R^{\ell} a_{13}^{\ell} + y_R^{\ell} a_{23}^{\ell} + z_R^{\ell} a_{33}^{\ell})^2}{2(\rho_R^{\ell})^3} \right] , \tag{A.25}$$

and

$$E_j^{\ell} = (a_{11}^{\ell} a_{13}^{\ell} + a_{21}^{\ell} a_{23}^{\ell} + a_{31}^{\ell} a_{33}^{\ell}) \left(\frac{1}{\rho_j^{\ell}} + \frac{1}{\rho_R^{\ell}} \right) - \frac{(x_j^{\ell} a_{11}^{\ell} + y_j^{\ell} a_{21}^{\ell} + z_j^{\ell} a_{31}^{\ell})(x_j^{\ell} a_{13}^{\ell} + y_j^{\ell} a_{23}^{\ell} + z_j^{\ell} a_{33}^{\ell})}{(\rho_j^{\ell})^3} - \frac{(x_R^{\ell} a_{11}^{\ell} + y_R^{\ell} a_{21}^{\ell} + z_R^{\ell} a_{31}^{\ell})(x_R^{\ell} a_{13}^{\ell} + y_R^{\ell} a_{23}^{\ell} + z_R^{\ell} a_{33}^{\ell})}{(\rho_R^{\ell})^3} . \tag{A.26}$$

The coefficient E_j^{ℓ} of the cross term $\xi\eta$ is the expansion of $r_R^{\ell} + R_j^{\ell}$ unduly complicates the evaluation of the integral in Eq. (A.10). Fortunately,

in cases of interest to us, its magnitude is 3/2 to 3 orders of magnitude smaller than that for the other coefficients. It is on this basis that E_j^ℓ has been omitted from our calculations.

A.2.1 Fresnel Case

In situations where the quadratic terms ξ and η are important in evaluating the integral in Eq. (A.10), the coefficients A_j^ℓ through D_j^ℓ are substituted into this equation to yield

$$E_\ell(\vec{X}_R) = \frac{j}{2\lambda\rho_R^\ell}\sum_j \frac{1}{p_j^\ell}\left\{|\cos\alpha_1(\vec{\rho}_j^{\,\ell})| + |\cos\alpha_2(\rho_R^\ell)|\right\} A_j$$

$$\times \exp j\left\{k\left[\rho_j^\ell+\rho_R^\ell - \tfrac{1}{4}\left(\frac{(A_j^\ell)^2}{B_j^\ell} + \frac{(C_j^\ell)^2}{D_j^\ell}\right)\right] + \varphi_j\right\}$$

$$\times \int_{a\ell/2}^{a\ell/2} e^{jkB_j\left(\xi + \frac{A_j^\ell}{2B_j^\ell}\right)^2} d\xi \int_{-b\ell/2}^{b\ell/2} e^{jkD_j^\ell\left(\eta + \frac{C_j^\ell}{D_j^\ell}\right)^2} d\eta \qquad (A.27)$$

where a_ℓ and b_ℓ represent the width and height of the ℓ^{th} screen, and we have "completed squares" to obtain the quadratic terms in the integrands. After a change of variables the integrals in Eq. (A.27) become

$$\frac{\pi}{2k\sqrt{B_j^\ell D_j^\ell}} \int_{\sqrt{\frac{kB_j^\ell}{2\pi}}\left(-a_\ell+\frac{A_j^\ell}{B_j^\ell}\right)}^{\sqrt{\frac{kB_j^\ell}{2\pi}}\left(a_\ell+\frac{A_j^\ell}{B_j^\ell}\right)} e^{j\frac{\pi}{2}\sigma^2} d\sigma \int_{\sqrt{\frac{kD_j^\ell}{2\pi}}\left(-b_j^\ell+\frac{C_j^\ell}{D_j^\ell}\right)}^{\sqrt{\frac{kD_j^\ell}{2\pi}}\left(b_j^\ell+\frac{C_j^\ell}{D_j^\ell}\right)} e^{j\frac{\pi}{2}\sigma^2} d\sigma$$

$$= \frac{\pi}{2k\sqrt{B_j^\ell D_j^\ell}} F_j^\ell G_j^\ell. \qquad (A.28)$$

Now

$$F_j^{\ell} = \int_{\aleph_1}^{\aleph_2} e^{j\frac{\pi}{2}\sigma^2} d\sigma$$

$$= \text{sgn}\,(\aleph_2)C(|\aleph_2|)-\text{sgn}(\aleph_1)C(|\aleph_1|)+i\left[\text{sgn}(\aleph_s)S(|\aleph_2|-\text{sgn}(\aleph_1)S(|\aleph_1|)\right], \tag{A.29}$$

and the same formula is used for

$$G_j^{\ell} = \int_{\aleph_3}^{\aleph_4} e^{i\frac{\pi}{2}\sigma^2} d\sigma \tag{A.30}$$

where $\aleph_1$ and $\aleph_2$ are the lower and upper limits, respectively, of the first integral on the left side of Eq. (A.28) and $\aleph_3$ and $\aleph_4$ have similar connotations for the second integral on the left side of Eq. (A.28). The C's and S's in Eq. (A.29) are the familiar Fresnel integrals

$$C(z) = \int_0^z \cos\,(\frac{\pi}{2}\sigma^2)d\sigma, \tag{A.31}$$

and

$$S(z) = \int_0^z \sin\,(\frac{\pi}{2}\sigma^2)d\sigma. \tag{A.32}$$

C(z) and S(z) were evaluated in this program using the approximations listed under routine CS in the IBM PALS manual[2]. On substituting Eq. (A.28) into Eq. (A.27) we get the final result

$$E_{\ell}(\vec{X}_R) = j\sum_j \left\{\frac{|a_{12}^{\ell}x_j^{\ell}+a_{22}^{\ell}y_j^{\ell}+a_{32}^{\ell}z_j^{\ell}|}{\rho_j^{\ell}} + \frac{|a_{12}^{\ell}x_R^{\ell}+a_{22}^{\ell}y_R^{\ell}+a_{32}^{\ell}z_R^{\ell}|}{\rho_R^{\ell}}\right\} A_j/8\rho_R^{\ell}\rho_j^{\ell}\sqrt{(B_j^{\ell}D_j^{\ell})}$$

$$\text{x exp } j\left\{k\left[\rho_j^{\ell}+\rho_R^{\ell}-\tfrac{1}{4}\left(\frac{(A_j^{\ell})^2}{B_j^{\ell}} + \frac{(C_j^{\ell})^2}{D_j^{\ell}}\right)\right] + \varphi_j\right\} F_j^{\ell}G_j^{\ell}. \tag{A.33}$$

A.2.2 Fraunhoffer Case

In cases where only the linear terms in ξ and η are appreciable, the much simpler Fraunhoffer integrals are used in Eq. (A.10) and this gives

$$E_\ell(\vec{X}_R) = \frac{j\lambda}{2\pi^2\rho_R^\ell} \sum_j \frac{A_j}{\rho_j^\ell} \left\{ \frac{|a_{12}^\ell x_j^\ell + a_{22}^\ell y_j^\ell + a_{32}^\ell z_j^\ell|}{\rho_j^\ell} + \frac{|a_{12}^\ell x_R^\ell + a_{22}^\ell y_R^\ell + a_{32}^\ell z_R^\ell|}{\rho_R^\ell} \right\}$$

$$\times \exp j \left\{ k[\rho_j^\ell + \rho_R^\ell] + \varphi_j \right\} F_j^\ell G_j^\ell, \qquad (A.34)$$

with

$$F_j^\ell = \frac{1}{A_j^\ell} \sin\left(\frac{kA_j^\ell a_\ell}{2} \right), \qquad (A.35)$$

and

$$G_j^\ell = \frac{1}{C_j^\ell} \sin\left(\frac{kC_j^\ell b_\ell}{2} \right) . \qquad (A.36)$$

The effects of ground reflections must be included in the formulation of this problem. The direct transmitter-to-receiver field was discussed at the beginning of this section. For the case of the ℓ^{th} scatterer, there are four paths that must be considered; these paths are sketched in Figure A-6. For the situation corresponding to Figure A-6(b), we replace the radiators by their images; this amounts to changing the third component of $\vec{r}_j$ from z_j to $-z_j$. Similarly, for the situation sketched in Figure A-6(c) we use the image of the receiver, and for that shown in Figure A-6(d) two images are used. If we express $E_\ell(\vec{X}_R)$ (using Eq. (A.33) or Eq. (A.34)) formally as

$$E_\ell(\vec{X}_R) = \Sigma_j \, E_{\ell j}, \qquad (A.37)$$

we obtain the situation described by Figure A-6(a). If ${}^tE_{\ell j}$ indicates the

field where the radiator image is used and $E_{\ell j}$ that where the receiver image is used, then for $E(\vec{X}_R)$ to include ground reflections it must be replaced by

$$E_\ell(\vec{X}_R) = \sum_j (E_{\ell j} - {}^tE_{\ell j} - E^t_{\ell j} + {}^tE^t_{\ell j}); \tag{A.38}$$

the negative signs express the phase change of 180° upon reflection at the ground. Finally, using Eq. (A.38) and Eq. (A.8) in Eq. (A.9) we get

$$E_{tot}(\vec{X}_R) = E_D - \sum_\ell \sum_j (E_{\ell j} - {}^tE_{\ell j} - E^t_{\ell j} + {}^tE^t_{\ell j}). \tag{A.39}$$

The validity of this formulation together with its limitations, and the selection of far field (fraunhoffer) versus near field (Fresnel) calculations are deferred until the latter part of Section A.3.

A.3 The Guidance Signal - DDM

The localizer and glide slope fields are generated at distinct frequencies and give azimuthal and vertical orientations, respectively. This is accomplished with current signals displayed visually for the pilot and called DDM (difference in depth of modulation). Each antenna radiates two characteristic signals for this detection - the carrier plus sideband (CSB) and the sideband only (SBO).

Moore, et. al.[3] have demonstrated an accurate and computationally simple representation of DDM in terms of the CSB and SBO fields for glide slope antennas. This formulation is valid for localizers as well and is given by

$$DDM = N\ Re\ (SBO/CSB) \tag{A.40}$$

where N is a normalization characteristic of the antenna. The total SBO and CSB signals in the presence of scatterers are of the form given by Eq. (A.39).

Using the glide path as reference, the localizer is normalized in terms of azimuthal readings at $\pm 3.5^{\circ}$ and the normalization constant is

$$N = \frac{180\ \mu\text{amps}}{\frac{1}{2}\left\{\left|\text{Re}\left(\frac{\text{SBO}}{\text{CSB}}\right)\right|_{+3.5^{\circ}} + \left|\text{Re}\left(\frac{\text{SBO}}{\text{CSB}}\right)\right|_{-3.5^{\circ}}\right\}} . \tag{A.41}$$

Using the same reference and vertical angular displacements, the normalization constant for the glide slope antenna is

$$N = \frac{75\ \mu\text{amps}}{\frac{1}{2}\left\{\left|\text{Re}\left(\frac{\text{SBO}}{\text{CSB}}\right)\right|_{+.35^{\circ}} + \left|\text{Re}\left(\frac{\text{SBO}}{\text{CSB}}\right)\right|_{-.35^{\circ}}\right\}} . \tag{A.42}$$

In the calculations we performed we used the 15 element localizer array of V-rings developed by the Avionics Research Group at Ohio University[4] and the null reference glide slope antenna[3].

The perturbations of CSB and SBO fields were manifested directly in terms of DDM in our calculations. In particular, we analyzed a difference in DDM which is defined as the DDM arising from the direct plus scattered fields minus that for the scattered field; this quantity is denoted Δ(DDM). It is convenient to express the (complex) fields as two-component real vectors and use the algebra of such vectors in our analysis. Correspondingly, we let

$$\vec{A} = (\text{Re}\ (\text{SBO}_D), \text{Im}\ (\text{SBO}_D)), \tag{A.43}$$

$$\vec{a} = \vec{A} - (\text{Re}\ (\text{SBO}_{TOT}), \text{Im}\ (\text{SBO}_{TOT})), \tag{A.44}$$

$$\vec{B} = (\text{Re}\ (\text{CSB}_D), \text{Im}\ (\text{CSB}_D)), \tag{A.45}$$

and

$$\vec{b} = \vec{B} - (\text{Re}\ (\text{CSB}_{TOT}), \text{Im}\ (\text{CSB}_{TOT})). \tag{A.46}$$

The vectors represented by lower case letters represent the perturbed fields. With this notation we have

$$\Delta(DDM)/N = \frac{(\vec{A}-\vec{a})\cdot(\vec{B}-\vec{b})}{\|\vec{B}-\vec{b}\|^2} - \frac{\vec{A}\cdot\vec{B}}{B^2} . \qquad (A.47)$$

Eq. (A.47) has been used in most of our numerical work, although linear approximations of $\Delta(DDM)$ are particularly useful in the vicinity of the glide path. We shall discuss various properties of $\Delta(DDM)$ in the remaining part of this section.

The concluding portions of this section detail the various representations of $\Delta(DDM)$ along with the limitations of these representations and the Kirchhoff diffraction theory. This discussion is confined to the localizer antenna, but analogous conditions hold for the glide slope antenna as well.

The azimuthal angle $\tilde{\varphi}$ is used to represent the variation of the fields and $\Delta(DDM)$ transverse to the glide path. In the next two paragraphs we use primarily transverse profiles to discuss qualitative features of $\Delta(DDM)$.

Although $\Delta(DDM)$ is not a linear function of $\vec{a}$ and $\vec{b}$ (the scattered SBO and CSB respectively), Figures A-7, A-8 and A-9 indicate that in a reasonably large neighborhood of $\tilde{\varphi} = 0$, it is indeed so (the sum of curves in Figures A-7 and A-8 closely approximate that in Figure A-9).

On the basis of this result we sought a linear representation of $\Delta(DDM)$ in $\vec{a}$ and $\vec{b}$. Expanding Eq. (A.47), assuming $\vec{a}$ and $\vec{b}$ to have magnitudes small relative to those of $\vec{A}$ and $\vec{B}$, we obtain

$$\Delta(DDM)/N = \frac{2(\vec{A}\cdot\vec{B})(\vec{B}\cdot\vec{b})}{B^4} - \frac{\vec{a}\cdot\vec{B}+\vec{b}\cdot\vec{A}}{B^2} + F \qquad (A.48)$$

where F represents the nonlinear terms in $\vec{a}$ and $\vec{b}$. In many instances of asymmetrically placed scatterers with reasonable small magnitudes of $\vec{a}$ and $\vec{b}$, $\Delta(DDM)/N$ has a smaller magnitude at $\tilde{\varphi} = -3.5^\circ$ than at $\tilde{\varphi} = +3.5^\circ$. A plausible explanation of this phenomenon follows from Eq. (A.48) where $\vec{A} = +\text{sgn}(\tilde{\varphi})\vec{B}$. In this case the linear terms in Eq. (A.48) reduce to

$$\Delta(DDM)/N \doteq -(\text{sgn}(\tilde{\varphi})\vec{B}\cdot\vec{b}+\vec{B}\cdot\vec{a})/B^2. \qquad (A.49)$$

If $\vec{b}$ is approximately equal to $\vec{a}$ at $\pm 3.5^\circ$, as it often is, then Eq. (A.48) gives a zero contribution to $\Delta(DDM)$ at $\tilde{\varphi} = -3.5^\circ$ but not at $\tilde{\varphi} = 3.5^\circ$.

Another manifestation of Eq. (A.48) occurs in the region of the glide path. In this case (corresponding roughly to $-.5^\circ \le \tilde{\varphi} \le +.5^\circ$) $\vec{A}$ is small in magnitude and Eq. (A.48) reduces further to the simple expression

$$\Delta(DDM)/N = -\vec{B}\cdot\vec{a}/B^2. \qquad (A.50)$$

In more familiar terms Eq. (A.50) has the form

$$\Delta(DDM)/N = -\frac{\overrightarrow{CSB}_D \cdot \overrightarrow{SBO}_{SCAT.}}{\|\overrightarrow{CSB}_D\|^2} \qquad (A.50)'$$

where CSB_D is the direct or unscattered CSB signal.

It is worth remarking that these two equations are very accurate along the glide path when the ideal unscattered CSB and SBO signals are valid. The validity of Eq. (A.50) can be seen on comparing Figures A-10 and A-11 where Eq. (A.47) was used to obtain the curve in Figure A.10 and Eq. (A.50) to obtain that in Figure A-11.

A comparison was made of $\Delta(DDM)$ values using the Kirchhoff theory and Keller's more accurate geometrical diffraction theory for a long narrow scattering screen. These results indicate that the $\Delta(DDM)$ resulting from

the two approaches were in good agreement for screen widths $\geq \lambda$. Consequently, we limited the use of Kirchhoff's theory to cases where the normal projection of the screen dimensions in the direction of the center of the radiating aperture were $\geq \lambda$.

Computational complexity is much greater when using Fresnel rather than Fraunhoffer integrals (compare Eqs. (A.29) and (A.30) with Eqs. (A.35) and (A.36). The Fresnel integrals give more accurate results (especially) in the near field, and, in general, the necessity of using them depends on the sizes of the radiating and receiving apertures and the scattering screen, the wavelength of radiation, and the distances of the scatterer from the radiating antenna and the receiver. Among the parameters involved in this study, the one involving greatest variations is distance; consequently, we based our selection of the quadrature approximation on distance alone. Specifically, comparisons of Δ(DDM) were made using the different quadratures for a 24' x 72' scatterer situated in the center of the runway at various distances D from the localizer and oriented normal to the runway centerline. Transverse profiles of Δ(DDM) were calculated, and we found that peak-to-peak excursions in Δ(DDM) using the two methods of approximation to be 1.5 μamps for D = 2200 ft., 3 μamps for D = 1500 ft., and 8 μamps for D = 1000 ft. On this basis we used the Fraunhoffer approximation when the object-to-transmitter or object-to-receiver distances exceeded 1500 ft.

A.4 Envelope Functions and Vector DDM

The envelope of DDM (or Δ(DDM)) is, roughly speaking, a smooth curve passing through the peaks of $|\text{DDM}|$ (or $|\Delta(\text{DDM})|$). An example of an envelope is given by the dashed curve in Figure A-10. It is this concept that has proved useful in correlating the transverse monitor data with data along the

flight path. The validity of this concept and methods of measuring it are discussed in the main body of this report (principally Section 3). In this section we present analytical definitions of the notions of "envelope" and "vector DDM" and discuss their relationship.

From the definition of DDM given by Eq. (A.40) we have

$$\begin{aligned} DDM &= N\ Re\left(\frac{SBO_{TOT}}{CSB_{TOT}}\right) \\ &= N\left(\frac{\overrightarrow{SBO}_{TOT} \cdot \overrightarrow{CSB}_{TOT}}{CSB^2_{TOT}}\right) \end{aligned} \tag{A.51}$$

where $\overrightarrow{SBO}_{TOT}$ and $\overrightarrow{CSB}_{TOT}$ are the real components of the complex waveforms. For brevity we express this equation as

$$\begin{aligned} DDM &= N\ \frac{(\vec{A} - \vec{a}) \cdot (\vec{B} - \vec{b})}{\|\vec{B} - \vec{b}\|^2} \\ &= N\ \frac{\vec{S} \cdot \vec{C}}{C^2}, \end{aligned} \tag{A.52}$$

where $\vec{S}$ and $\vec{C}$ represent total SBO and CSB signals. Clearly,

$$\begin{aligned} |DDM| &= NSC\ Cos\ (\vec{S}, \vec{C})/C^2 \\ &= \frac{NS}{C}\ \cos\ (\vec{S}, \vec{C}), \end{aligned}$$

and the <u>envelope function</u> relation to DDM is

$$\mathcal{E} \equiv N\frac{S}{C}\left(-1 \leq \max_{\cos\ (\vec{S}, \vec{C})} \leq +1\right) |\cos\ (\vec{S}, \vec{C})| = N\frac{S}{C} \tag{A.53}$$

It should be remarked that $\mathcal{E}$ is very accurately represented by

$$\mathcal{E}'' = Na/B \tag{A.54}$$

in a neighborhood of $\tilde{\varphi} = 0$.

One of the most promising approaches to correlating monitor data to flight path data is to relate $\mathcal{E}$ to a quantity we call "vector DDM". Vector

DDM is a two-component vector with total DDM as its first component and an experimentally measurable quadrature component of DDM as its second component. Specifically, it is defined as

$$\overrightarrow{DDM} \equiv N\left(\frac{\vec{S}\cdot\vec{C}}{C^2}\,,\ \frac{(\vec{S}\times\vec{C})_3}{C^2}\right) \tag{A.55}$$

where $(\vec{S}\times\vec{C})_3$ is the third and only non-zero component of the cross product $\vec{S}\times\vec{C}$. Expressing $\overrightarrow{DDM}$ as

$$\overrightarrow{DDM} = \frac{N}{C}\left(\frac{\vec{S}\cdot\vec{C}}{C}\,,\ \frac{(\vec{S}\times\vec{C})_3}{C}\right) \tag{A.55}'$$

we obtain the geometrical relations:

$$\frac{\vec{S}\cdot\vec{C}}{C} = \text{scalar projection of } \vec{S} \text{ along } \vec{C}, \tag{A.56}$$

and

$$\frac{(\vec{S}\times\vec{C})_3}{C} = \text{scalar projection of } \vec{S} \text{ normal to } \vec{C}. \tag{A.57}$$

The vector $\overrightarrow{DDM}$ is sometimes expressed as

$$\overrightarrow{DDM} = (DDM_{TOT},\ QDDM), \tag{A.58}$$

where the second component is called quadrature DDM. An illustration of the vector components in Eqs. (A.56) and (A.57) are given in Figure A-12. One should realize that in a reasonably large neighborhood of $\tilde{\varphi}$ (say $-3.5^\circ \le \tilde{\varphi} \le 3.5^\circ$) the components in Eq. (A.58) are simply those in the previous two equations multiplied by the slowly varying amplitude N/C.

A simple relationship between $\overrightarrow{DDM}$ and $\mathcal{E}$ exists which allows us to relate the desired quantity (for correlation studies) with the measurable quantity $\overrightarrow{DDM}$. Suppose the real components of the complex waveforms $\vec{C}$ and

$\vec{S}$ are $\vec{C} = (C_1, C_2)$ and $\vec{S} = (S_1, S_2)$. Then

$$\| \overrightarrow{DDM} \| = N \left\| \left(\frac{\vec{S} \cdot \vec{C}}{C^2}, \frac{(\vec{S} \times \vec{C})_3}{C^2} \right) \right\|$$

$$= \frac{N}{C^2} \left\{ (S_1C_1+S_2C_2)^2 + (S_1C_2-S_2C_1)^2 \right\}^{\frac{1}{2}}$$

$$= \frac{N}{C^2} \left\{ (S_1^2 + S_2^2)(C_1^2 + C_2^2) \right\}^{\frac{1}{2}}$$

$$= NS/C, \tag{A.59}$$

and on comparison with Eq. (A.53) we have

$$\mathcal{E} = \| \overrightarrow{DDM} \|. \tag{A.60}$$

A more appropriate quantity than vector DDM is the perturbation on vector DDM caused by scatterers. Such a quantity can be defined by

$$\overrightarrow{\Delta\ (DDM)} = \left(\Delta\ (DDM), \frac{(\vec{S} \times \vec{C})_3}{C^2} \right) \tag{A.61}$$

where Δ (DDM) is defined by Eq. (A.47) and its second component is the same quadrature component given in Eq. (A.55). Related to $\overrightarrow{\Delta\ (DDM)}$ is an envelope function $\mathcal{E}' = \| \overrightarrow{\Delta\ (DDM)} \|$ corresponding to the envelope of Δ (DDM) such as that given by the dashed line in Figure A-16. So long as we are concerned with vector DDM at $\tilde{\varphi} = 0$ it is sufficient to use either formulation of the vector concept, for

$$\| \overrightarrow{\Delta\ (DDM)} \|_{\tilde{\varphi} = 0} = \| \overrightarrow{DDM} \|_{\tilde{\varphi} = 0} . \tag{A.62}$$

A.5 Numerical Results

The numerical results introduced in this section comprise a number of trials of DDM, Δ (DDM) and vector DDM calculations. Each figure in the sequence is identified by a set of parameters corresponding to antenna type, the position of scatterers and the data field. If certain parameters are not listed in the data list then they are understood to take nominal

values. A few examples should make this clear; $\lfloor$ indexes the number of scattering screens, and if it is omitted from the data list then $\lfloor$ is understood to be 1; if an angle is omitted then it is understood to be 0. The flight path is considered a straight line inclined at 3° from the horizontal and intersecting the ground plane at touch down.

The localizer is centered at the far end of the runway a distance of 10,000 feet from touchdown. The transverse DDM calculations were taken on an arc 3000 feet from touchdown and with z = 25 or 50 feet above the ground plane. An illustration of this situation is given in Figure A-15 this figure includes the azimuthal angle $\tilde{\varphi}$ and its limiting range $-3.5^{\circ} \leq \tilde{\varphi} \leq +3.5^{\circ}$.

The glide slope antenna is located on the horizontal line with the x-y-z coordinate system and 300 feet from this origin. The angle θ is used as a verticle inclination from this main coordinate center with $\theta = 0$ at the ground plane, and RR is the distance from touchdown where the data field was computed.

The parameter data listed on the individual figures adhere to the following general rules:

- Antenna type
- X, Y, Z (indexed by $\lfloor$ for $\lfloor > 1$) coordinates of scattering center
- φ, ϵ, ψ (indexed by $\lfloor$ for $\lfloor > 1$) orientation of scatterer
- a, b (indexed by $\lfloor$ for $\lfloor > 1$) width and height of scatterer
- X_R, Y_R, Z_R receiver coordinates (points where DDM is determined).

Figures A-16 through A-27 contain results of a study of localizer signal disturbances caused by ground based aircraft. The first four of these figures are typical of data collected in region I of Figure A-15, the second four correspond to region II and the third set of four correspond to region III.

A comparison of envelopes along the flight path and 50' above the ground, both at X_R = -3000 ft., indicate excellent correlation since the difference $|\mathcal{E}(\text{flight path}) - \mathcal{E}(\text{monitor})|$ is less than 1 μamp.

Figures A-28 through A-39 contain results of a study of localizer signal disturbances caused by departing aircraft in the vicinity of the localizer. The reader is cautioned that these data might be in error by as much as 20% since they were gathered using the Fraunhoffer field at distances of the order of 1000 ft. from the localizer. It is interesting to note the large variations in Δ (DDM) that are possible - especially along the null reference line when the departing aircraft is tilted slightly relative to the horizontal (i.e., $\psi \neq 0$).

Figures A-40 through A-49 contain data relating to the perturbation of glide slope fields. It is interesting to note the similar character of transverse Δ (DDM) data for both localizer and glide slope antennas.

A.6 List of References

1. H. Goldstein, Classical Mechanics, Addison-Wesley, 1957.
2. PALS, IBM Manual, System/360 Scientific Subroutine Package, Version II, Programmer's Manual.
3. R. A. Moore, G. J. Moussally, T. Parker and S. F. Payer, "Analysis of Instrument Landing System Glide Slope Broadside Antennas", Report No. FAA-RD-72-139, Federal Aviation Administration, Washington, D.C., p. 3-1, 1972.
4. Avionics Research Group, Dept. of Electrical Engineering, Ohio University, "Instrument Landing System Improvement Program", The Third Interim Report on FAA Contract FA69WA-2066, June, 1972. See Chapter III entitled "ILS Localizer".

FIGURE A-1

FAR FIELD MONITOR AT A RUNWAY ENVIRONMENT

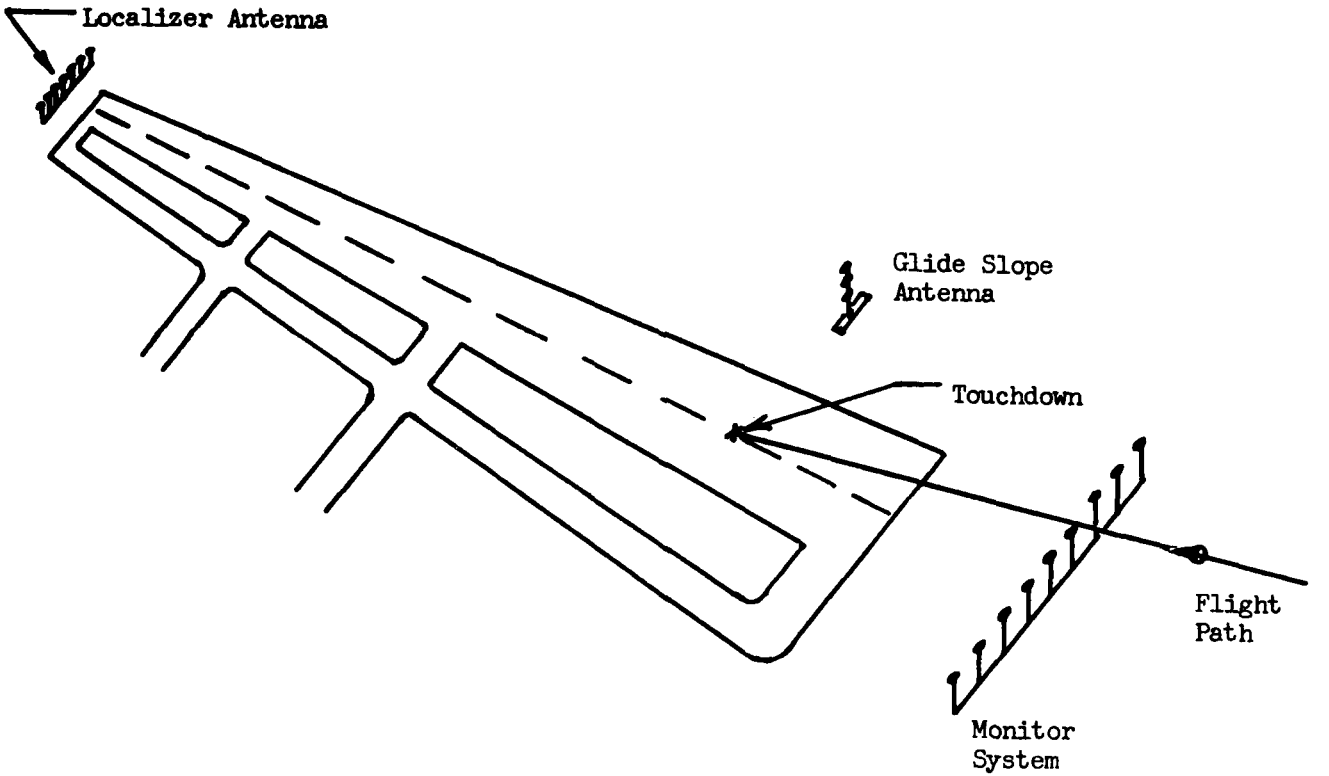

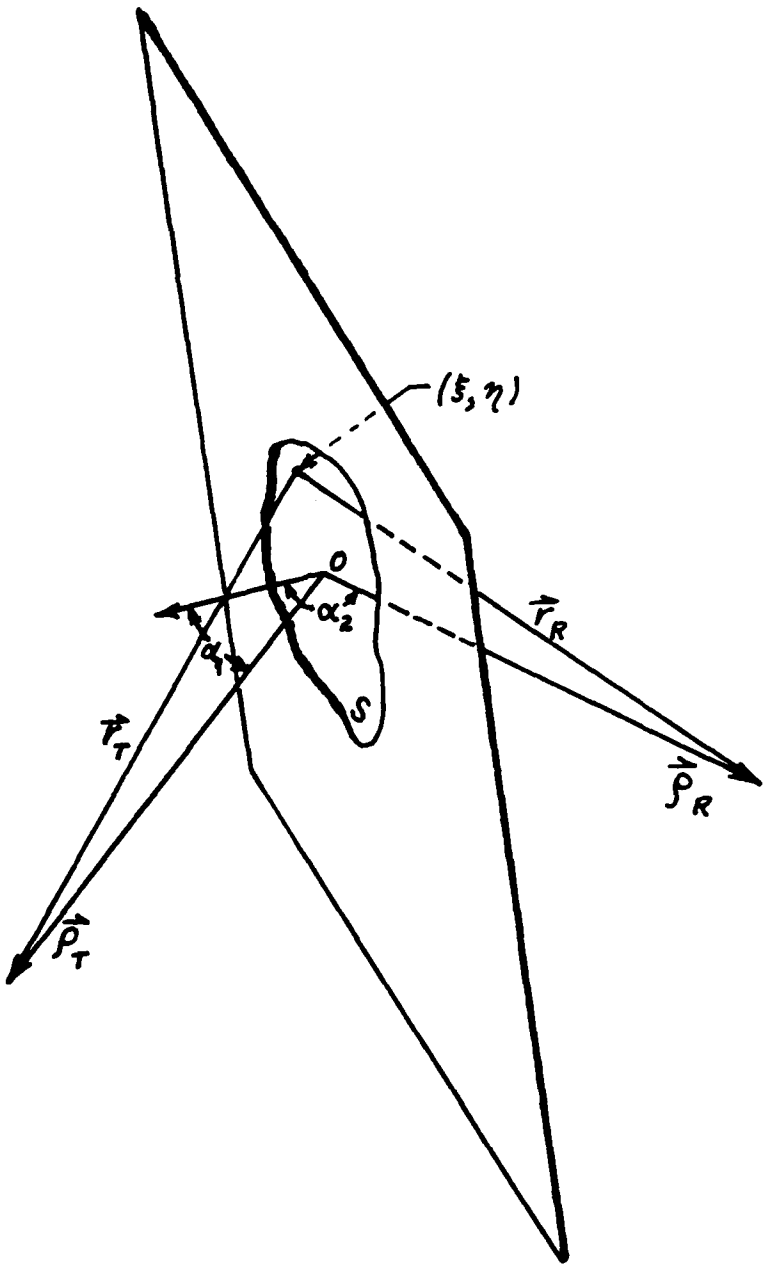

FIGURE A-2.

FIELD DIFFRACTED BY AN APERTURE S

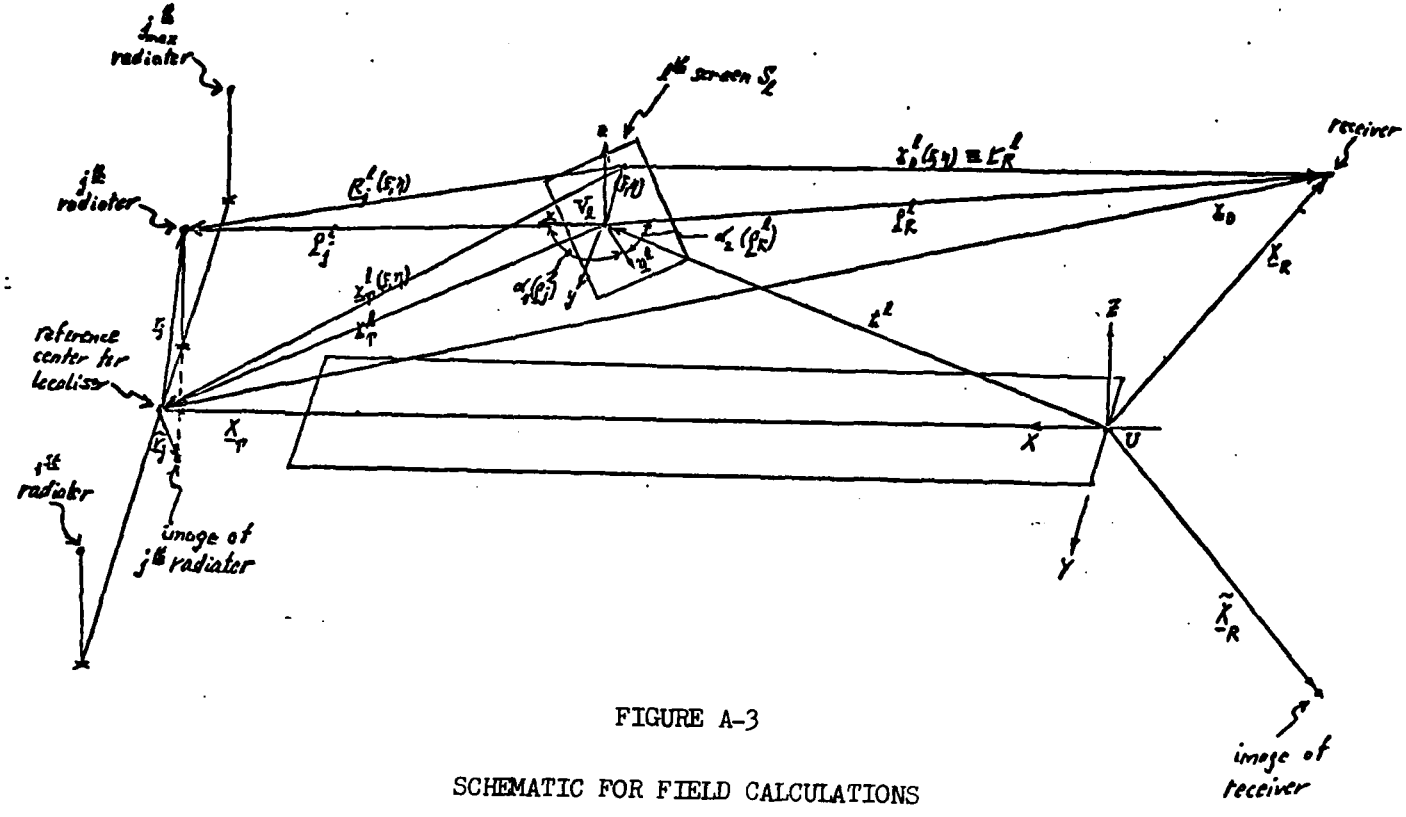

FIGURE A-3

SCHEMATIC FOR FIELD CALCULATIONS

FIGURE A-4

EULER ANGLES φ, ε, χ

$$\begin{pmatrix} \alpha \\ \beta \\ \gamma \end{pmatrix} = \begin{pmatrix} \cos\varphi & \sin\varphi & 0 \\ -\sin\varphi & \cos\varphi & 0 \\ 0 & 0 & 1 \end{pmatrix} \begin{pmatrix} x \\ y \\ z \end{pmatrix}$$

B_1

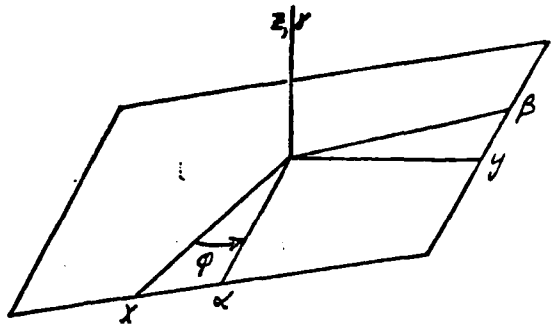

$$\begin{pmatrix} \alpha' \\ \beta' \\ \gamma' \end{pmatrix} = \begin{pmatrix} 1 & 0 & 0 \\ 0 & \cos\varepsilon & \sin\varepsilon \\ 0 & -\sin\varepsilon & \cos\varepsilon \end{pmatrix} \begin{pmatrix} \alpha \\ \beta \\ \gamma \end{pmatrix}$$

B_2

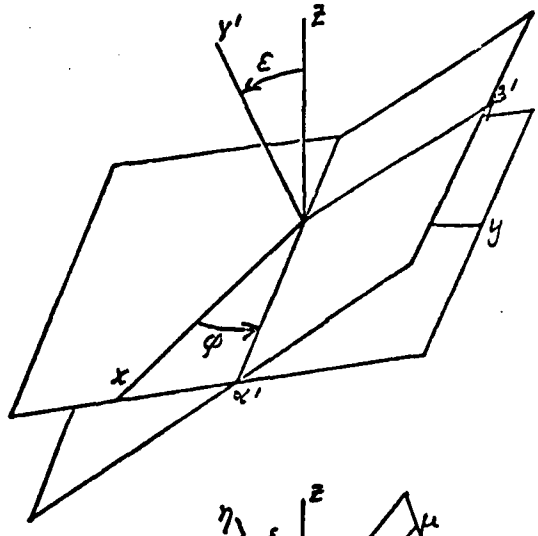

$$\begin{pmatrix} \xi \\ \mu \\ \eta \end{pmatrix} = \begin{pmatrix} \cos\psi & \sin\psi & 0 \\ -\sin\psi & \cos\psi & 0 \\ 0 & 0 & 1 \end{pmatrix} \begin{pmatrix} \alpha' \\ \beta' \\ \gamma' \end{pmatrix}$$

B_3

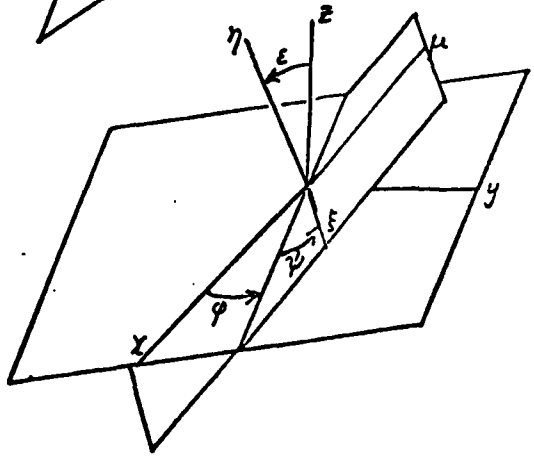

FIGURE A-5

ILLUSTRATION OF SOME POSITION VECTORS

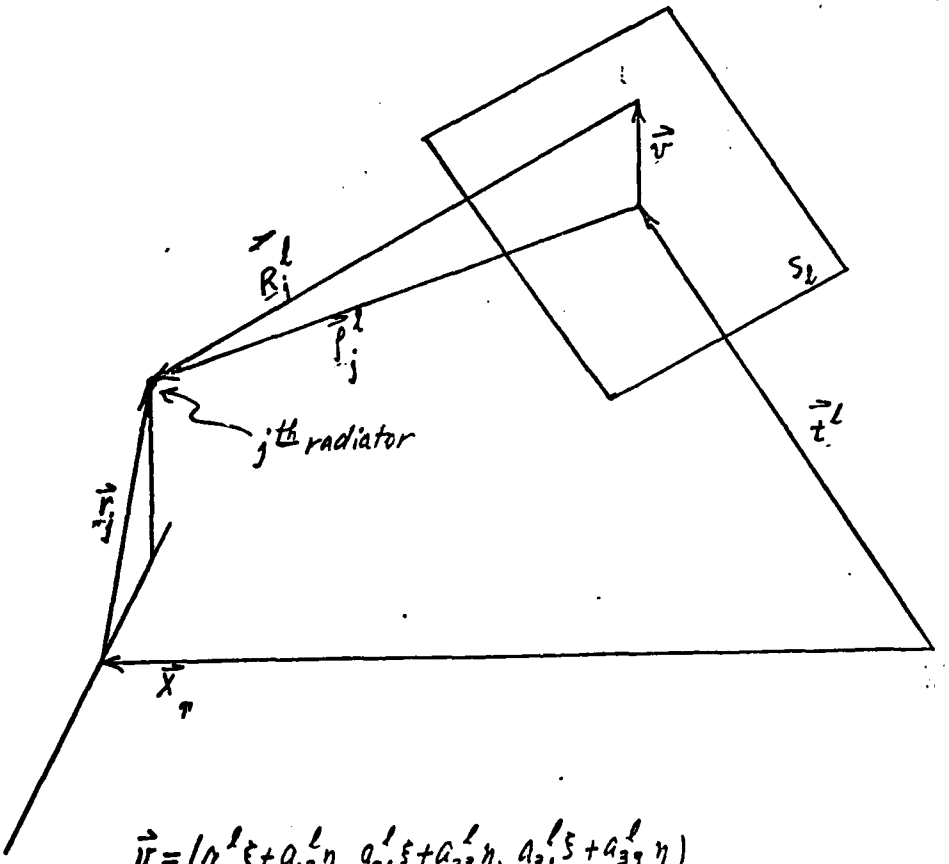

$$\vec{v} = (a_{11}^l \xi + a_{12}^l \eta,\ a_{21}^l \xi + a_{23}^l \eta,\ a_{31}^l \xi + a_{33}^l \eta)$$

FIGURE A-6. GROUND REFLECTIONS

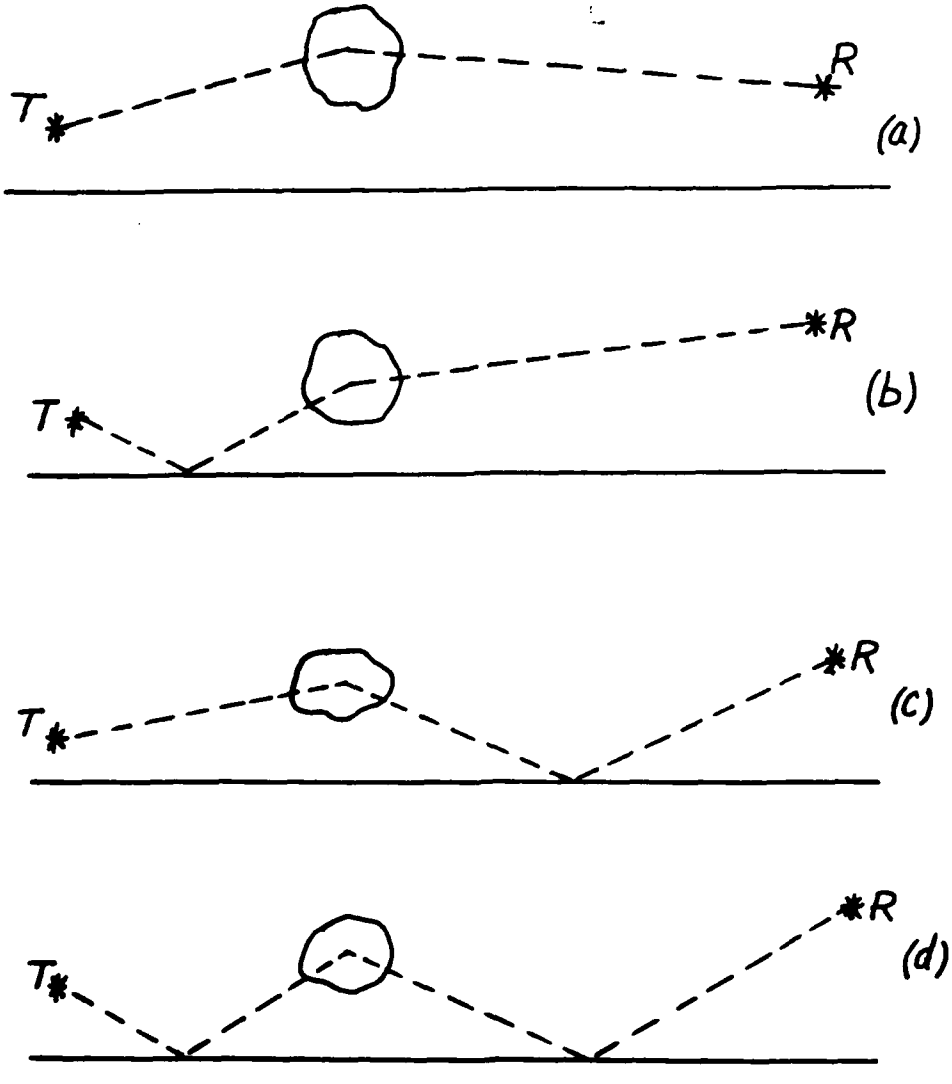

Key:

Localizer

X = 5000'

Y = 250'

Z = 36'

φ = 90°

A = 24' } tail approx.

B = 72' }

Z_R = 25'

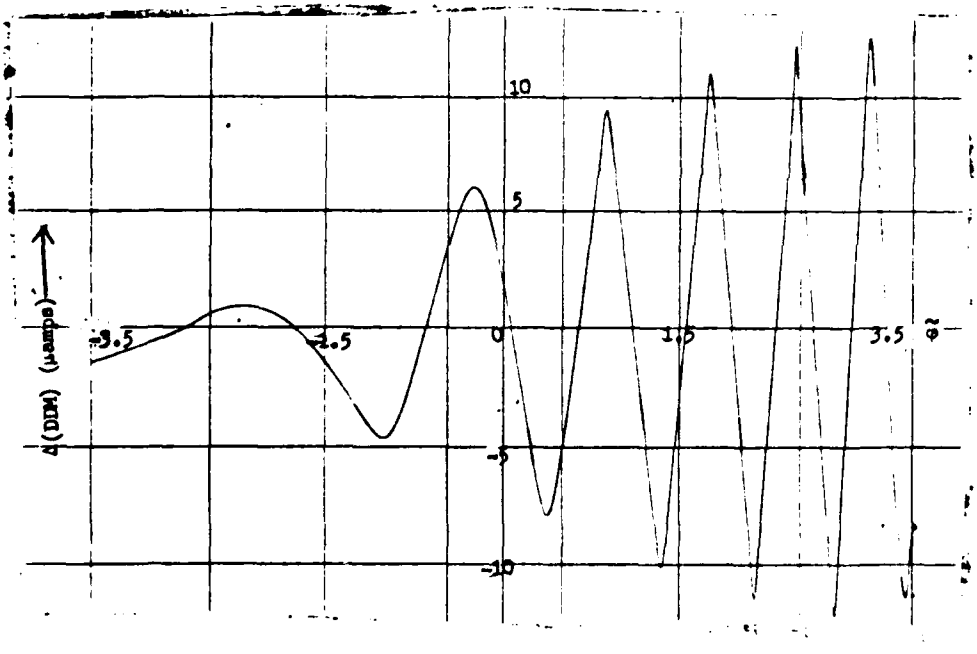

FIGURE A-7. TRANSVERSE VARIATION OF Δ (DDM)

Key:

Localizer

X = 8500'

Y = 250'

Z = 36'

$\Phi = 90^0$

A = 24' } tail
B = 72' } approx.

Z_R = 25'

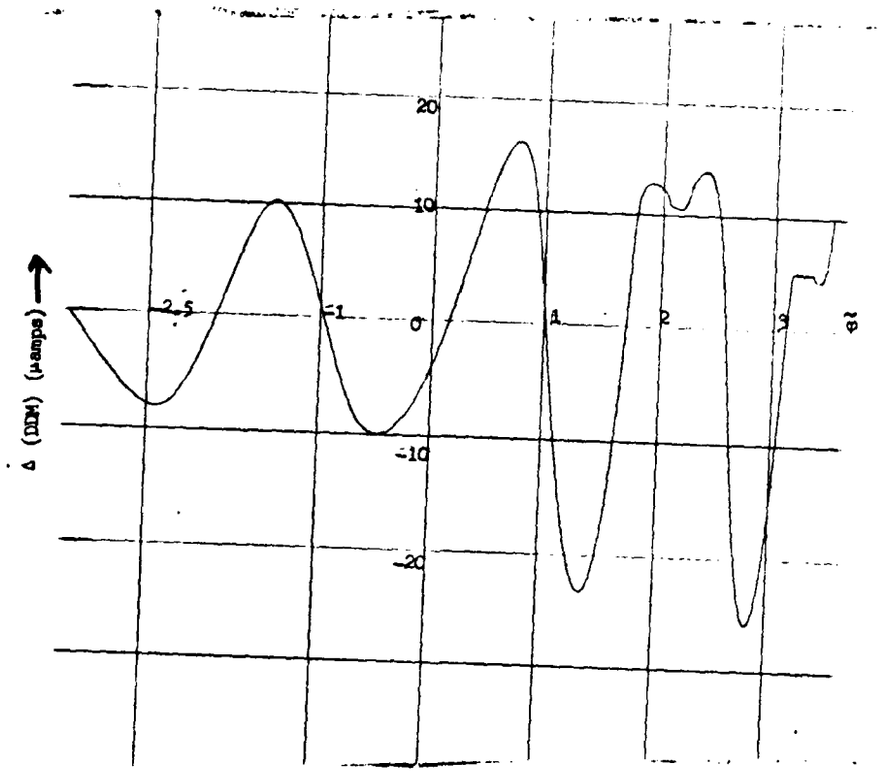

FIGURE A-8. TRANSVERSE VARIATION OF Δ (DDM)

Key:

Localizer

$X(1) = 8500'$

$X(2) = 5000'$

$Z(L) = 250'$

$\Phi(L) = 36'$

$A(L) = 24'$ } tail approx.

$B(L) = 72'$ }

$Z_R = 25'$

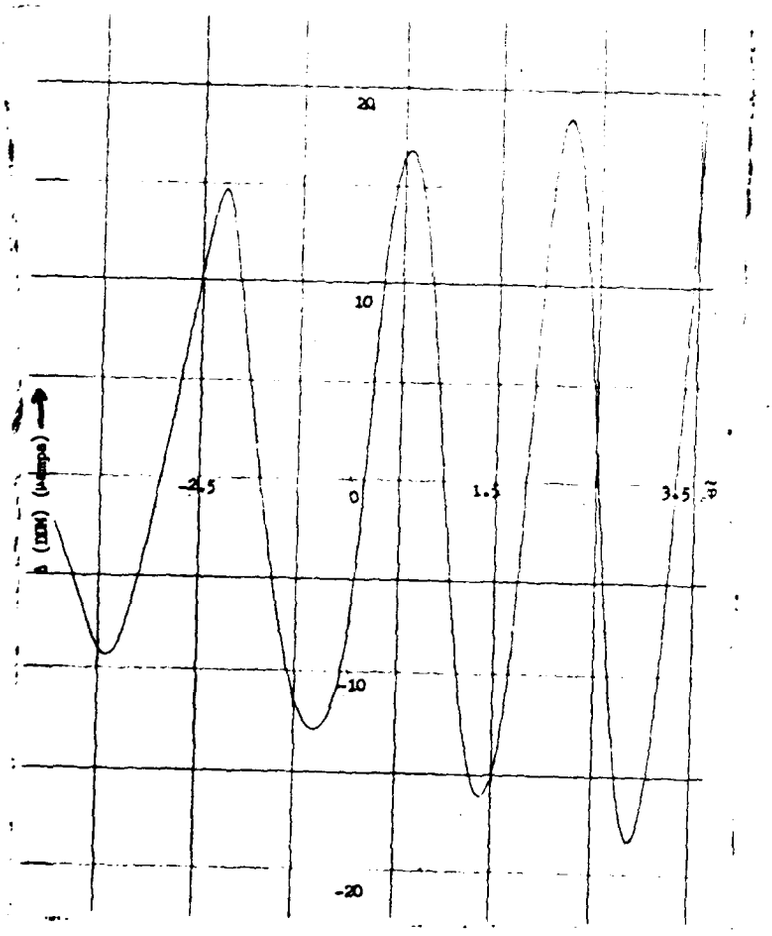

FIGURE A-9. TRANSVERSE VARIATION OF Δ (DDM)

Key:

Localizer

X = 1500'

Y = 250'

Z = 36'

φ = 90°

A = 24' } tail approx.

B = 72' }

Z_R = 25'

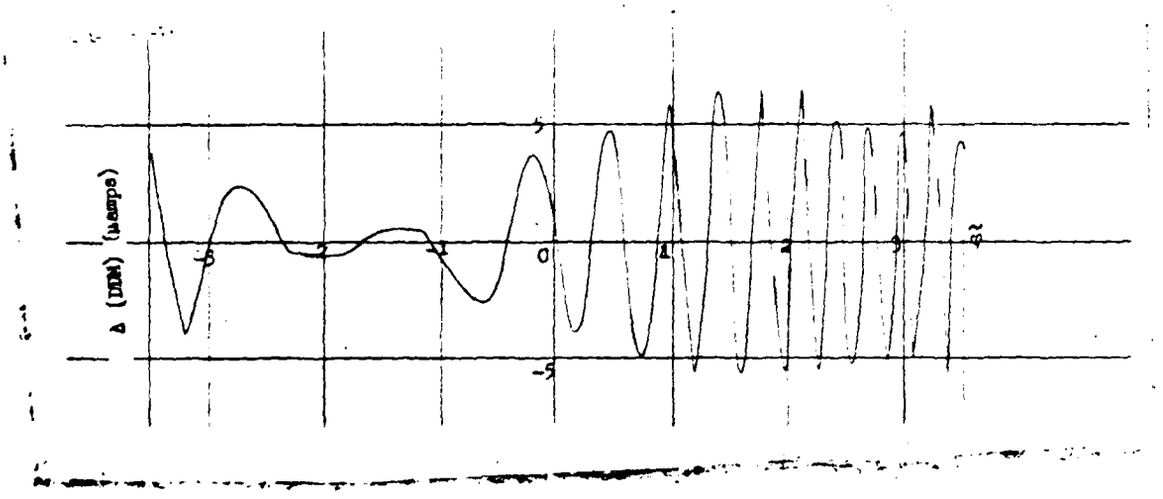

FIGURE A-10. TRANSVERSE VARIATION OF Δ (DDM)

Key:

Localizer

X = 1500'

Y = 250'

Z = 36'

A = 24' } tail
B = 72' } approx.

Z_R = 25'

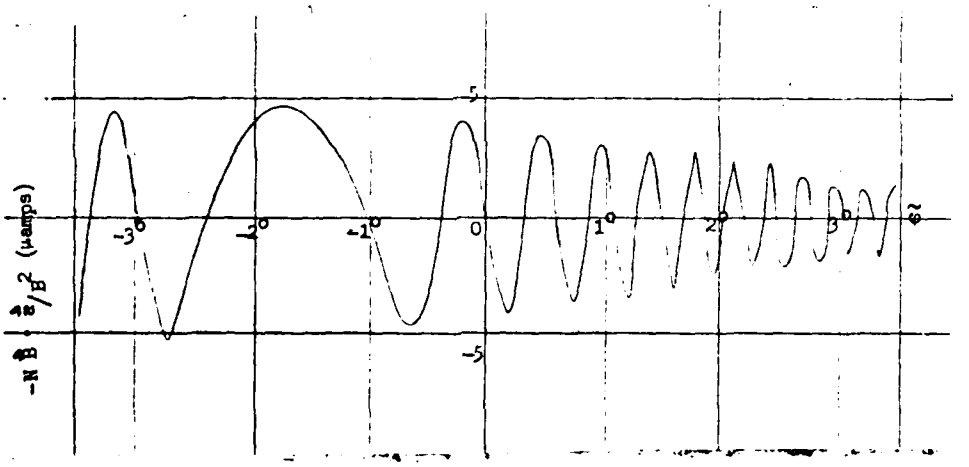

FIGURE A-11. TRANSVERSE VARIATION OF $-N\vec{B}\cdot\vec{a}/B^2$

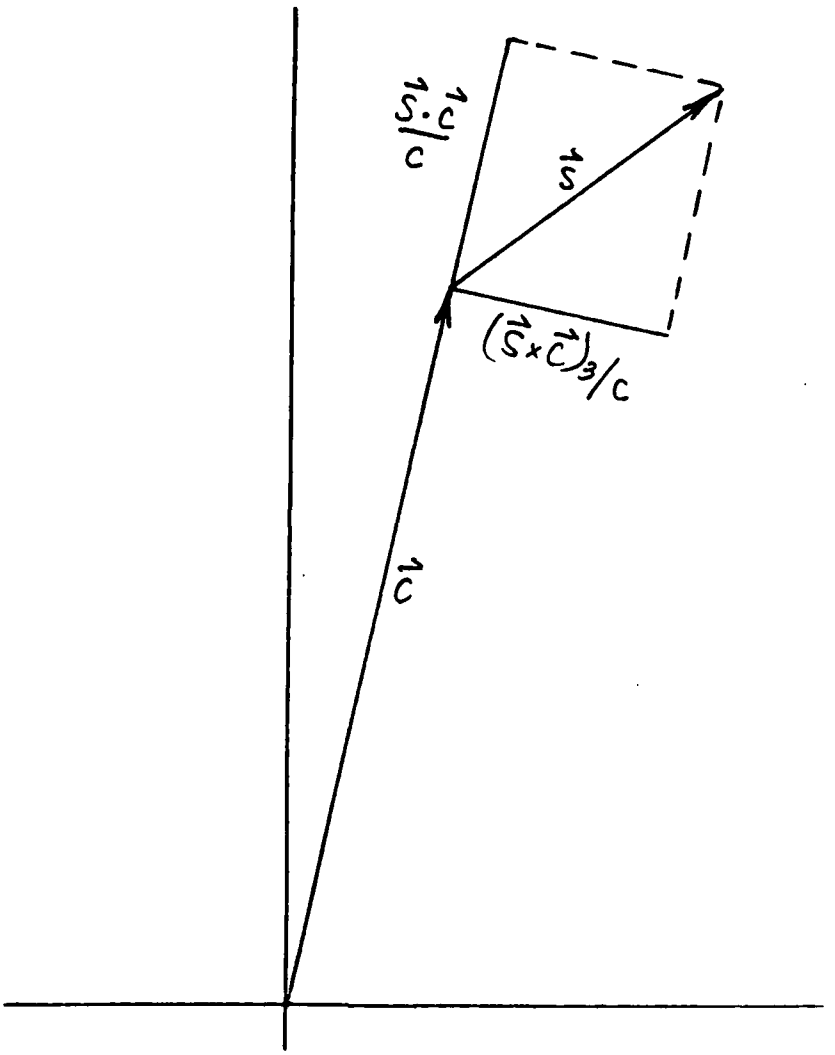

FIGURE A-12. COMPONENTS OF VECTOR DDM

Key:

Null Reference
$(300', 3^{\circ})$

Glide Sloper

$X = 1000'$

$Y = 240'$

$Z = 36'$

$\varphi = 90^{\circ}$

$A = 24'$
$B = 72'$
} tail approx.

$Y_R = 0$

$Z_R = X_R \tan 3^{\circ}$

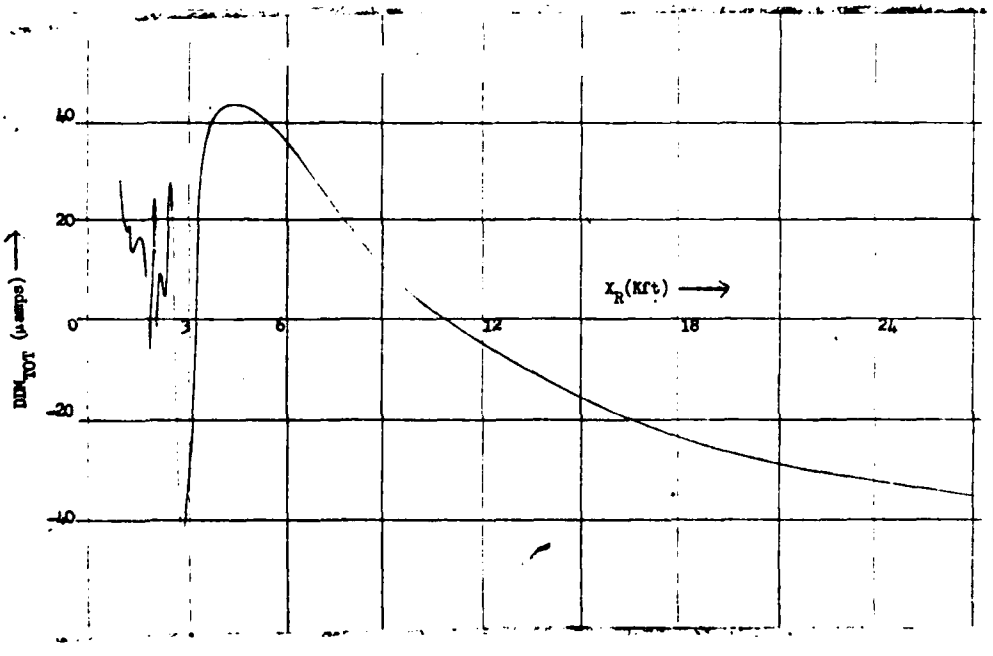

FIGURE A-13. GLIDE SLOPE Δ (DIM) VS.
FLIGHT PATH GROUND COORDINATE

Key:

Null Reference
$(300', 3^{\circ})$

$X = 1000'$

$Y = 240'$

$Z = 36'$

$\varphi = 90'$

$A = 24'$ } tail approx.
$B = 72'$ }

$Y_R = 0$

$Z_R = X_R \tan 3^{\circ}$

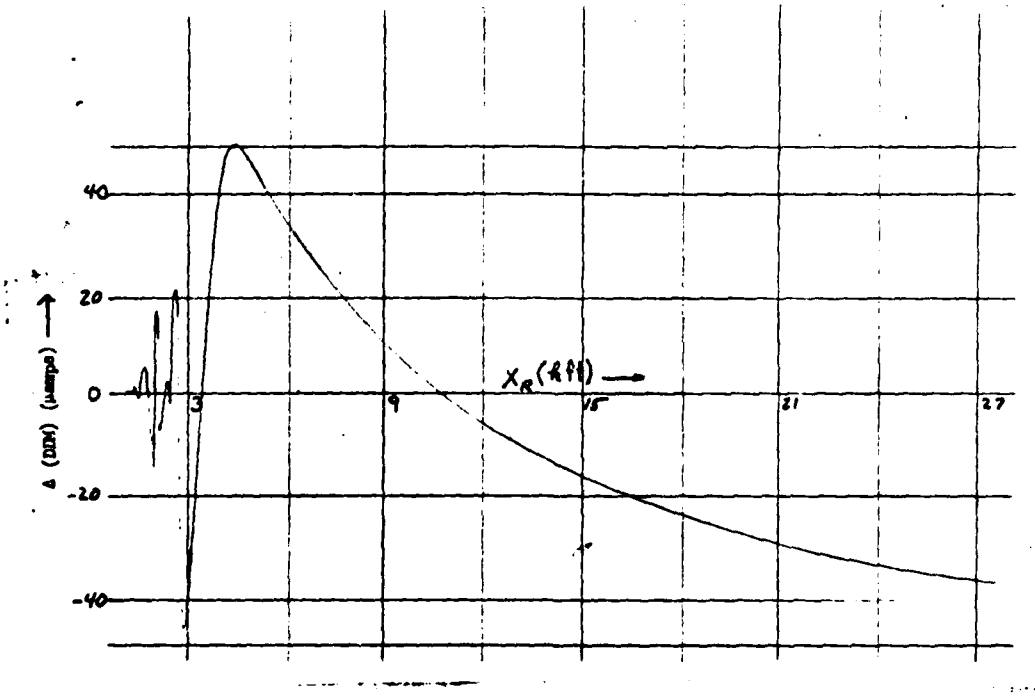

FIGURE A-14. GLIDE SLOPE DDM_{TOT} VS.
FLIGHT PATH GROUND COORDINATE

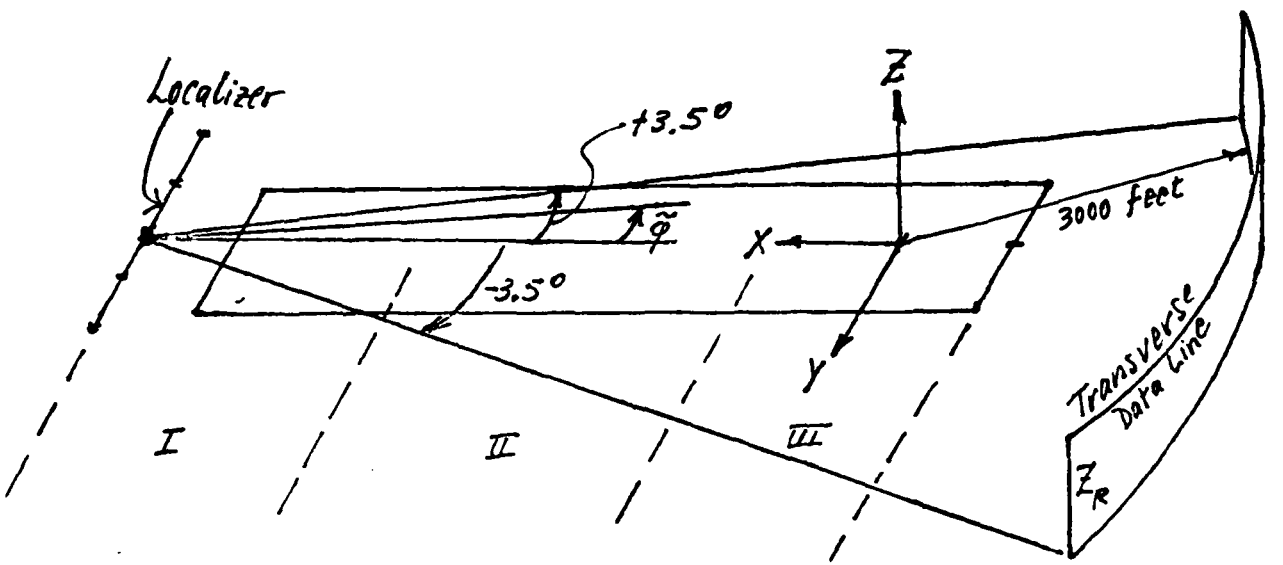

FIGURE A-15. SCHEMATIC ILLUSTRATION OF
LOCALIZER TRANSVERSE DATA FIELD

Key:

Localizer

X = 7500'

Y = 250'

Z = 36'

φ = 90°

A = 24' } tail approx.

B = 72' }

Z_R = 50'

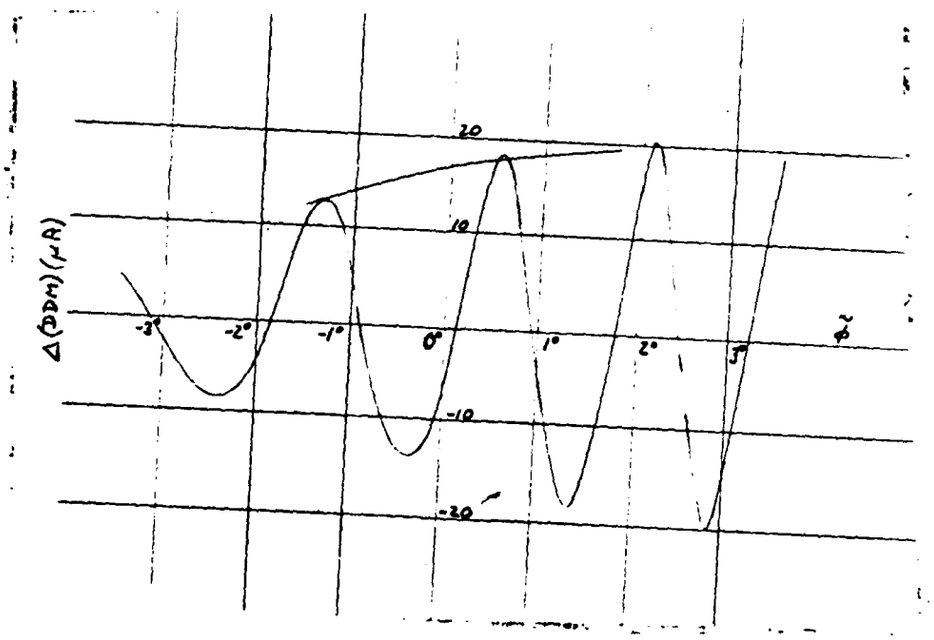

FIGURE A-16. TRANSVERSE VARIATION OF Δ (DDM)

Key:

Localizer

X = 7500'

Y = 250'

Z = 36'

Φ = 90°

A = 24' } tail
B = 72' } approx.

Z_R = 50'

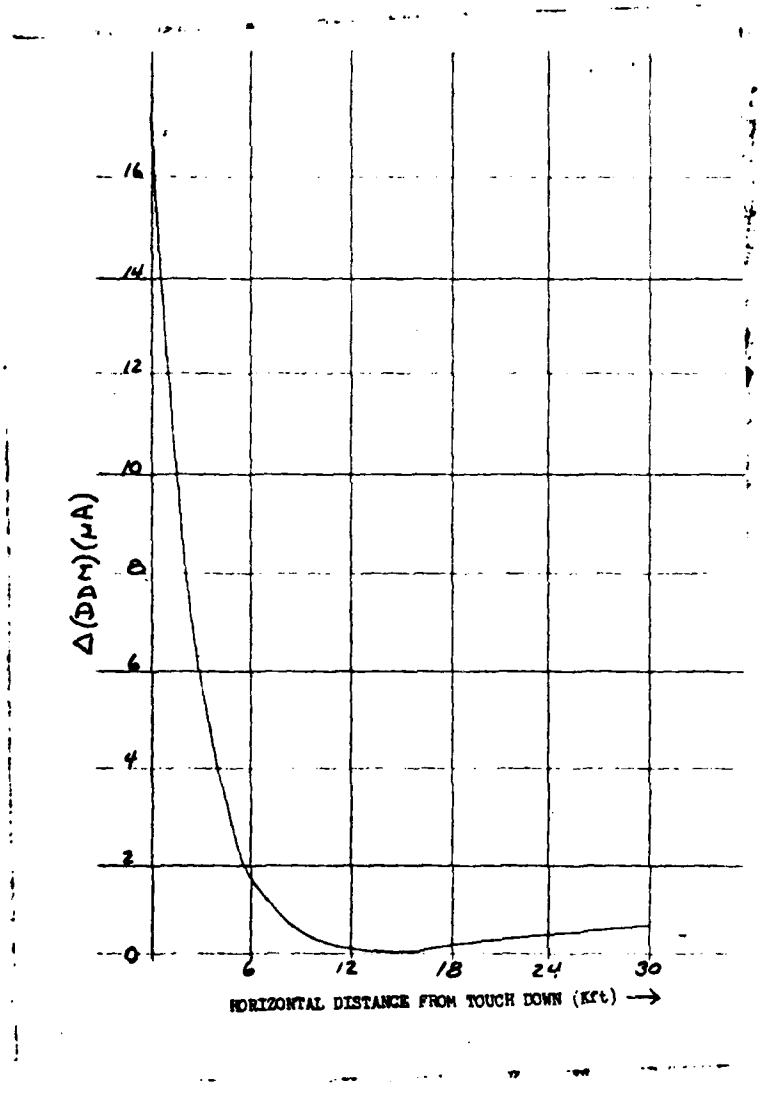

FIGURE A-17. FLIGHT PATH Δ (DDM)

Key:

Localizer

X = 7500'

Y = 250'

Z = 36'

φ = 90°

A = 24' } tail approx.

B = 72' }

Z_R = 50'

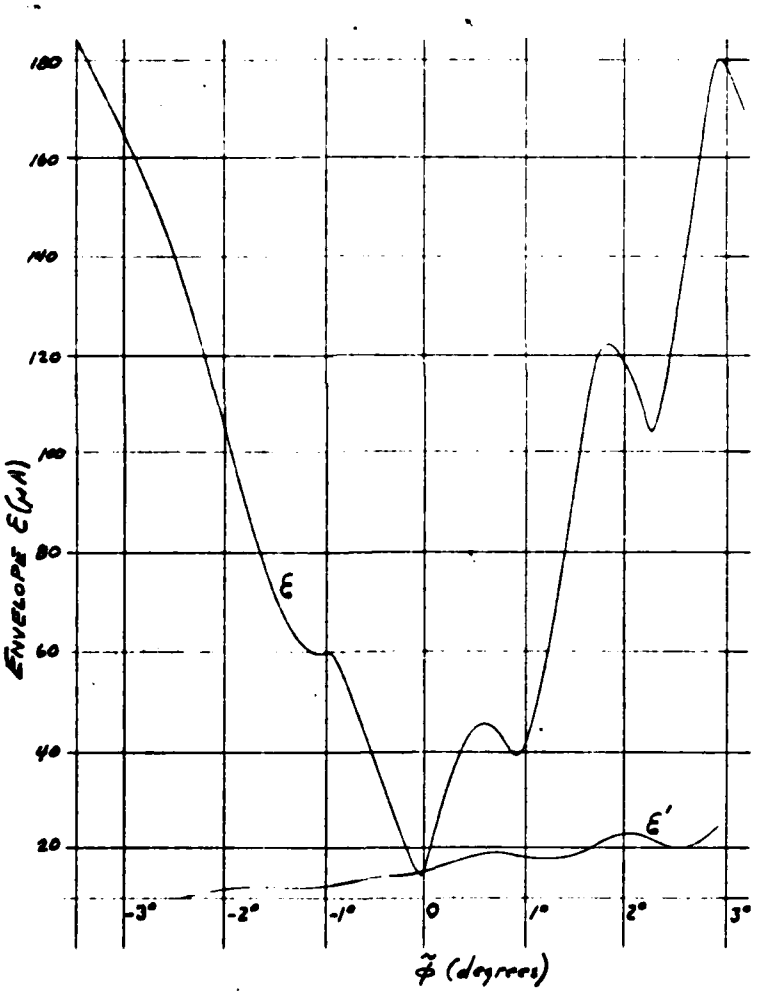

FIGURE A-18. TRANSVERSE VARIATION OF $\mathcal{E}$ AND $\mathcal{E}'$

Key:

Localizer

X = 7500'

B = 250'

Z = 36'

φ = 90°

A = 24' } tail
B = 72' } approx.

Z_R = 50'

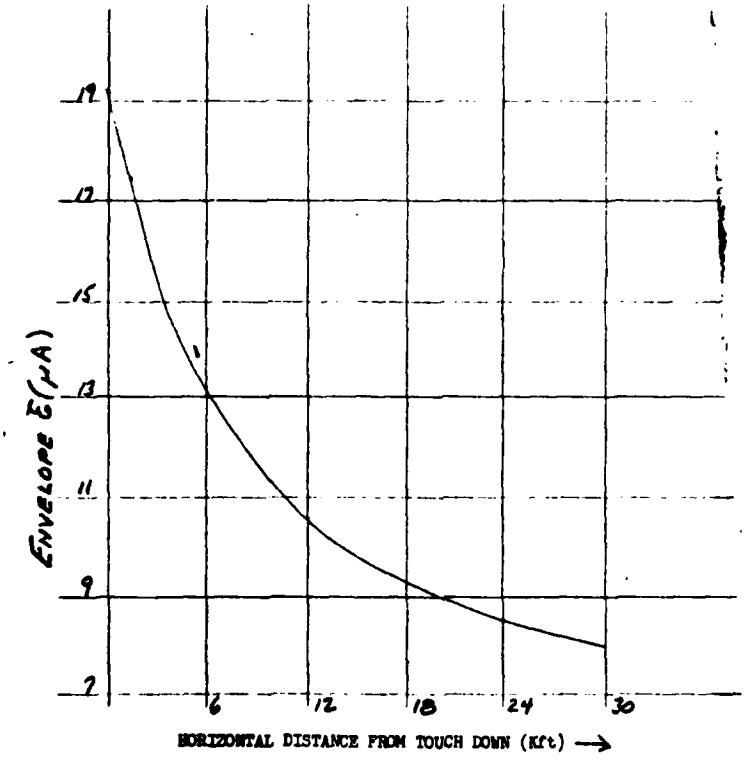

FIGURE A-19. E VS. HORIZONTAL DISTANCE GLIDE PATH

Key:

Localizer

X = 4500'

Y = 250'

Z = 36'

φ = 90°

A = 24' } tail
B = 72' } approx.

Z_R = 50'

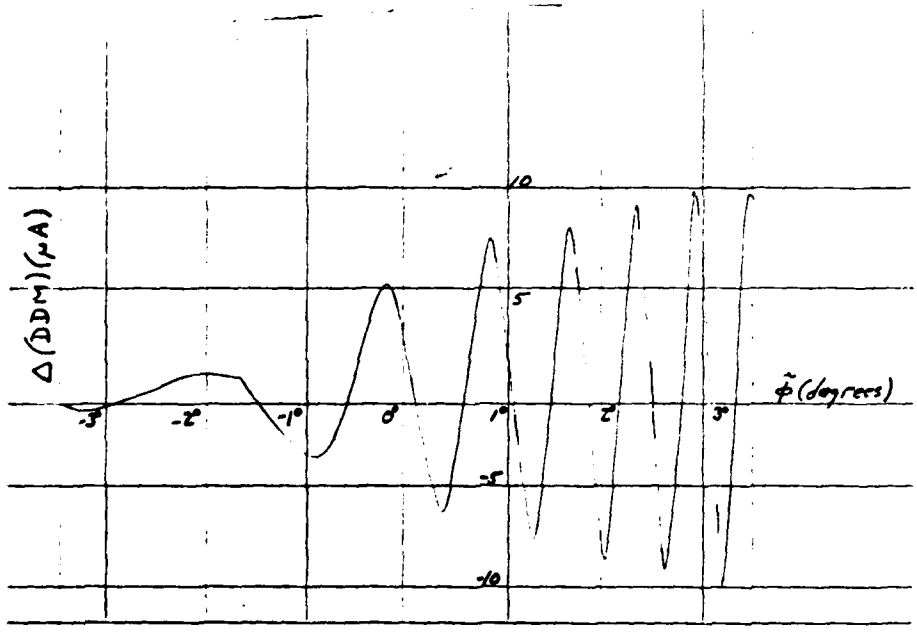

FIGURE A-20. TRANSVERSE VARIATION OF Δ (DDM)

Key:

Localizer

X = 4500'

Y = 250'

Z = 36'

α = 90°

A = 24' } tail approx.

B = 72' }

Z_R = 50'

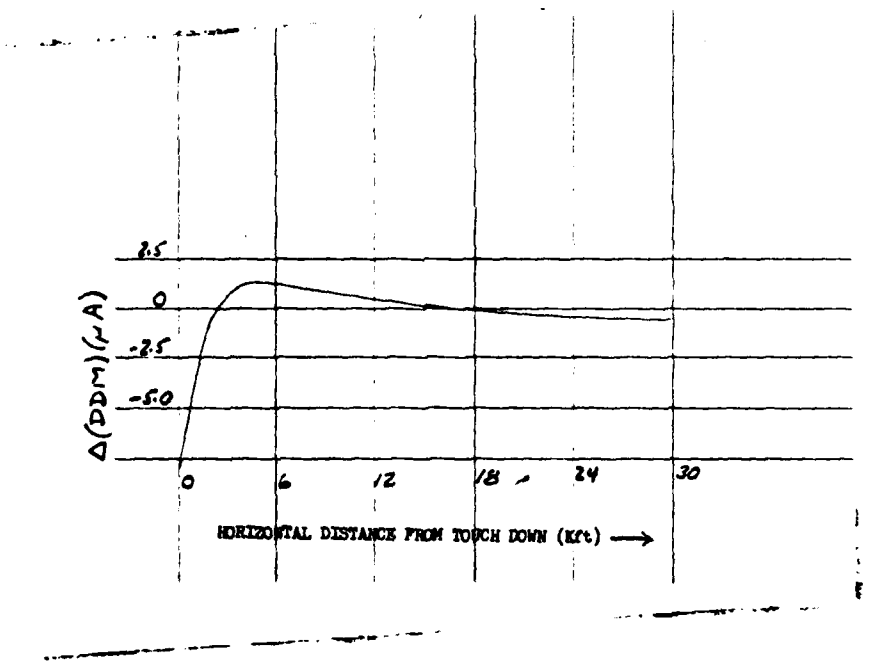

FIGURE A-21. FLIGHT PATH Δ (DDM)

Key:

Localizer

X = 1500'

Y = 250'

Z = 36'

φ = 90°

A = 24' } tail approx.

B = 72' }

Z_R = 50'

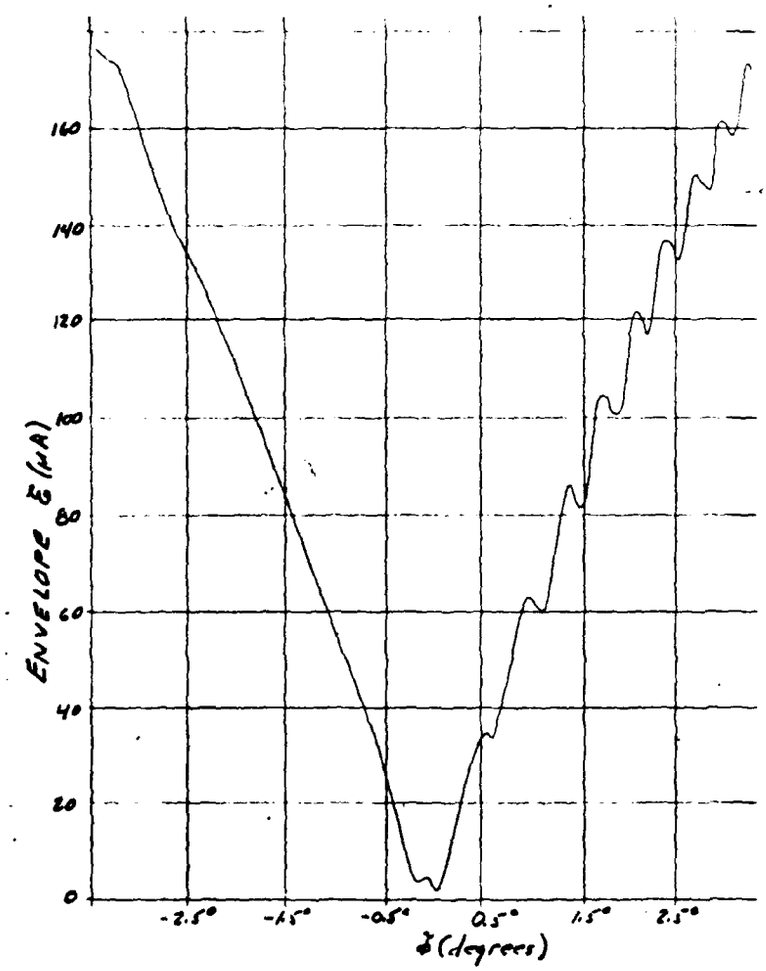

FIGURE A-22. TRANSVERSE VARIATION OF ξ

Key:

Localizer

X = 4500'

Y = 250'

Z = 36'

ϕ = 90°

A = 24' } tail
B = 72' } approx.

Z_R = 50'

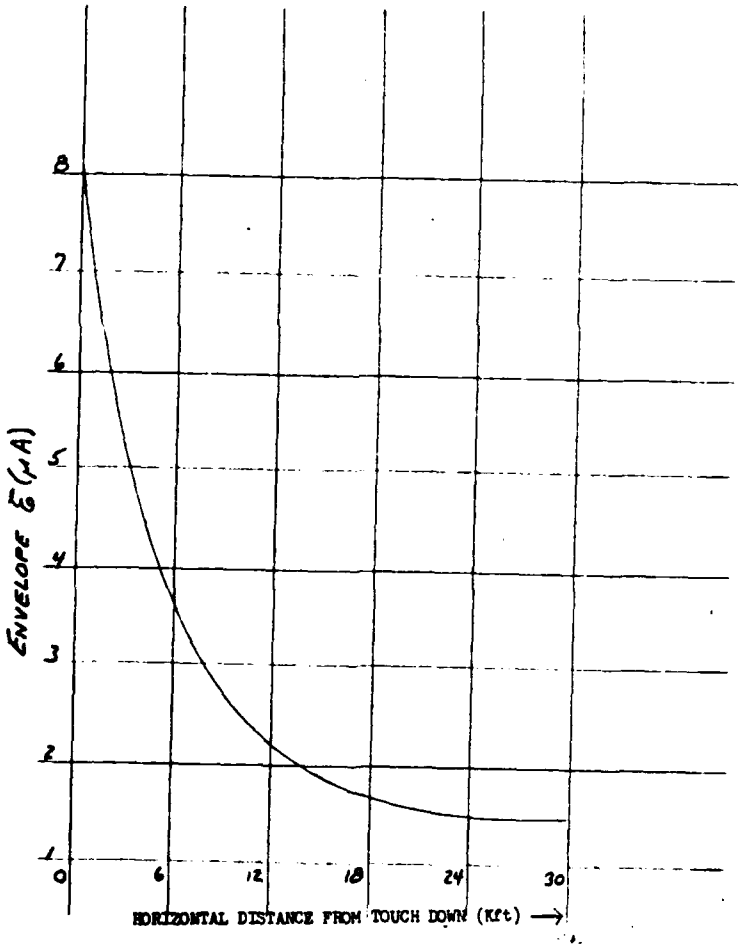

FIGURE A-23. $\mathcal{E}$ VS. HORIZONTAL DISTANCE ALONG GLIDE PATH

Key:

Localizer

X = 1500'

Y = 250'

Z = 36'

φ = 90°

A = 24' } wing approx.

B = 72' }

Z_R = 50'

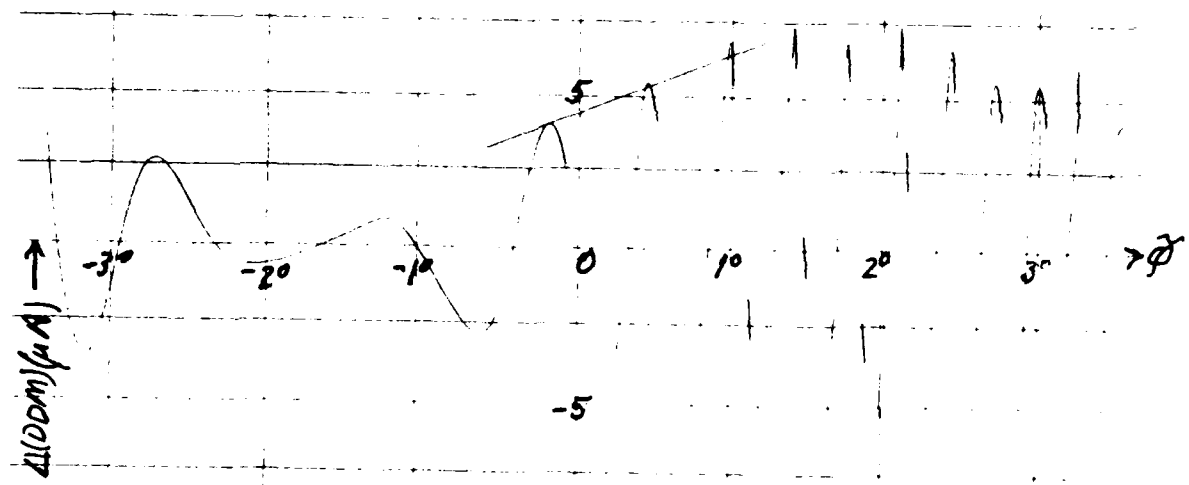

FIGURE A-24. TRANSVERSE VARIATION OF Δ (DDM)

Key:

Localizer

X = 1500'

Y = 250'

Z = 36'

φ = 90°

A = 24' } tail
B = 72' } approx.

Z_R = 50'

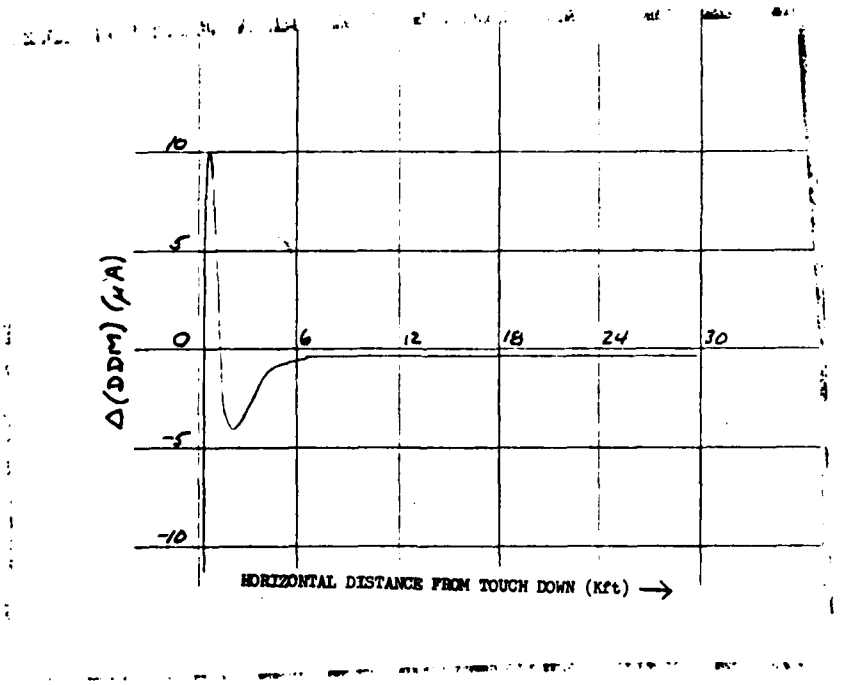

FIGURE A-25. FLIGHT PATH Δ (DDM)

Key:

Localizer

X = 1500'

Y = 250'

Z = 36'

φ = 90°

A = 24' } tail approx.

B = 72' }

Z_R = 50'

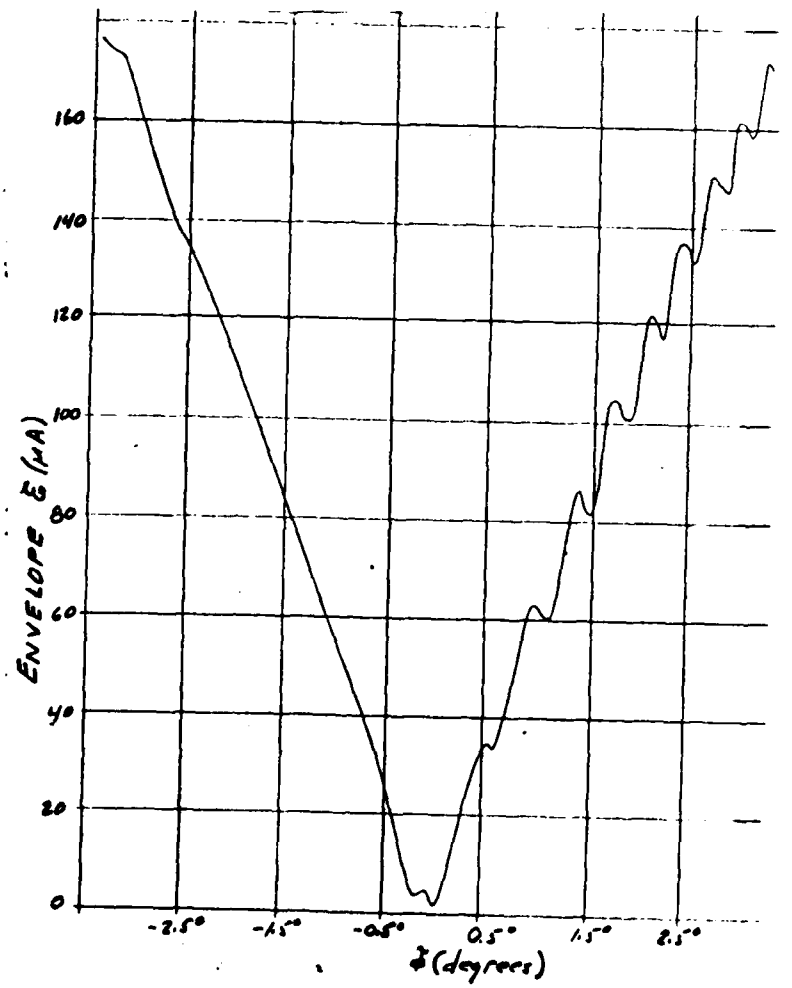

FIGURE A-26. TRANSVERSE VARIATION OF E_φ

Key:

Localizer

X = 1500'

Y = 250'

Z = 36'

$\varphi = 90^{\circ}$

A = 24' } tail
B = 72' } approx.

Z_R = 50'

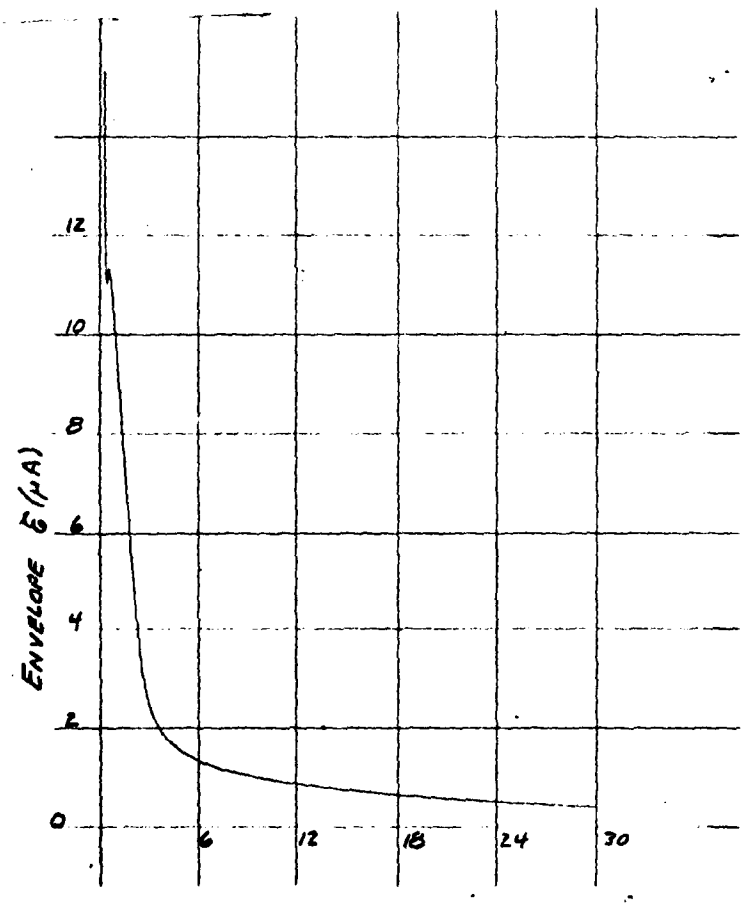

FIGURE A-27. $\mathcal{E}$ VS. HORIZONTAL DISTANCE ALONG GLIDE PATH

Key:

Localizer

X = 8500'

Y = 0

Z = 360'

φ = 90°

ϵ = 60°

A = 195' } wing approx.

B = 60' }

Z_R = 25'

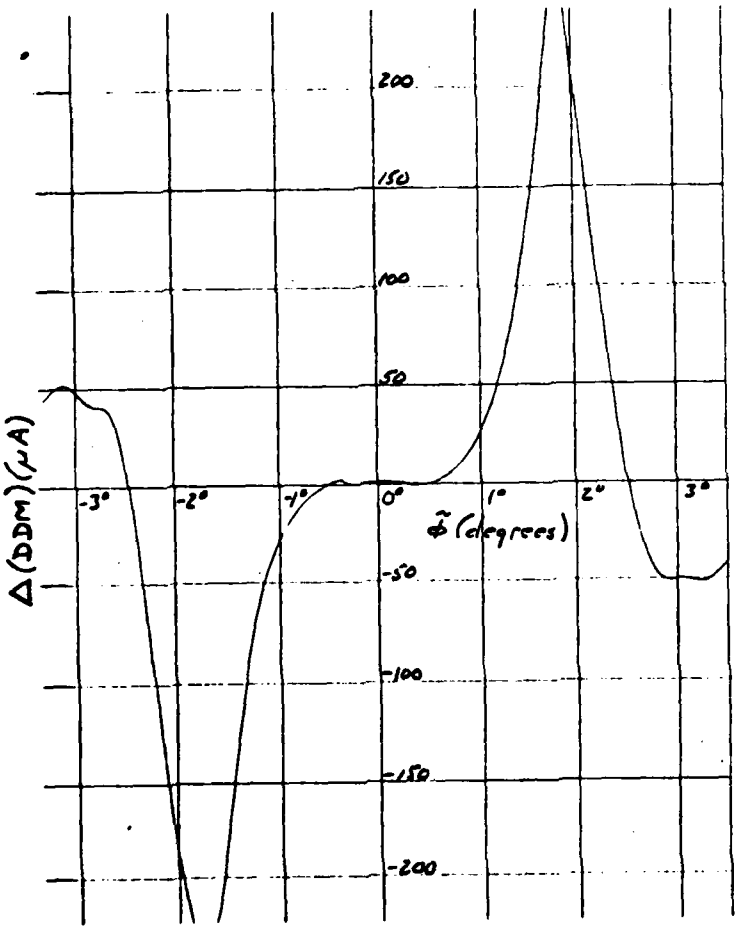

FIGURE A-28. TRANSVERSE VARIATION OF Δ (DDM) (FLYOVER)

Key:

Localizer

$X = 8500'$

$Y = 0$

$Z = 360'$

$\varphi = 90^{\circ}$

$\varepsilon = 60^{\circ}$

$A = 195'$, $B = 60'$ } wing approx.

$Y_R = 25'$

$Z_R = X_R \tan 3^{\circ}$

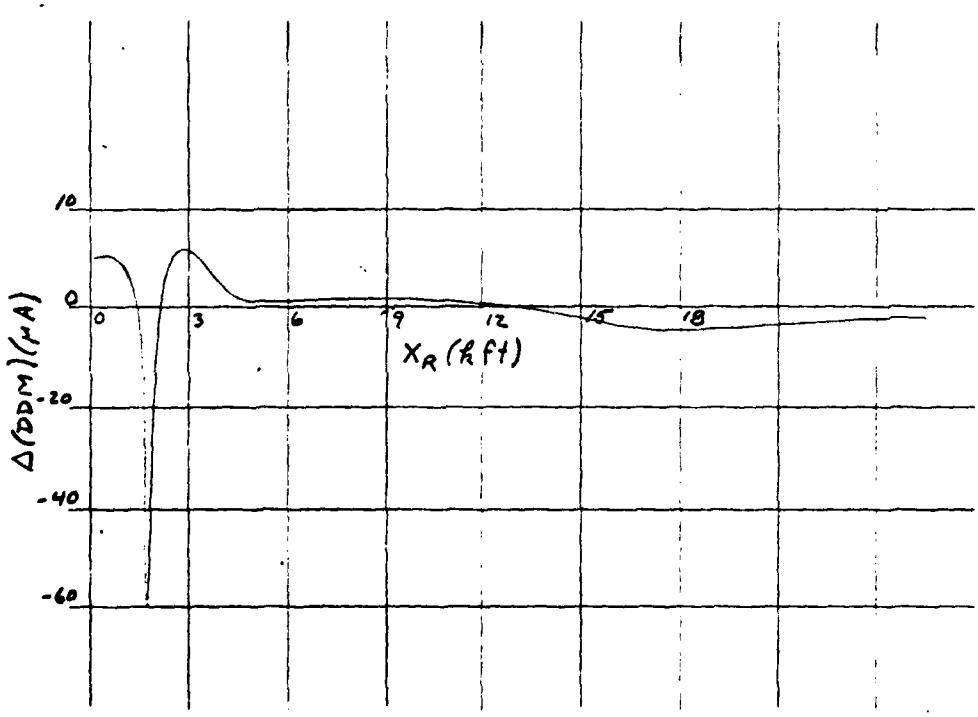

FIGURE A-29. FLIGHT PATH Δ (DDM) (FLYOVER)

Key:

Localizer

X = 8500'

Y = 0

Z = 360'

$\varphi = 90^{\circ}$

$\varepsilon = 60^{\circ}$

A = 195' } wing
B = 60' } approx.

$Z_R = 25'$

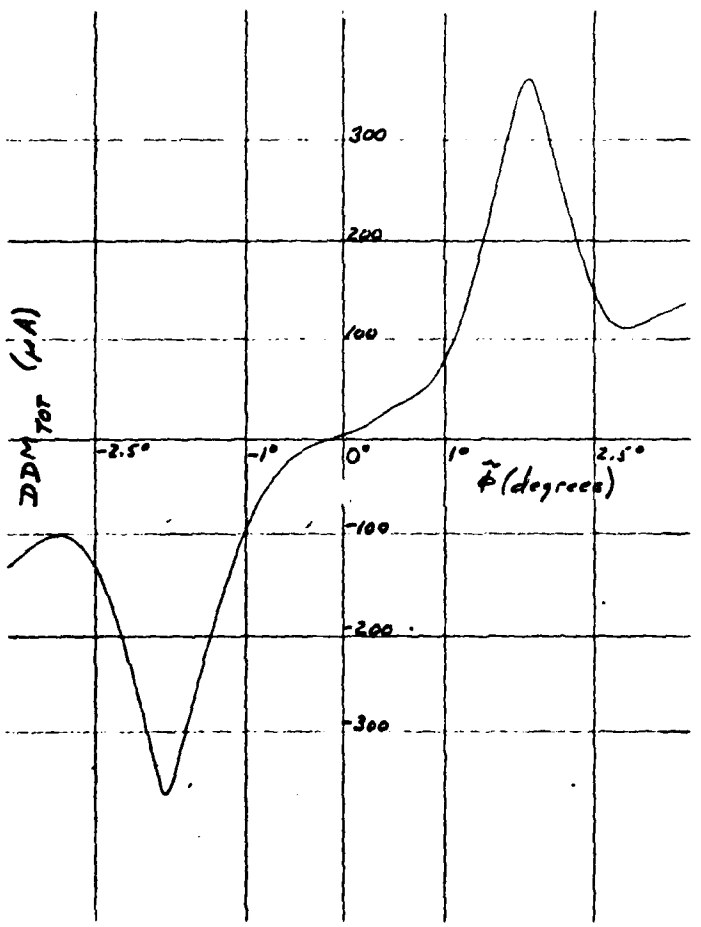

FIGURE A-30. TRANSVERSE VARIATION OF DDM_{TOT} (FLYOVER)

Key:

Localizer

$X = 8500'$

$Y = 200'$

$Z = 360'$

$\varphi = 90^{\circ}$

$\epsilon = 60^{\circ}$

$A = 195'$ } wing
$B = 60'$ } approx.

$Y_R = 0$

$Z_R = X_R \tan 3^{\circ}$

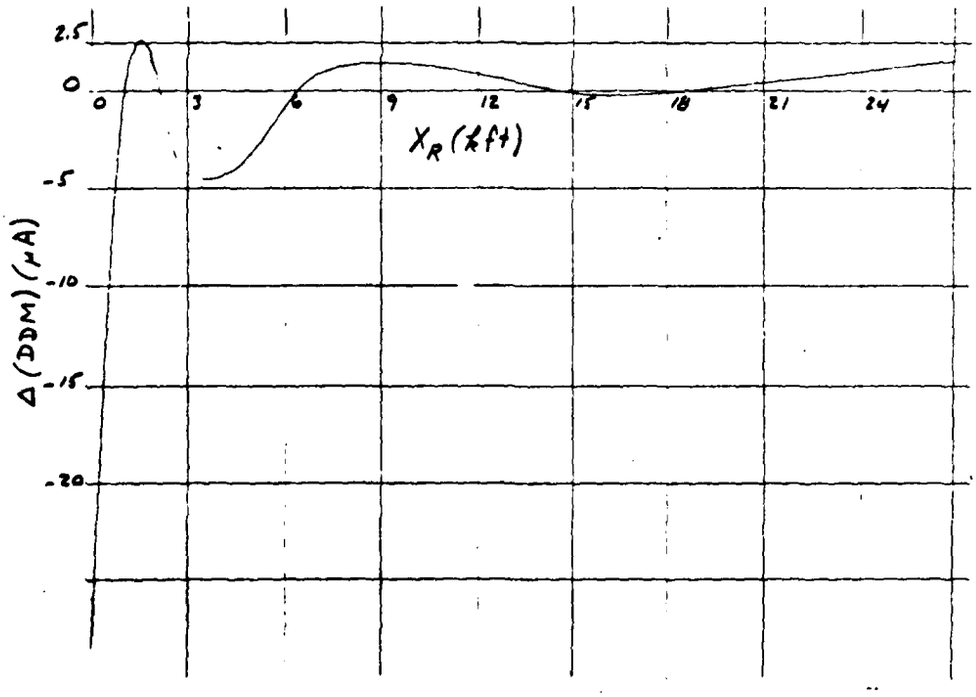

FIGURE A-31. FLIGHT PATH Δ (DDM) (FLYOVER)

Key:

Localizer

$X = 9000'$

$Y = 0$

$Z = 360'$

$\varphi = 80^{\circ}$

$\varepsilon = 60^{\circ}$

$\chi = 10^{\circ}$

$A = 195'$ } wing approx.

$B = 60'$ }

$X_R = -3000'$

$Y_R = 0$

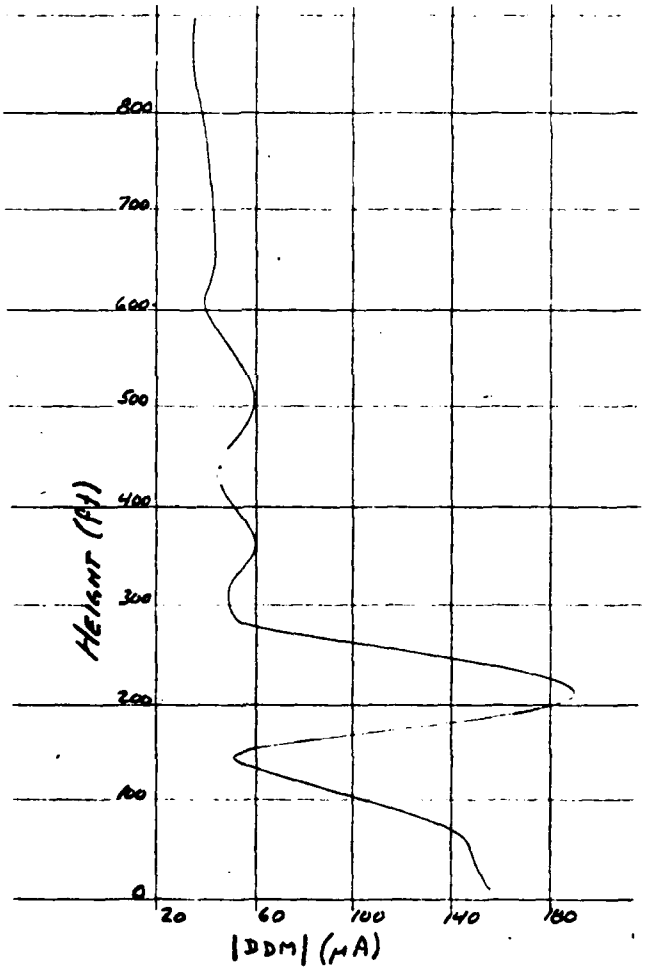

FIGURE A-32. VERTICAL VARIATION OF 180 $\left|\frac{SBO}{CSB}\right|$ (FLYOVER)

Key:

Localizer

$X = 9000'$

$Y = 150'$

$Z = 360'$

$\varphi = 80^{\circ}$

$\epsilon = 60^{\circ}$

$\chi = 10^{\circ}$

$A = 195'$ } wing approx.

$B = 60'$ }

$X_R = -3000'$

$Y_R = 0$

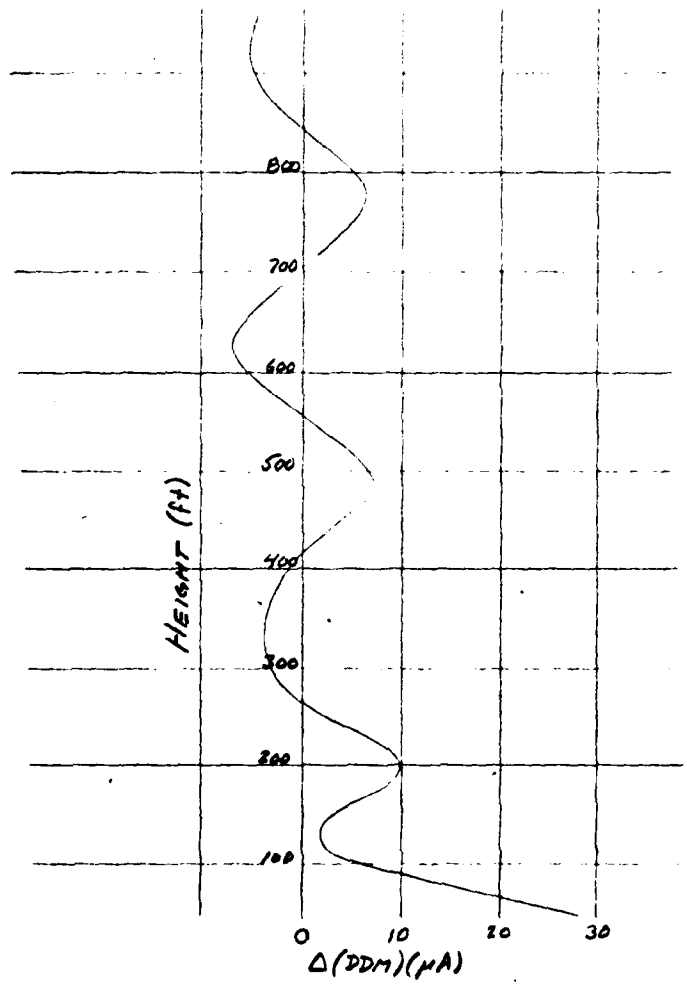

FIGURE A-33. VERTICAL VARIATION OF Δ (DDM) (FLYOVER)

Key:

Localizer

X = 9000'

Y = 0

Z = 360'

φ = 80°

$\mathfrak{E}$ = 60°

χ = 10°

A = 195' } wing approx.

B = 60' }

X_R = -3000'

Y_R = 0

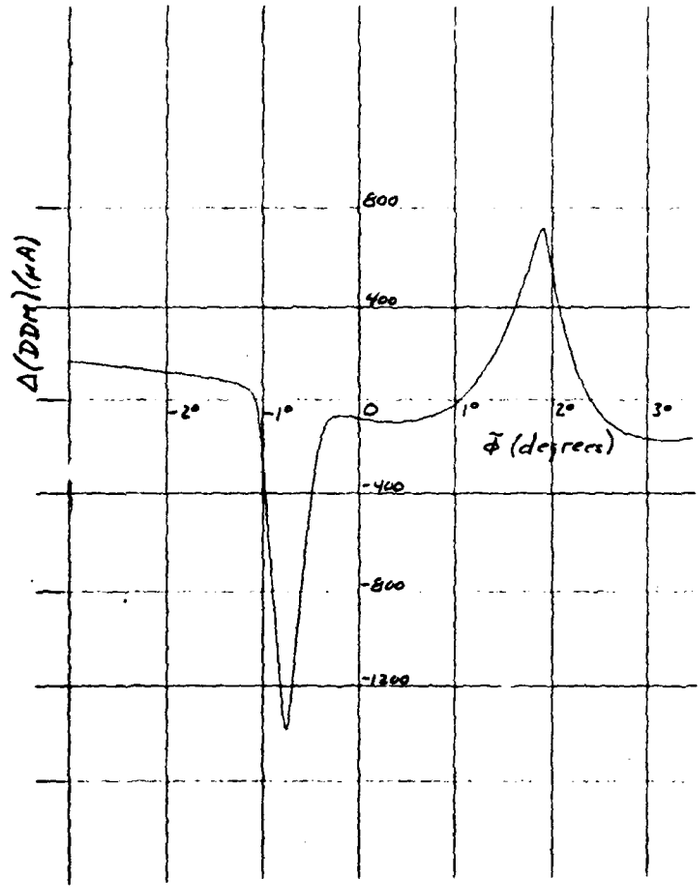

FIGURE A-34. TRANSVERSE Δ (DDM) (FLYOVER)

Key:

Localizer

$X = 9000'$

$Y = 0$

$Z = 360'$

$\varphi = 75^{\circ}$

$\varepsilon = 60^{\circ}$

$\chi = 15^{\circ}$

$A = 195'$ } wing approx.

$B = 60'$ }

$X_R = -3000'$

$Y_R = 0$

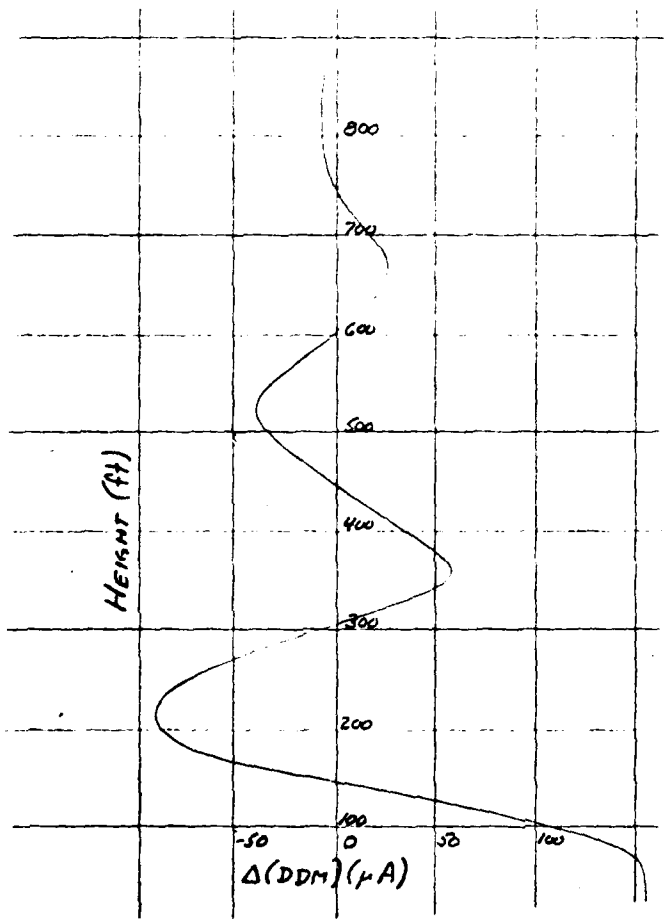

FIGURE A-35. VERTICAL VARIATION OF Δ (DDM) (FLYOVER)

Key:

Localizer

$X = 9000'$

$Y = 0$

$Z = 360'$

$\varphi = 80^{\circ}$

$\varepsilon = 60^{\circ}$

$\chi = 10^{\circ}$

$A = 195'$ } wing approx.

$B = 60'$ }

$X_R = -3000^{\circ}$

$Y_R = 0$

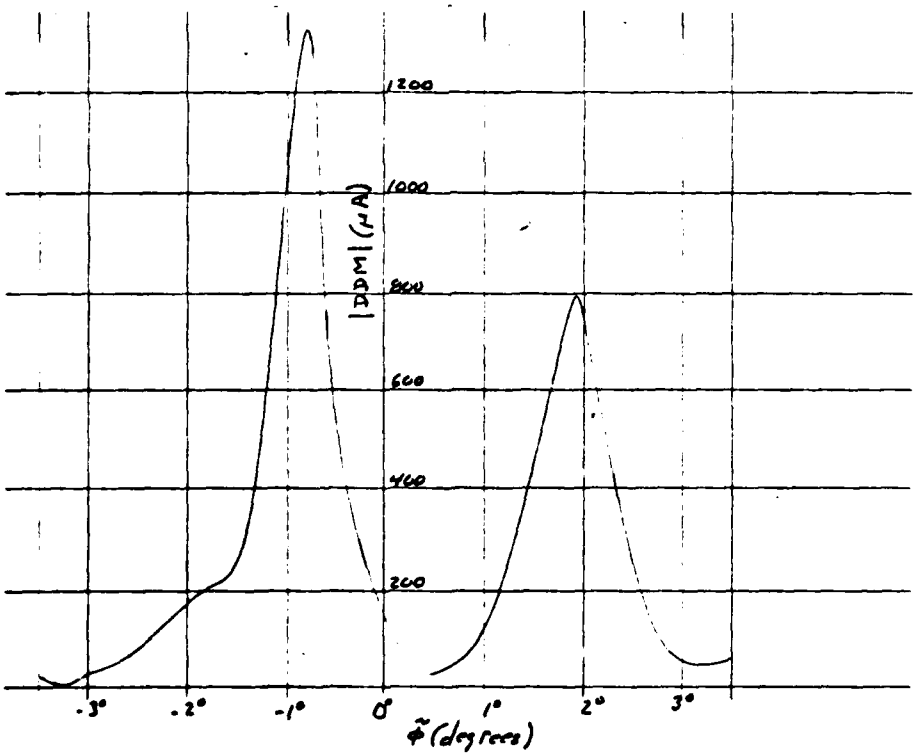

FIGURE A-36. TRANSVERSE VARIATION OF (DDM) (FLYOVER)

Key:

Localizer

$X = 9000'$

$Y = 0$

$Z = 360'$

$\varphi = 80^{\circ}$

$\varepsilon = 60^{\circ}$

$\chi = 10^{\circ}$

$A = 195'$, $B = 60'$ } wing approx.

$X_R = -3000'$

$Y_R = 0$

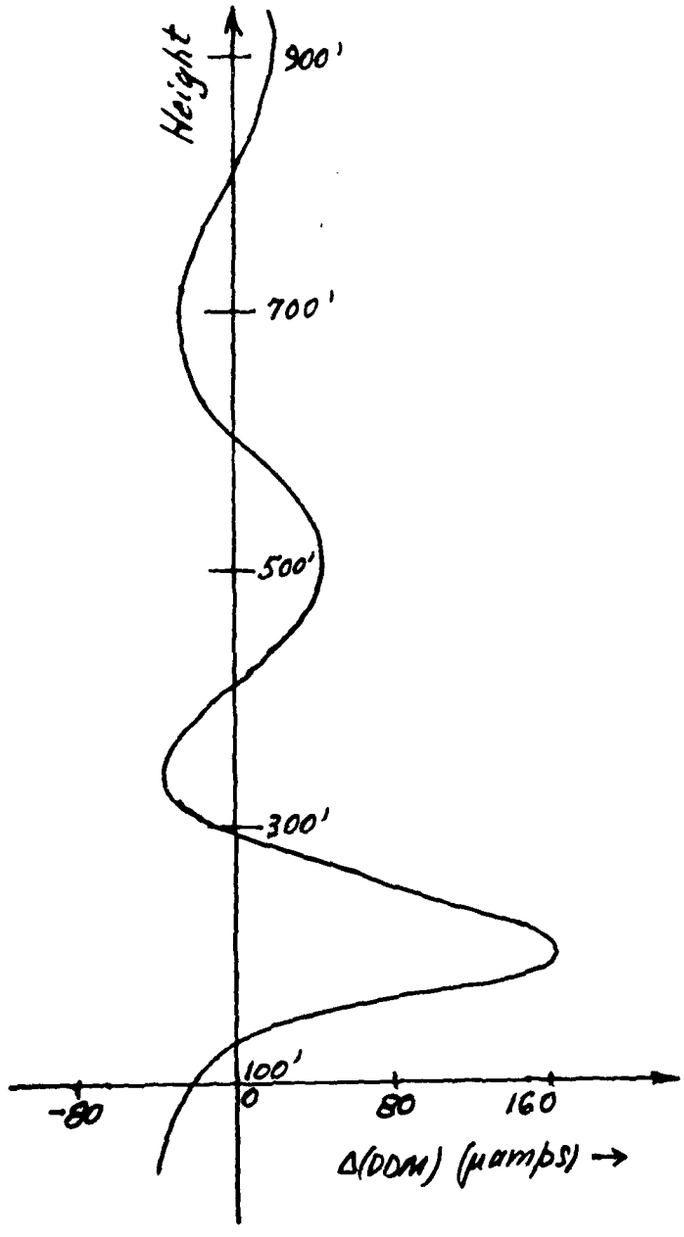

FIGURE A-37.

VERTICAL VARIATION OF Δ (DDM) (FLYOVER)

Key:

Localizer

$X = 9000'$

$Y = 0$

$Z = 360'$

$\phi = 80^{\circ}$

$\varepsilon = 60^{\circ}$

$\chi = 10^{\circ}$

$A = 195'$, $B = 60'$ } wing approx.

$Y_R = 0$

$Z_R = X_R \sin 3^{\circ}$

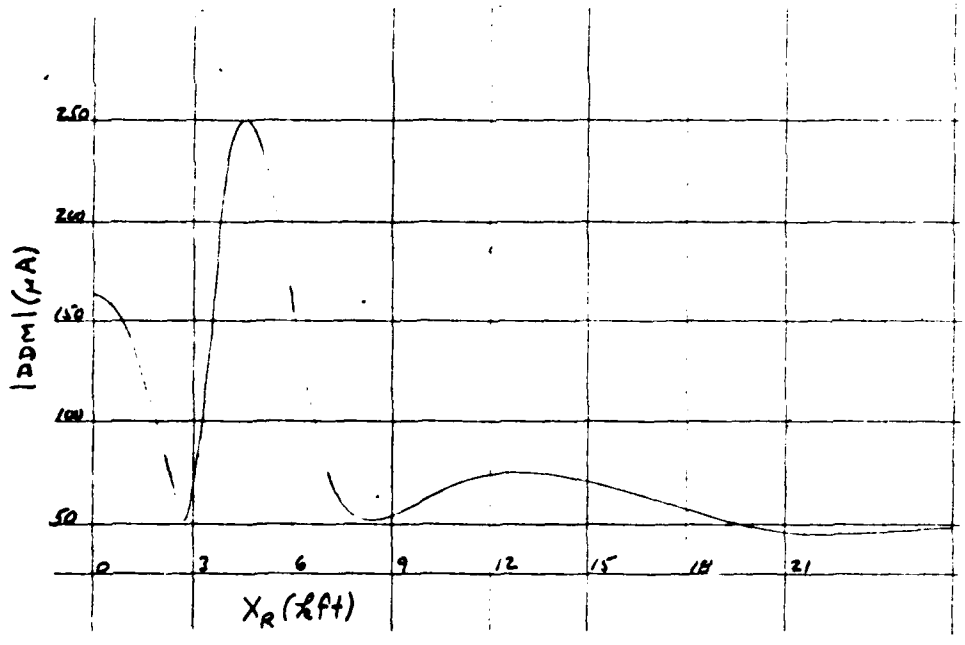

FIGURE A-38. |DDM| (FLYOVER)

Key:

L Localizer

$X = 9000'$

$Y = 0$

$Z = 360'$

$\varphi = 80'$

$\epsilon = 60^{\circ}$

$\chi = 10^{\circ}$

$A = 195'$, $B = 60'$ } wing approx.

$Y_R = 0$

$Z_R = X_R \sin 3^{\circ}$

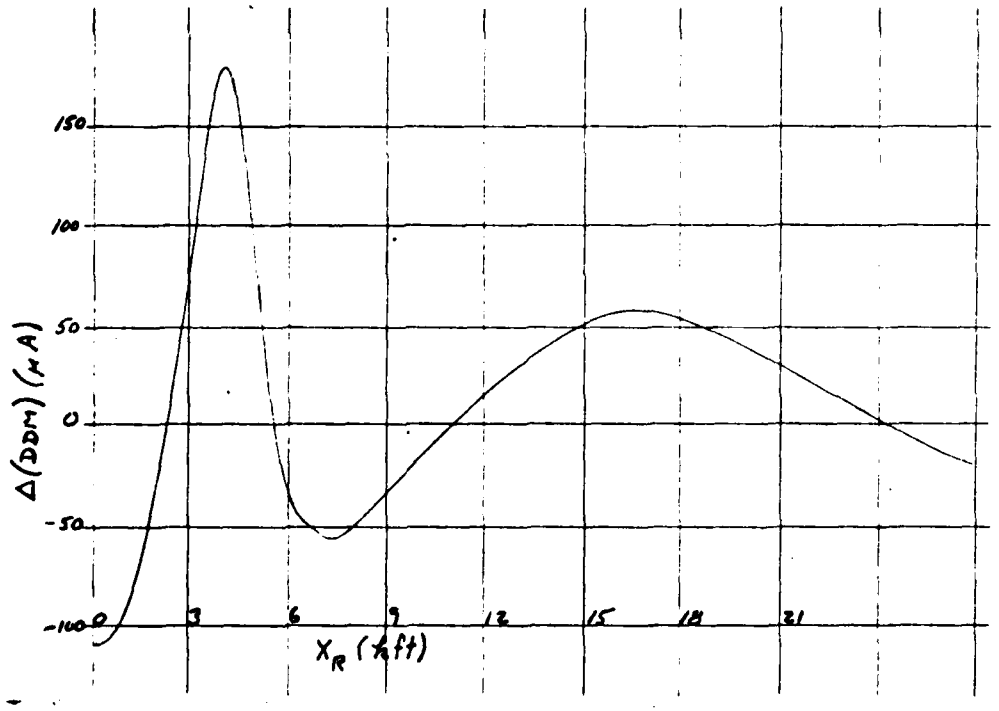

FIGURE A-39. FLIGHT PATH Δ (DDM) (FLYOVER)

Key:

Glide Slope

Null Reference (300', 3°

X = 1000'

Y = 240'

Z = 36'

φ = 90°

A = 24' } tail
B = 72' } approx.

Y_R = 0

RR = 5000'

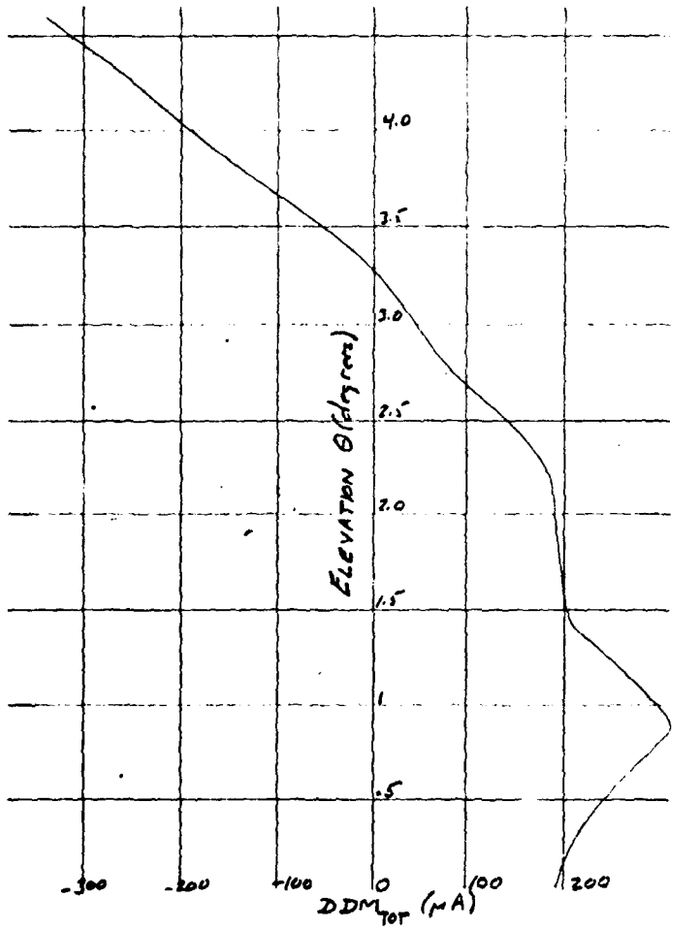

FIGURE A-40. DIM_{TOT} VS. ELEVATION

Key:

Glide Slope

Null Reference (300', 3°)

X = 1000'

Y = 240'

Z = 36'

φ = 90°

A = 24' } tail approx.

B = 72' }

Y_R = 0

RR = 5000'

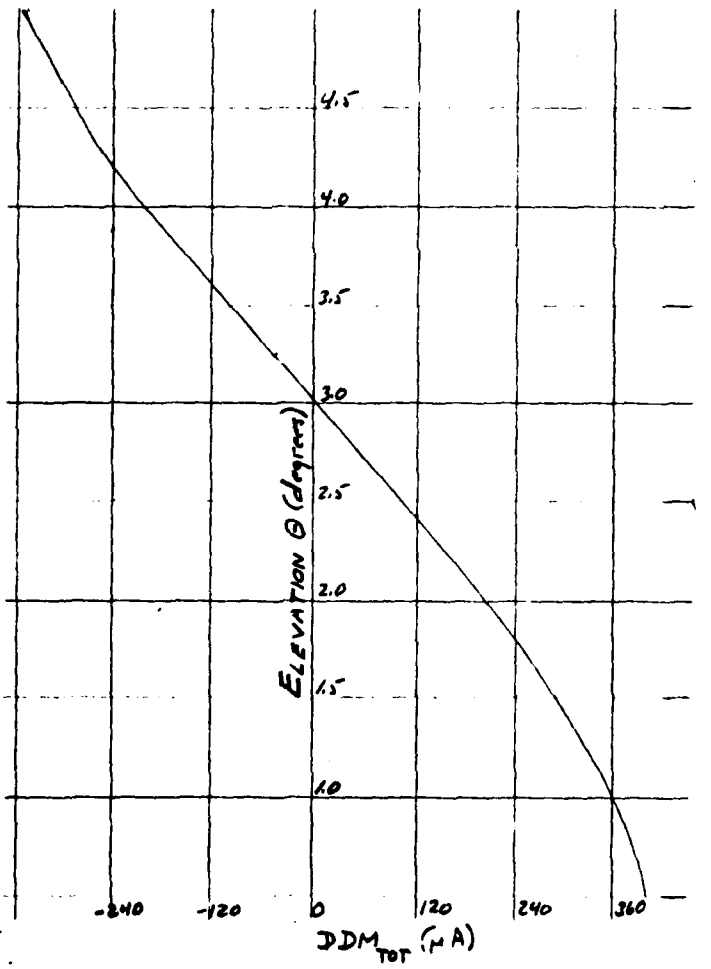

FIGURE A-41. DDM_Δ VS. ELEVATION

Key:

Glide Slope

Null Reference (300', 3°)

X = 1000'

Y = 75'

Z = 36'

φ = 90°

A = 24' } tail approx.

B = 72' }

Y_R = 0

RR = 5000'

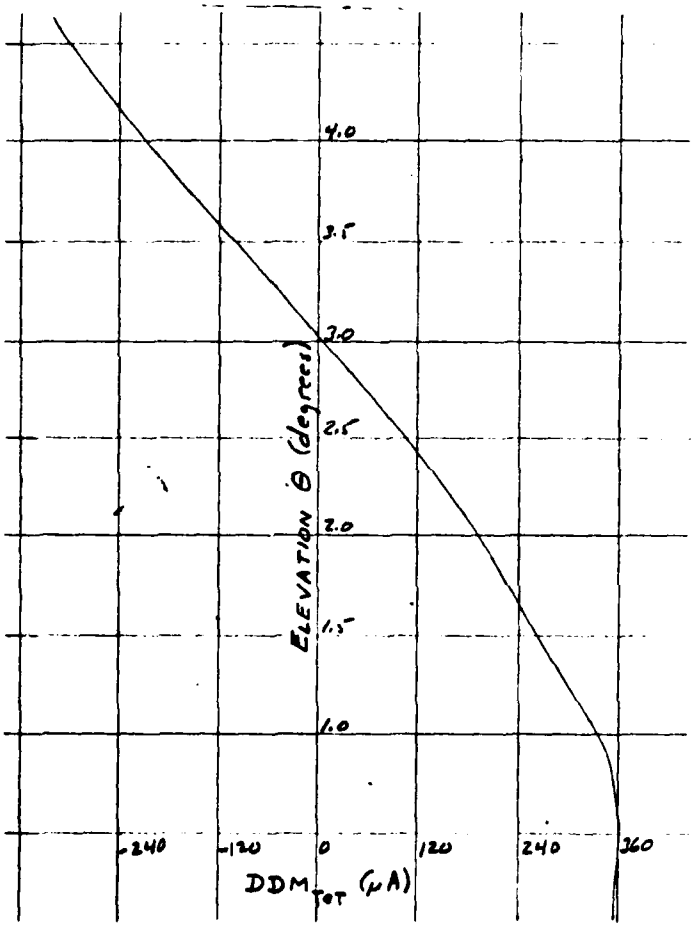

FIGURE A-42. DDM_{TOT} VS. ELEVATION

Key:

Glide Slope

Null Reference (300', 3°)

X = 1000'

Y = 240'

Z = 36'

φ = 90°

A = 24' } tail approx.

B = 72' }

$Y_R = 0$

$Z_R = X_R \tan 3^\circ$

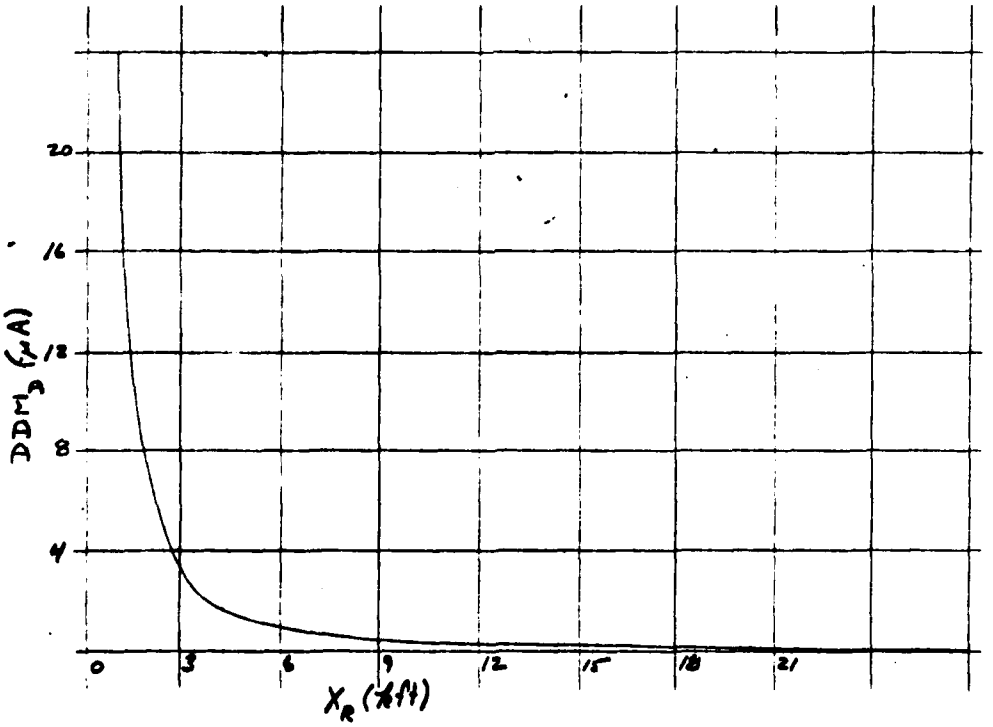

FIGURE A-43. FLIGHT PATH DDM_D

Key:

Glide Slope

Null Reference

X = 1000'

Y = 240'

Z = 36'

φ 90°

A = 24' } tail approx.

B = 72' }

Y_R = 0

RR = 5000'

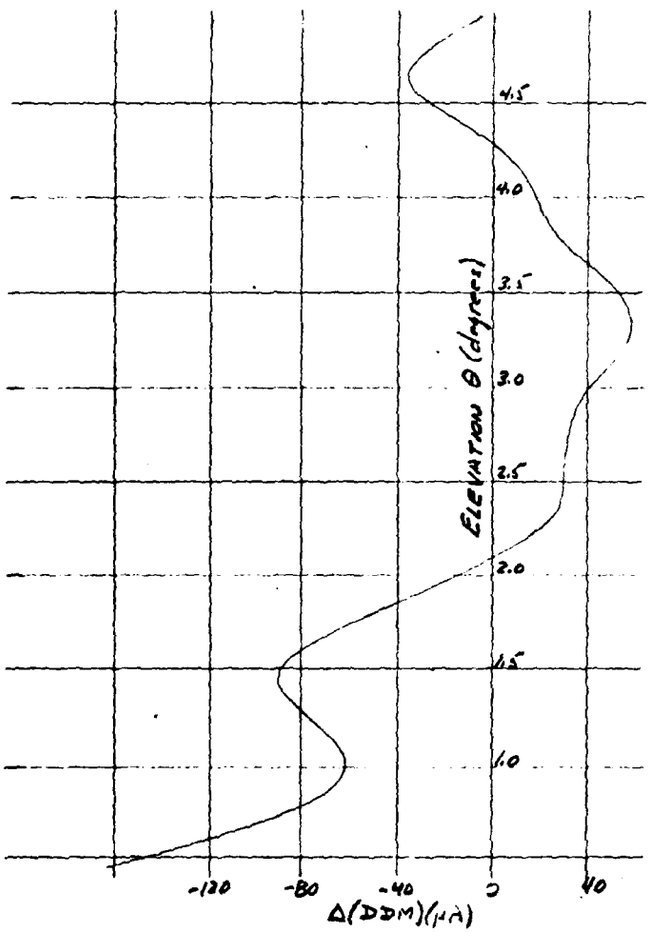

FIGURE A-44. Δ (DDM) VS. ELEVATION

Key:

Glide Slope

Null Reference (300', 3°)

X = 1000'

Y = 75'

Z = 36'

φ = 90°

A = 24' } tail approx.

B = 72' }

Y_R = 0

RR = 5000'

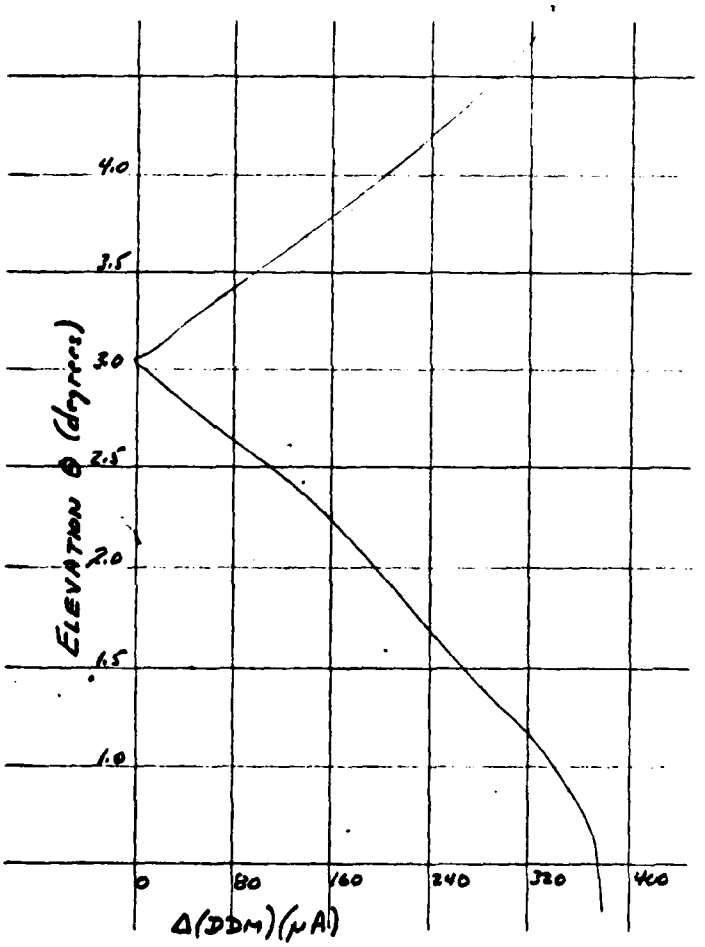

FIGURE A-45. VDDM VS. ELEVATION

Key:

Glide Slope

Null Reference (300', 3°)

X = 1000'

Y = 75'

Z = 36'

φ = 90°

A = 24' } tail approx.

B = 72' }

X_R = -5000 sin 3°

Z_R = 25'

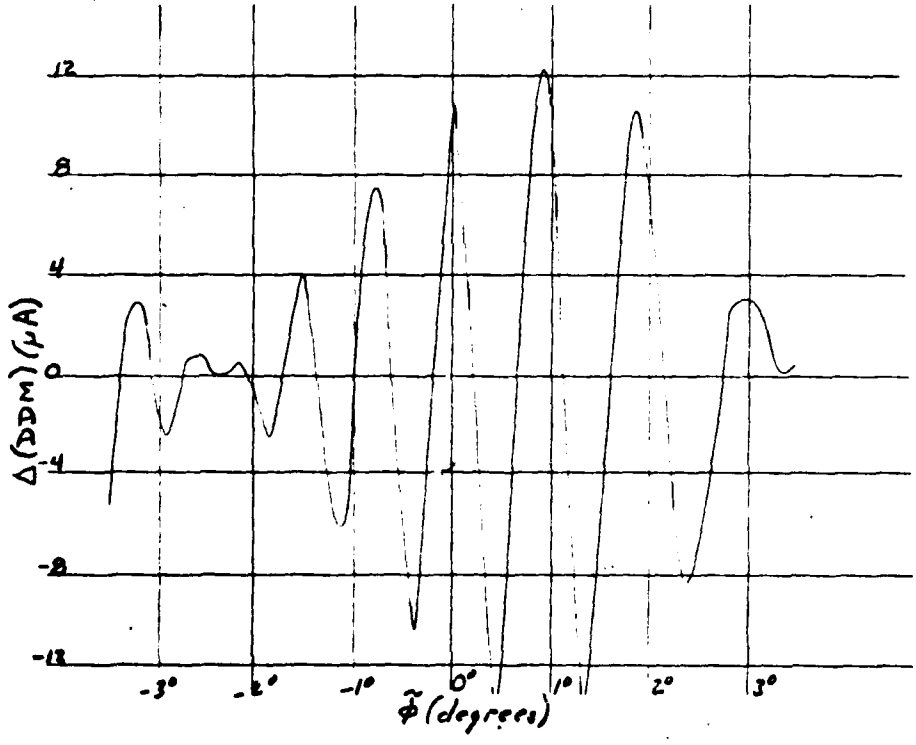

FIGURE A-46. TRANSVERSE VARIATION OF Δ (DDM)

Key:

Glide Slope

Null Reference (300', 3°)

X = 1000

Y = 75'

Z = 36'

φ = 90°

A = 24' } tail
B = 72' } approx.

Y_R = 0

Z_R X_R tan 3°

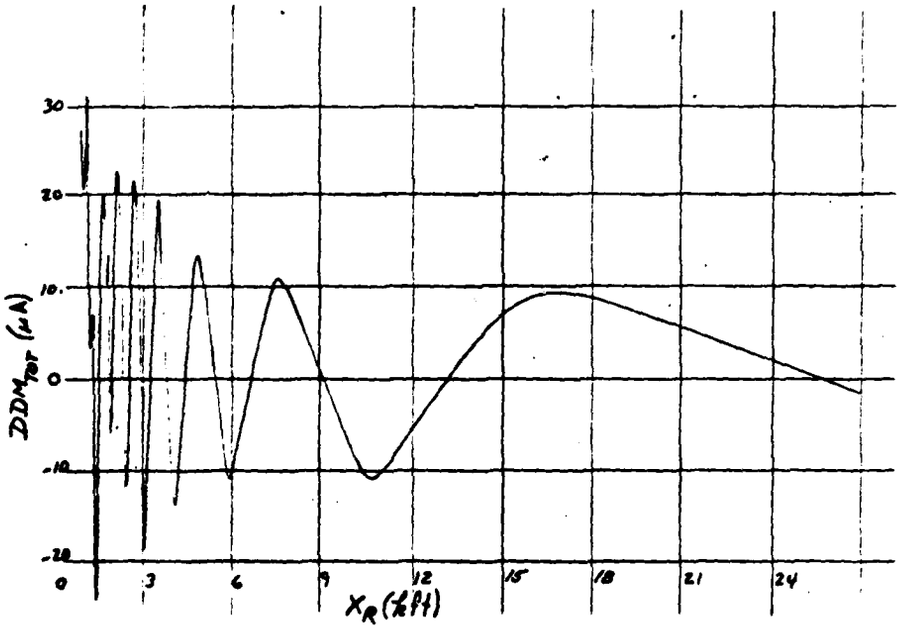

FIGURE A-47. FLIGHT PATH DDM_{TOT}

Key:

Glide Slope

Null Reference (300', 3°)

X = 1000'

Y = 75'

Z = 36'

φ = 90°

A = 24' } tail
B = 72' } approx.

X_R = -2500'

Z_R = 25'

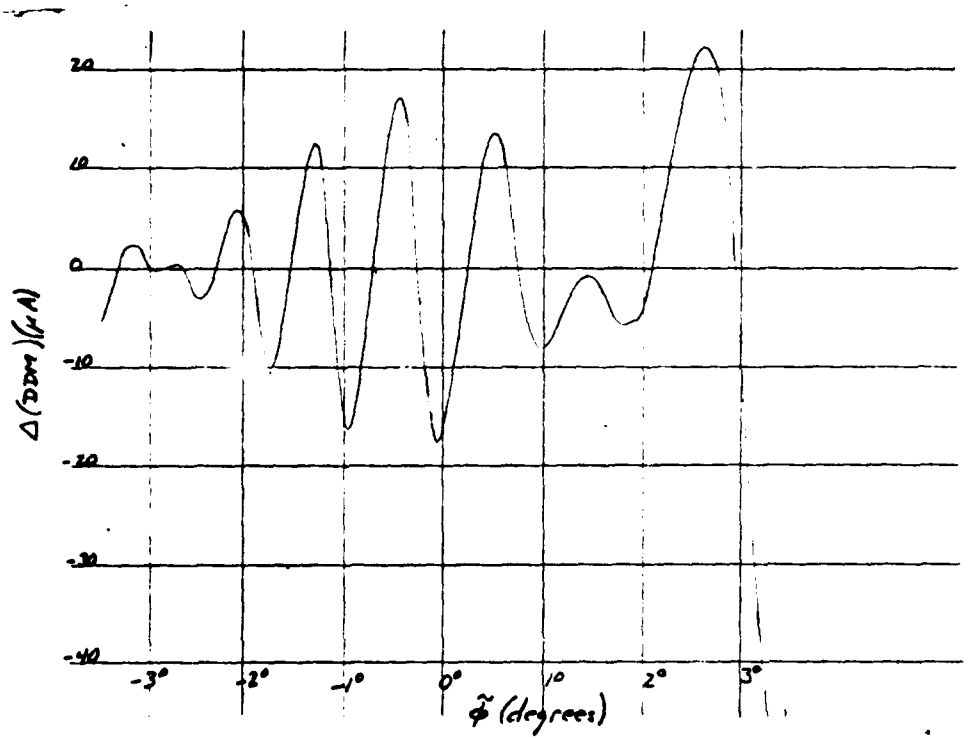

FIGURE A-48. TRANSVERSE VARIATION OF Δ (DDM)

Key:

Glide Slope

Null Reference (300', 3°)

X = 1000'

Y = 75'

Z = 36'

φ = 90°

A = 24' } tail approx.

B = 72' }

$X_R = -10^4 \cdot \sin 3°$

Z_R = 25'

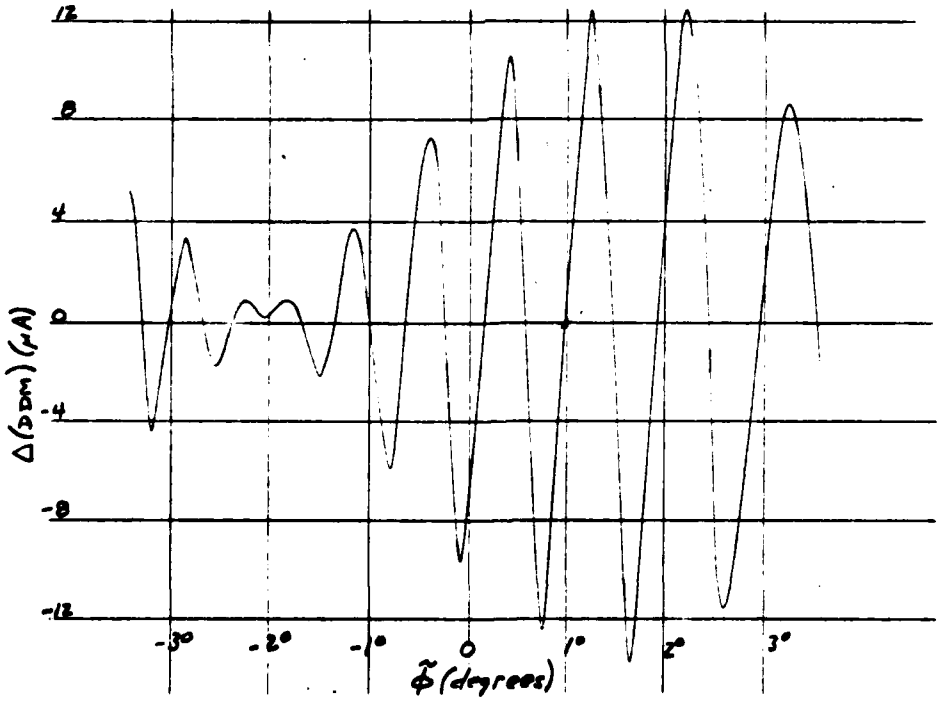

FIGURE A-49. TRANSVERSE VARIATION OF Δ (DDM)

Key:

Localizer

X = 8500'

Y = 260'

Z = 36'

φ = 90°

A = 24' } tail approx.

B = 72' }

Z_R = 25'

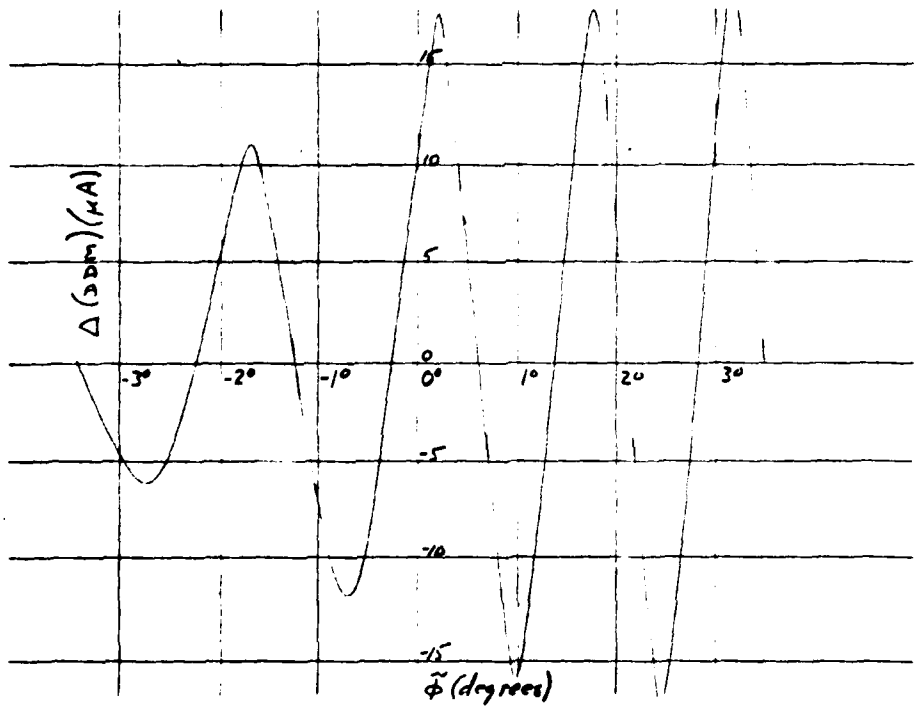

FIGURE A-50. TRANSVERSE VARIATION OF Δ (DDM)

APPENDIX B

EXPERIMENTAL PROCEDURE

Experimental investigations were carried out in two distinct areas. The first, included model range measurements of interference patterns for model aircraft, profiles and rectangular sheets. This avenue was pursued to illustrate the fact that the diffraction produced by aircraft can be approximated by that produced by a rectangular flat sheet. This fact enabled a radical simplification in the computer modeling of diffraction patterns and, hence, allowed for a more exhaustive computer analysis of scattering phenomena. The second area of experimental investigation involved full scale tests carried out at Stansted, England. Although they were pursued for the interferometric method only, it is felt that these experimental results support the vector monitor as well since the essential verification was that of a phase independent monitor able to detect derogation resulting from scatterers located anywhere on the airport.

B.1 Model Range Measurements.

B.1.1 Method of Measurement.

To ascertain that no rogue scatterer would contribute to the patterns to be measured and also as a check on the performance of the equipment the receiver was first made to scan the environment with no known object present between the receiver and the transmitter. The clear site response is shown dotted in the results and shows only the amplitude variation expected from the equipment over the angle of scan.

A 100th scale model (an early prototype of the C5A) was then placed on the site such that its tail fin/rudder was central about the range center line with the body of the aircraft normal to the center line-see Figure B-1. The side was carefully marked to record the location of the model aircraft and the receiving equipment made to transverse scan the environment. The resultant interference pattern due to the scattering by diffraction is shown in Figure B-2 (d).

The model aircraft was then removed, and a full flat sheet profile was carefully positioned on the site in the same position as the model aircraft. The resultant pattern recorded is shown in Figure B-2 (c).

The full flat sheet profile was then divided, and only that part of the profile representing the tail fin/rudder was allowed to remain on the site. The resultant pattern recorded is shown in Figure B-2 (b).

The tail-fin/rudder profile was then removed and the part of the profile representing the body of the aircraft was carefully repositioned on the site. The resultant pattern recorded is shown in Figure B-2 (a).

The body only profile was then removed and the interference patterns resulting from two rectangular flat sheets were recorded. Each of the sheets were of the same height as the tail fin/rudder of the model aircraft (0.645 ft. representing a full scale height of 64.5 ft.). The first sheet was 0.2 ft. wide (20 ft. full scale) and the interference pattern recorded is shown in Figure B-2 (e). The second sheet was 0.25 ft. wide (25 ft. full scale) and its interference pattern is shown in Figure B-2 (f).

B.1.2 Interference Patterns

All the interference patterns obtained are shown together for ease of comparison. The horizontal scale gives the transverse position of the

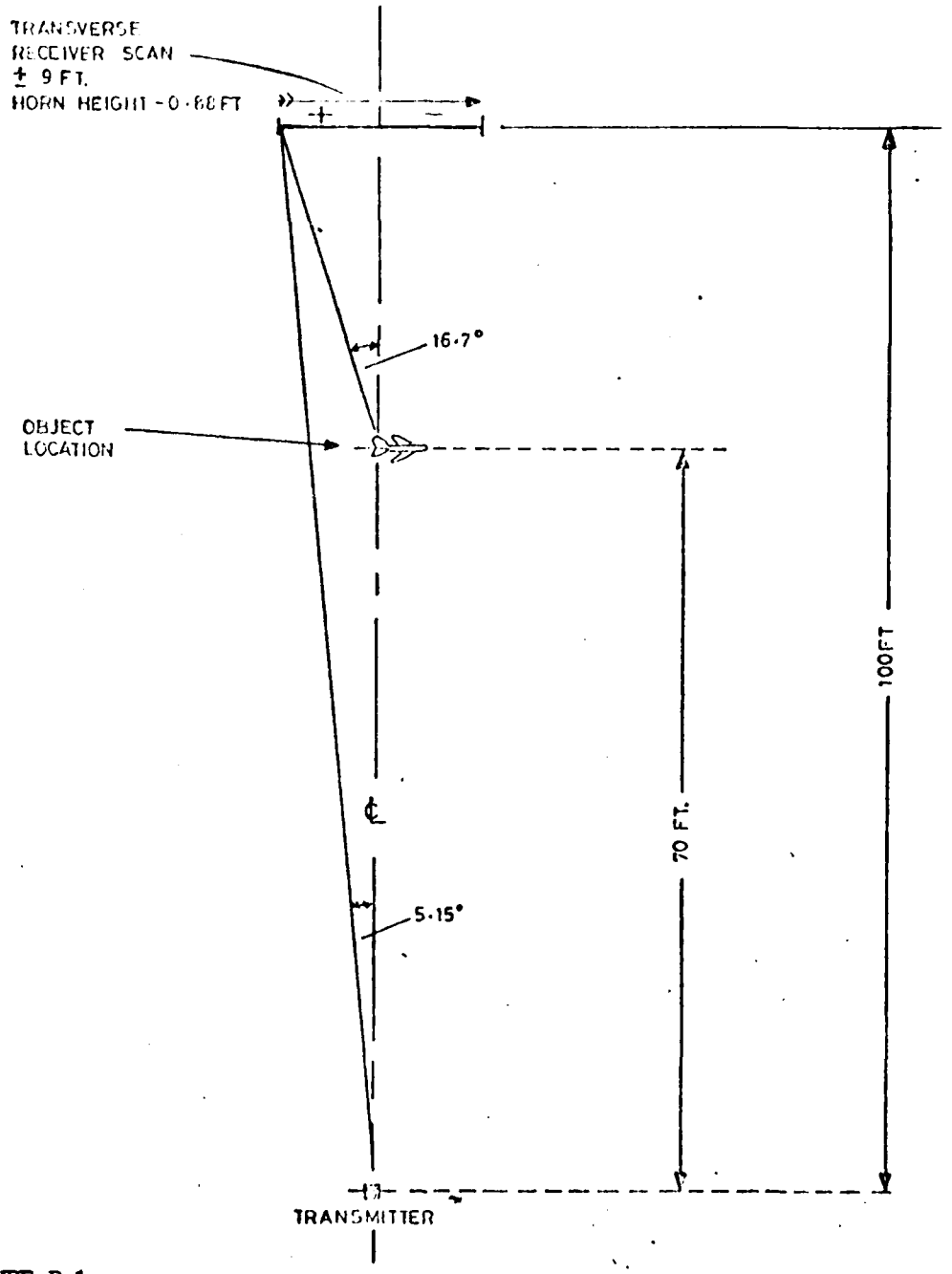

FIGURE B-1.

GEOMETRY FOR INTERFERENCE MEASUREMENTS FROM MODEL AIRCRAFT, PROFILES AND RECTANGULAR SHEETS

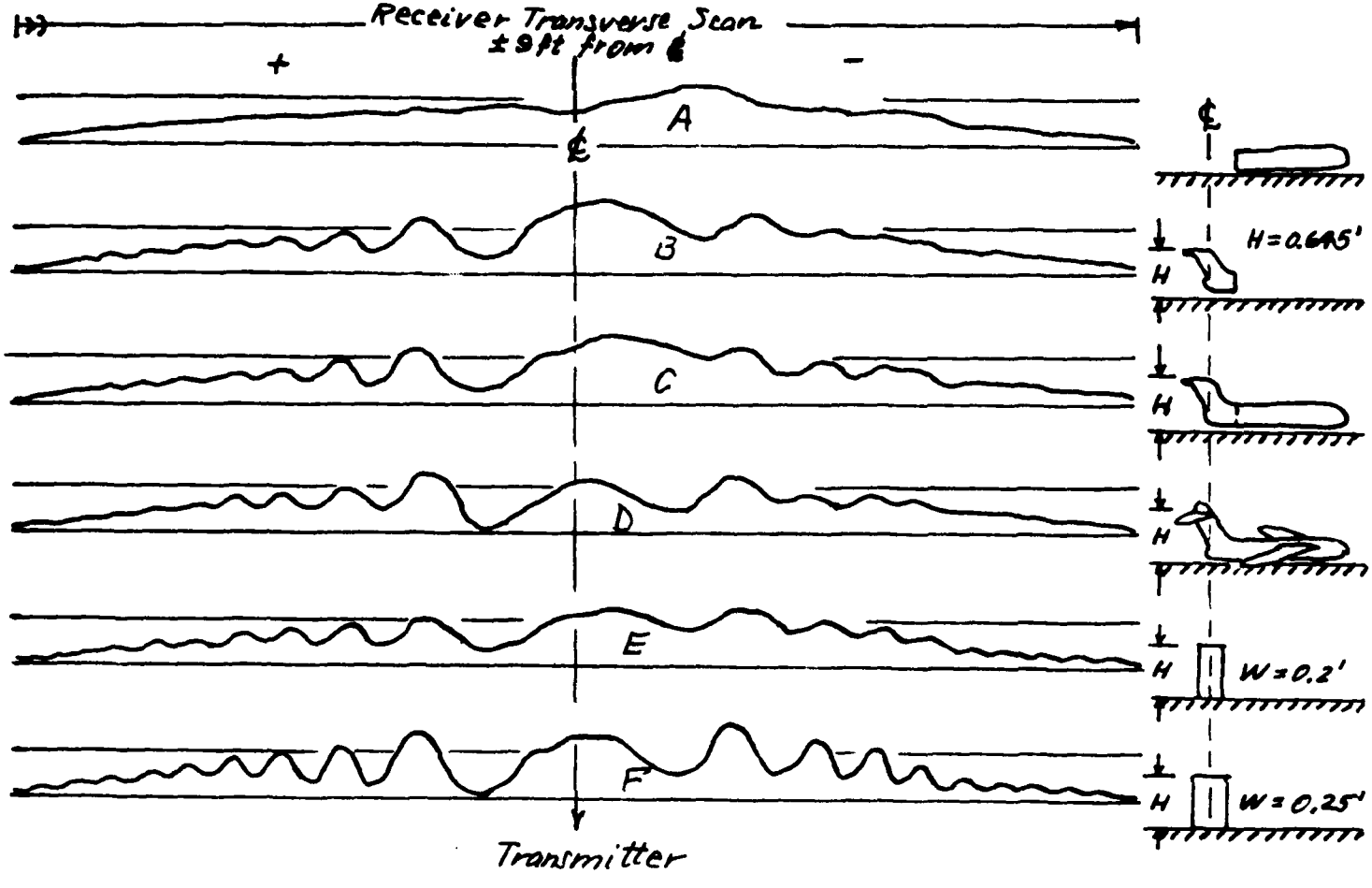

FIGURE B-2.
MODEL-SITE INTERFERENCE FOR MODEL AIRCRAFT, PROFILES AND RECTANGULAR SCREEN

receiving equipment and the point on the scale where the receiver was exactly on the model range center line is indicated. The vertical scale gives the relative amplitude of the received signal with the heavy scale markings representing 1 dB change in amplitude. The clear site response is shown dotted on each recording to emphasize the effect of the various objects.

B.1.2.1 Representation of Model Aircraft by Flat Sheet Profile.

The interference pattern obtained with the model aircraft (Figure B-2 (d)) and that obtained with the full flat sheet profile (Figure B-2 (c)) show the excursion of the received signal to be similar particularly away from the center line. It will be noted that both patterns show a slight lack of symmetry due to the non-symmetrical characteristics of the diffracting scatterer.

Examination of the interference patterns due to the two main constituent parts in isolation ((a)-body only and (b)-tail-fin/rudder only) shows that the major contributor of interference is the taller tail-fin/rudder part of the object. The non-symmetry of the full object is clearly indicated in the two patterns; the interference due to the body only appears mainly behind the object on the side of the center line, whereas the interference due to the tail only is apparent over a much greater part of the transverse scan and is virtually symmetrical about the center line.

When added, the interference pattern (a) (body only) and pattern (b) (tail-fin/rudder only) gives almost exactly the pattern recorded for the full profile (c).

B.1.2.2 Representation of Model Aircraft by Rectangular Sheet.

With the rectangular sheets placed on the center line the expected symmetrical interference patterns are shown in (e) and (f). Pattern (e)

shows close correspondence with the pattern obtained with the three dimensional model aircraft (d) except perhaps over a small length of size immediately behind the object about the center line.

Flat sheet (f) gives a closer approximation to the effect about the center line but produces a greater scattered signal at wider angles.

B.1.3 Experimental Results of Scale Model Range Measurements

The Scale Model operates at 10.5 GHz which represents a 100:1 scaling factor for VHF ILS localizer studies. The facility is set up on a level area of tarmac of 30m x 100m (equivalent to 10000ft x 30000ft). At one end the transmitting horn is fixed to the ground: the receiving horn is mounted on an electrically driven support structure which enables the horn to be moved transversely (across the centre line) or longitudinally (along the centre line). Optionally the receiving horn may be varied in height to simulate the 3^{o} approach path of an incoming aircraft. The signal level at the receiving horn is plotted on a pen recorder.

In the region between the transmitter and the receiver, scattering objects such as model aircraft, and hangars, etc. may be placed on the ground. The interference pattern produced by such an object is then detected at the receiver as it moves along its programmed track, and is recorded automatically.

During the two exercises reported here, the scatterers were rectangular with a greater height than width. The heights lay in the range 60 ft. - 125 ft. (equivalent full-scale) and the widths 11 ft. - 33 ft. Interference patterns were obtained with the scatterers placed at various positions singly and in pairs, and in one test four scatterers were present.

The computer simulation follows the scalar theory based on the Kirchhoff Diffraction Integral, given in Appendix A. The free-space field scattered from the object is calculated for each of the four propatation paths taking ground reflections into account:

(i) Transmitter - Object - Receiver,

(ii) Transmitter Image - Object - Receiver,

(iii) Transmitter - Object - Receiver Image,

(iv) Transmitter Image - Object - Receiver Image.

With a ground reflection coefficient of -1 attached to the field from each image, the sum of the four resulting fields gives the scattered field at the receiver.

The azimuth polar diagrams of the transmitting and receiving horns are taken into account simply as factors multiplying the calculated field strengths, and the resultant field printed out for each receiver position is the vector sum of the direct field and the scattered fields from the objects placed in the illuminated region.

The two series of test carried out are referred to here as Exercise I and Exercise II. Fig. B-3 shows the layout of the site for Ex. I, and it is seen that the four scatterers were of identical dimensions and placed at four positions. In this case the receiver was scanned laterally along a line 100 ft. from the transmitter. Fig. B-4 shows the layout for Ex. II in which the results are given for one longitudinal run and three lateral runs at different distances. Two of the objects used in this exercise were cylindrical.

Exercises and Results

Exercise I was carried out using four scattering objects A, B, C, D placed singly and in pairs in the positions shown in Fig. B-3. During each run the receiver probe was scanned through 18 ft. laterally along a line 100 ft. from the transmitter. The results obtained with the various scattering configurations are given in Figs. 3-7. On each trace obtained from the pen recorder the corresponding computed interference pattern is drawn for comparison. The total number of runs was nine.

For Exercise II three objects were used at the positions shown in Fig. B-4. At first a longitudinal set of receiver runs was carried out along the centre line beginning and ending 110 ft. and 143 ft. from the transmitter respectively. The object configurations used for this set of six runs were:

(i) Clear Site,

(ii) A only,

(iii) B only,

(iv) C only,

(v) A+B,

(vi) A+C.

Three sets of lateral runs were then carried out at 110, 125 and 140 ft. from the transmitter with a transverse scan of $\pm$ 4 ft. For each set of runs the six configurations listed above were used, and the total number of runs for Ex. II was therefore twenty-four. The results of these runs and the corresponding computer simulations are shown in Figs. 8-13 (longitudinal runs) and 14-19 (transverse runs).

The figures are laid out as follows:

Exercise I

Figure	
3	Computed and Measured - objects A and B
4	" " " - " C and D
5	" " " - " A+B and A+C
6	" " " - " C+D and B+D
7	" " " - " A+B+C+D

Exercise II

Figure	
8	Longitudinal run - Clear Site
9	" " - Object A
10	" " - Object B
11	" " - Object C
12	" " - Objects A+B
13	" " - Objects A+C
14	Transverse run at 110 ft. - Clear site, objects A and B
15	" " " " " - Objects C, A+B, A+C
16	" " " 125 " - Clear site, objects A and B
17	" " " " " - Objects C, A+B, A+C
18	" " " 140 " - Clear site, objects A and B
19	" " " " " - Objects C, A+B, A+C

Conclusions

Examination of the figures reveals a close correlation between computed and measured results for all tests. A slight nonlinearity in the recording

mechanism is noticeable, especially in the longitudinal clear-site run (fig. 8) where the dynamic range of signal level is greatest. In the same figure the short-period fluctuations observed on the experimental trace give an indication of the low level of errors due to roughness of the site surface.

The largest discrepancy arises in the transverse runs carried out at a range of 140 ft. from the transmitter. These results are given in Figs. 18 and 19, and the dual-object cases show the greatest discrepancies. In view of the short wavelength used (1 inch) the errors are considered to be due to inaccuracies in the precise location of the objects, since very small displacemnts in the dimensions of the site can lead to noticeable changes in the phases of the contributing scattered field. The resulting received field, which is the vector sum of the direct signal and the individual scattered fields, is evidently sensitive to these small perturbations.

Some estimate of the effect of positional errors may be made by reference to Fig. 20, which gives computed interference patterns for objects A + B and A + C displaced outwards from the centre line by 0.02 ft. These should be compared with the corresponding computed patterns in Fig. 19. It may be seen that the alterations produced in the computed patterns by moving the objects ½ inch are of a similar magintude to the discrepancy between the measured and computed patterns. Thus it is reasonable to attribute the discrepancies to this cause.

With this proviso, the dual-object traces and the quadruple-object trace (Fig. 7) show that the overall scattered field may be calculated as the vector sum of the individual contributions. This applies even in the

case of Ex. I, object A + C, where the two scatters and the transmitter were collinear. In this case the objects were separated by approximately 10 ft. and shadowing was not in evidence. It remains to be seen how close two in-line scatterers may be placed before shadowing does affect the result.

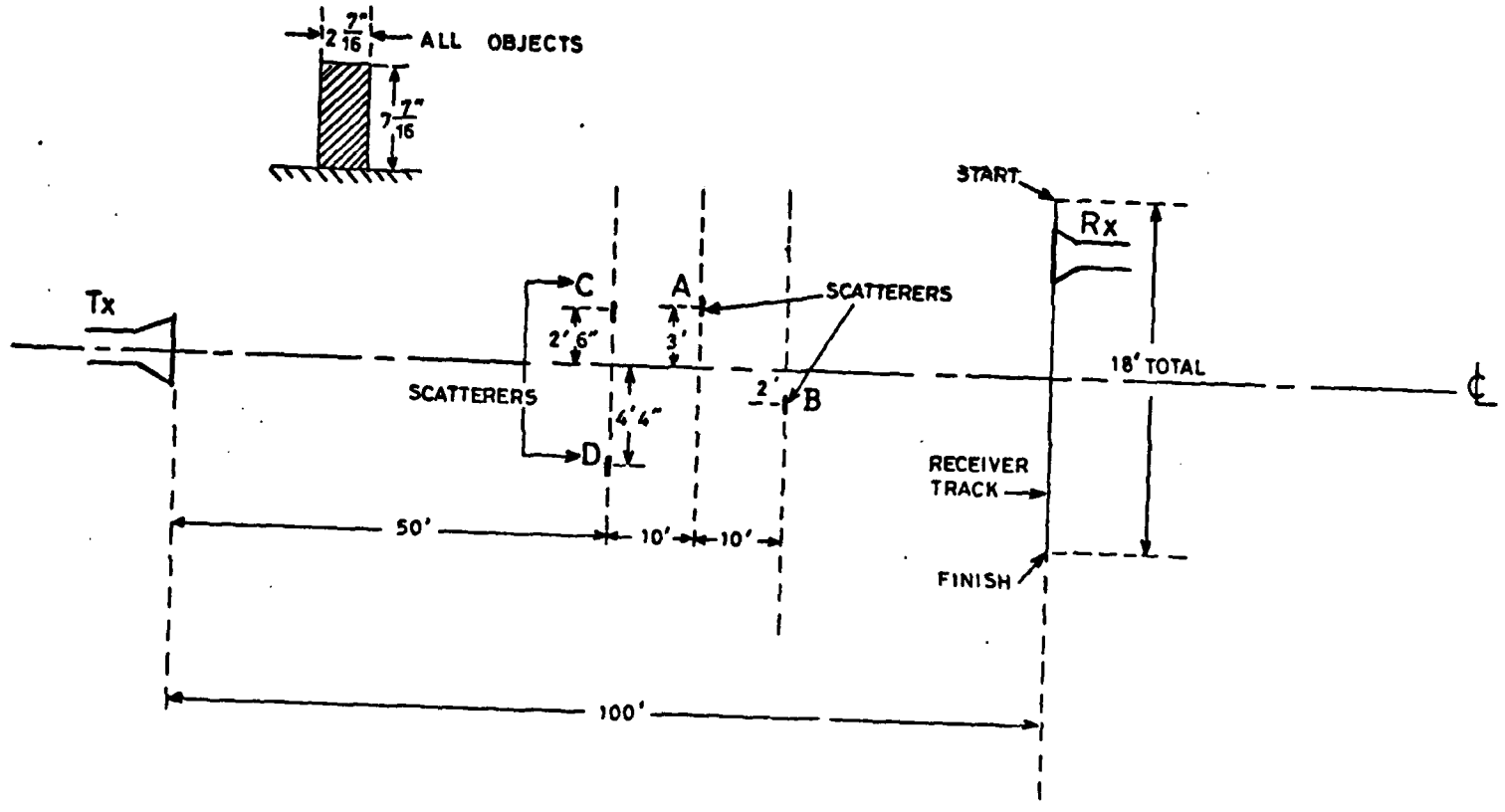

Figure B-3 Site Layout For Scattering Exercise I

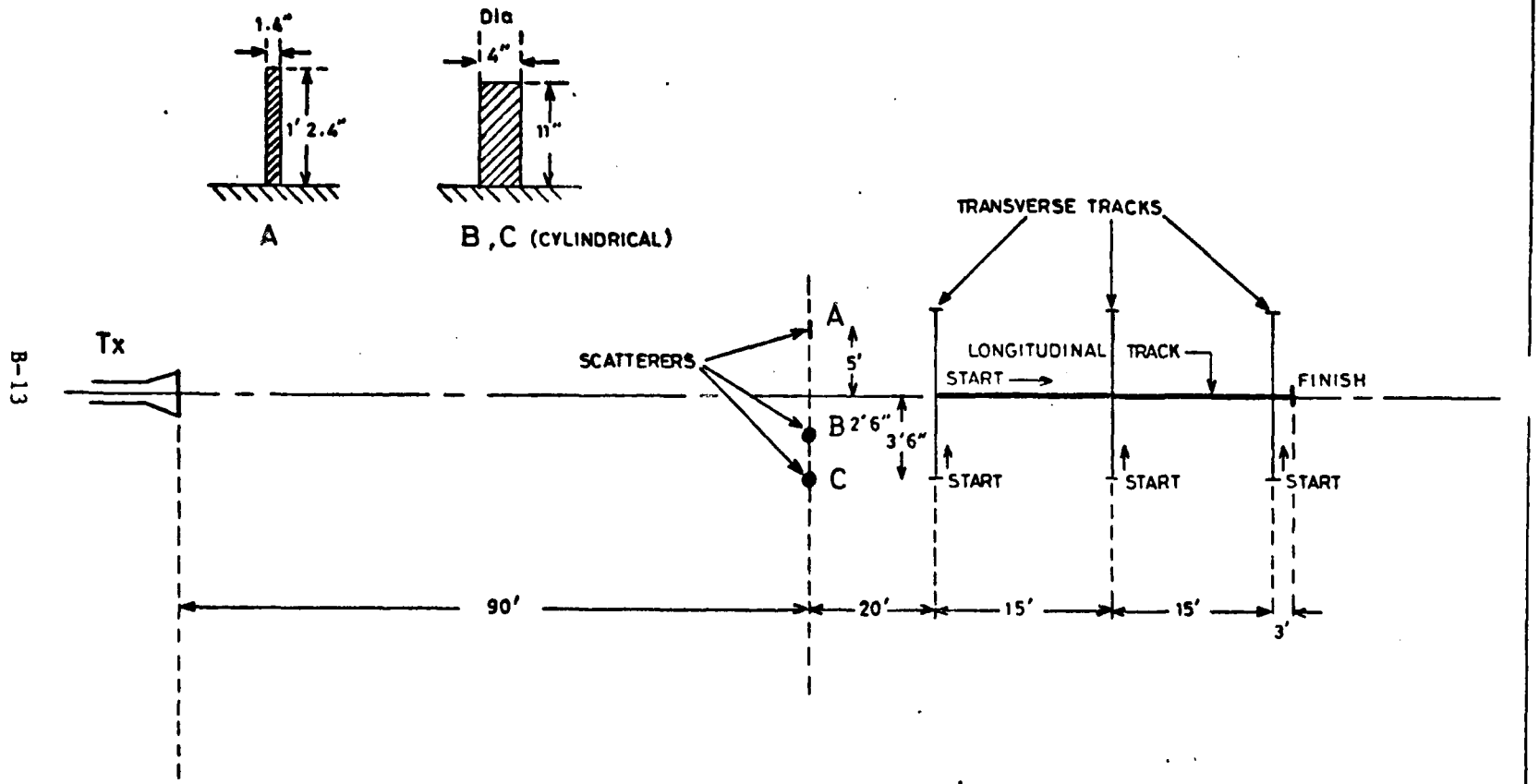

Figure B-4 Site Layout For Scattering Exercise II

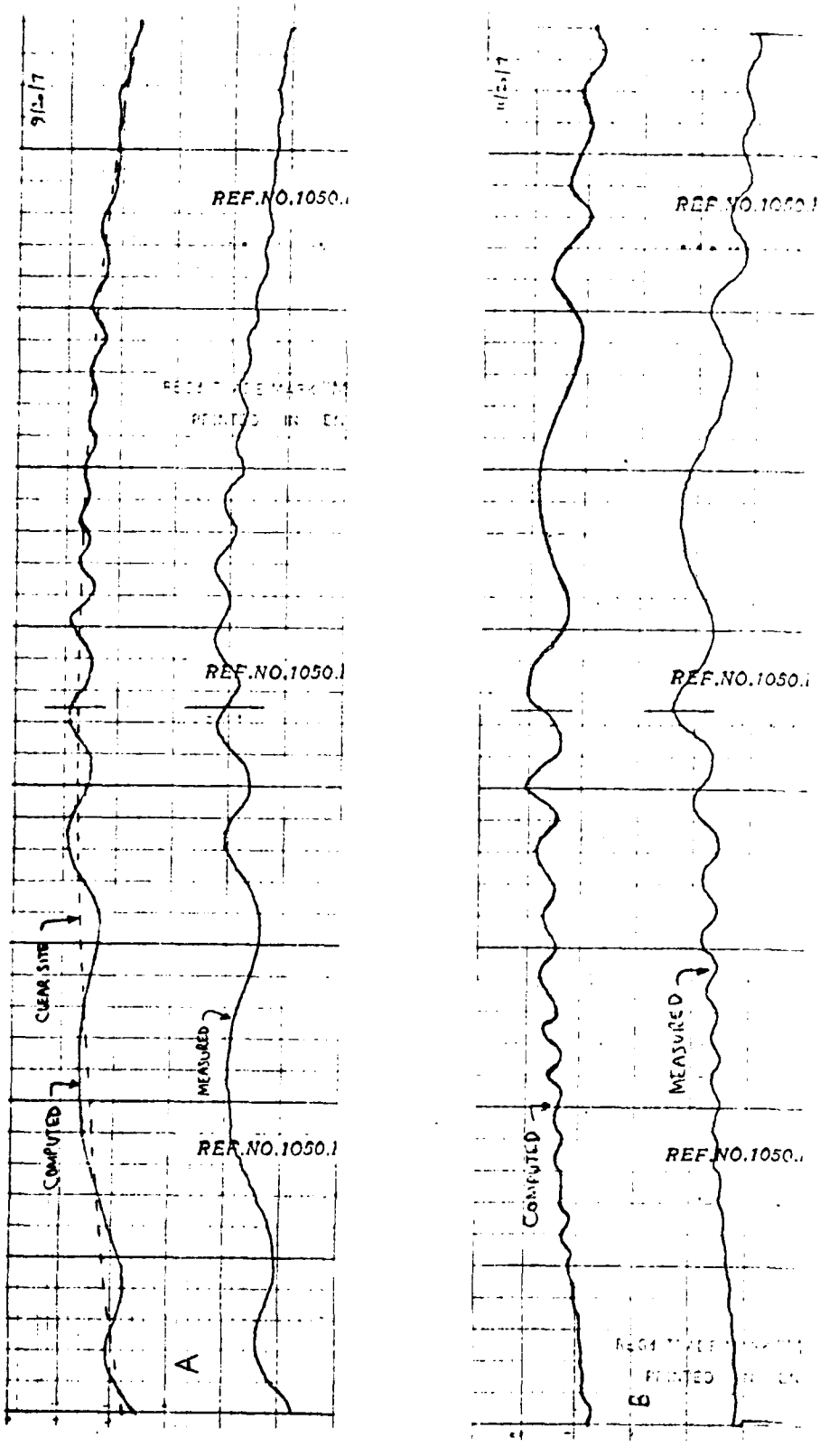

Fig.3 Exercise I - Objects A and B.

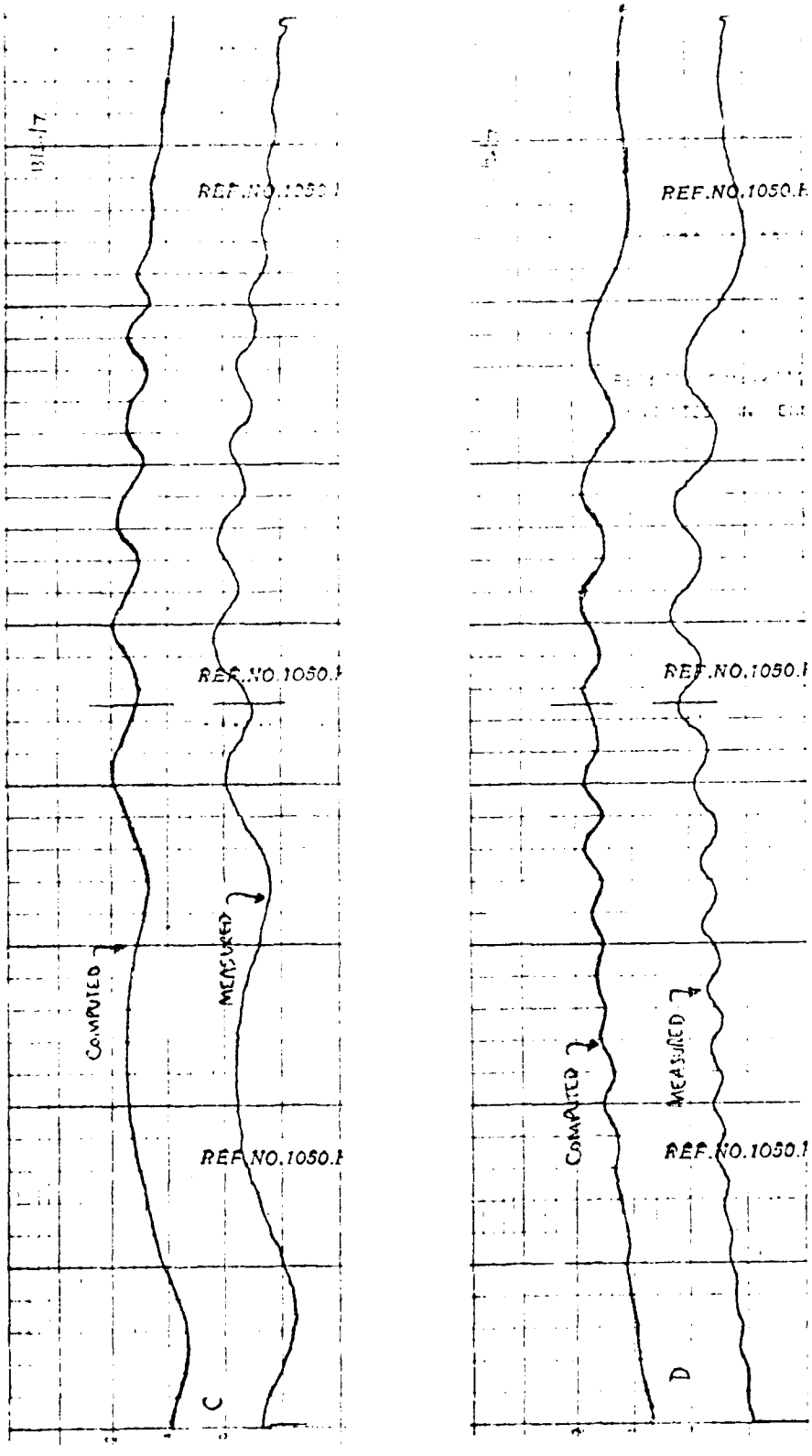

Fig.4 Exercise I - Objects C and D.

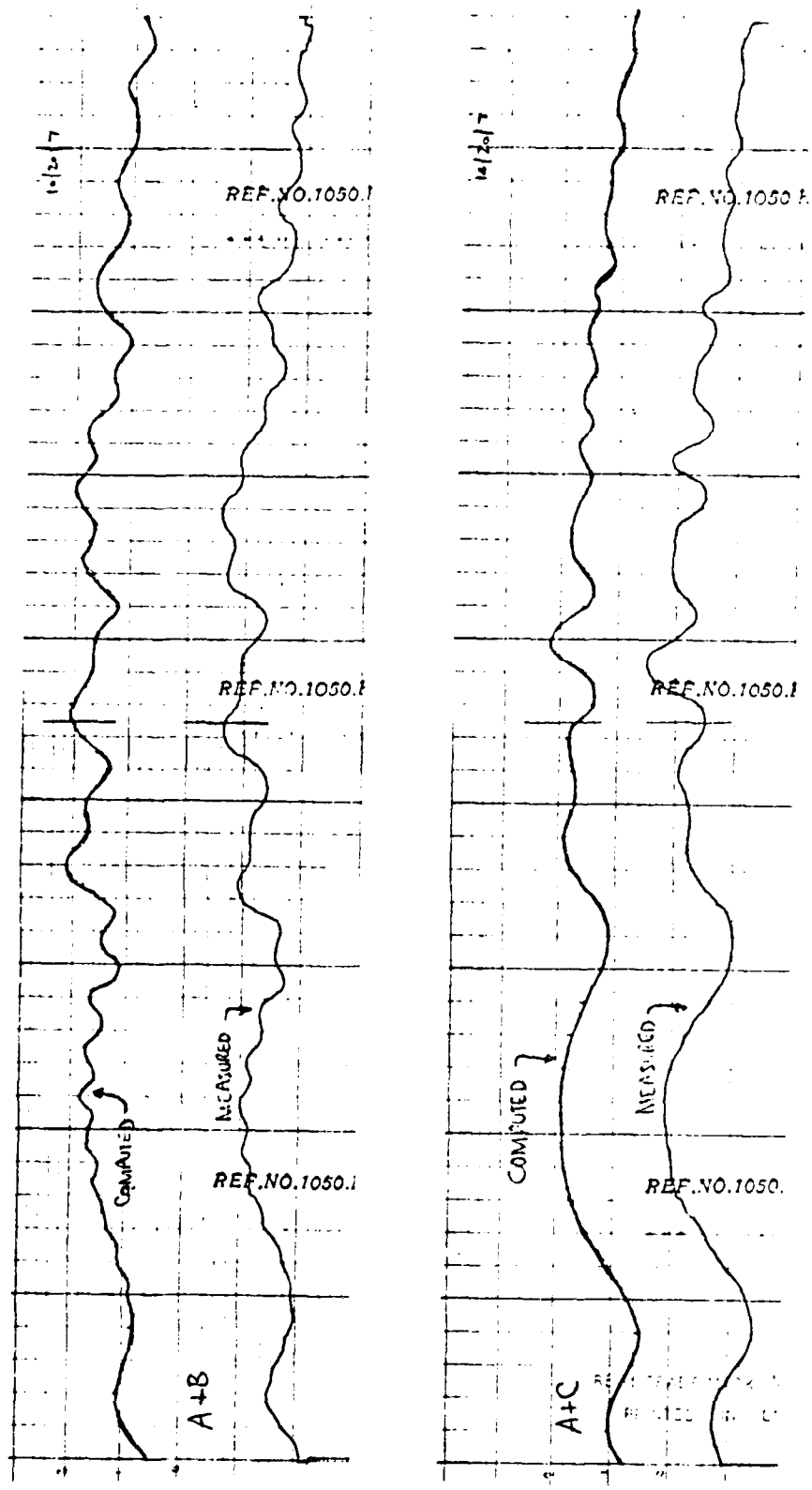

Fig.5 Exercise I - Objects A+B and A+C.

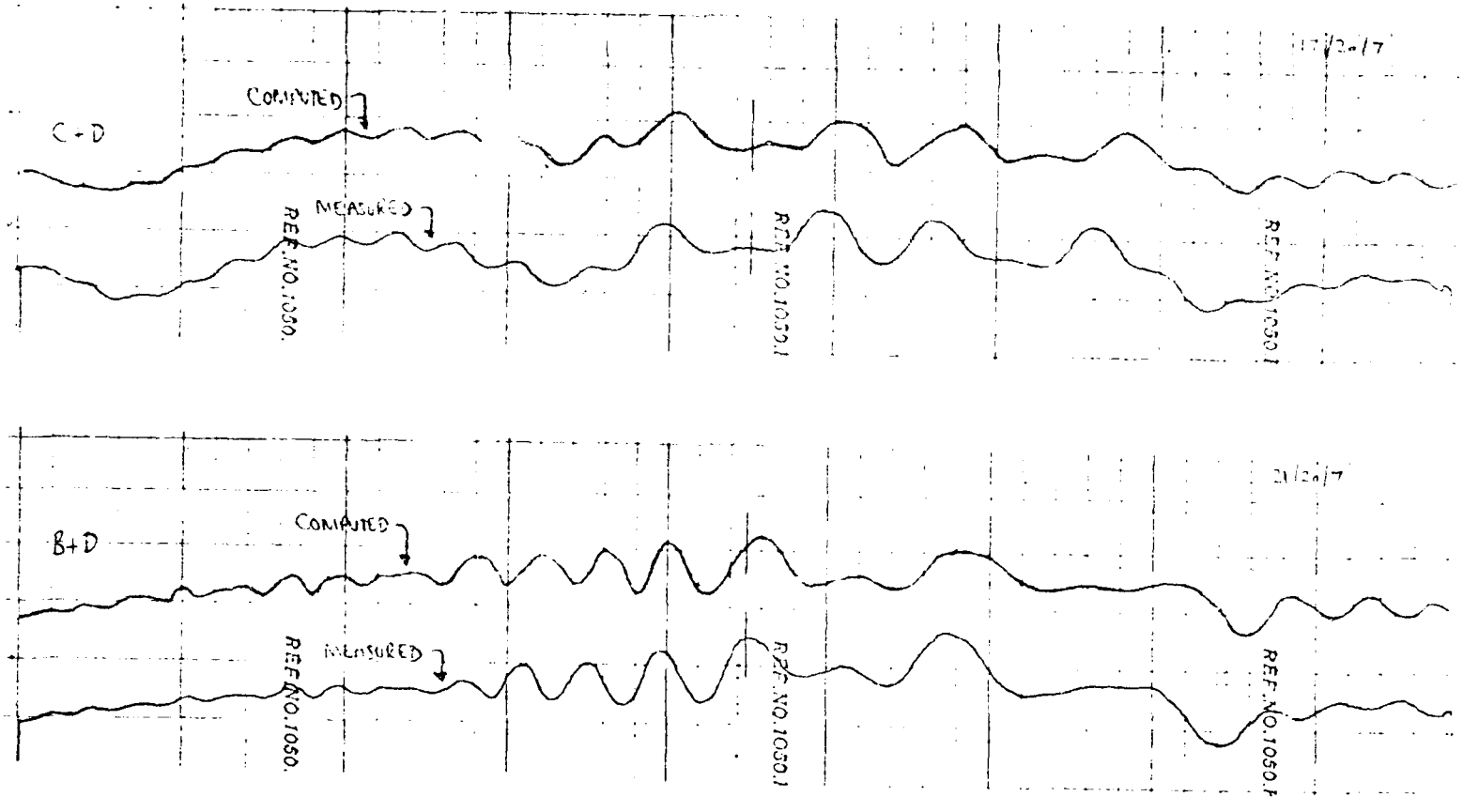

Fig.6 Exercise I - Objects C+D and B+D.

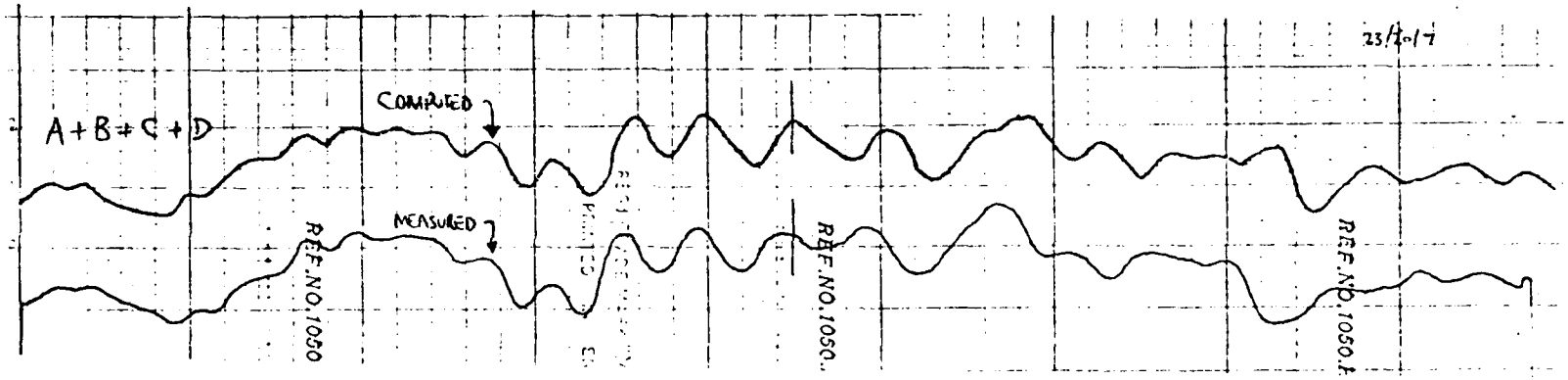

Fig.7 Exercise I - Objects A+B+C+D.

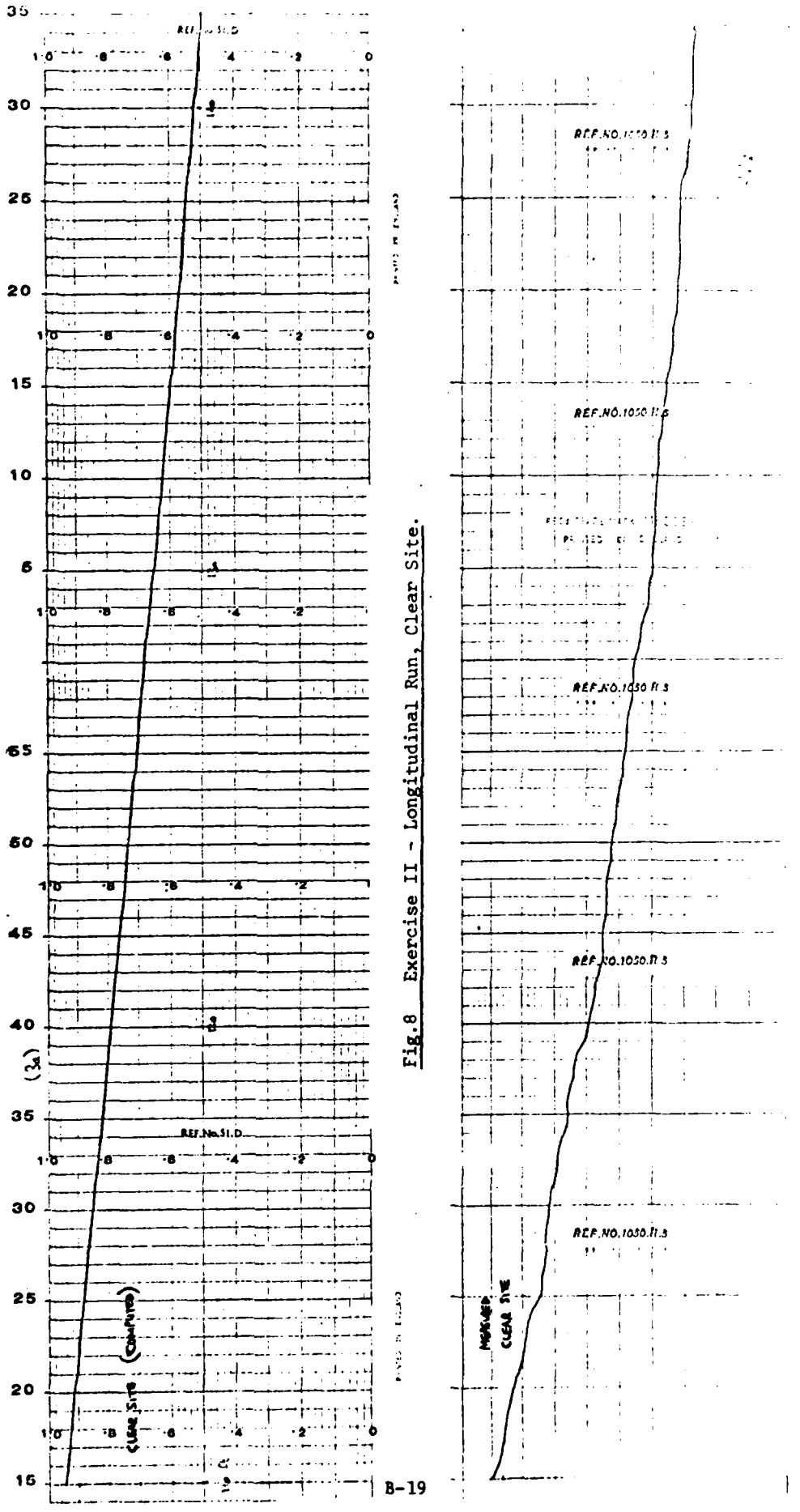

Fig.8 Exercise II - Longitudinal Run, Clear Site.

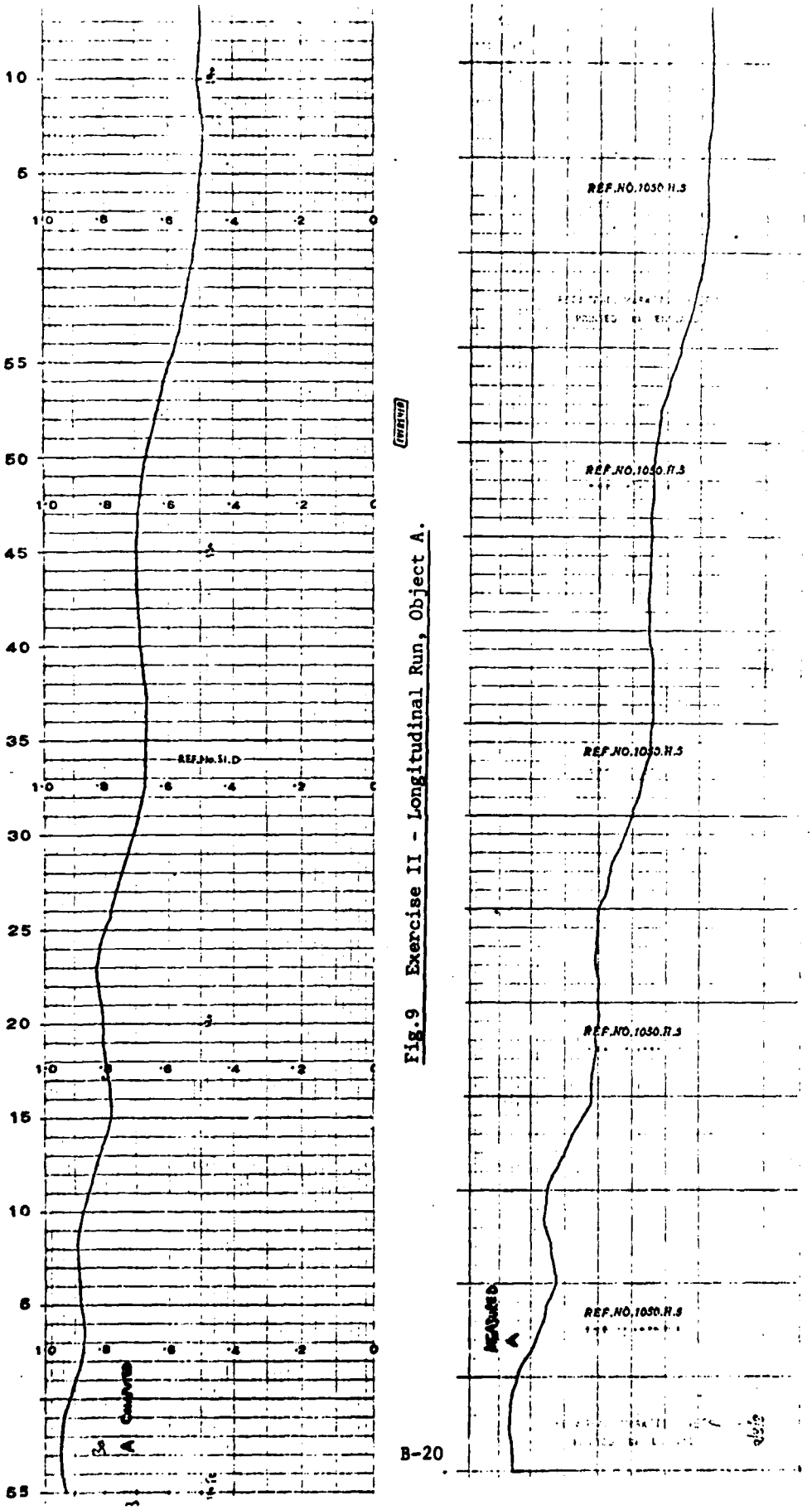

Fig.9 Exercise II - Longitudinal Run, Object A.

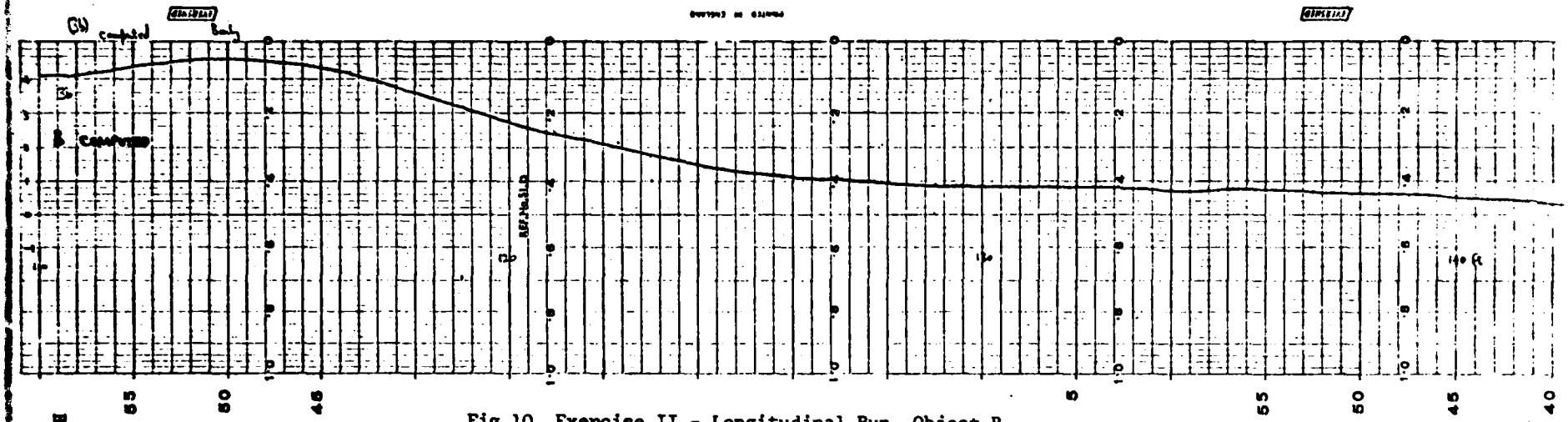

Fig.10 Exercise II - Longitudinal Run, Object B.

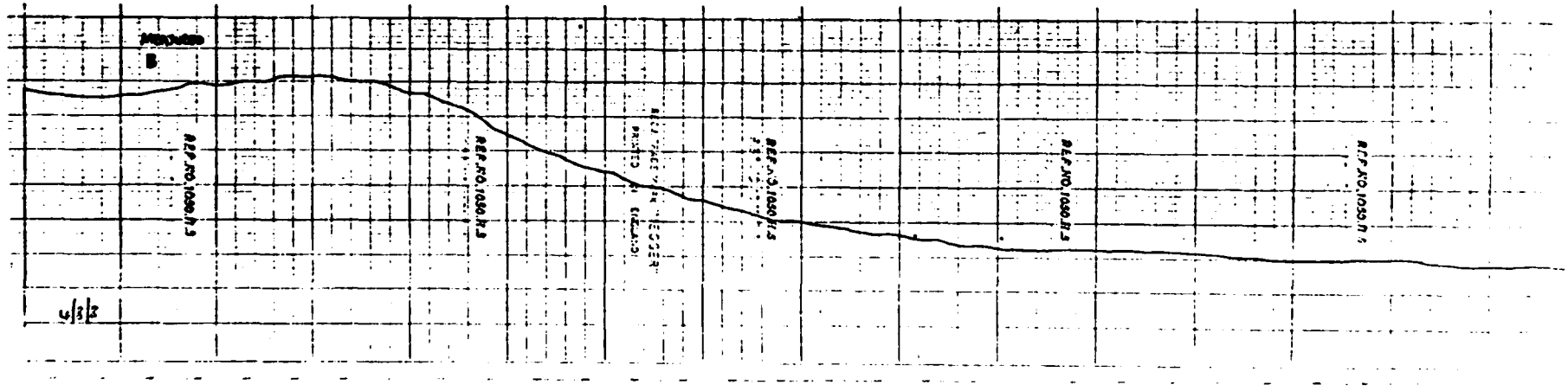

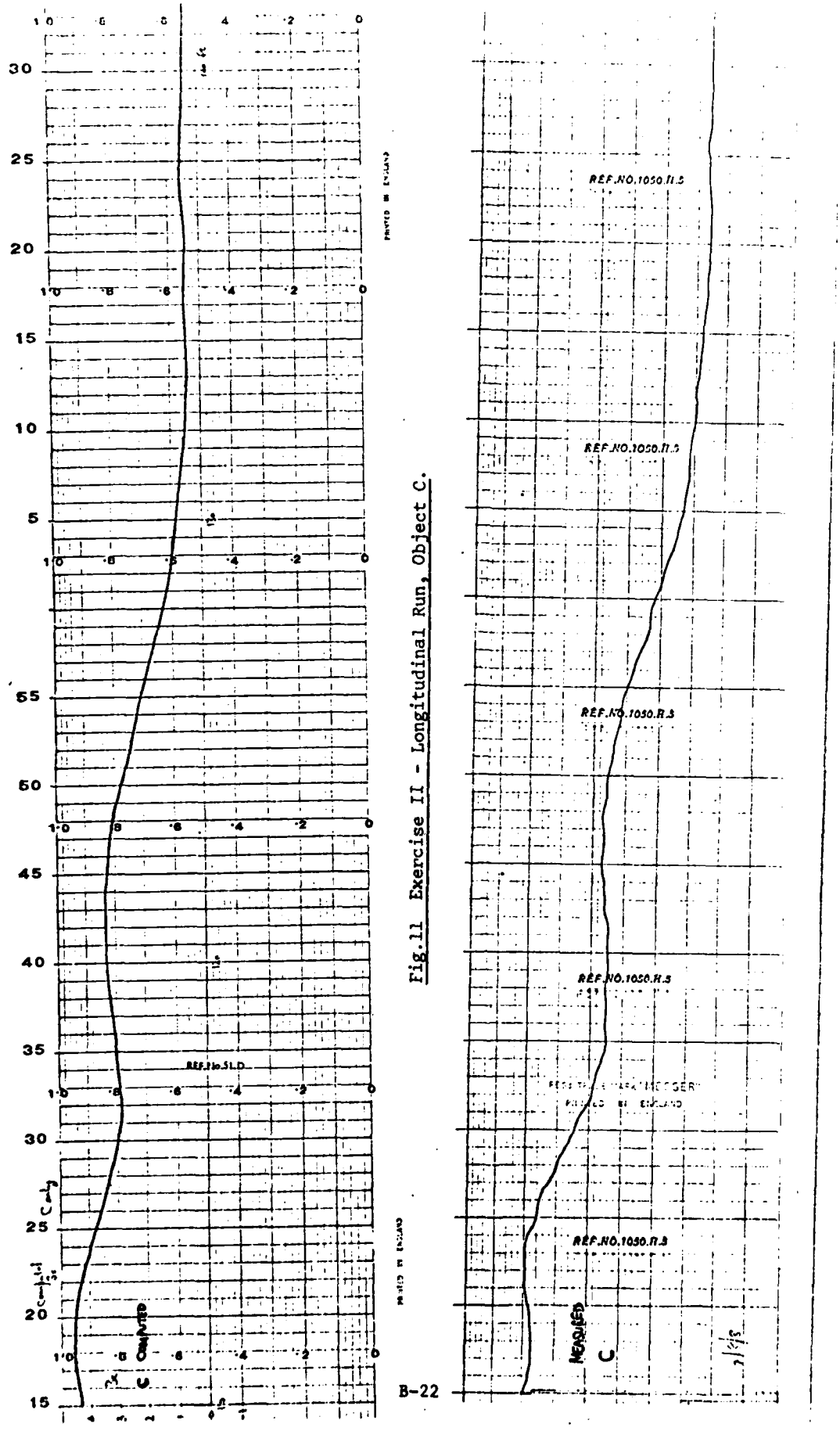

Fig.11 Exercise II - Longitudinal Run, Object C.

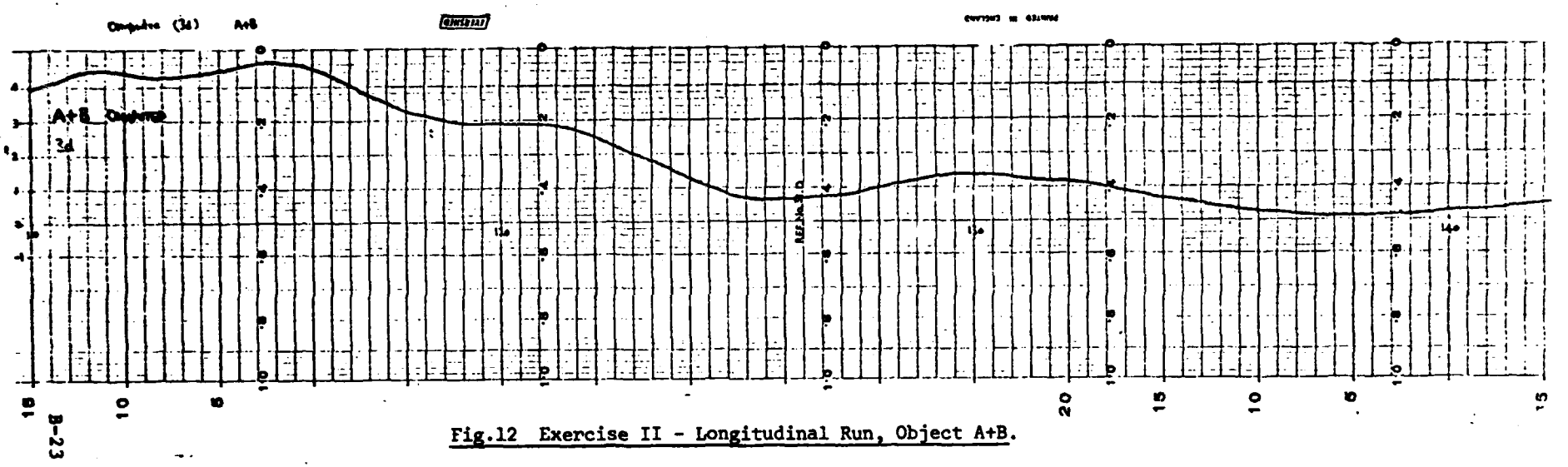

Fig.12 Exercise II - Longitudinal Run, Object A+B.

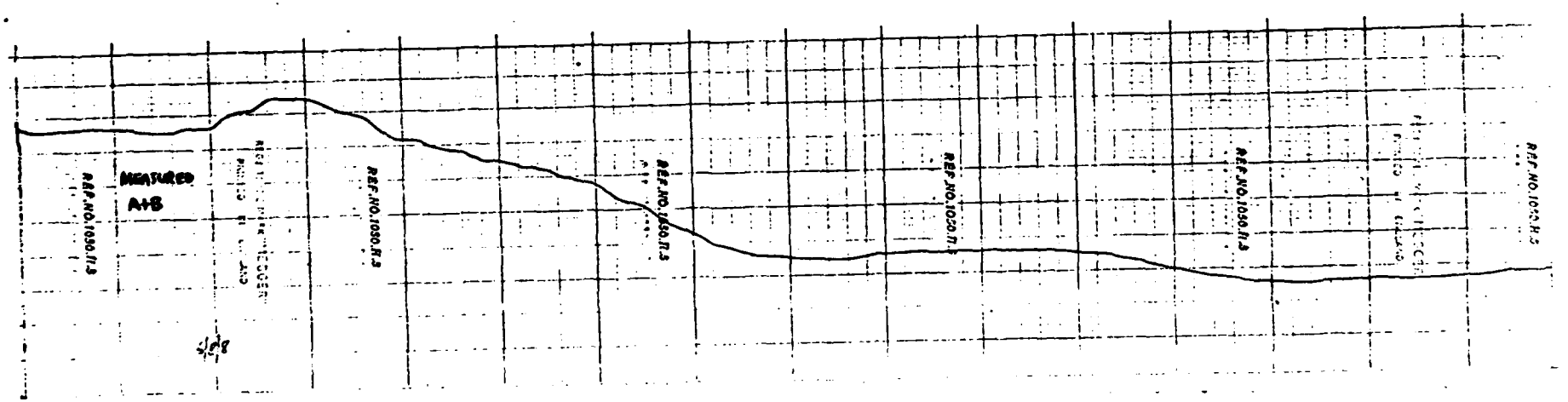

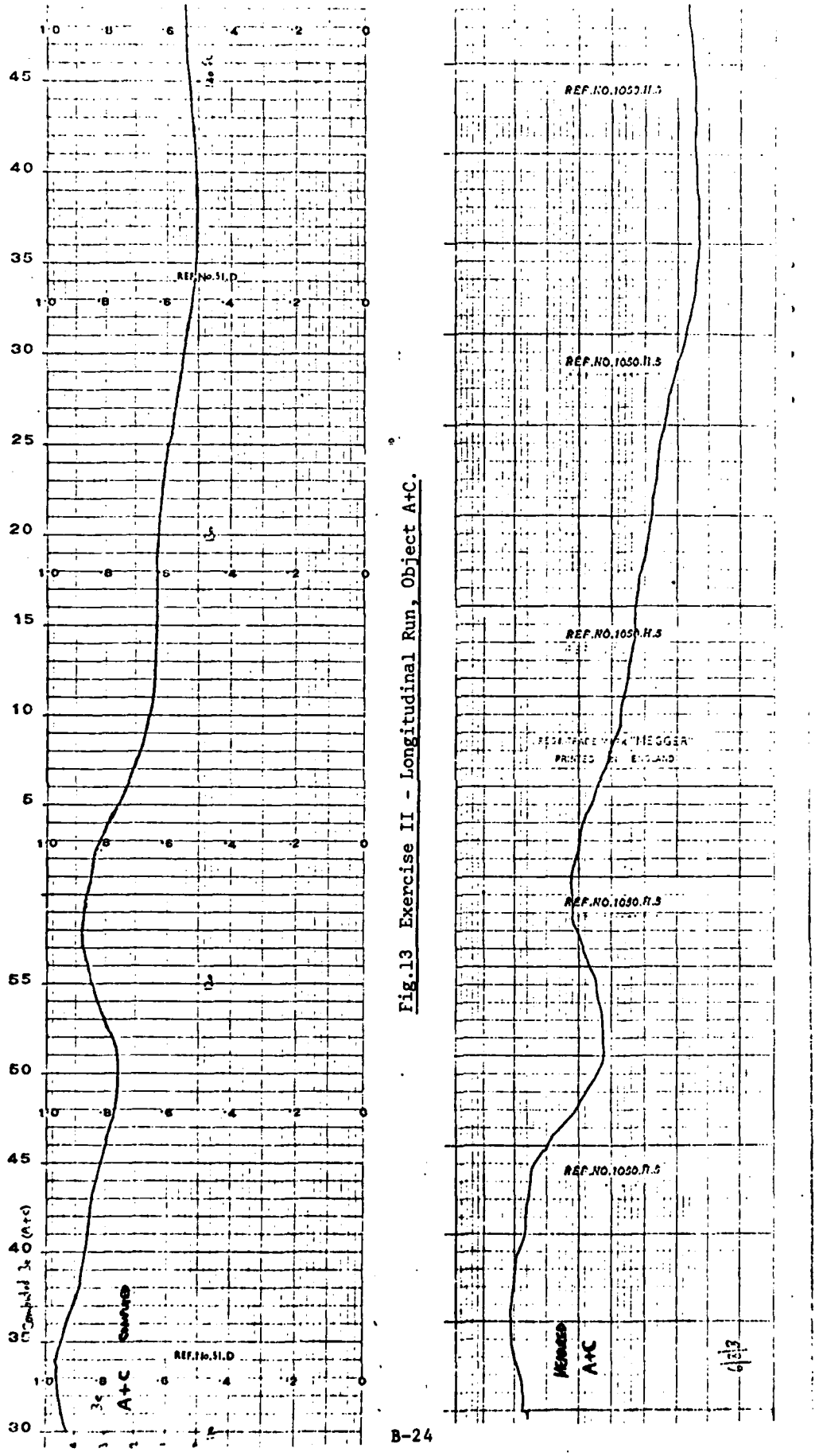

Fig.13 Exercise II - Longitudinal Run, Object A+C.

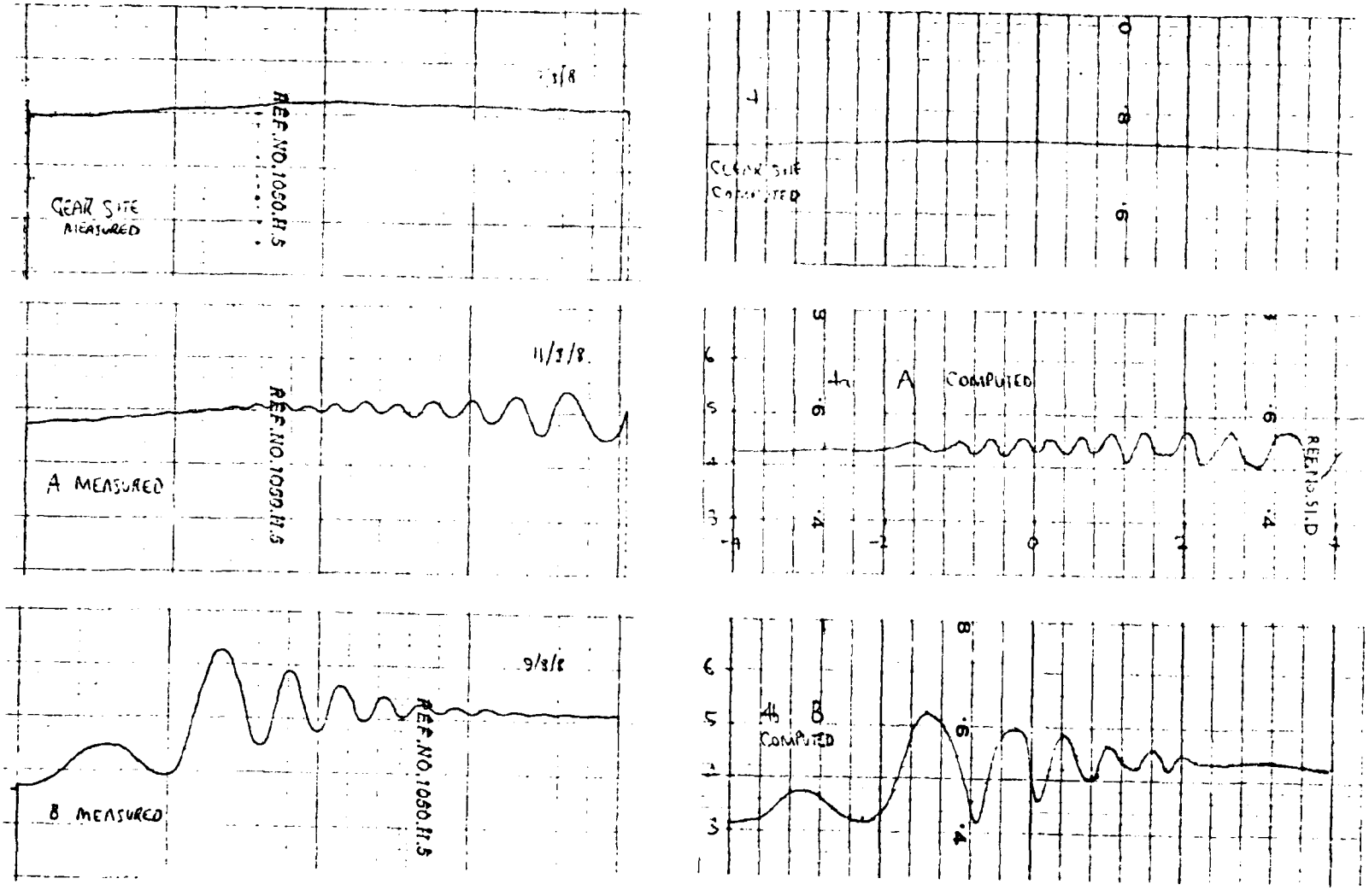

Fig.14 Exercise II - Transverse Runs, Clear Site and Objects A,B,Distance 110 ft.

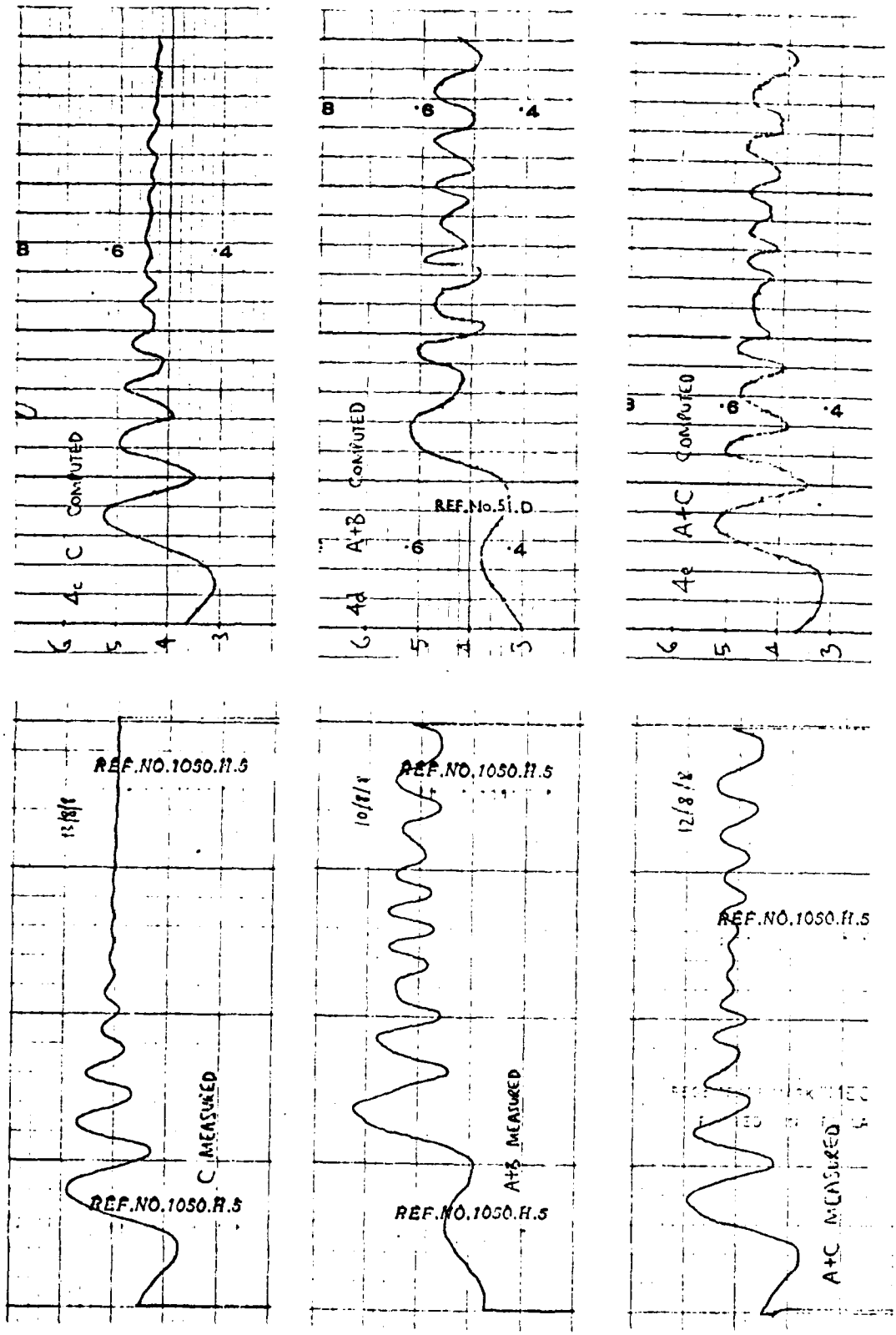

Fig.15 Exercise II - Transverse Runs, Objects C, A+B, A+C, Distance 110 ft.

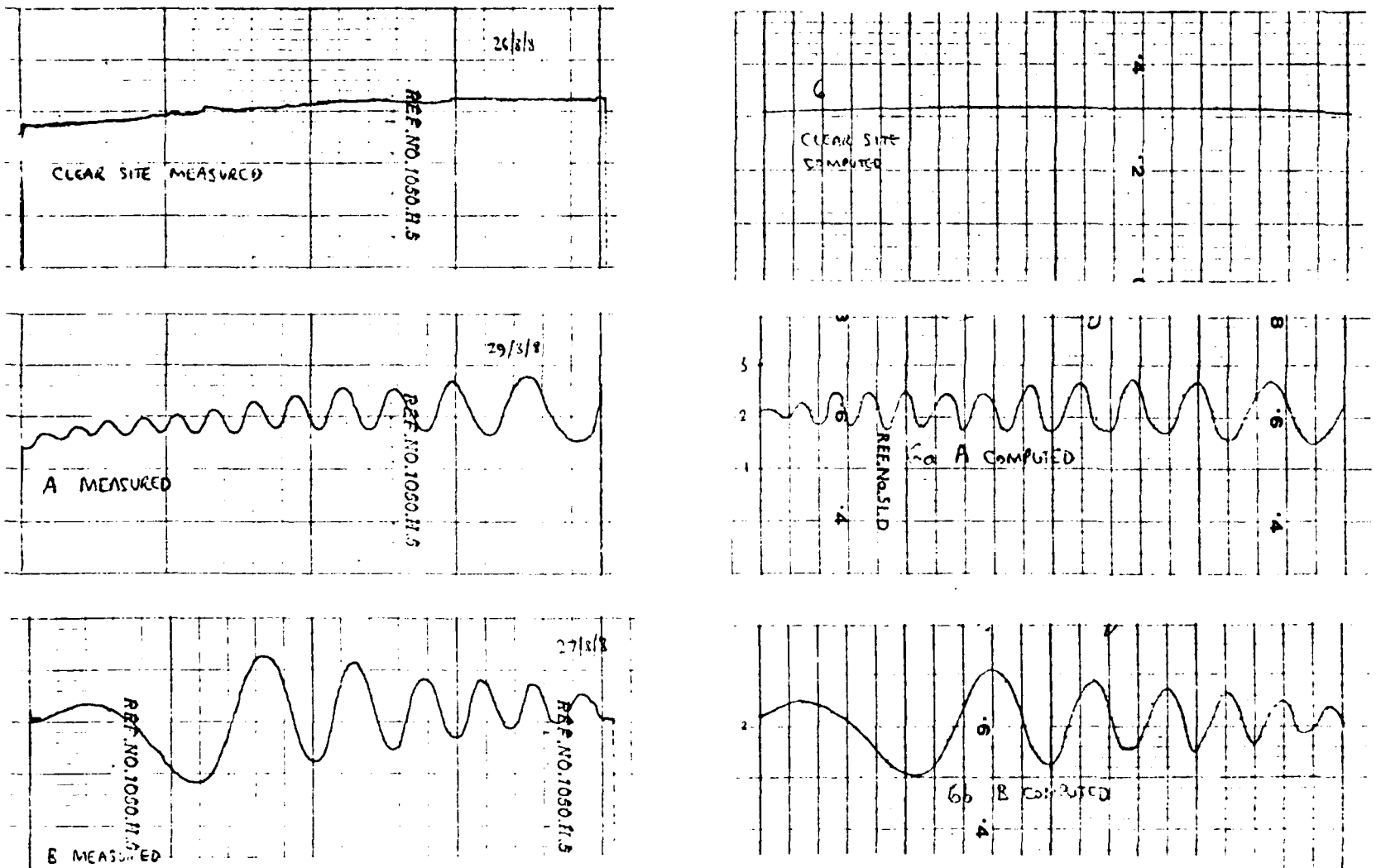

Fig.16 Exercise II - Transverse Runs, Clear Site and Objects A,B,Distance 125 ft.

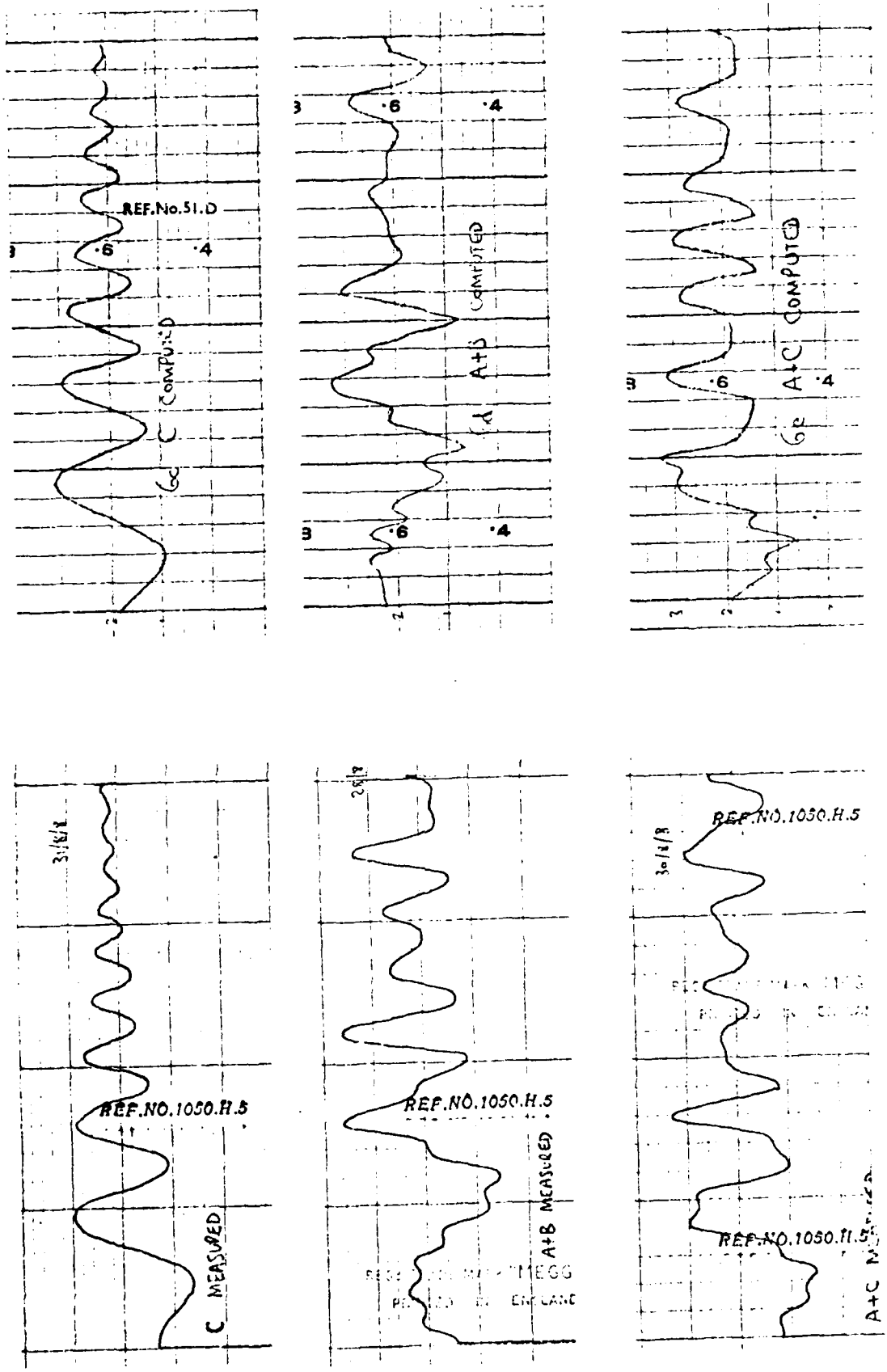

Fig.17 Exercise II - Transverse Runs, Objects C,A+B,A+C,Distance 125 ft.

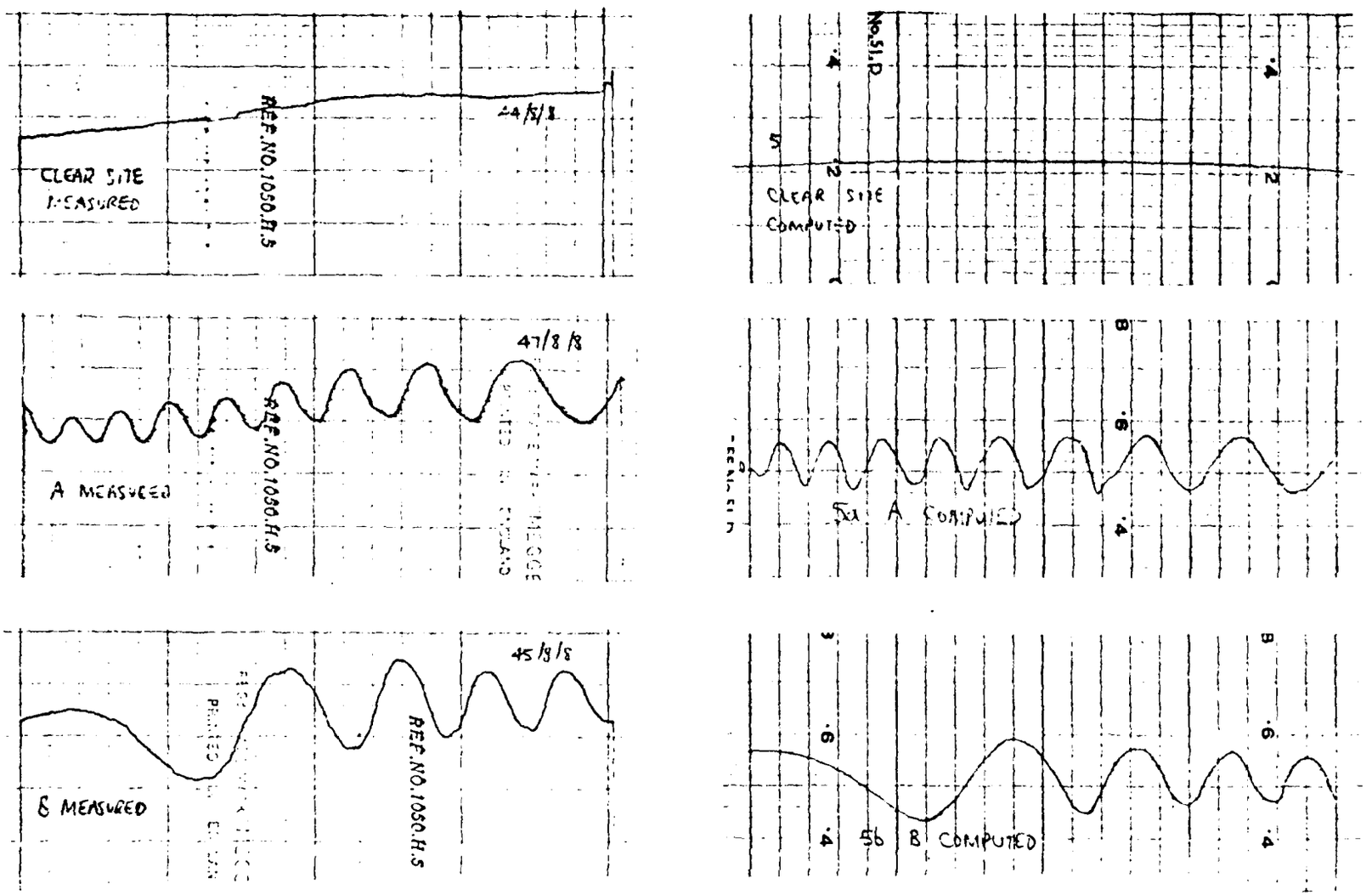

Fig.18 Exercise II - Transverse Runs, Clear site and Objects A,B,Distance 140 ft.

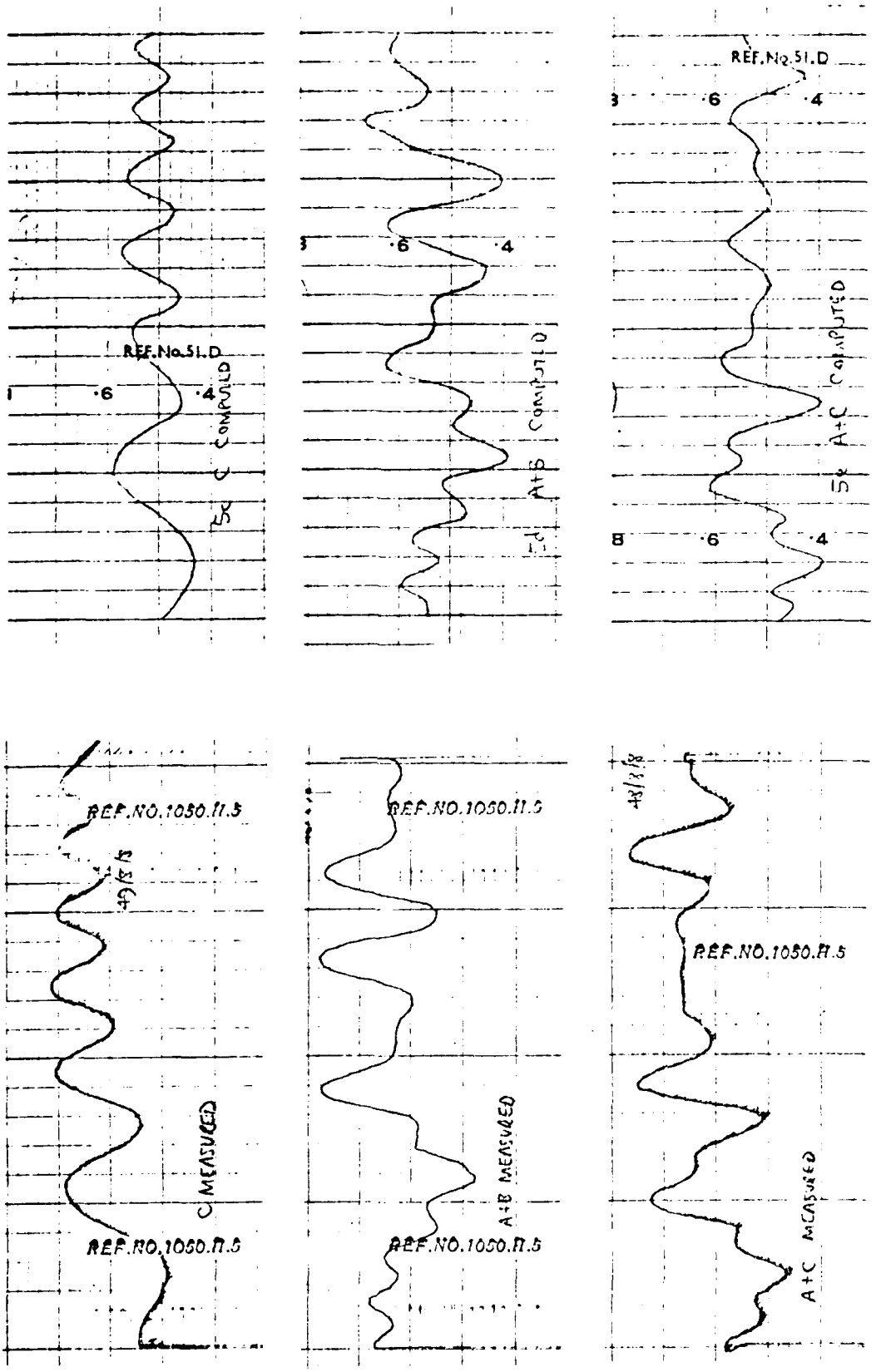

Fig.19 Exercise II - Transverse Runs, Objects C, A+B, A+C, Distance 140 ft.

AD-A079 663 WESTINGHOUSE ELECTRIC CORP BALTIMORE MD F/G 17/7
FAR FIELD MONITOR FOR INSTRUMENT LANDING SYSTEMS.(U)
NOV 79 R MORE, J C BRADLEY, B NEWMAN DOT-FA75WA-3689
UNCLASSIFIED FAA-RD-79-78 NL

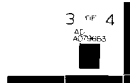

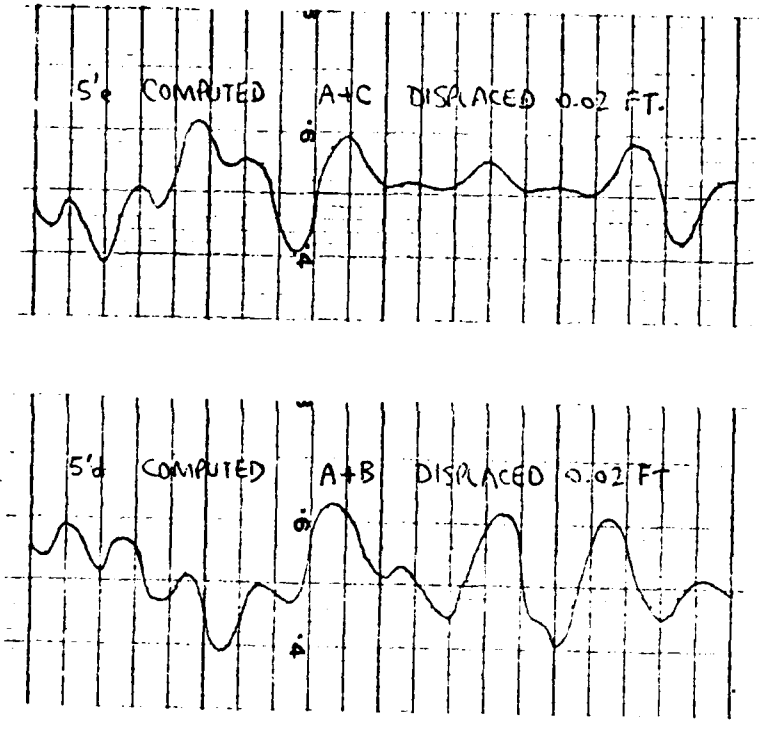

Fig. 20. Exercise II Transverse Runs, Objects A+B,A+C displaced by 0.02 ft,Distance 140 ft.

B.2 Experimental Test Of Interferometric Monitor

B.2.1 Arrangement.

The arrangement of the equipment used to assess the Interferometer type of Far Field Monitor is shown in Figure B-3. The four Aerials 1,2,3 and 4 were spaced 50 ft. apart along a line at right angles to the extended runway center line at a distance of 12,500 ft. from the localizer transmitter. The 4 main aerials were 2 element yagi arrays mounted 20 ft. above the local ground level. An additional aerial (2L) was also mounted 10 ft. above ground level on the mast situated on the extended runway center line.

Referring to Figure B-3 it can be seen that the incoming signal at each aerial must be isolated and split or time shared to give an input to both tone cancellation circuits. There was insufficient time and funds to build such circuits so initial attempts were made to use two aerials on the same mast to give the two signals required. This resulted in unacceptable coupling effects and so for the purposes of experiment separate aerial pairs whose centeres were 50' apart were used.

Two separate, although identical, processing limbs were thus constructed, one for each localizer tone. The third limb shown was used to process, with a conventienal ILS Receiver and Navigation unit, the signal received by the single center line aerial 2L. This facility was included to allow some reference output to be available of the DDM magnitude from the moving scatterers, against which the performance of the interferometric pairs might be assessed.

B.2.2 Description.

Aerials 1 and 3 (100 ft. apart) formed one interferometric pair and their

signals were combined in a simple resistor combining network which enabled the amplitudes of the 90 Hz sidebands to be equalized at the take off point of the potentiometer. The length of the aerial feeder from one aerial was made adjustable by means of a line stretching device, which permitted the sideband signal from one aerial to be combined with the signal from the other aerial in anti-phase.

The resultant signal, after combining, was supplied to a conventional ILS receiver whose detector output was then further processed by an Audio amplifier and Filter unit. This unit amplified the detected signal to a suitable level, which was then filtered to separate the individual 90 Hz and 150 Hz components using a standard navigation unit filter assembly. The outputs from the filter were rectified and loaded individually to allow 90 Hz tone amplitude to be observed and recorded. In order to permit the equipment previously constructed to supply DDM signals to the Ultra Violet and Tape Recorders, the d.c. level out of the filter unit was reduced by the potentiometer arrangement shown. It also allowed the same degree of low frequency filtering as previously used to be readily incorporated.

The signals from the other inferometric pair of aerials (2 and 4) were processed with similar equipment, with the combining arrangement being adjusted to suit the amplitude and phase of the 150 Hz sideband signals. The output for observation and recording was thus taken from the 150 Hz filter as shown.

B.2.3 Setting Up Operation.

The nulling of the sideband signals was carried out by adjustment of the phase and amplitude variables alternately until the d.c. amplitude appearing at the output of the appropriate tone filter was a minimum. The conditions

of balance were relatively easy to attain but slight re-adjustment was necessary from day to day, as no attempt had been made to stabilize the characteristics of the aerial feeders which were up to 200 ft. in length and exposed to the elements.

After the 'nulls' had been adjusted the residue carrier level in the ILS Receiver was checked to coincide with the expected level to confirm that the correct conditions for nulling only one sideband signal had been attained and not the conditions for nulling the carrier.

The setting (or checking) of the 'null' conditions was only attempted during the times when no ground or air activity involving aircraft was taking place, and Stansted Airport was a fortunate choice in this respect because there were periods when there were a low number of movements. The calibration of the recording devices was checked by applying a variable d.c. potential to the input to the amplifiers supplying the Ultra Violet and Tape Recorders, and the effective 'depth' of the nulled output of each filter was observed by noting the recording response when only one aerial was connected to each limb and comparing that response with that obtained when both pairs of aerials were connected.

It was immediately observed that the depth of the null from the 150 Hz pair was not so great as that obtained from the 90 Hz pair of aerials, and no adjustment enabled the depth to be equalized. All recording made thus showed a higher residue level on the 150 Hz tone signal than the 90 Hz signal.

Wherever possible the effect of single ground movements were recorded, and careful logging of such movements by an observer in the airports control tower enabled the effects of similar movements by different aircraft to be compared. These are discussed elsewhere. One particular feature that was

apparent from all landing aricraft was that multipath disturbance was detected from each aircraft before it overflew the monitor aerials. It was noticeable that when the multipath effects were first 'seen' for each landing they appeared much earlier in the flight on the interferometric monitors than on the standard DDM receiver.

B.2.4 Equipment Performance.

To ascertain the reasons for the consistently different null depths obtained from the 90 Hz and 150 Hz processing limbs a series of laboratory and on-site measurements were taken.

B.2.4.1 Null Adjusting Circuits

Using a stable signal generator at 110 MHz, two coherent signals were supplied to the nulling circuits. The two signals were different in amplitude by 0.5 dB. With the output of the nulling cicuit supplied to a standard signal strength measuring set. (Eddystone Noise Measuring Set No.31A) the amplitude and phase adjustments were carried out, and the resultant signal was 50 dB down on the signal level in either arm of the nulling arrangement.

B.2.4.2 Audio Amplifier and Filter Unit

Using a standard Audio Signal Generator with an output amplitude similar to that obtained from the ILS Receiver Type 6401, the responses of the two filters was checked. Each response showed similar and acceptable characteristics and it was particularly noted that the rejection of either filter at center frequency of other filter was -23 dB. The -6 dB bandwidths of each filter was 40 Hz for the 90 Hz filter and 60 Hz for the 150 Hz filter.

B.2.4.3 Independent Tones from Localizer

With the co-operation of the Station Tels. Officer at Stansted, it was arranged for each of the localizer tones to be muted in turn, to enable the

observation of the on-site nulled signals of one tone in the absence of the second tone. It was postulated that because of the low level of operation of the ILS Receiver's detector, second harmonics, particularly of the 90 Hz tone, were being generated and were the probable cause of the enhanced 150 Hz nulled signal.

With single tones only modulating the ILS transmitter the null amplitude measured for each tone was -20 dB to the tone level from a single aerial. When only the 90 Hz modulation was present the output of the 150 Hz filter was measured with the null components adjusted to give a 90 Hz null. The signal level at the output of the 150 Hz filter was -11 dB relative to the amplitude of the 90 Hz signal from one aerial in the 90 Hz filter.

When only the 150 Hz modulation was present, the output of the 90 Hz filter, with the null components adjusted to give a 150 Hz null, was-16 dB relative to the amplitude of the 150 Hz signal from one aerial in the 150 Hz filter.

The localizer transmitter was restored to normal operation, with both tones present and the nulled amplitudes were -16 dB at the output of the 90 Hz filter and -11 dB at the output of the 150 Hz filter.

B.2.5 Summary of Operation and Performance and Future Considerations.

Within the limitations of the experimental arrangement the essential facets for an interferometric type Far Field Monitor have been explored. The ability to cancel two R.F. signals with the required rejection is demonstrated, although some form of stabilization of the feeder characteristics is essential for any final equipment.

A number of factors make the quantitative interpretation of the results difficult as discussed in Section B.2.6.1, the tone filters and harmonics

and their relation to the cancellation residues particularly requires further investigation.

The recordings and on-site observations clearly indicate that multi-path interference due to ground based or airborne scatterers was more apparent with the interferometric system than with a conventional ILS receiver monitor. This feature illustrates the relative sensitivity of the alternative forms of multipath detection, and suggests that a Far Field Monitor based on the principle explored should provide useful information to ATC.

The equipment used for the experimental tests should not be regarded as the form of any final equipment. The use of separate aerials was an expedient, and any final equipment could use for example a switched aerial system with time sharing of the processing equipment.

One possible form of switched system for a single pair of aerials is shown in Figure B-4. For a system using several aerial pairs to provide complete coverage of an airports runway environment, the input switch could be extended to scan all aerial pairs. The speed of switching, and the possible consequential generation of switch harmonics needs assessment, but the feature of time sharing affords a considerable reduction in equipment hardware.

B.2.6 Experimental Observations.

B.2.6.1 General

With the simplified single pair per tone equipment described in Section B.2 a large number of measurements of aircraft movements were recorded on the tape recorder shown in Figure B-3. These outputs were fed via an A/D converter into a MYRIAD computer and studied using the MIDAS * system. Plots 1-70 were selected for further discussion and are included. Since a full monitor was

not constructed a number of effects which will not normally be present interact in the results and interpretation is required.

The following points should be noted:

1) As different center positions were used for the tones the separate tone responses are modulated by Sin ($\frac{2\pi d}{\lambda}$ Sin x) terms with different origins for angle x.

2) Off the shelf ILS receivers and filters were used in which the isolation between tones was 23 dB or less due to filter responses and harmonics. Consequently the smaller tone disturbances oscillate about this residual. If the tone disturbance is larger than the residual the response will vary with the tone level at the scatterer modified by the Sin ($\frac{2\pi d}{\lambda}$ Sin x) factor as expected. Interaction of this signal with the residual will give oscillations of residual amplitude about this response. The oscillatory response about the residual for the smaller tone disturbances is not acceptable in terms of a final monitor since phase dependence is re-introduced. We could tolerate it in our experiments since the objects observed were moving so that the peak became visible at some stage. With improved filters or alternative means of detection, and receiver design to avoid harmonics the residual may be reduced to the limit set by basic tone cancellation described in Section B.2.6.2 below.

3) The separate, carrier detection, and comparison with the carrier residual circuits which enable the interferometer tone outputs to be related to DDM were not constructed.

4) The exact position of the aircraft relative to the observations was not known.

5) The diode detectors used have a non-linear characteristic which results in a reduced response to small signals. This was allowed for in the null level measurements using separate bench measurement of levels in to level out of the detector. However, the plots are of the output of the detectors so the smaller signals are further reduced by this effect.

6) The part-cancellation of the direct carrier means that the interfering carrier becomes of the same order as the direct carrier residual. This means that the AGC level changes and in a complete monitor this is allowed for by comparing the AGC with a separately detected direct carrier signal. This circuit is not included in our experimental equipment and so the carrier interference will affect the levels in the plots. This is corroborated by plot 52. If the sections just before and just after the stationary period are examined it can be seen that the interference oscillation does not pick up where it ceased as would be expected with simple tone interference with its residual. This is consistent with an AGC time constant lag and indicates that the interference pattern is in part due to the carrier.

7) Effects 1-6 mean that it is difficult to relate the tone observations to DDM so as an aid a separate measurement of DDM was made with a single ILS receiver. Since all the observed objects were moving the peak DDM seen by this was an estimate of the DDM being reradiated.

B.2.6.2 Basic Tone Cancellation.

As described above the inadequancies of the standard receiver used meant that each tone cancellation residual was limited by the breakthrough from the other tone. In order to investigate the basic tone cancellation achievable

on site measurements of the cancellations were made with the other tone off.

The following measurements were made

	Cancellation Both Tones On		Cancellation Other Tone Off	
	Measured dB	True dB	Measured dB	True dB
150 Hz Null	-11	-31	-21	41
90 Hz Null	-16	-36	-21	41

The 20 dB difference between the measured and true levels is because the residuals are amplified by 20 dB by the receiver AGC. The carrier is cancelled by 20 dB in the canceller and the receiver AGC acts to restore this hence introducing a gain of 20 dB. The expected output levels of the canceller can be seen by tracing the signals through one tone cancellation, the 90 Hz say

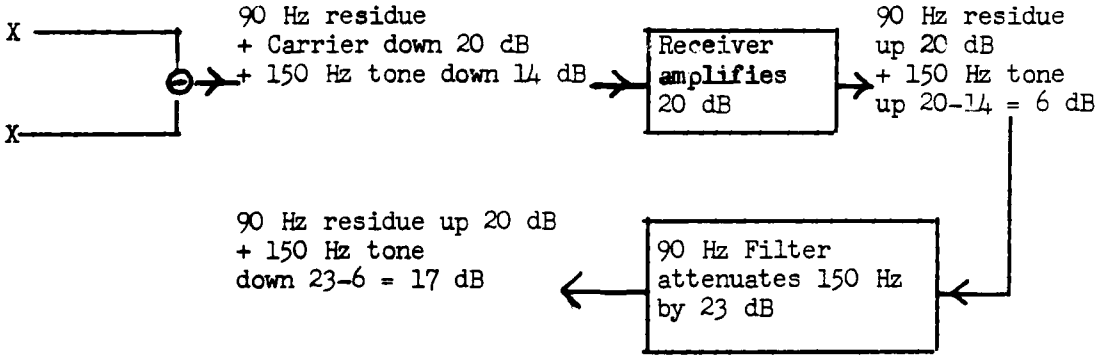

The expected output level is -17 dB relative to the direct signal which agrees well with the measured figure of - 16 dB for the 90 Hz tone. In the case of the 150 Hz tone the breakthrough level is 5 dB higher and it is postulated that this is due to a 180 Hz harmonic of the 90 Hz. The cancel-

lations achieved with each tone if the other tone is switched off are identical, as would be expected.

The 20 dB gain must be remembered when viewing the plots.

B.2.7 Discussion of Measurements

This discussion should be viewed in conjunction with the airport map shown in Figure B-5.

Plots 1-18 show the 90 Hz, 150 Hz and DDM disturbances due to various aircraft taxying from the head of taxiway 4 to the 23 threshold. Plots 1 to 6 are of a Hercules. The cancelled tone outputs are typical for this maneuver showing oscillations due to path length change interference as the aircraft moves towards the center line culminating in a broad disturbance as the aircraft turns onto the center line. Note there is a y scale change between Plots 1-3 and 4-6. The associated DDM receiver shows a smaller amplitude oscillatory disturbance which disappears as the center line is approached, that is as the DDM illuminating the aircraft decreases. The final swing onto the center line is not detected. It can be seen that the noise levels between cancelled tone and DDM plots are similar indicating that the amplitude comparison is reasonable fair.

Plots 7-9 show the disturbance due to a small f28 airliner. The distrubance is clearly seen on the tones but the DDM receiver totally fails to detect the aircraft. Plots 10-18 show two examples of the disturbance due to a CL44. The large disturbance on the cancelled tone outputs due to the turn onto the center line is shown very well and may be contrasted with the DDM receiver output on which nothing is seen.

Plots 19 to 24 show the disturbances due to a 737 and F28 turning on the center line at the 23 threshold after taxying up the main runway. The

disturbance is clearly seen on the cancelled tone outputs but is invisible to the DDM receiver.

Plots 25 to 30 show the outputs due to an F28 and 737 taxying across 5½ crossing. Again the maneuver is detected on the cancelled tones but not by the DDM receiver.

Plots 31-40 are of an F28 and 737 taxying from the bottom of taxiway to the 05 threshold in preparation for a reverse direction take off. The aircraft are on the 150 Hz side of the runway and the tone disturbances are seen most strongly on this tone. The aircraft are detected over a longer section of the maneuver on the tones than they are on the DDM. Plot 39 shows the DC offset expected as discussed further below.

Plots 41-52 show a very interesting example of the same maneuver and demonstrate the response expected from a cancelled tone pair when the disturbance is sufficiently larger than the residual. The plot is of a 737 taxying to the 05 threshold with a halt during the maneuver. Consider the 150 Hz tone on plot 52 (center trace). It can be seen that during the halt the tone shows a steady offset from the level when no aircraft is present. That this is not due to chance phase is shown by the steady rise to, and fall from, the level which is at a much slower rate than the accompanying oscillation due to path length pahse change. The effect is also shown clearly on plot 42 which is a compressed abscissa plot of the same signal. The plots demonstrate that the tone cancellers will give an output independent of the relative phase between the direct and multipath signals when the cancellation residual is reduced sufficiently relative to the multipath. Plot 35 also demonstrates this.

The fine structure at the beginning and end of the halt indicates as

discussed in Step 6 of Section B.2.6.1 that the oscillations which occur while the aircraft is moving are in part at least due to carrier interference.

The plots were obtained as a feasibility demonstration using off the shelf equipment as far as possible and a number of interacting factors make complete interpretation difficult as discussed in Section B.2.6.1. The main difficulty was that the cancellation residue on the tones was much larger than it would be in a practical monitor as the performance of the tone filters was inadequate. As a consequence unless the disturbance is large it oscillates about this residual rather than providing a steady measurement which varies with the strength of the tone signal and the $\mathrm{Sin}(\frac{2\pi d}{\lambda} \sin x)$ response of the cancellation pair. The 150 Hz channel for the larger aircraft maneuvers near the localizer (i.e. larger multipath signals) show this expected response. The difference in response between 150 Hz and 90 Hz channels for near localizer maneuvers is not fully explicable. The aircraft is on the 150 Hz side of the runway so one would expect the 150 Hz measurement to be larger and the action of the square law detector with the interference plus larger residual would also give the 150 Hz signal a larger amplitude than the 90 Hz. However, the 90 Hz does not show the expected steady offset anywhere. To explain this and to obtain measurements more directly relatable to DDM improved equipment is necessary. Specifically the tone filters must be improved, the tone pairs must be calibrated.

However, the measurements obtained with our initial simple equipment demonstrate the potential of the system both in terms of phase independence and the high sensitivity of the tone measurements.

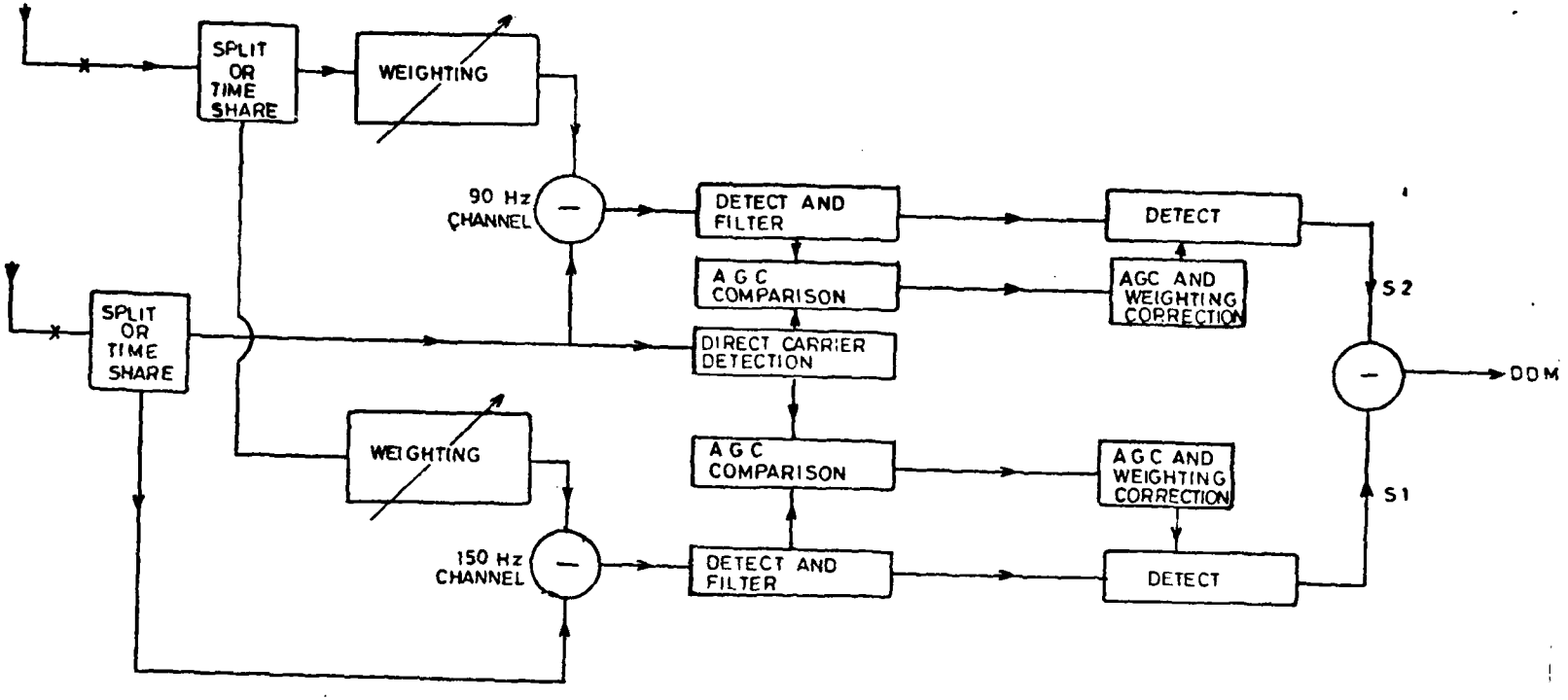

FIG. B-5 BASIC MONITOR PAIR

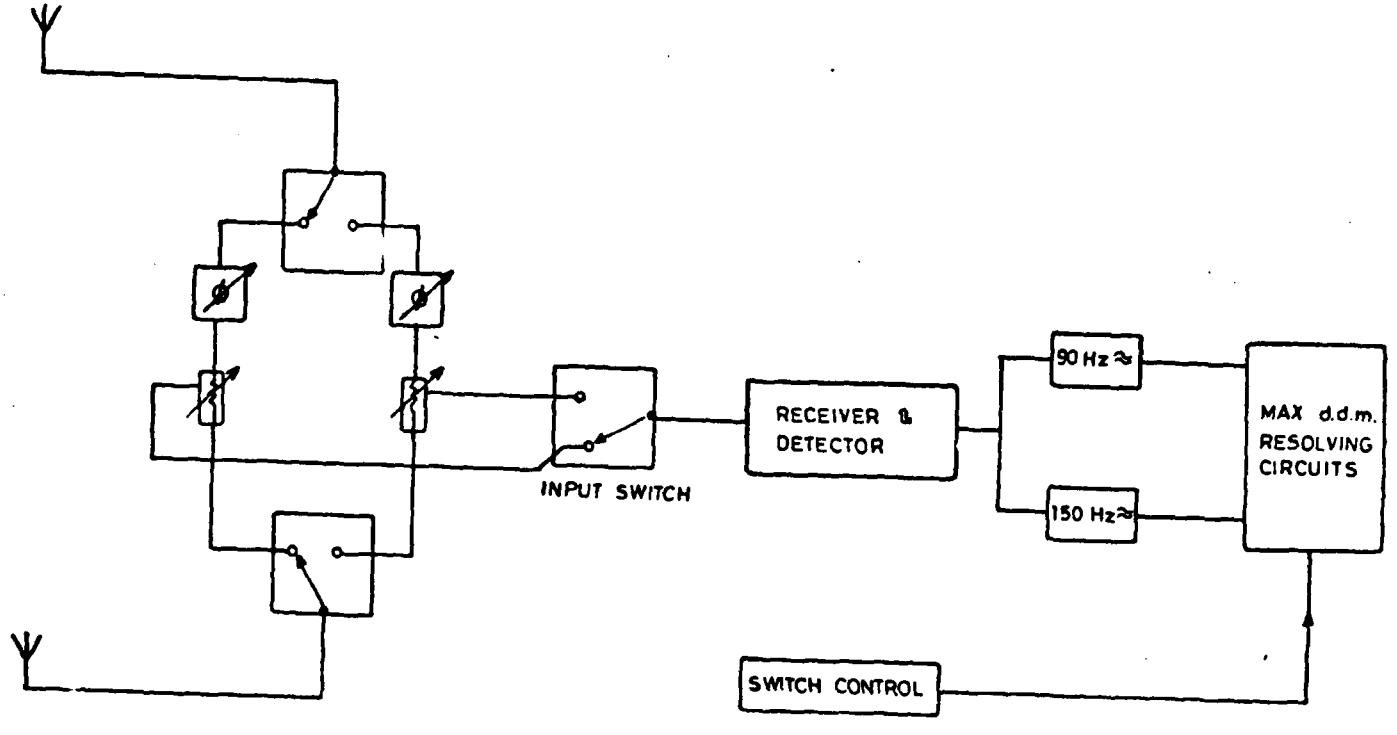

FIG. B-6 SWITCHED AERIAL SYSTEM FOR INTERFEROMETER TYPE FAR FIELD MONITOR

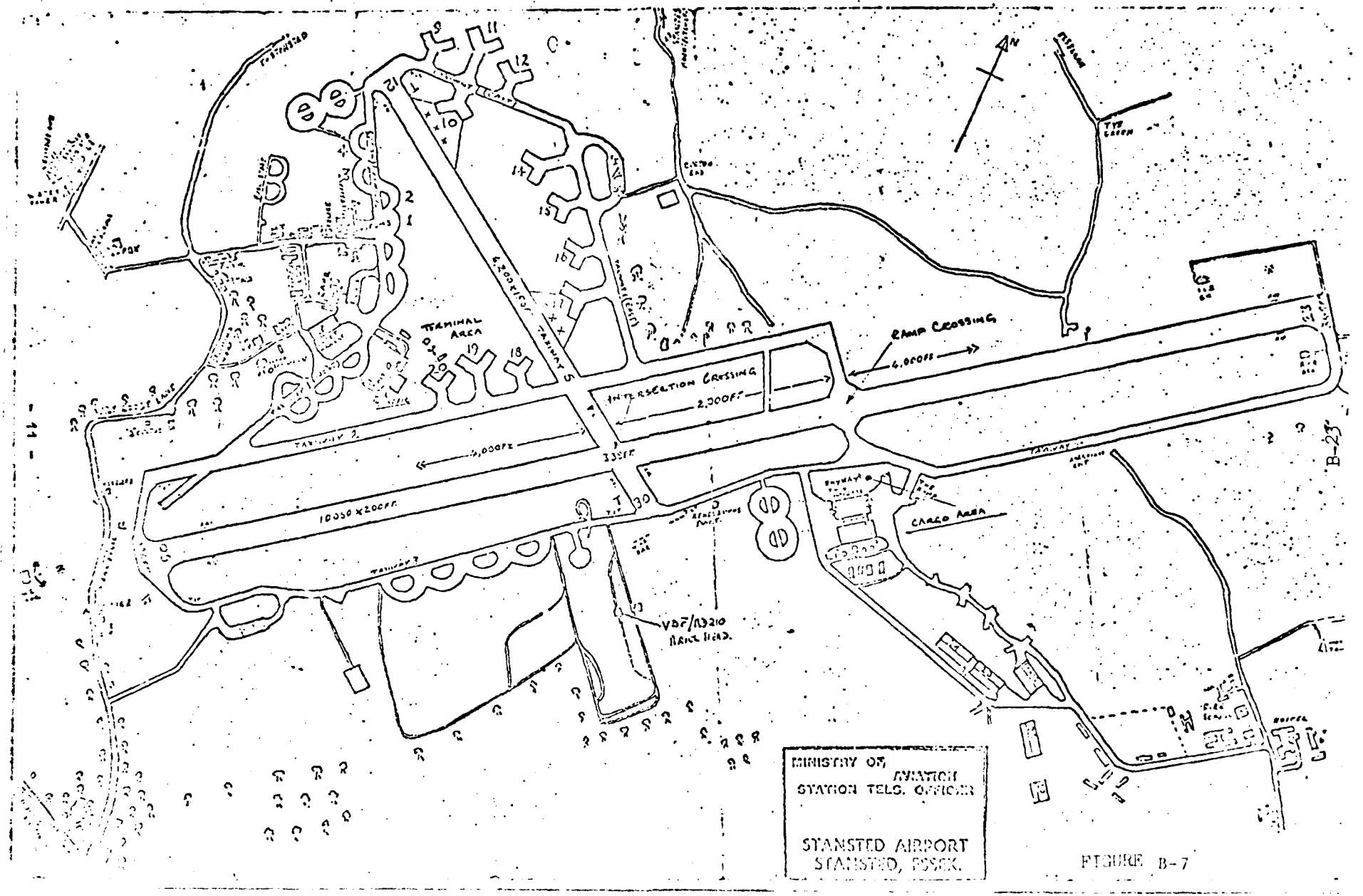
TERMINAL AREA
RAMP CROSSING
4,000FT
INTERSECTION CROSSING
2,000FT
TAXIWAY 2
TAXIWAY 5
TAXIWAY 7
10050 X 200FT
CARGO AREA
VDF/13210
MINISTRY OF AVIATION
STATION TELG. OFFICER
STANSTED AIRPORT
STANSTED, ESSEX.

FIGURE B-7

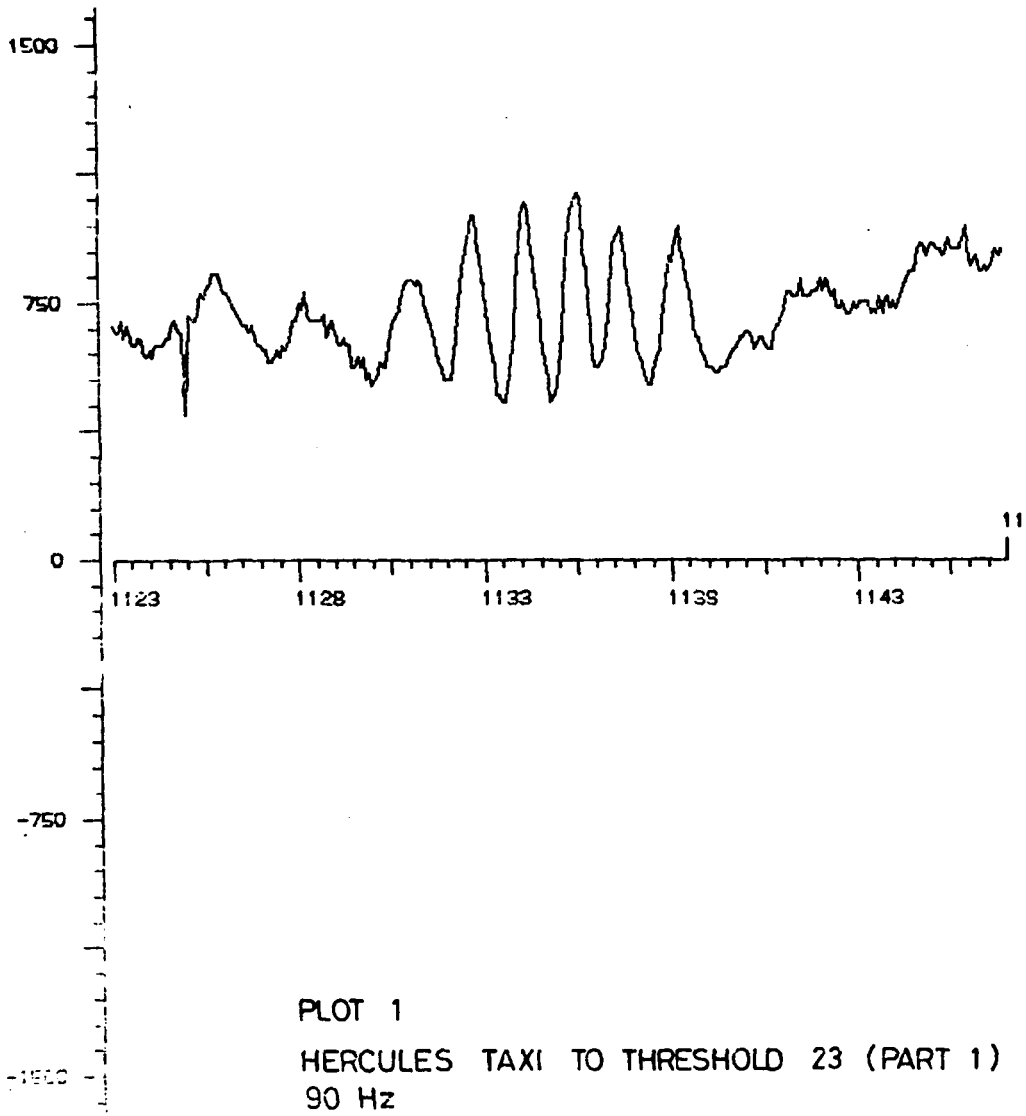

STANSTED TAPE 4
U.V.NO. 4
180 FT (APPROX)

GRAPH A2

WAIT

PARAMETER=1
SAMPLE RATE=15
DISC 3=RICETAP4-200-3
Y SCALE= $_{10}$-2 C4/1
X SCALE=200/200

PLOT 1
HERCULES TAXI TO THRESHOLD 23 (PART 1)
90 Hz

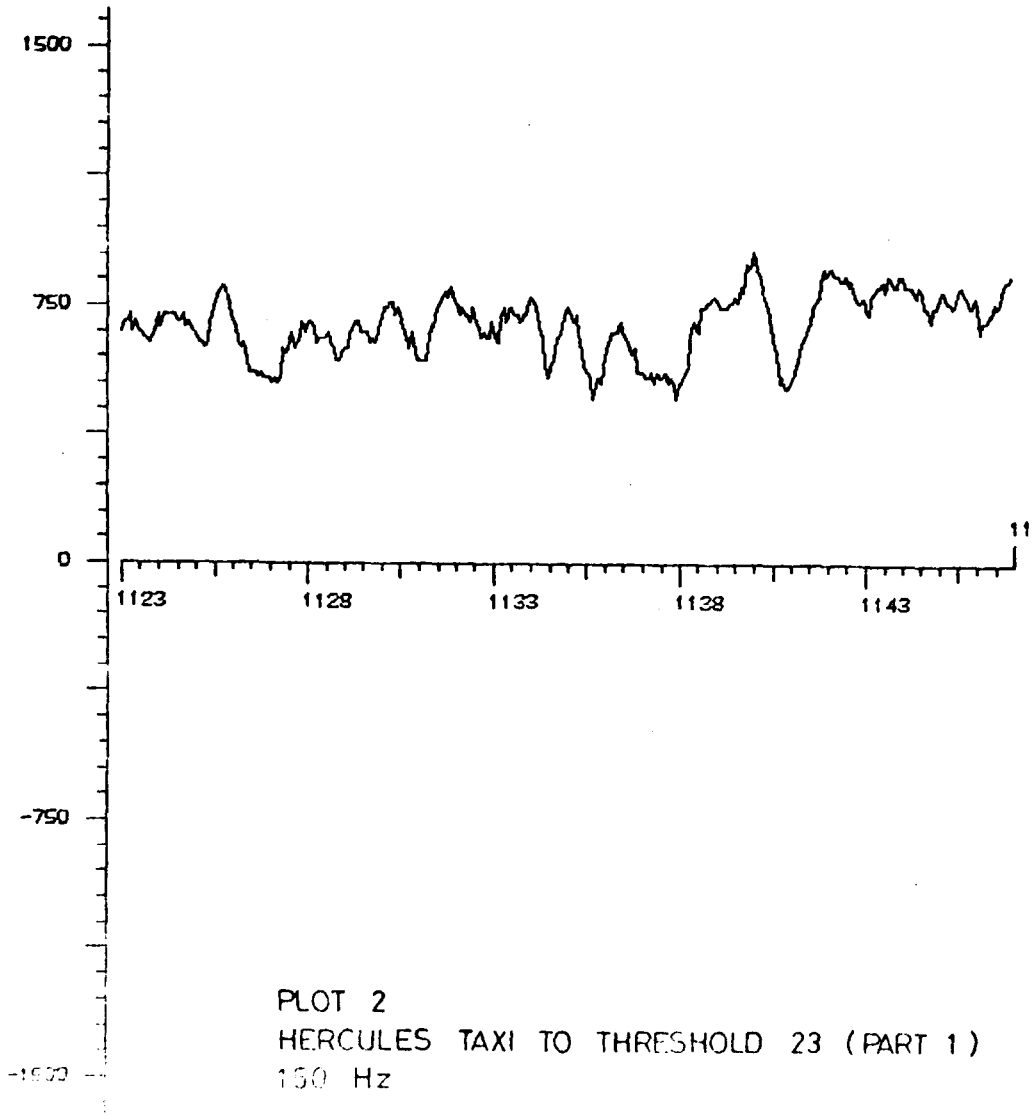

STANSTED TAPE 4
U.V.NO. 4
180 FT (APPROX)

GRAPH A3

WAIT

PARAMETER=2
SAMPLE RATE=15
DISC 3=RICETAP4-200-3
Y SCALE= $_{10}$-2 C4/1
X SCALE=200/200

PLOT 2
HERCULES TAXI TO THRESHOLD 23 (PART 1)
150 Hz

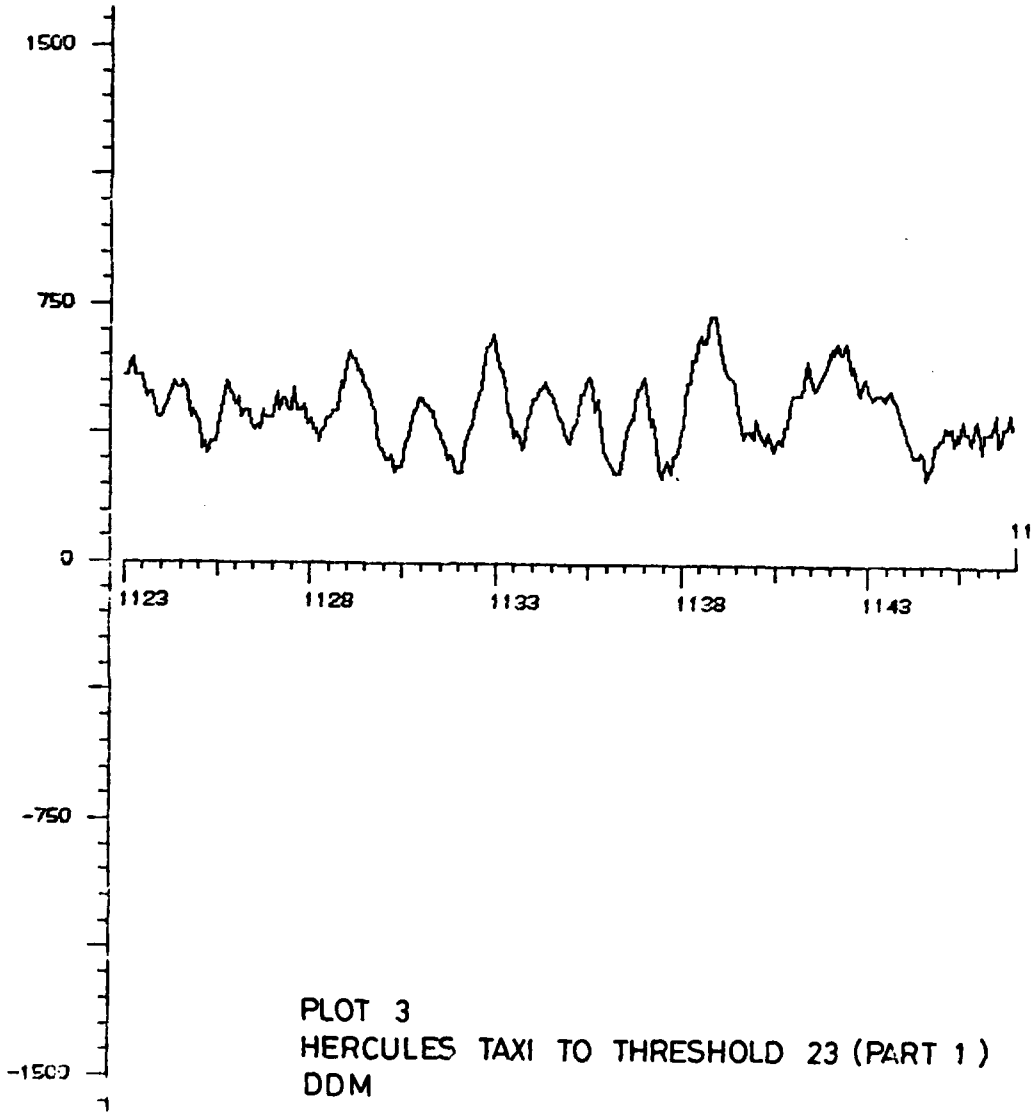

STANSTED TAPE 4
U.V.NO. 4
180 FT (APPROX)

GRAPH A4

WAIT

PARAMETER=3
SAMPLE RATE=15
DISC 3=RICETAP4-200-3
Y SCALE= $_{10}$-2 C4/1
X SCALE=200/200

PLOT 3
HERCULES TAXI TO THRESHOLD 23 (PART 1)
DDM

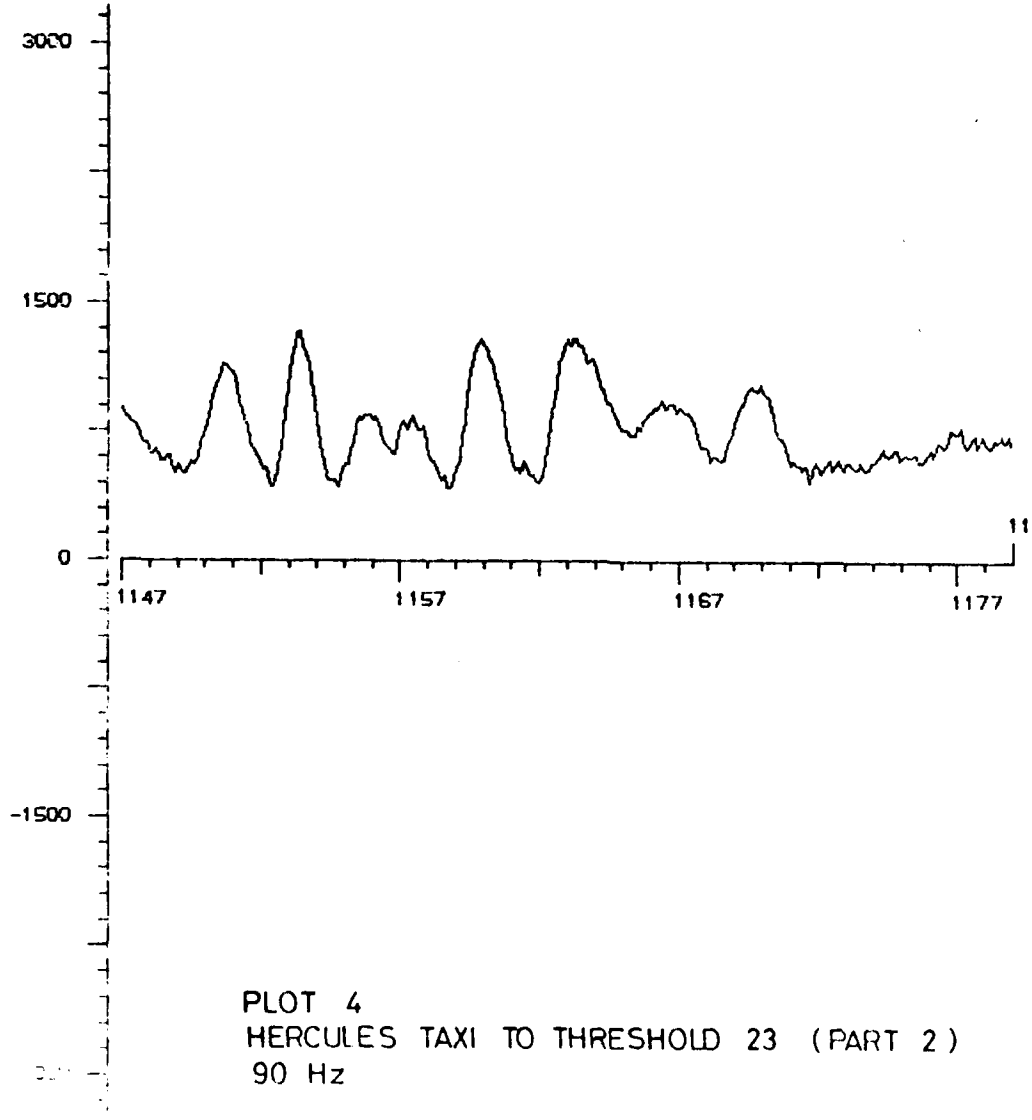

STANSTED TAPE 4
U.V.NO. 4
180 FT (APPROX)

GRAPH A5

WAIT

PARAMETER=1
SAMPLE RATE=20
DISC 3=RICETAP4-200-3
Y SCALE= $_{10}$-2 C4/1
X SCALE=200/200

PLOT 4
HERCULES TAXI TO THRESHOLD 23 (PART 2)
90 Hz

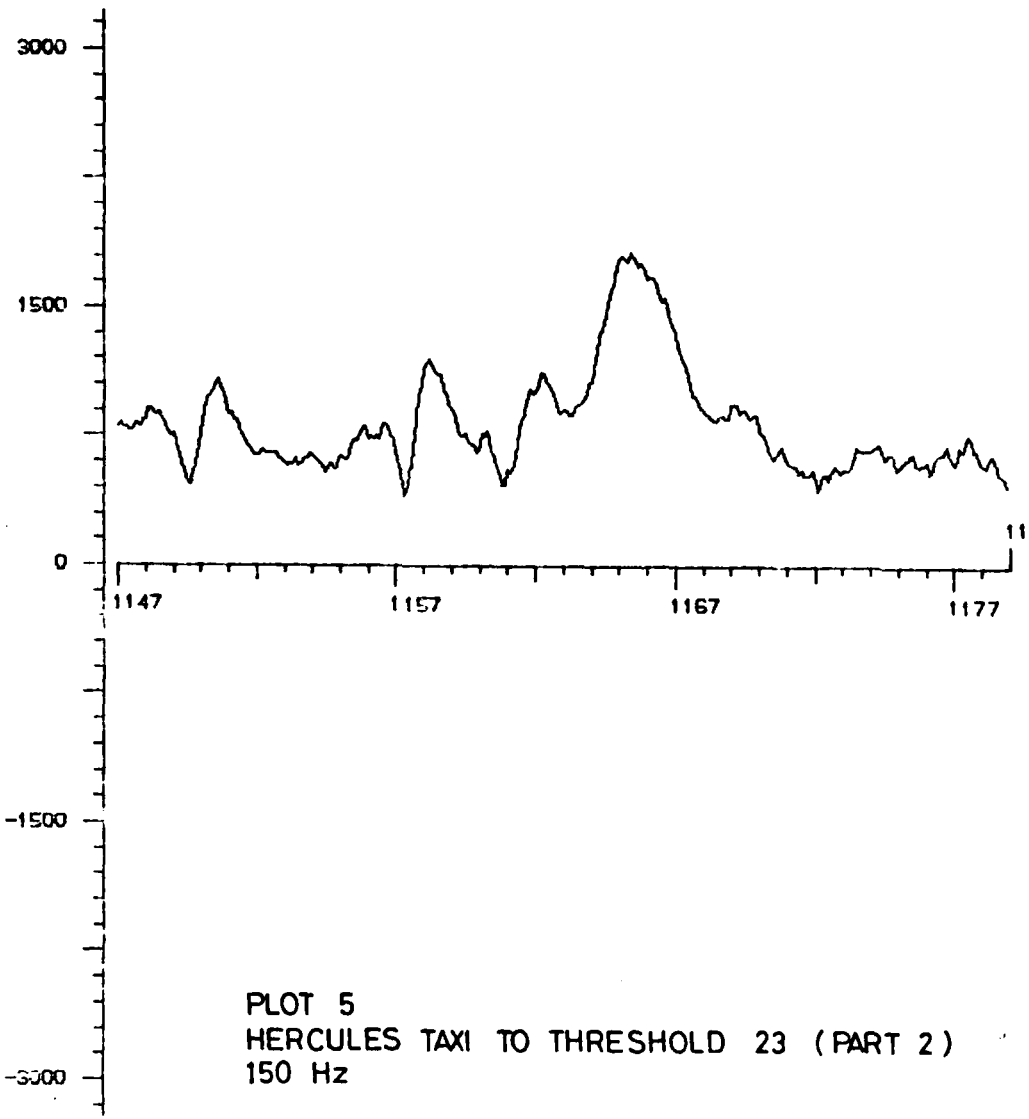

STANSTED TAPE 4
U.V.NO. 4
180 FT (APPROX)

GRAPH A6

WAIT

PARAMETER=2
SAMPLE RATE=20
DISC 3=RICETAP4-200-3
Y SCALE= $_{10}$-2 C4/1
X SCALE=200/200

PLOT 5
HERCULES TAXI TO THRESHOLD 23 (PART 2)
150 Hz

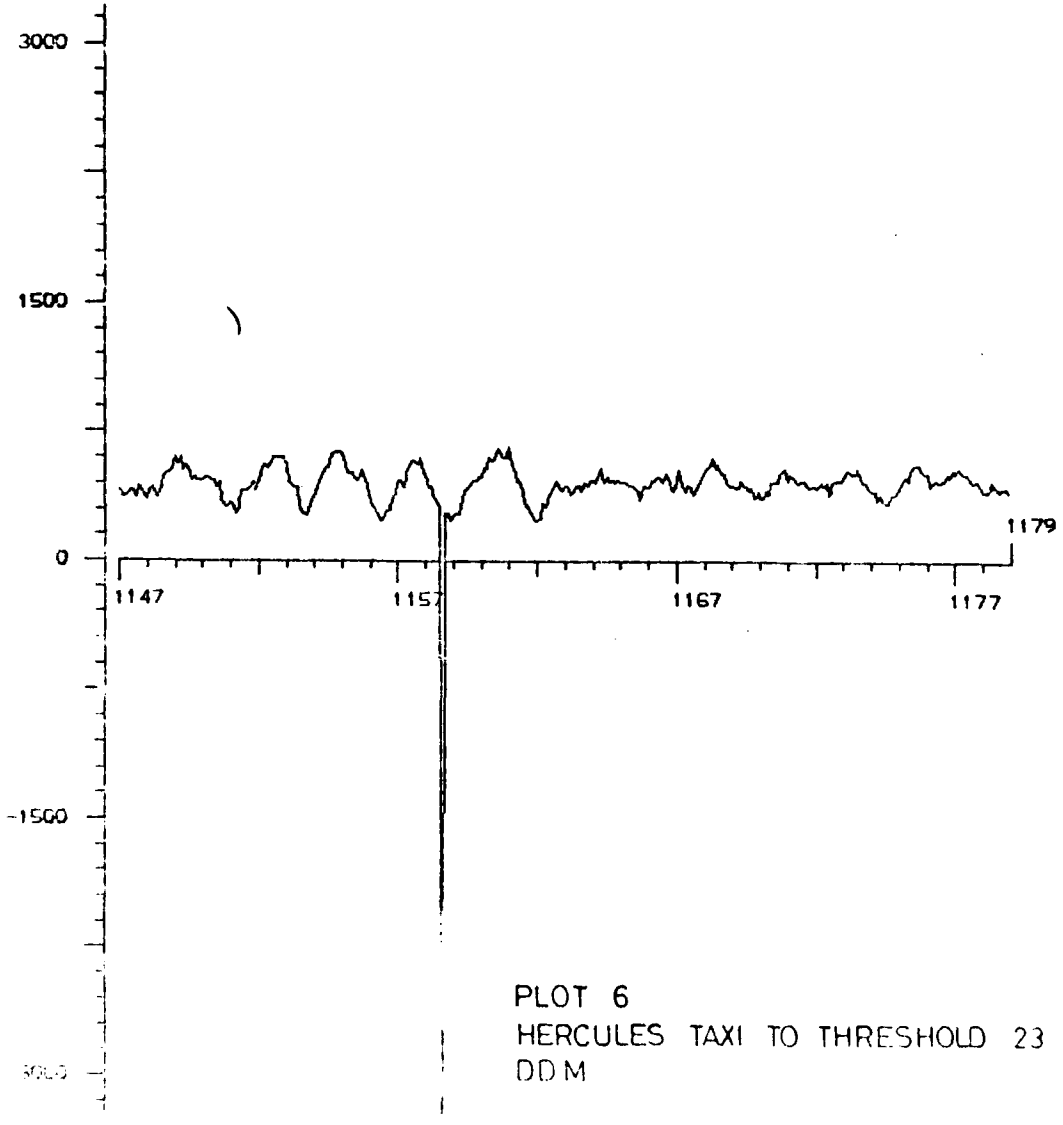

STANSTED TAPE 4
U.V.NO. 4
180 FT (APPROX)

GRAPH A7

WAIT

PARAMETER=3
SAMPLE RATE=20
DISC 3=RICETAP4-200-3
Y SCALE= $_{10}$-2 C4/1
X SCALE=200/200

PLOT 6
HERCULES TAXI TO THRESHOLD 23 (PART 2)
DD M

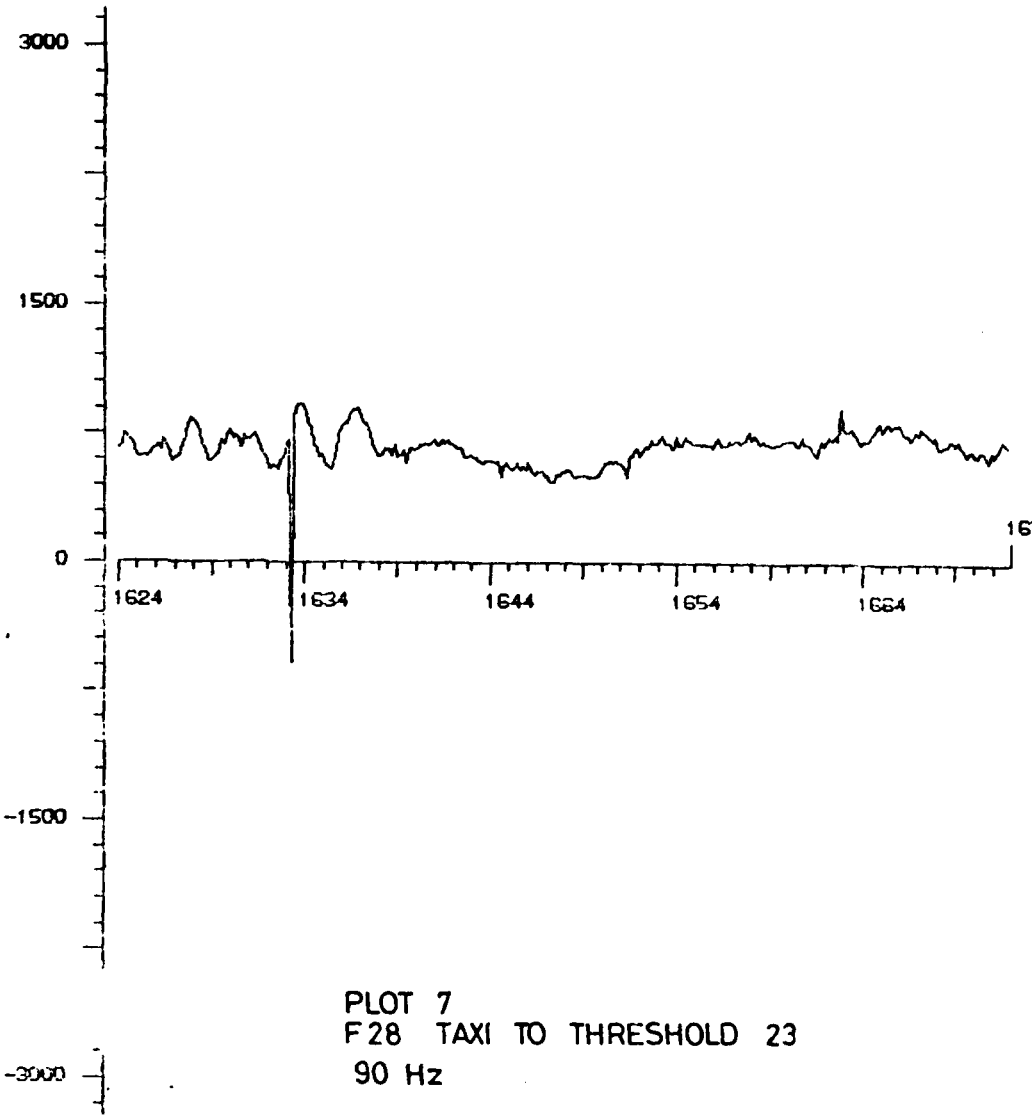

STANSTED TAPE 4
U V.NO. 5
287 FT (APPROX)
ON CL

GRAPH A8

WAIT

PARAMETER=1
SAMPLE RATE=30
DISC 3=RICETAP4-200-3
Y SCALE= $_{10}$-2 C4/1
X SCALE=200/200

PLOT 7
F28 TAXI TO THRESHOLD 23
90 Hz

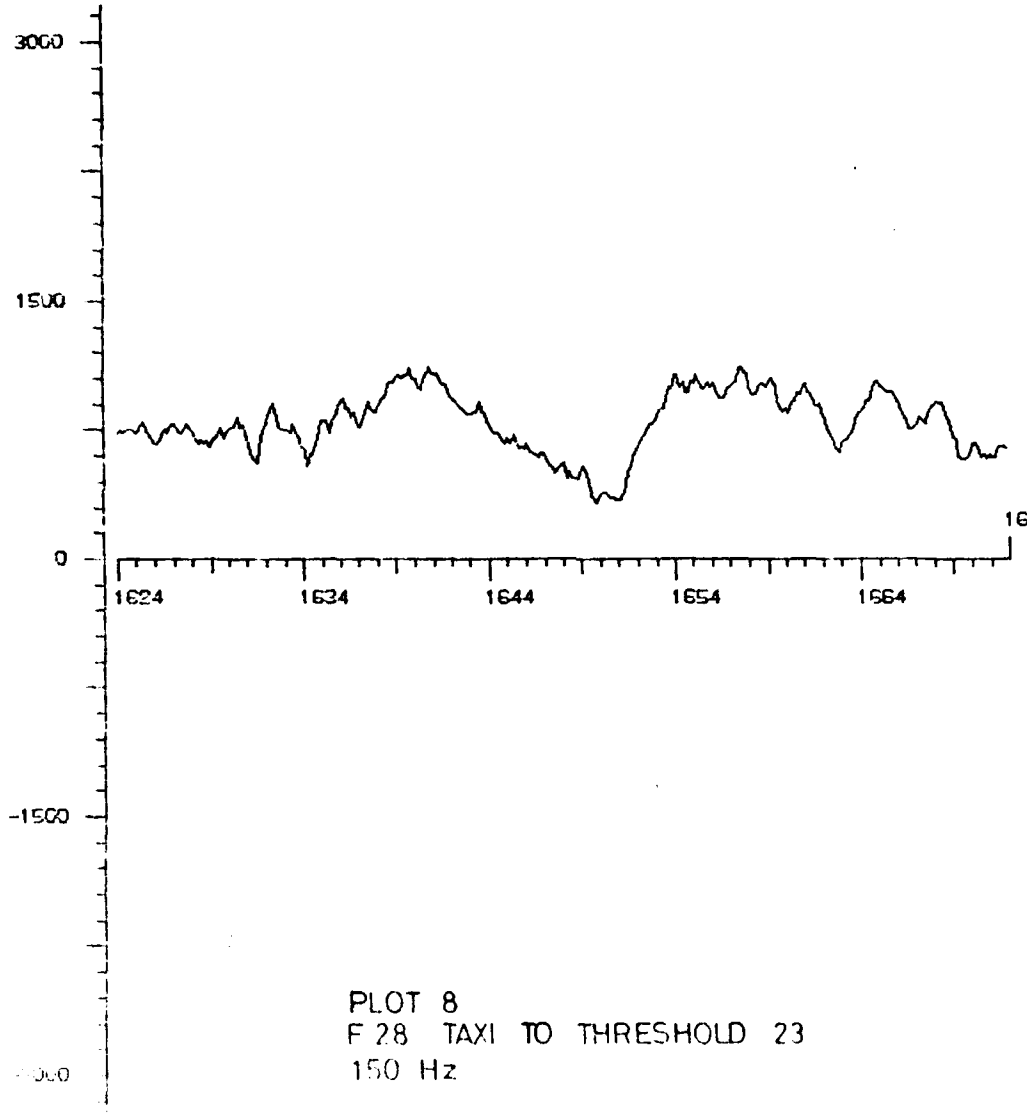

STANSTED TAPE 4
U.V.NO. 5
287 FT (APPROX)
ON CL

GRAPH A9

WAIT

PARAMETER=2
SAMPLE RATE=30
DISC 3=RICETAP4-200-3
Y SCALE= $_{10}$-2 C4/1
X SCALE=200/200

PLOT 8
F 28 TAXI TO THRESHOLD 23
150 Hz

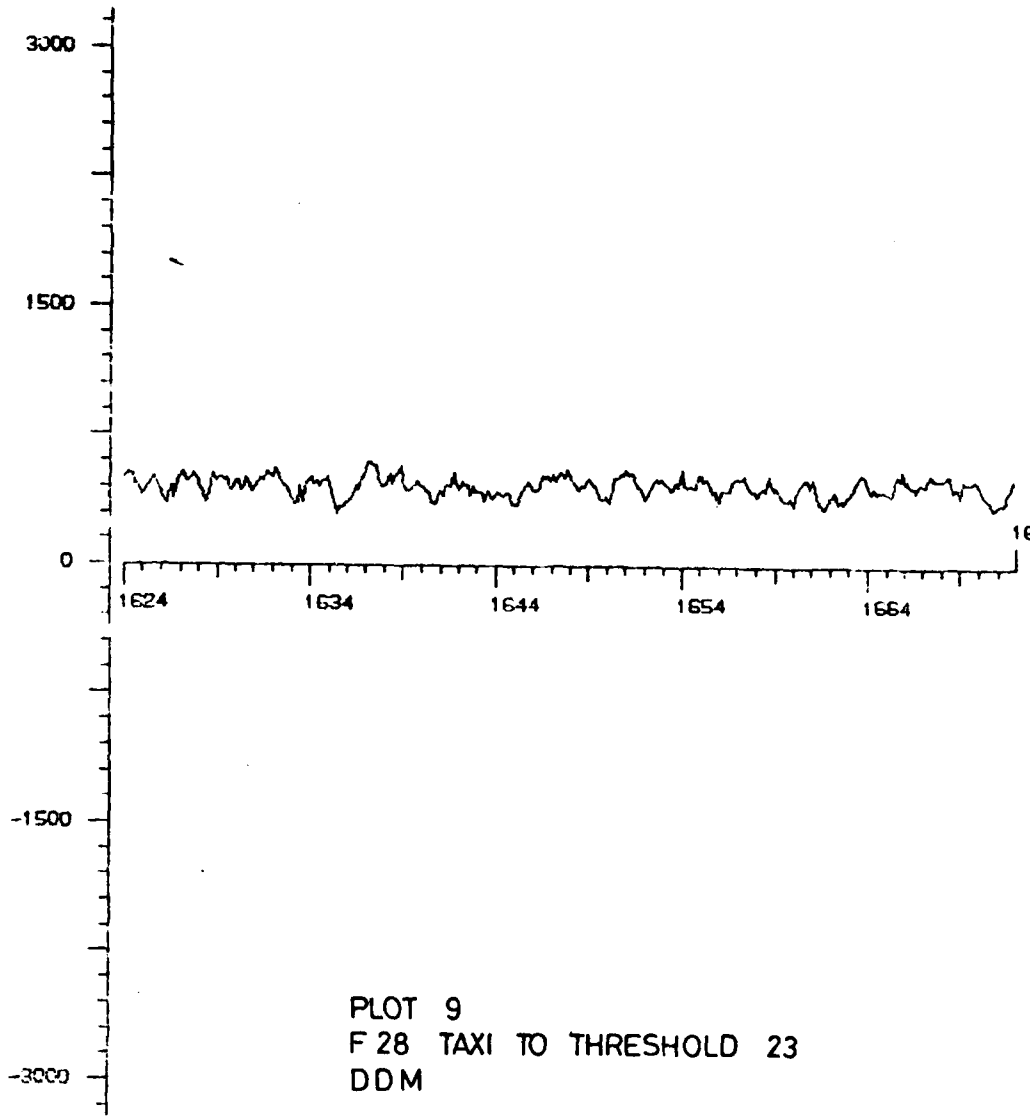

STANSTED TAPE 4
U.V.NO. 5
287 FT (APPROX)
ON. CL

GRAPH A10

WAIT

PARAMETER=3
SAMPLE RATE=30
DISC 3=RICETAP4-200-3
Y SCALE= $_{10}$-2 C4/1
X SCALE=200/200

PLOT 9
F 28 TAXI TO THRESHOLD 23
DDM

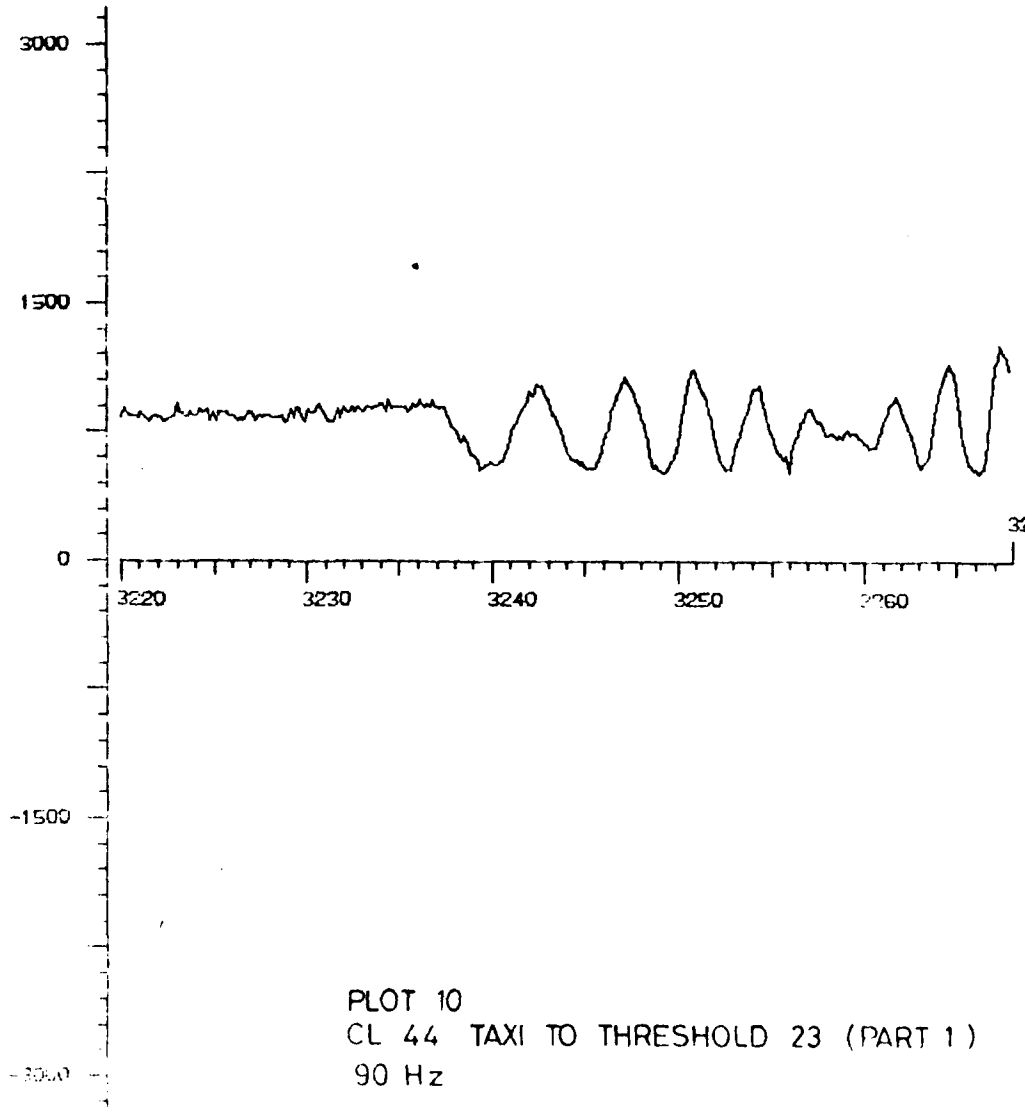

STANSTED TAPE 4
U.V.NO. 9
728 FT (APPROX)
CL44 STARTS TO MOVE

GRAPH A26

WAIT

PARAMETER=1
SAMPLE RATE=30
DISC 3=RICETAP4-200-3
Y SCALE= $_{10}$-2 C4/1
X SCALE=200/200

PLOT 10
CL 44 TAXI TO THRESHOLD 23 (PART 1)
90 Hz

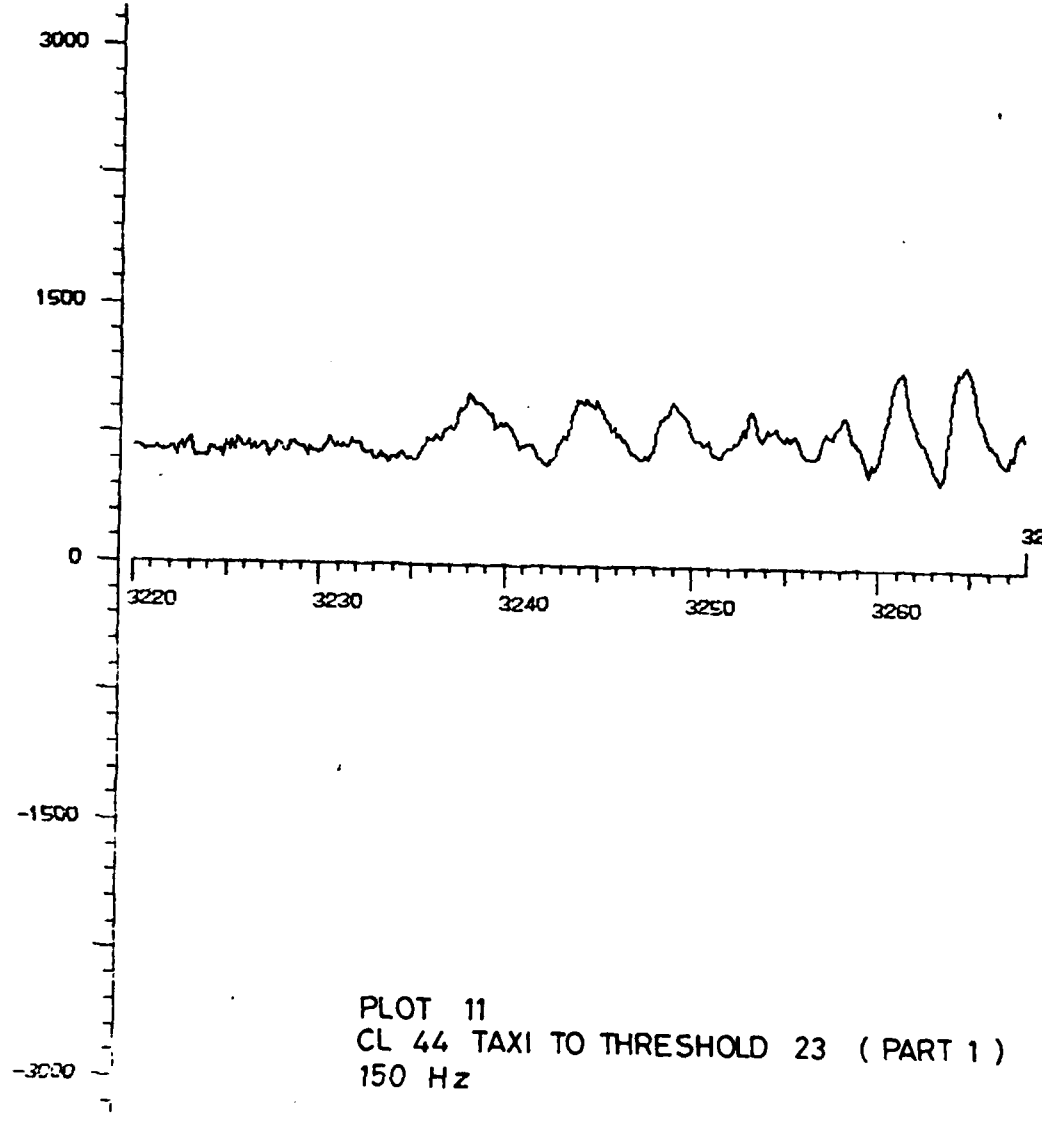

STANSTED TAPE 4
U.V.NO. 9
728 FT (APPROX)
CL44 STARTS TO MOVE

GRAPH A27

WAIT

PARAMETER=2
SAMPLE RATE=30
DISC 3=RICETAP4-200-3
Y SCALE= $_{10}$-2 C4/1
X SCALE=200/200

PLOT 11
CL 44 TAXI TO THRESHOLD 23 (PART 1)
150 Hz

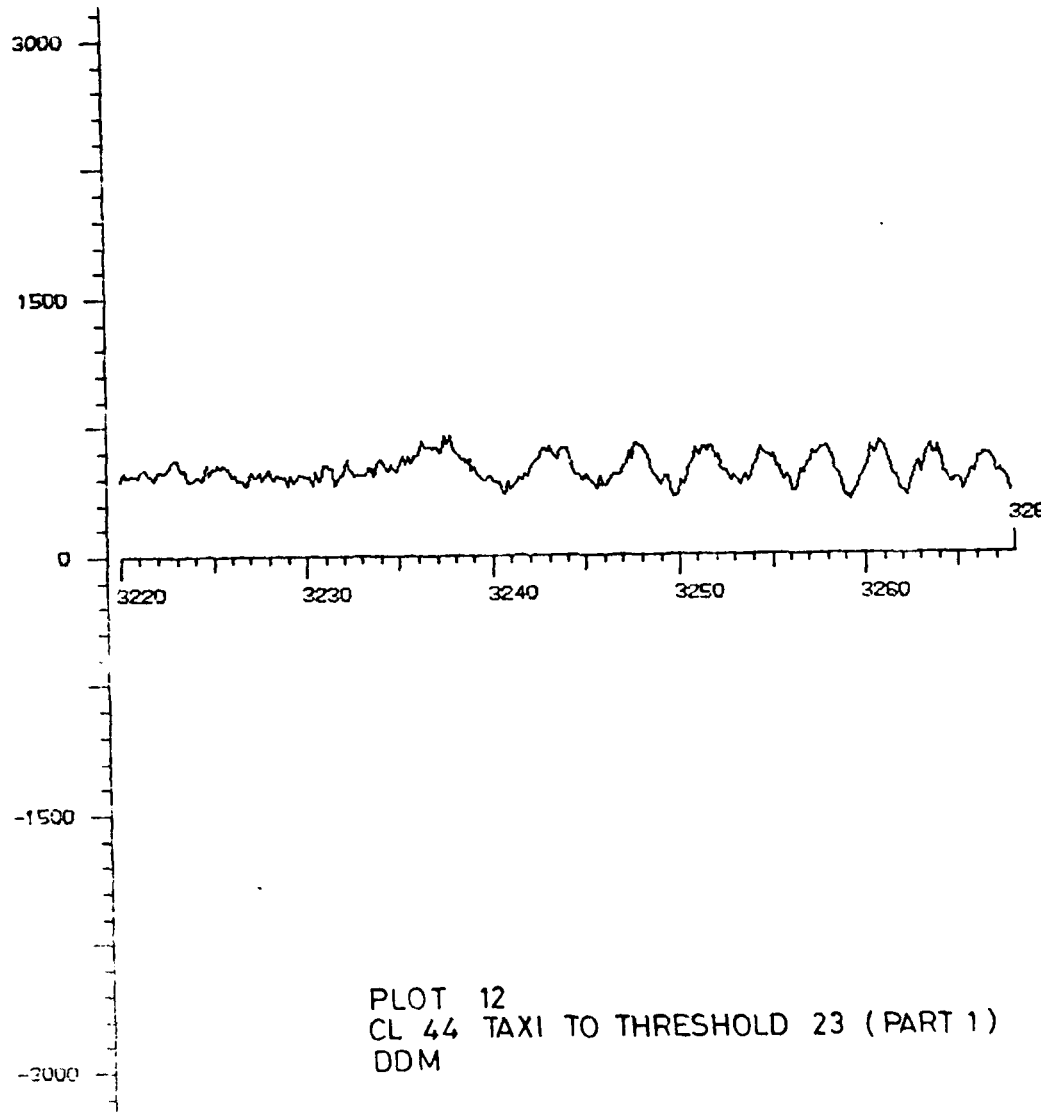

STANSTED TAPE 4
U.V.NO. 9
728 FT (APPROX)
CL44 STARTS TO MOVE

GRAPH A28

WAIT

PARAMETER=3
SAMPLE RATE=30
DISC 3=RICETAP4-200-3
Y SCALE= $_{10}$-2 C4/1
X SCALE=200/200

PLOT 12
CL 44 TAXI TO THRESHOLD 23 (PART 1)
DDM

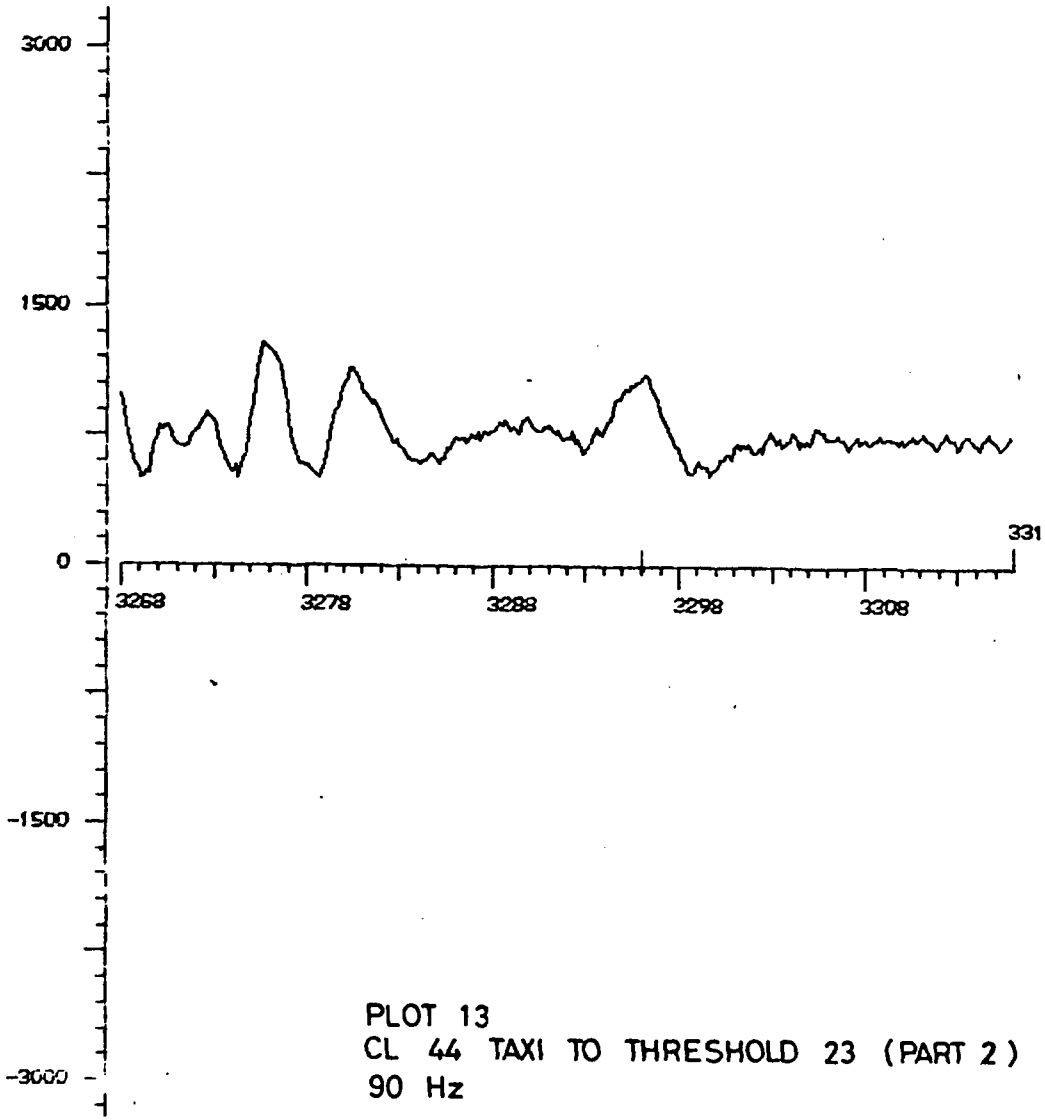

STANSTED TAPE 4
U.V.NO. 9
728 FT (APPROX)
CL44 STARTS TO MOVE

GRAPH A29

WAIT

PARAMETER=1
SAMPLE RATE=30
DISC 3=RICETAP4-200-3
Y SCALE= $_{10}$-2 C4/1
X SCALE=200/200

PLOT 13
CL 44 TAXI TO THRESHOLD 23 (PART 2)
90 Hz

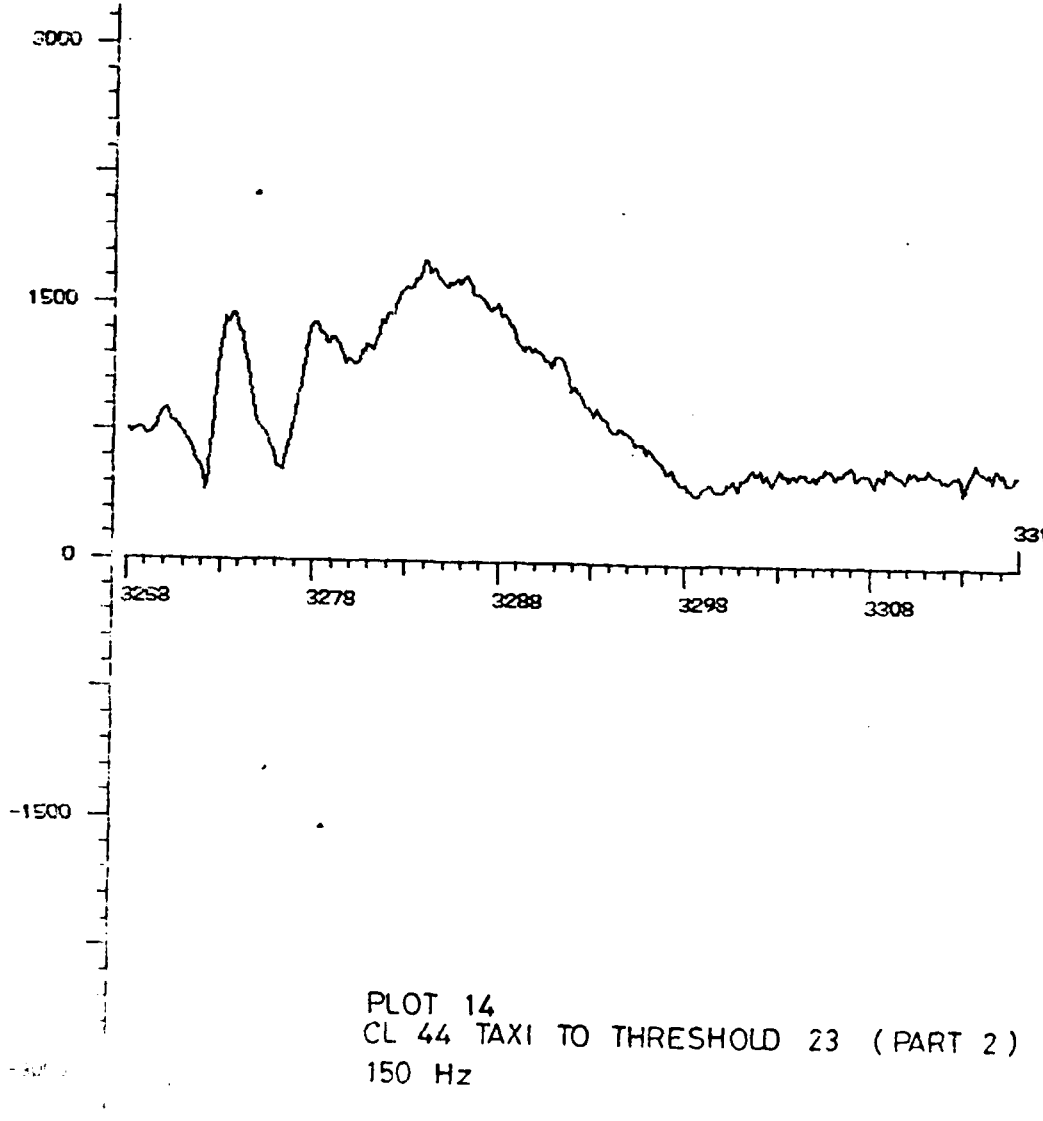

STANSTED TAPE 4
U.V.NO. 9
728 FT (APPROX)
CL44 STARTS TO MOVE

GRAPH A30

WAIT

PARAMETER=2
SAMPLE RATE=30
DISC 3=RICETAP4-200-3
Y SCALE= $_{10}$-2 C4/1
X SCALE=200/200

PLOT 14
CL 44 TAXI TO THRESHOLD 23 (PART 2)
150 Hz

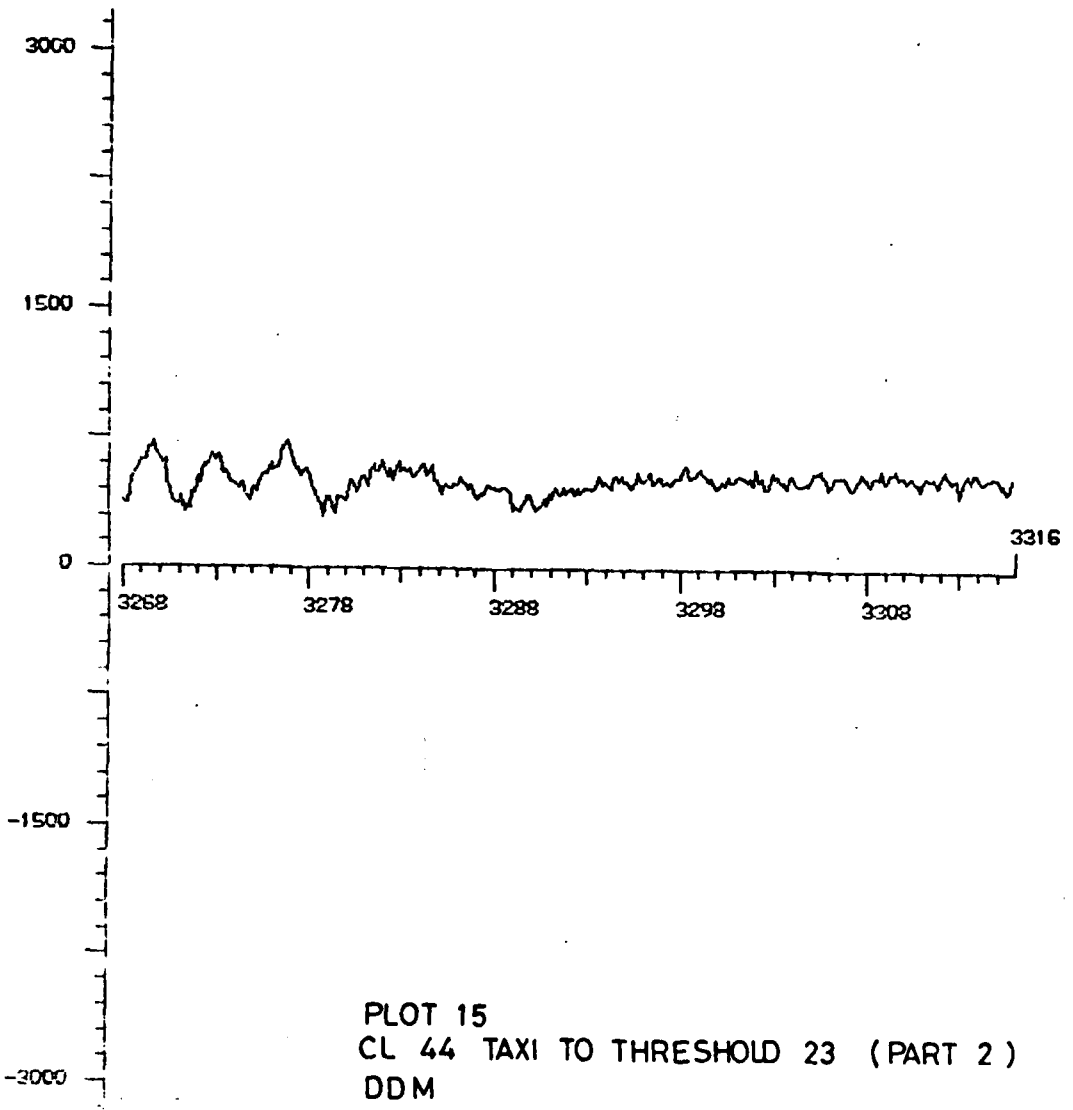

STANSTED TAPE 4
U.V.NO. 9
728 FT (APPROX)
CL44 STARTS TO MOVE

GRAPH A31

WAIT

PARAMETER=3
SAMPLE RATE=30
DISC 3=RICETAP4-200-3
Y SCALE= ,,-2 C4/1
X SCALE=200/200

PLOT 15
CL 44 TAXI TO THRESHOLD 23 (PART 2)
DDM

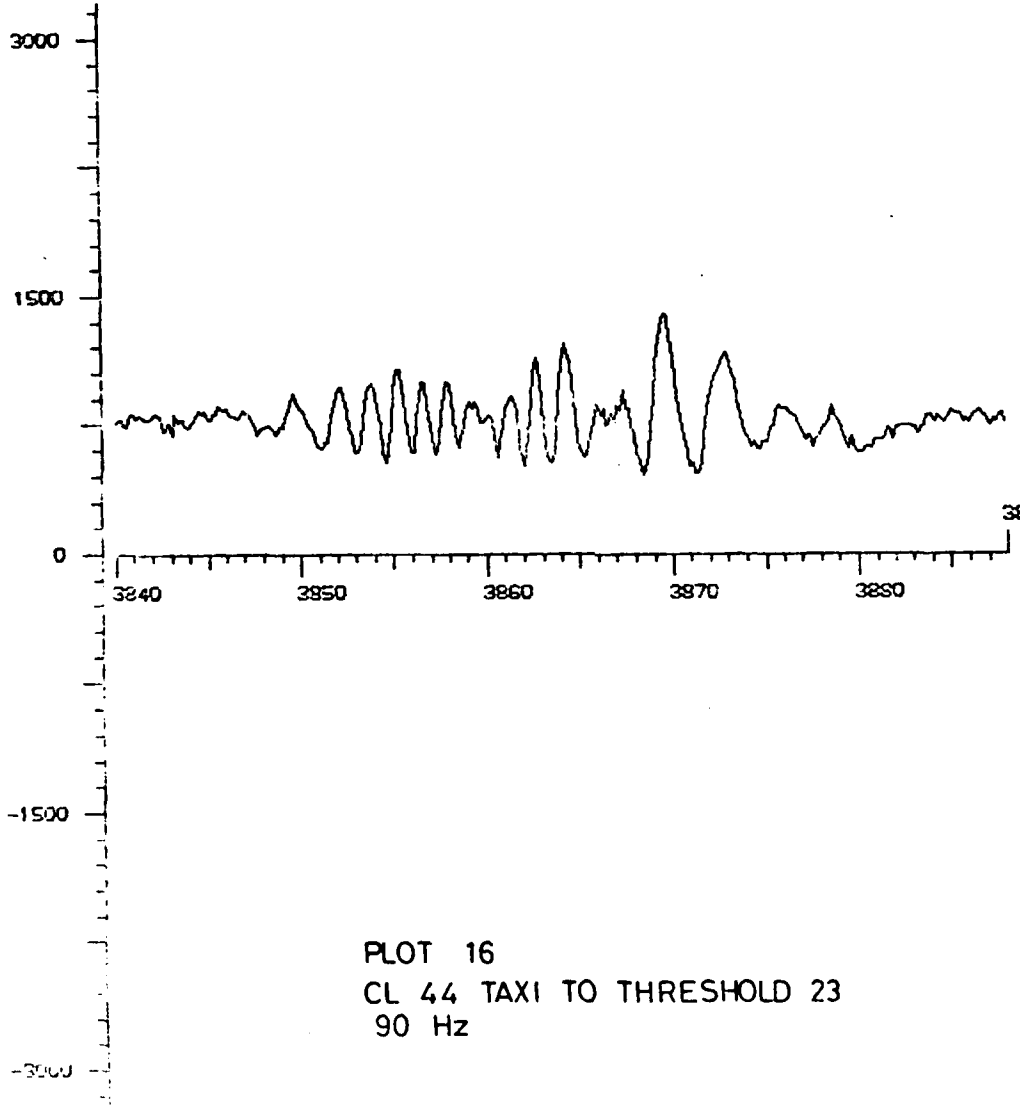

STANSTED TAPE 4
U.V.NO. 10
823 FT (APPROX)
CL44

GRAPH A35

WAIT

PARAMETER=1
SAMPLE RATE=30
DISC 3=RICETAP4-200-3
Y SCALE= $_{10}$-2 C4/1
X SCALE=200/200

PLOT 16
CL 44 TAXI TO THRESHOLD 23
90 Hz

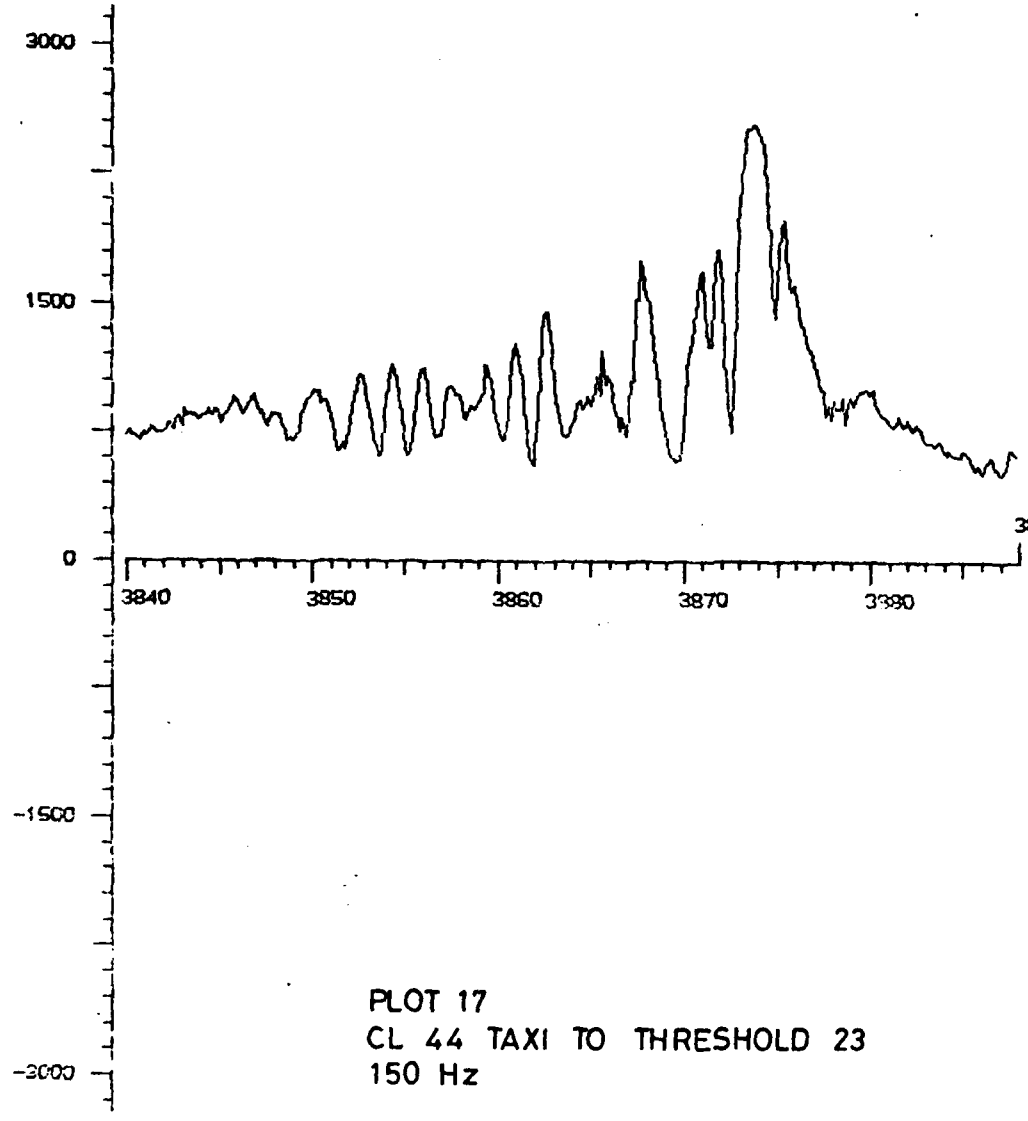

STANSTED TAPE 4
U.V.NO. 10
823 FT (APPROX)
CL44

GRAPH A36

WAIT

PARAMETER=2
SAMPLE RATE=30
DISC 3=RICETAP4-200-3
Y SCALE= $_{10}$-2 C4/1
X SCALE=200/200

PLOT 17
CL 44 TAXI TO THRESHOLD 23
150 Hz

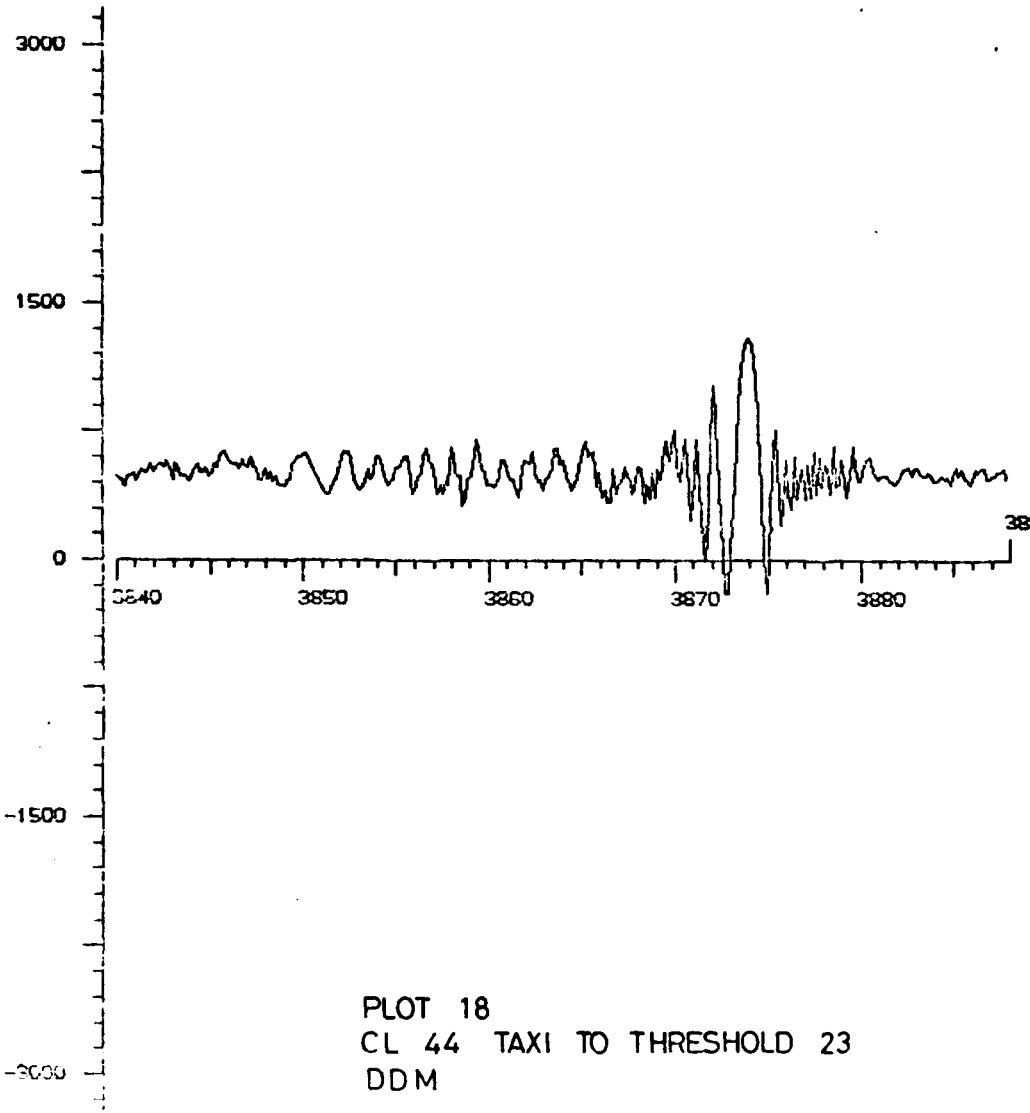

STANSTED TAPE 4
U.V.NO. 10
823 FT (APPROX)
CL44

GRAPH A37

WAIT

PARAMETER=3
SAMPLE RATE=30
DISC 3=RICETAP4-200-3
Y SCALE= $_{10}$-2 C4/1
X SCALE=200/200

PLOT 18
CL 44 TAXI TO THRESHOLD 23
DDM

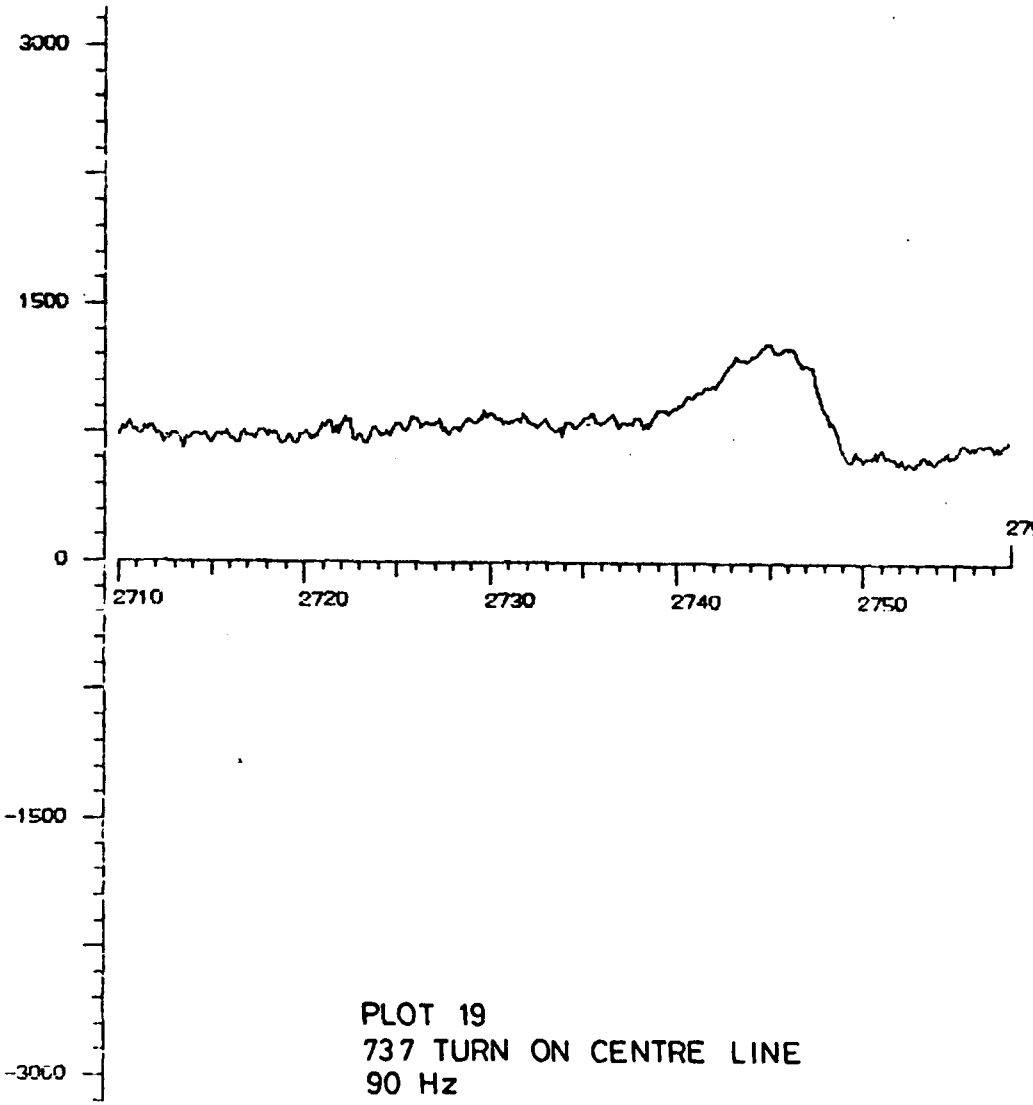

STANSTED TAPE 4
U.V.NO. 89
648 FT (APPROX)
TURNS

GRAPH A23

WAIT

PARAMETER=1
SAMPLE RATE=30
DISC 3=RICETAP4-200-3
Y SCALE= $_{10}$-2 C4/1
Y SCALE=200/200

PLOT 19
737 TURN ON CENTRE LINE
90 Hz

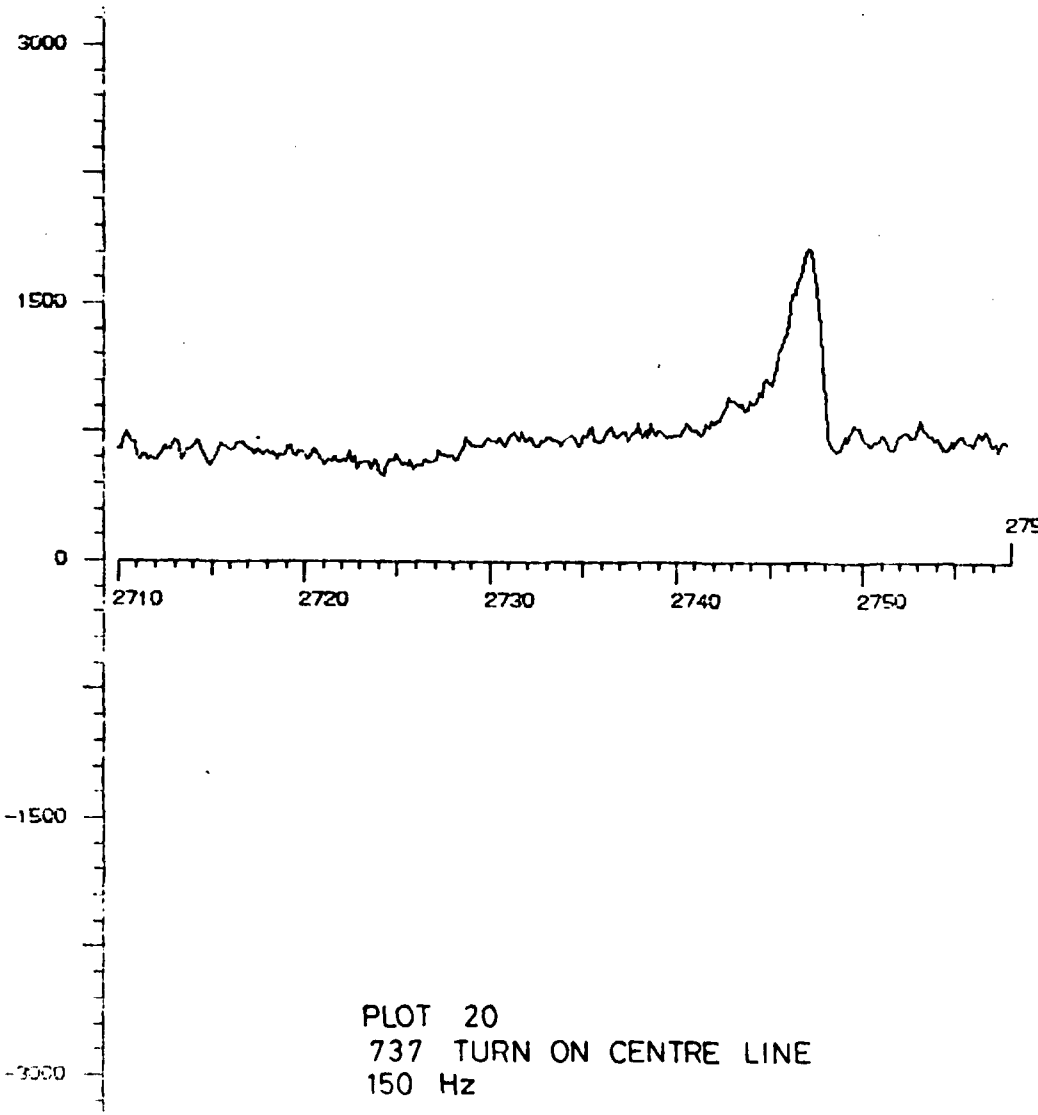

STANSTED TAPE 4
U.V.NO. 89
648 FT (APPROX)
TURNS

GRAPH A24

WAIT

PARAMETER=2
SAMPLE RATE=30
DISC 3=RICETAP4-200-3
Y SCALE= $_{10}$-2 C4/1
X SCALE=200/200

PLOT 20
737 TURN ON CENTRE LINE
150 Hz

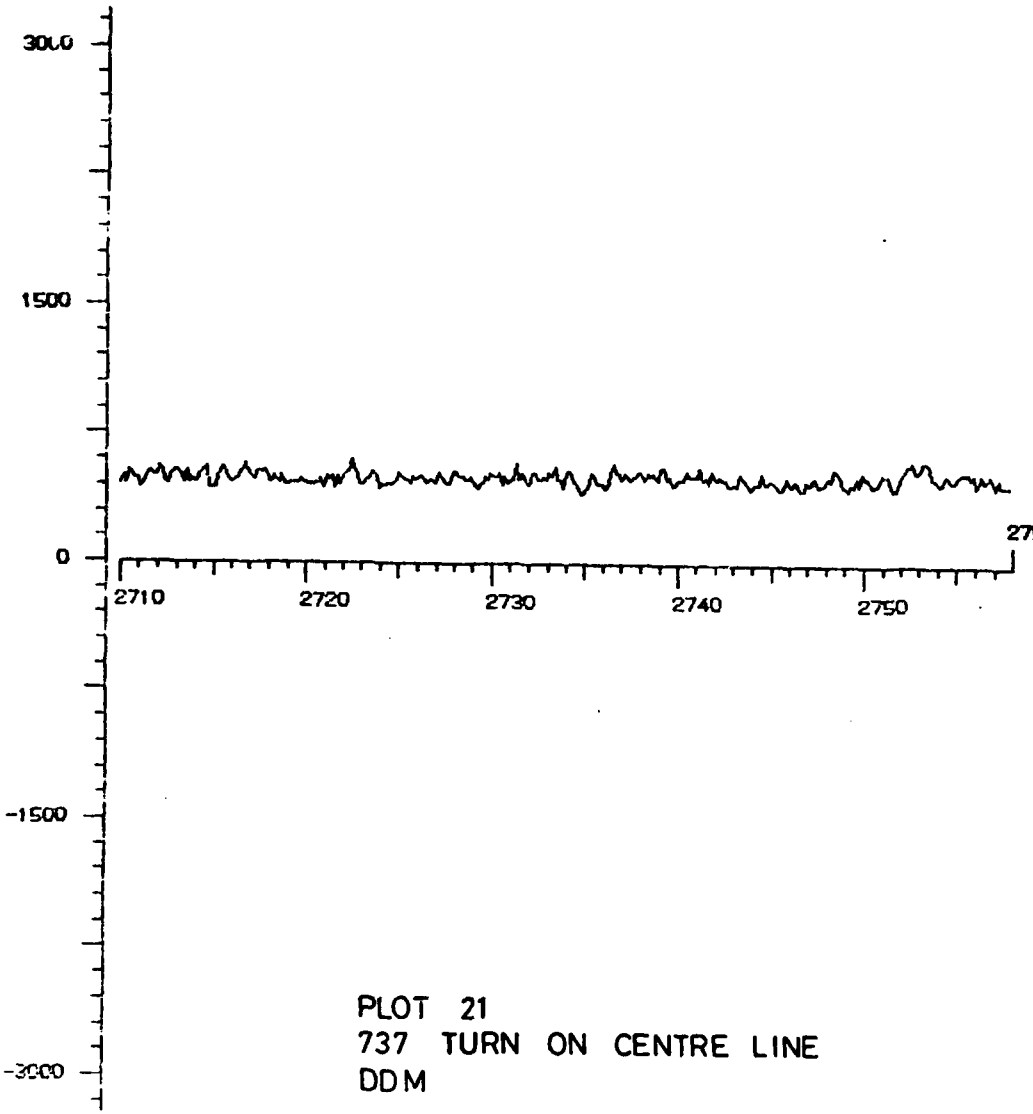

STANSTED TAPE 4
U.V.NO. 89
648 FT (APPROX)
TURNS

GRAPH A25

WAIT

PARAMETER=3
SAMPLE RATE=30
DISC 3=RICETAP4-200-3
Y SCALE= $_{10}$-2 C4/1
X SCALE=200/200

PLOT 21
737 TURN ON CENTRE LINE
DDM

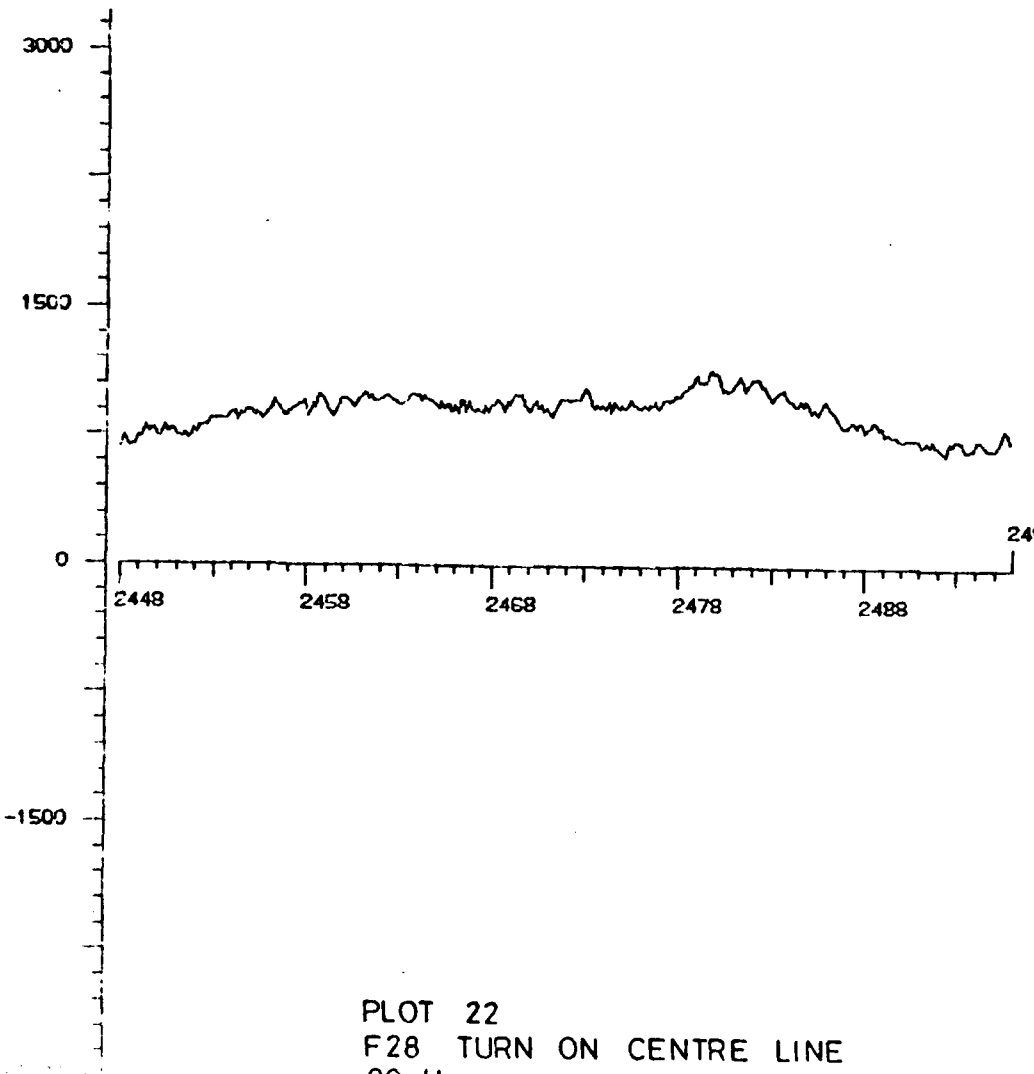

STANSTED TAPE 4
U.V.NO. 8
609 FT (APPROX)
TURN STARTS

GRAPH A17

WAIT

PARAMETER=1
SAMPLE RATE=30
DISC 3=RICETAP4-200-3
Y SCALE= $_{10}$-2 C4/1
X SCALE=200/200

PLOT 22
F28 TURN ON CENTRE LINE
90 Hz

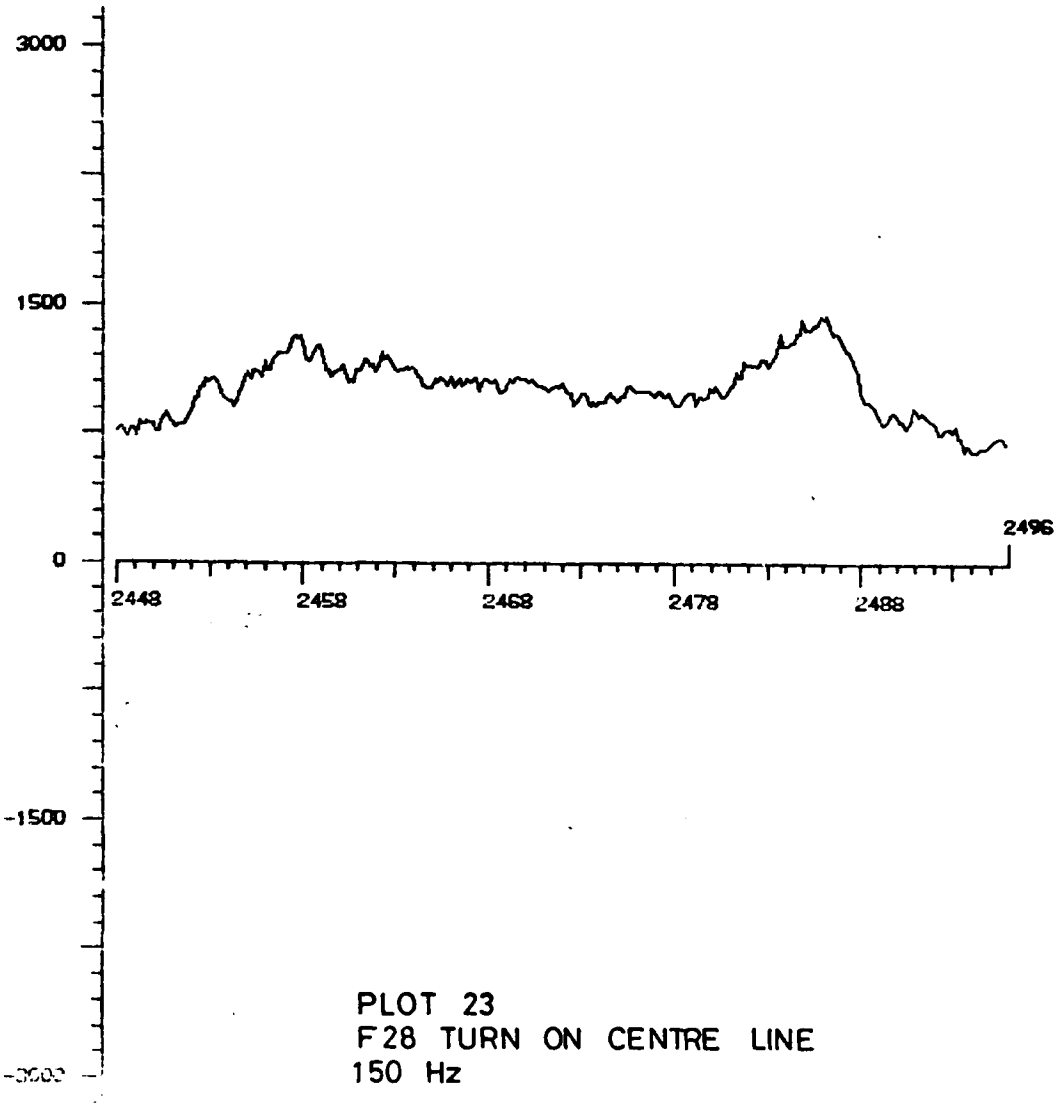

STANSTED TAPE 4
U.V.NO. 8
609 FT (APPROX)
TURN STARTS

GRAPH A18

WAIT

PARAMETER=2
SAMPLE RATE=30
DISC 3=RICETAP4-200-3
Y SCALE= $_{10}$-2 C4/1
X SCALE=200/200

PLOT 23
F28 TURN ON CENTRE LINE
150 Hz

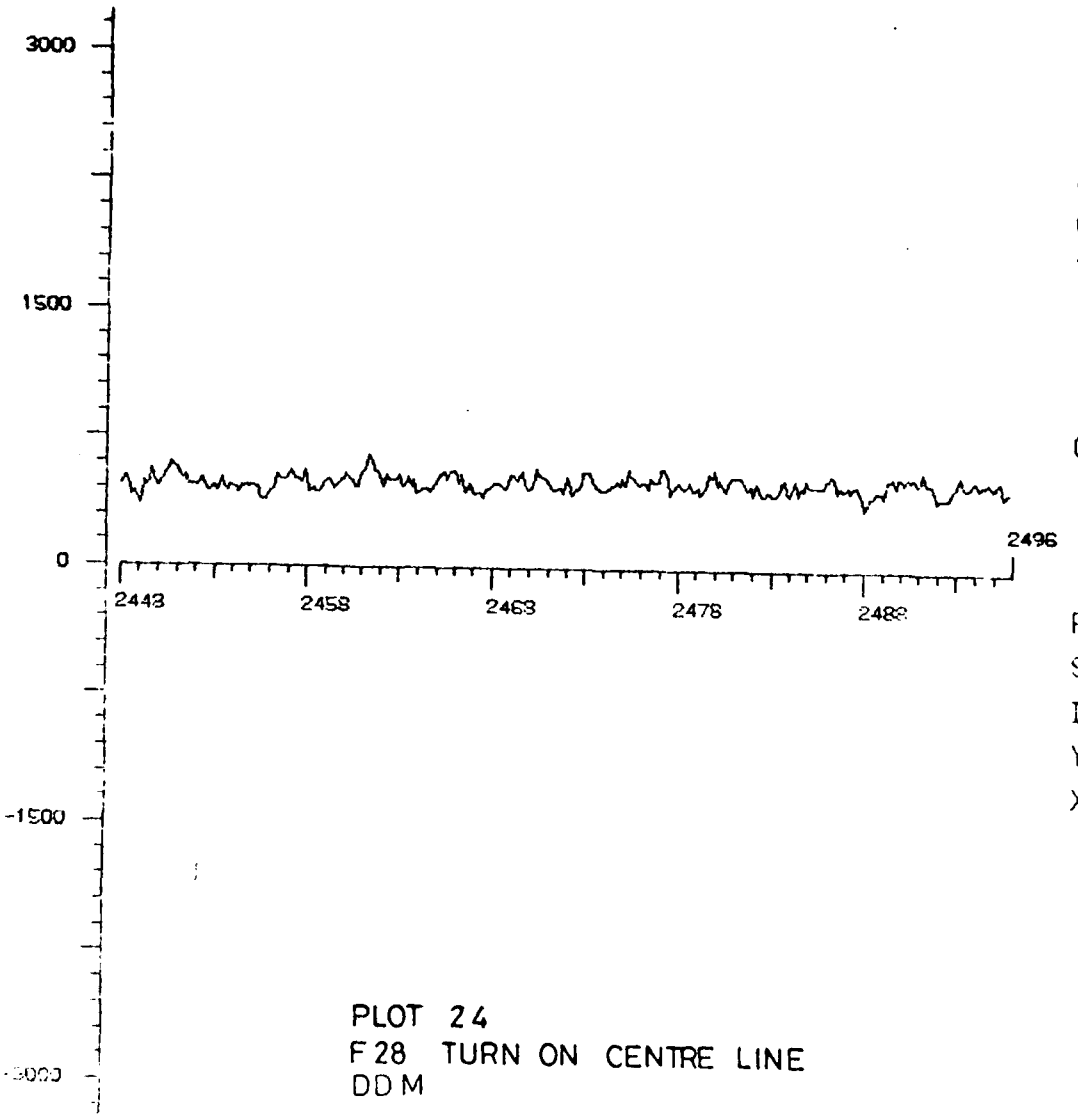

STANSTED TAPE 4
U.V. NO. 8
609 FT (APPROX)
TURN STARTS

GRAPH A19

WAIT

PARAMETER=3
SAMPLE RATE=30
DISC 3=RICETAP4-200-3
Y SCALE= $_{10}$-2 C4/1
X SCALE=200/200

PLOT 24
F28 TURN ON CENTRE LINE
DD M

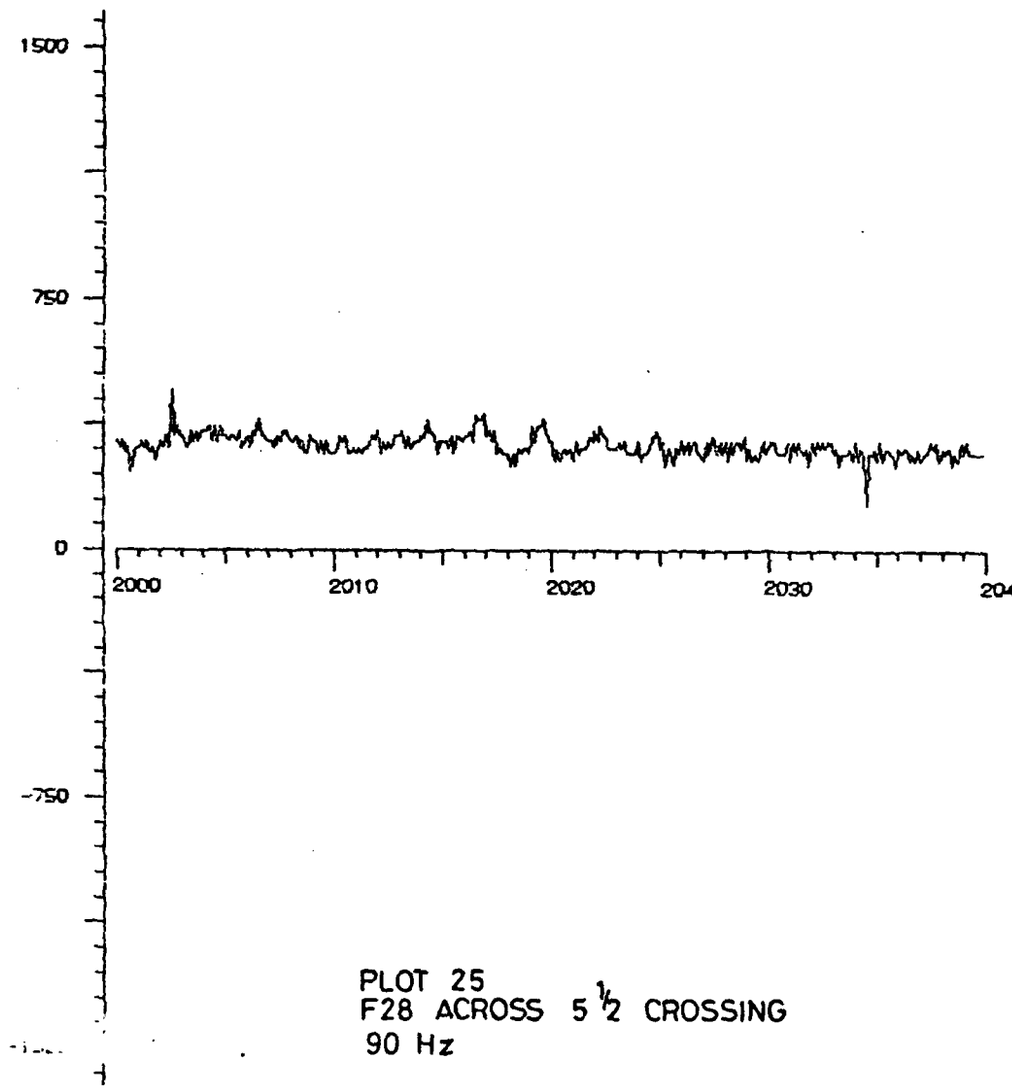

7/19/12 737
ACROSS 5.5

GRAPH B1

WAIT

PARAMETER=1
SAMPLE RATE=25
DISC 3=RICETAP5-200-3
Y SCALE= $_{10}$-2 C5/1
X SCALE=200/200

PLOT 25
F28 ACROSS 5 ½ CROSSING
90 Hz

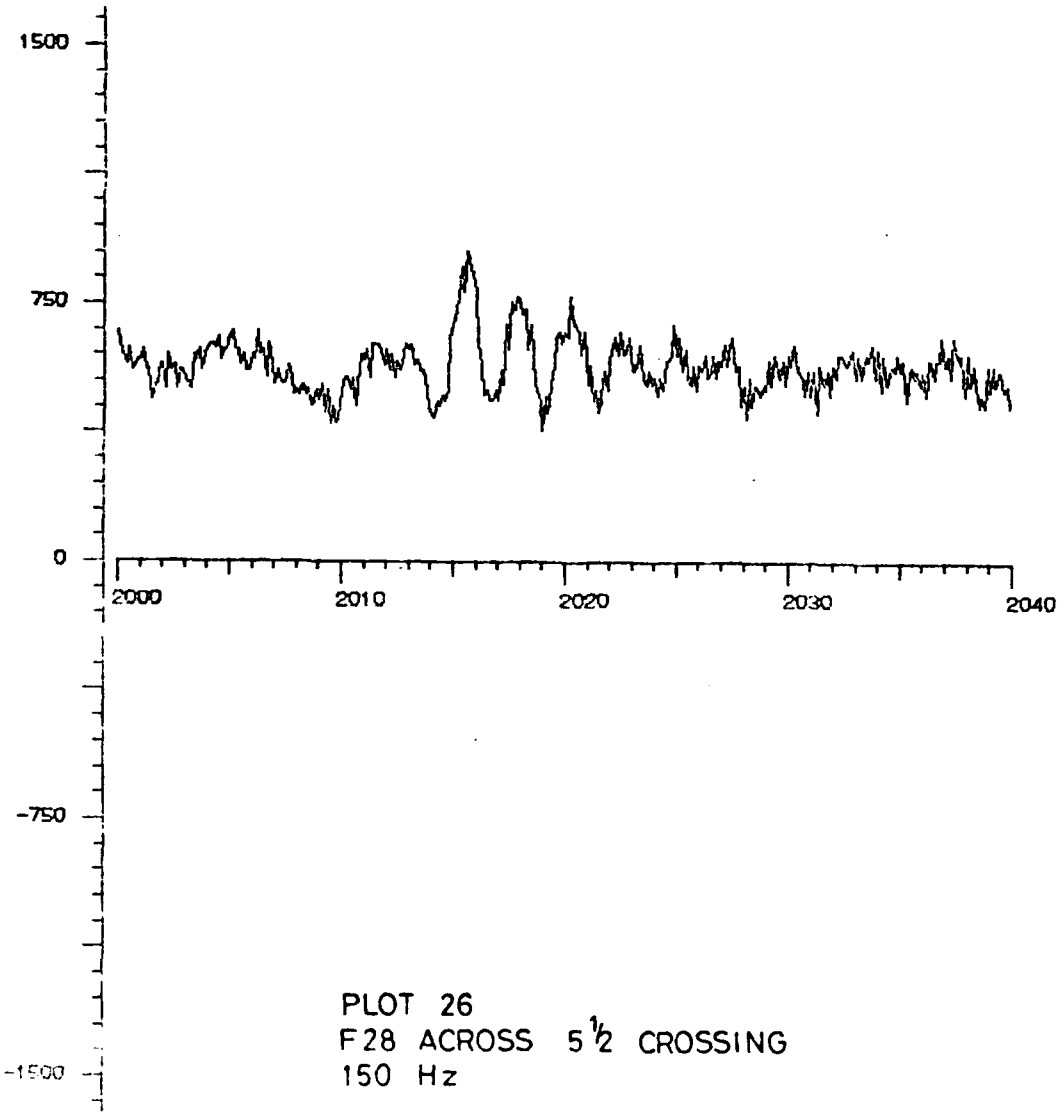

7/19/12 737
ACROSS 5.5

GRAPH B2

WAIT

PARAMETER=2
SAMPLE RATE=25
DISC 3=RICETAP5-200-3
Y SCALE= $_{10}$-2 C5/1
X SCALE=200/200

PLOT 26
F28 ACROSS 5 1/2 CROSSING
150 Hz

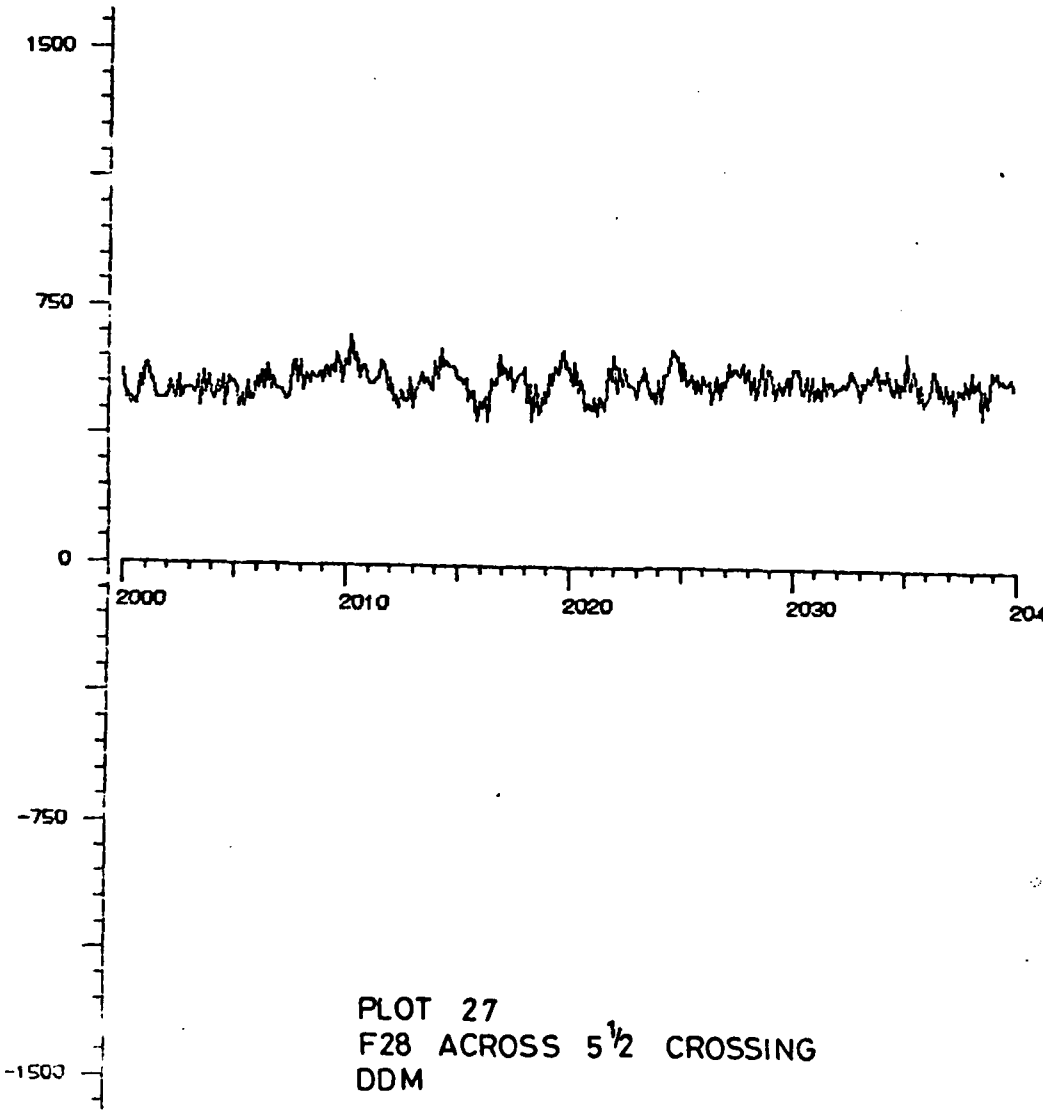

7/19/12 737
ACROSS 5.5

GRAPH B3

WAIT

PARAMETER=3
SAMPLE RATE=25
DISC 3=RICETAP5-200-3
Y SCALE= $_{10}$-2 C5/1
X SCALE=200/200

PLOT 27
F28 ACROSS 5½ CROSSING
DDM

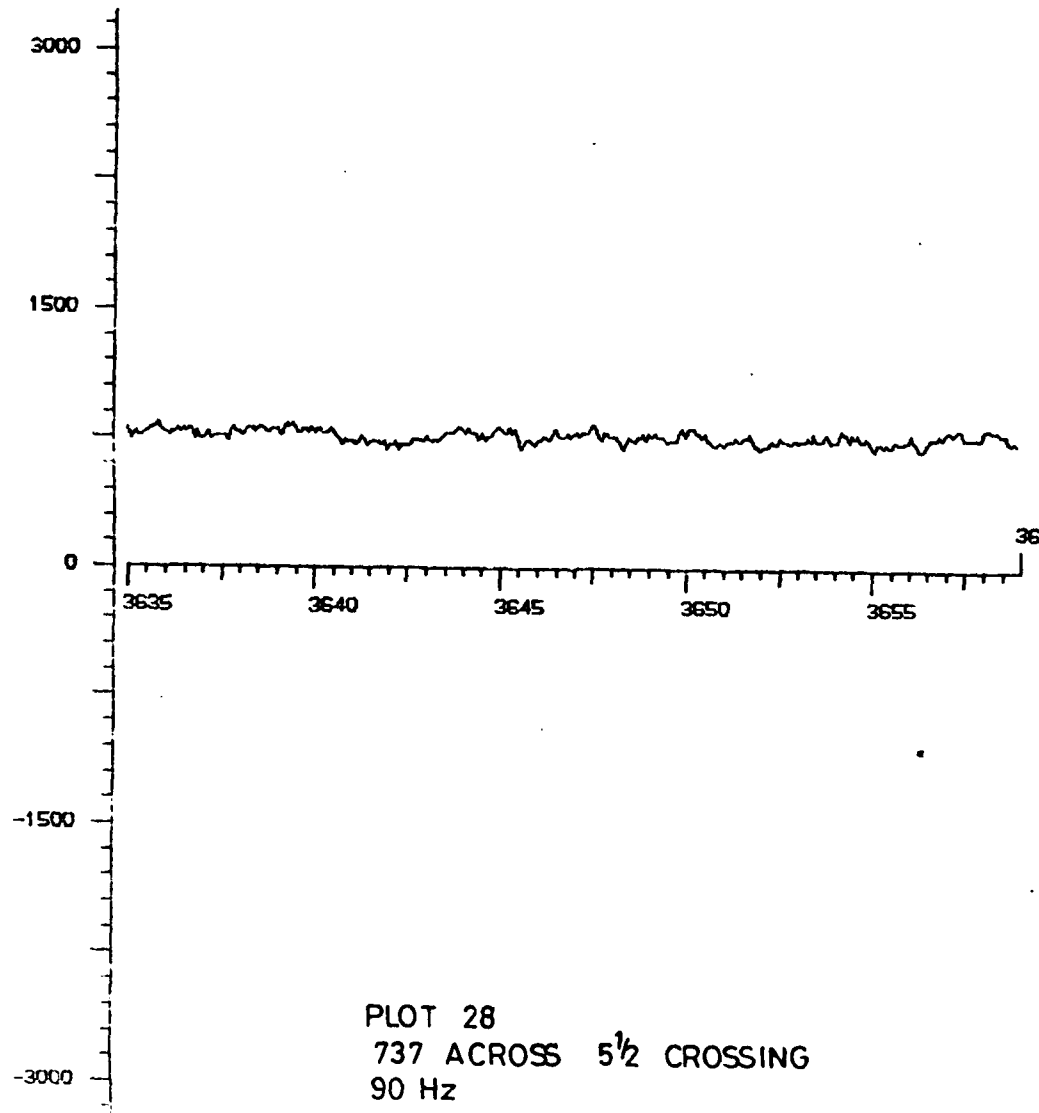

STANSTED TAPE 4
U.V.NO. 10
792 FT (APPROX)
TW2

GRAPH A32

WAIT

PARAMETER=1
SAMPLE RATE=15
DISC 3=RICETAP4-200-3
Y SCALE= $_{10}$-2 C4/1
X SCALE=200/200

PLOT 28
737 ACROSS 5½ CROSSING
90 Hz

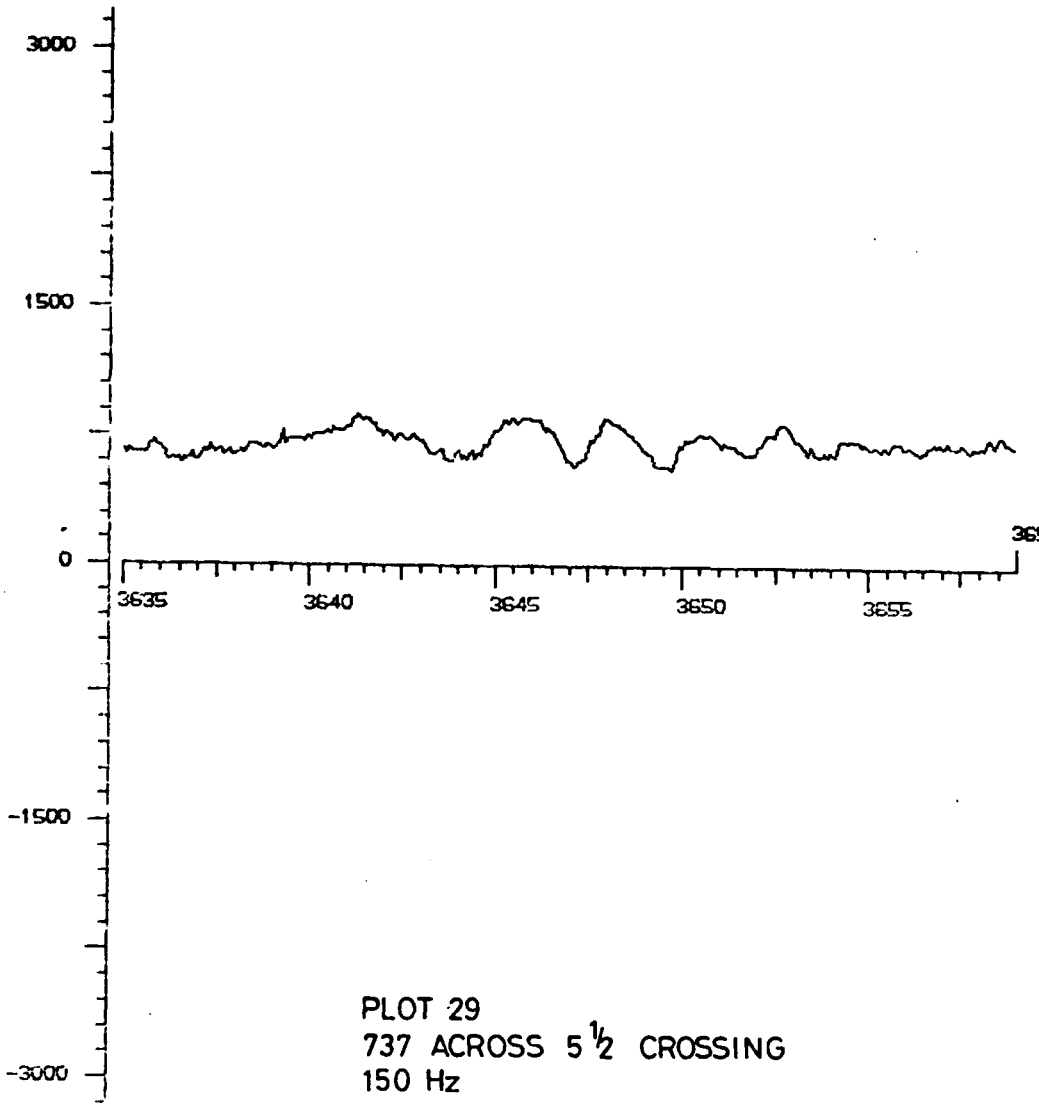

STANSTED TAPE 4
U.V.NO. 10
792 FT (APPROX)
TW2

GRAPH A33

WAIT

PARAMETER=2
SAMPLE RATE=15
DISC 3=RICETAP4-200-3
Y SCALE= $_{16}$-2 C4/1
X SCALE=200/200

PLOT 29
737 ACROSS 5 ½ CROSSING
150 Hz

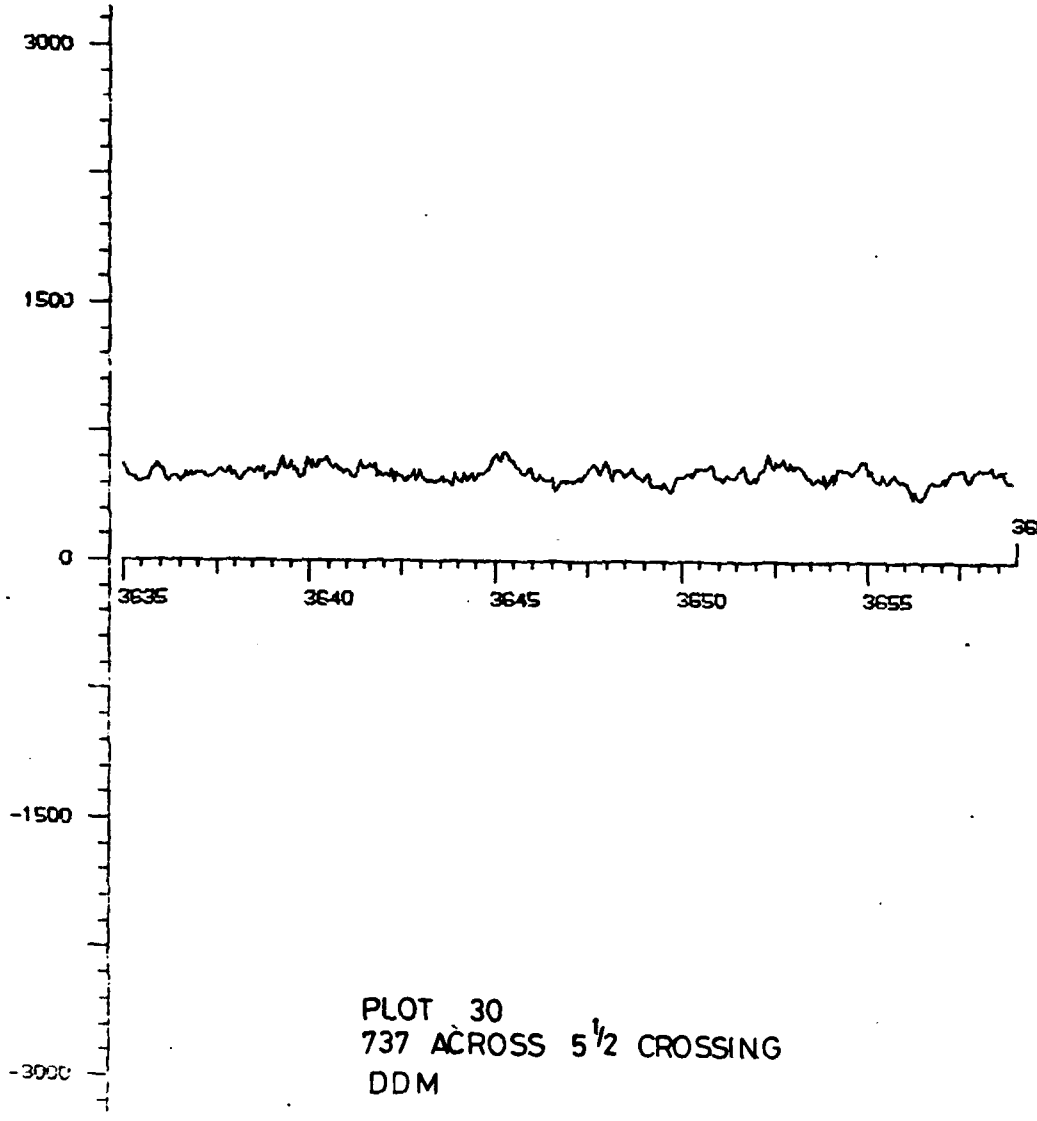

STANSTED TAPE 4
U.V.NO. 10
792 FT (APPROX)
TW2

GRAPH A34

WAIT

PARAMETER=3
SAMPLE RATE=15
DISC 3=RICETAP4-200-3
Y SCALE= $_{10}$-2 C4/1
X SCALE=200/200

PLOT 30
737 ACROSS 5 1/2 CROSSING
DDM

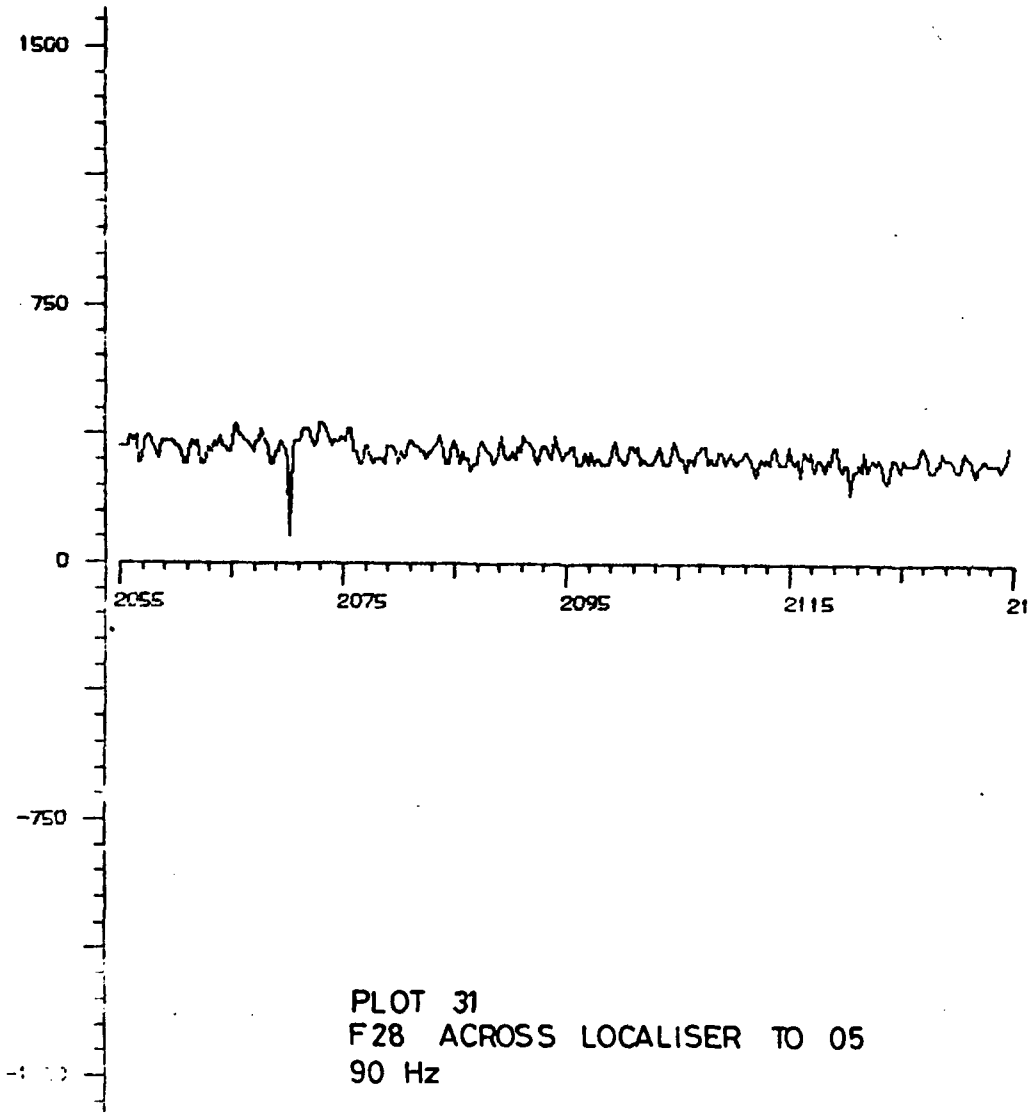

7/19/12 F28
TO 05 THRESHOLD

GRAPH B4

WAIT

PARAMETER=1
SAMPL_ RATE=50
DISC 3=RICETAP5-200-3
Y SCALE= $_{10}$-2 C5/1
X SCALE=200/200

PLOT 31
F28 ACROSS LOCALISER TO 05
90 Hz

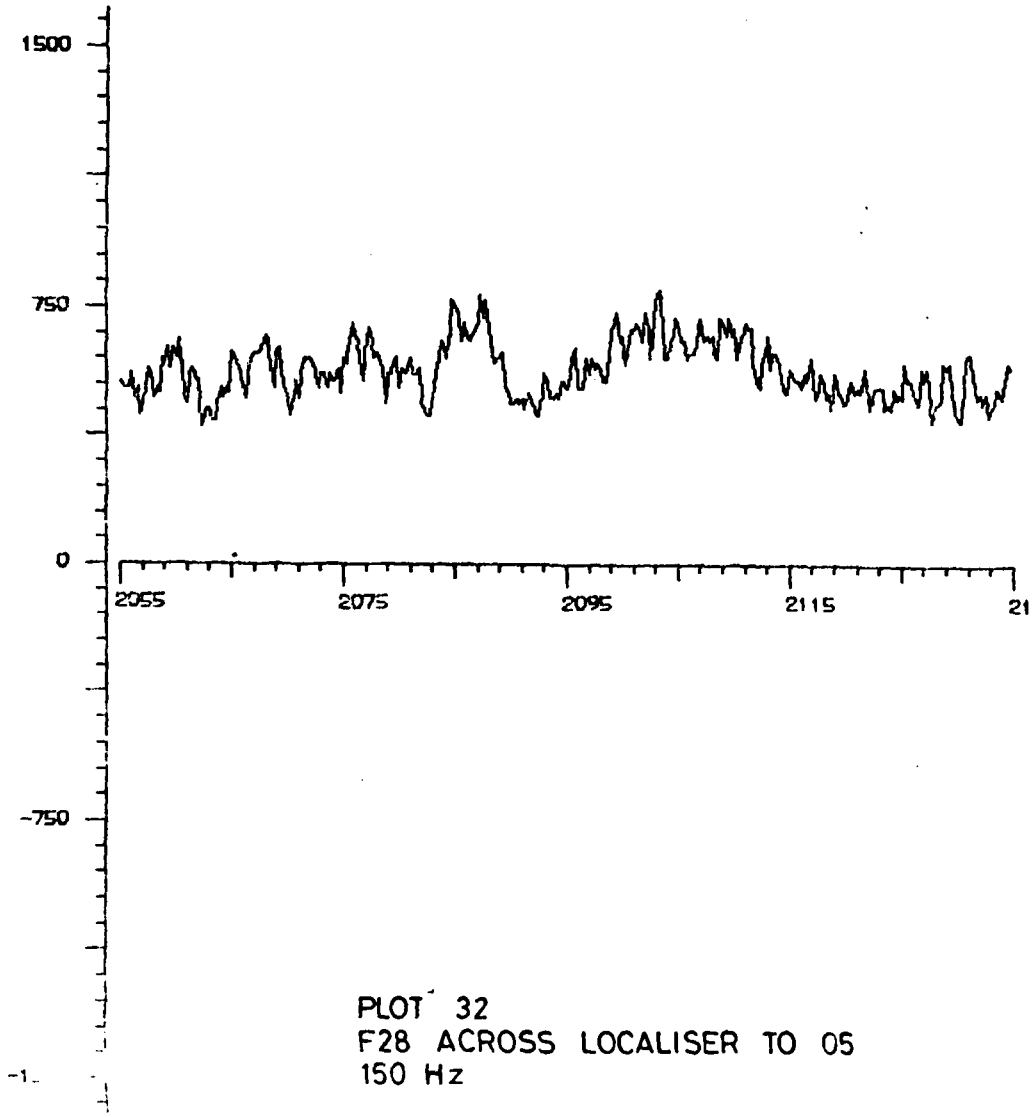

7/19/12 F28
TO 05 THRESHOLD

GRAPH B5

WAIT

PARAMETER=2
SAMPLE RATE=50
DISC 3=RICETAP5-200-3
Y SCALE= $_{10}$-2 C5/1
X SCALE=200/200

PLOT 32
F28 ACROSS LOCALISER TO 05
150 Hz

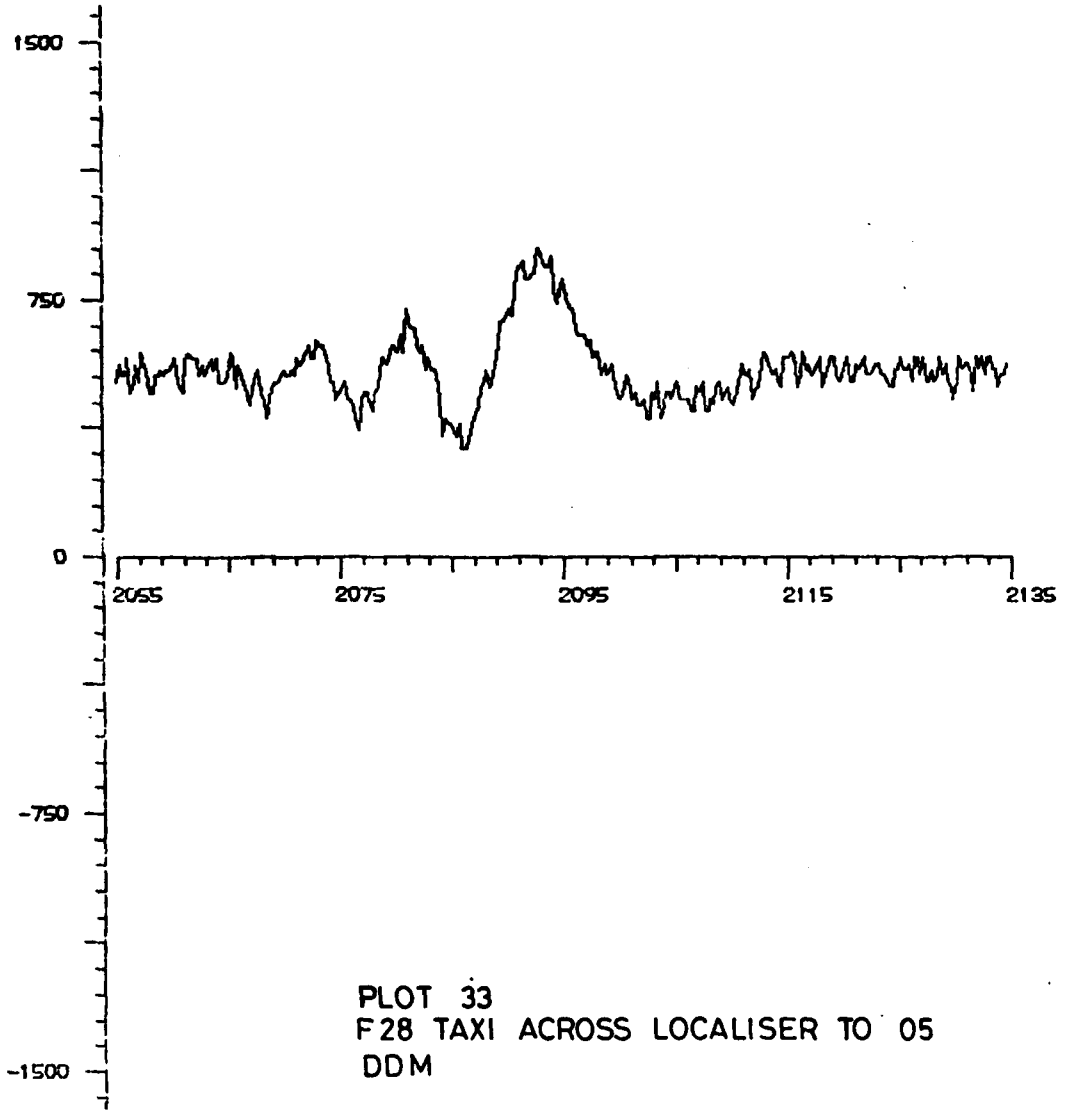

7/19/12 F28
TO 05 THRESHOLD

GRAPH B6

WAIT

PARAMETER=3
SAMPLE RATE=50
DISC 3=RICETAP5-200-3
Y SCALE= $_{10}$-2 C5/1
X SCALE=200/200

PLOT 33
F28 TAXI ACROSS LOCALISER TO 05
DDM

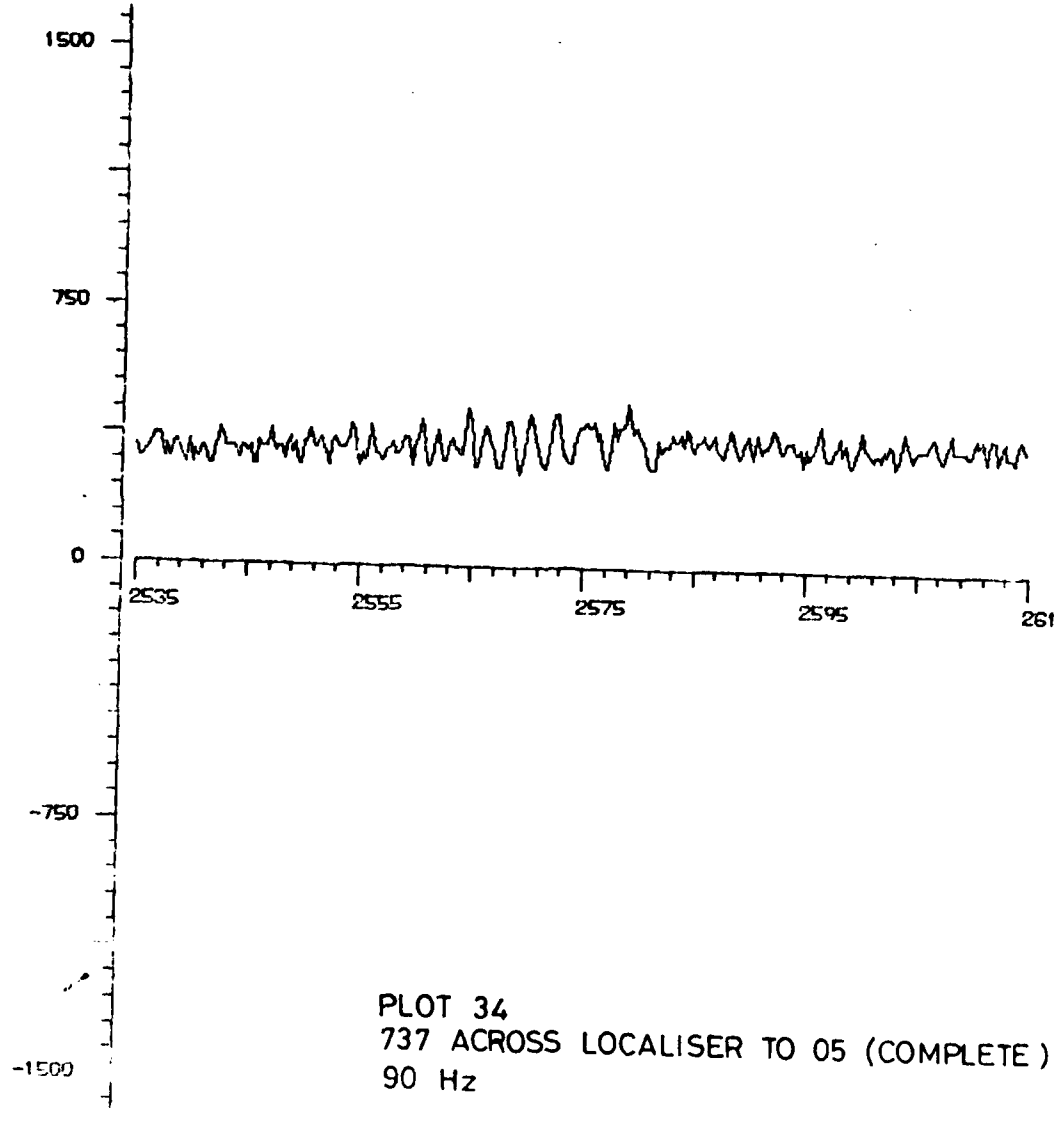

9/19/12 737
TO 05 THRESHOLD

GRAPH B7

WAIT

PARAMETER=1
SAMPLE RATE=50
DISC 3=RICETAP5-200-3
Y SCALE= $_{10}$-2 C5/'
X SCALE=200/200

PLOT 34
737 ACROSS LOCALISER TO 05 (COMPLETE)
90 Hz

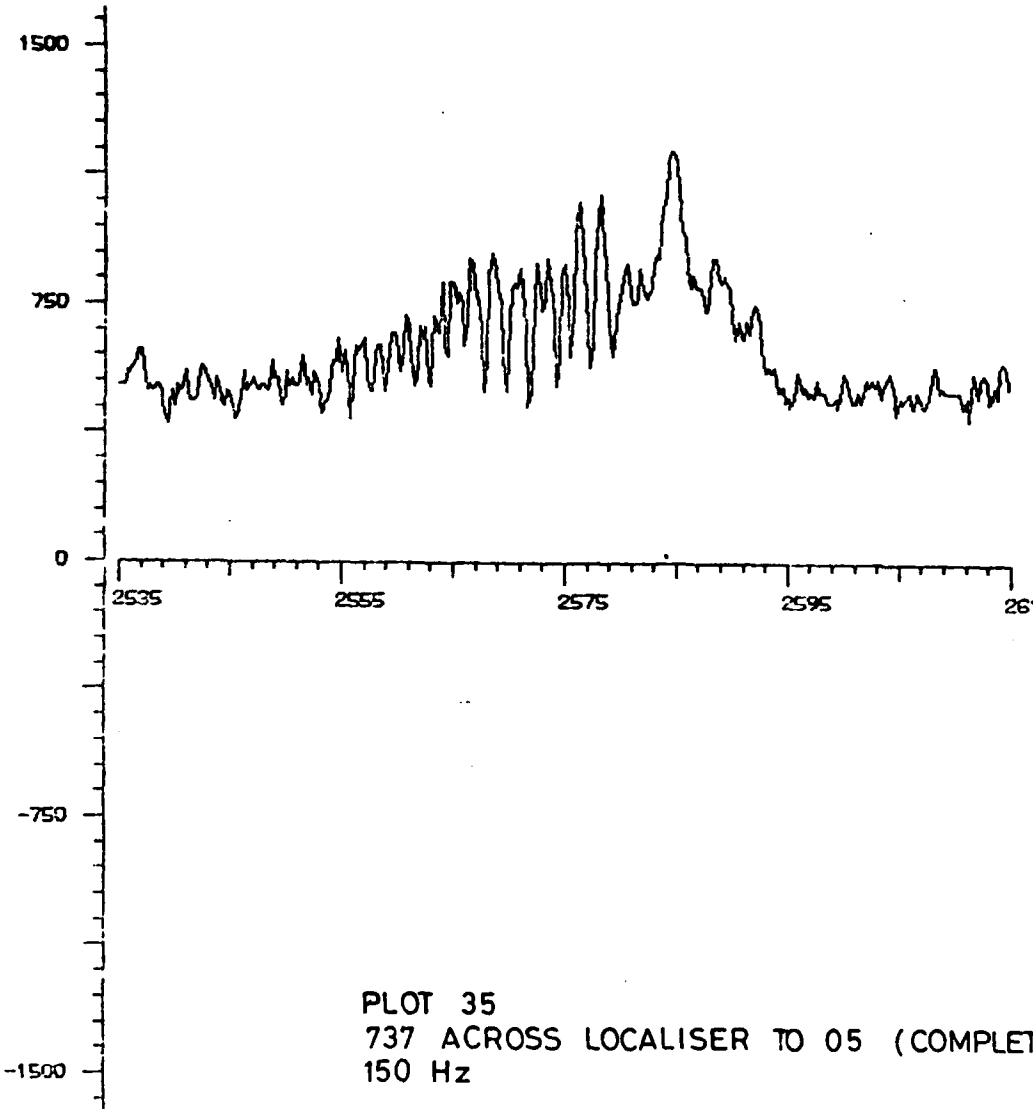

9/19/12 737
TO 05 THRESHOLD

GRAPH B8

WAIT

PARAMETER=2
SAMPLE RATE=50
DISC 3=RICETAP5-200-3
Y SCALE= $_{10}$-2 C5/1
X SCALE=200/200

PLOT 35
737 ACROSS LOCALISER TO 05 (COMPLETE)
150 Hz

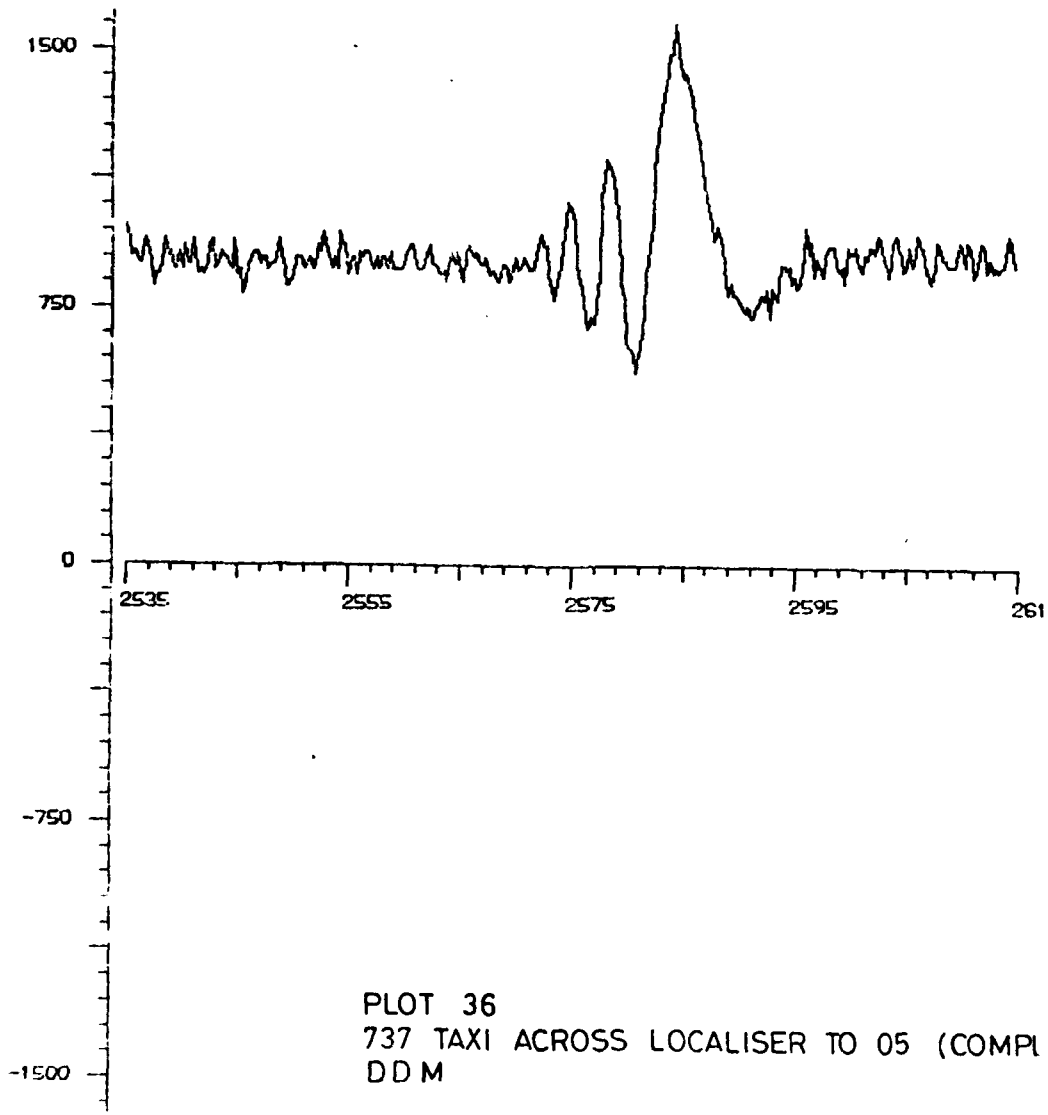

9/19/12 737
TO 05 THRESHOLD

GRAPH B9

WAIT

PARAMETER=3
SAMPLE RATE=50
DISC 3=RICETAP5-200-3
Y SCALE= $_{10}$-2 C5/1
X SCALE=200/200

PLOT 36
737 TAXI ACROSS LOCALISER TO 05 (COMPLETE)
DDM

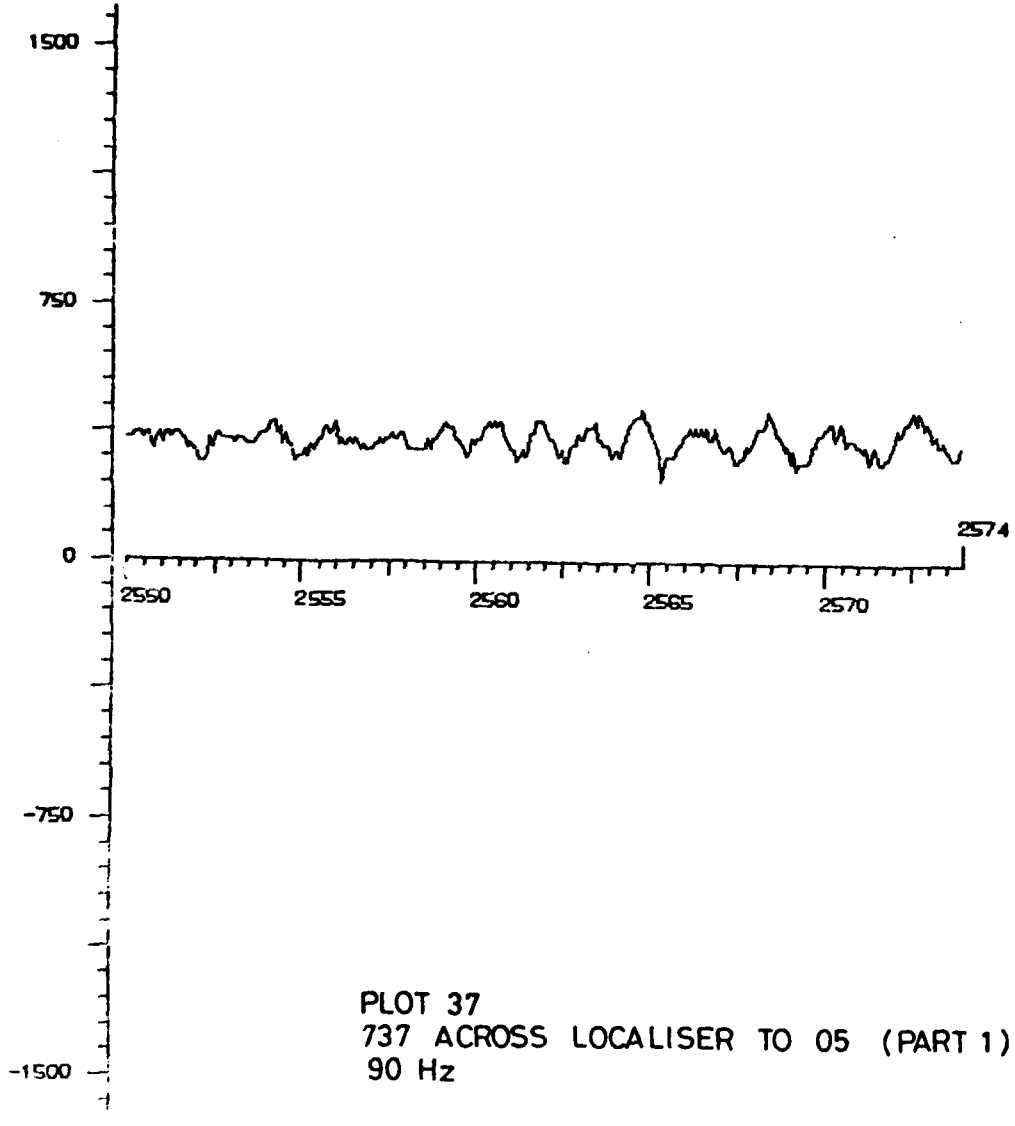

9/19/12 737
TO 05 THRESHOLD

GRAPH B10

WAIT

PARAMETER=1
SAMPLE RATE=16
DISC 3=RICETAP5-200-3
Y SCALE= $_{10}$-2 C5/1
X SCALE=200/200

PLOT 37
737 ACROSS LOCALISER TO 05 (PART 1)
90 Hz

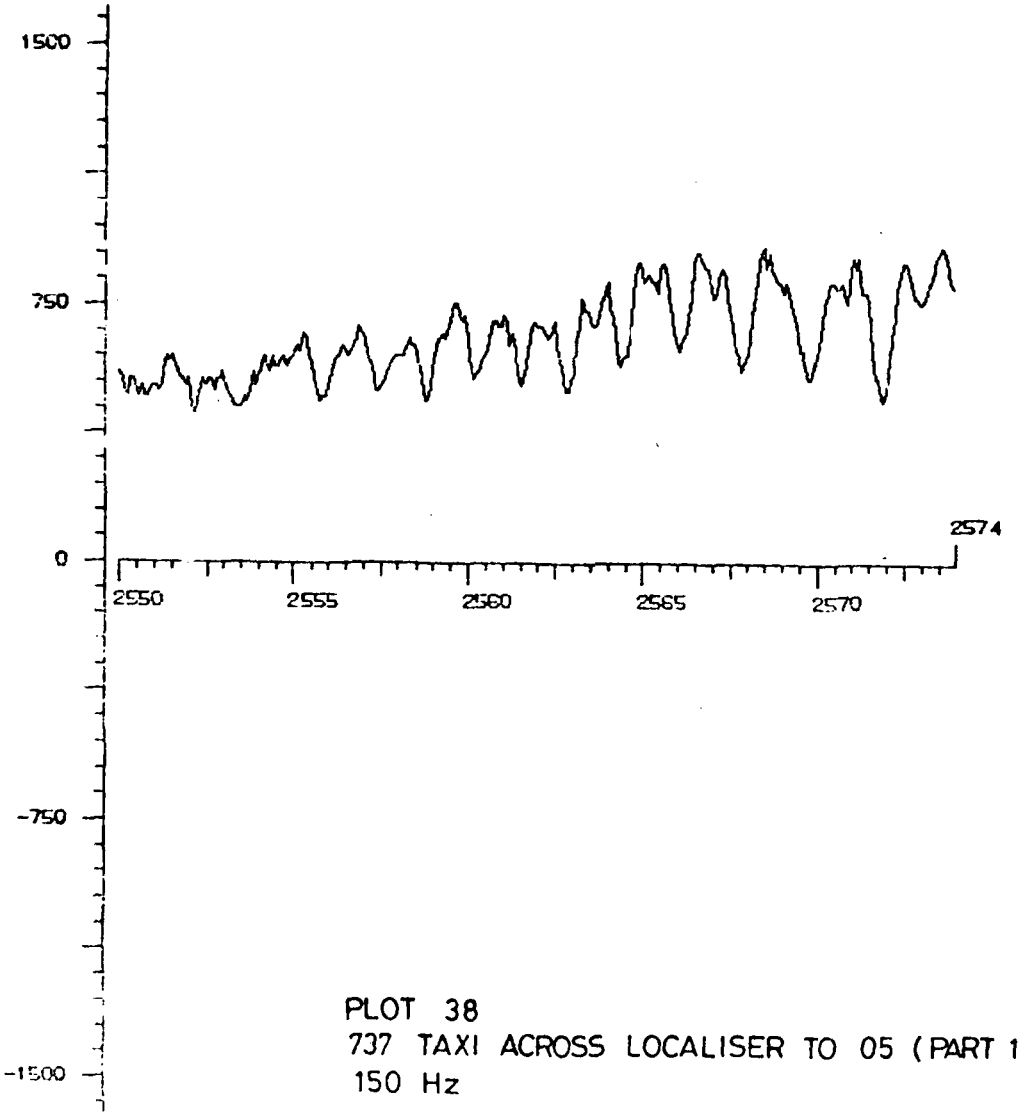

9/19/12 737
TO 05 THRESHOLD

GRAPH B11

WAIT

PARAMETER=2
SAMPLE RATE=16
DISC 3=RICETAP5-200-3
Y SCALE= $_{10}$-2 C5/1
X SCALE=200/200

PLOT 38
737 TAXI ACROSS LOCALISER TO 05 (PART 1)
150 Hz

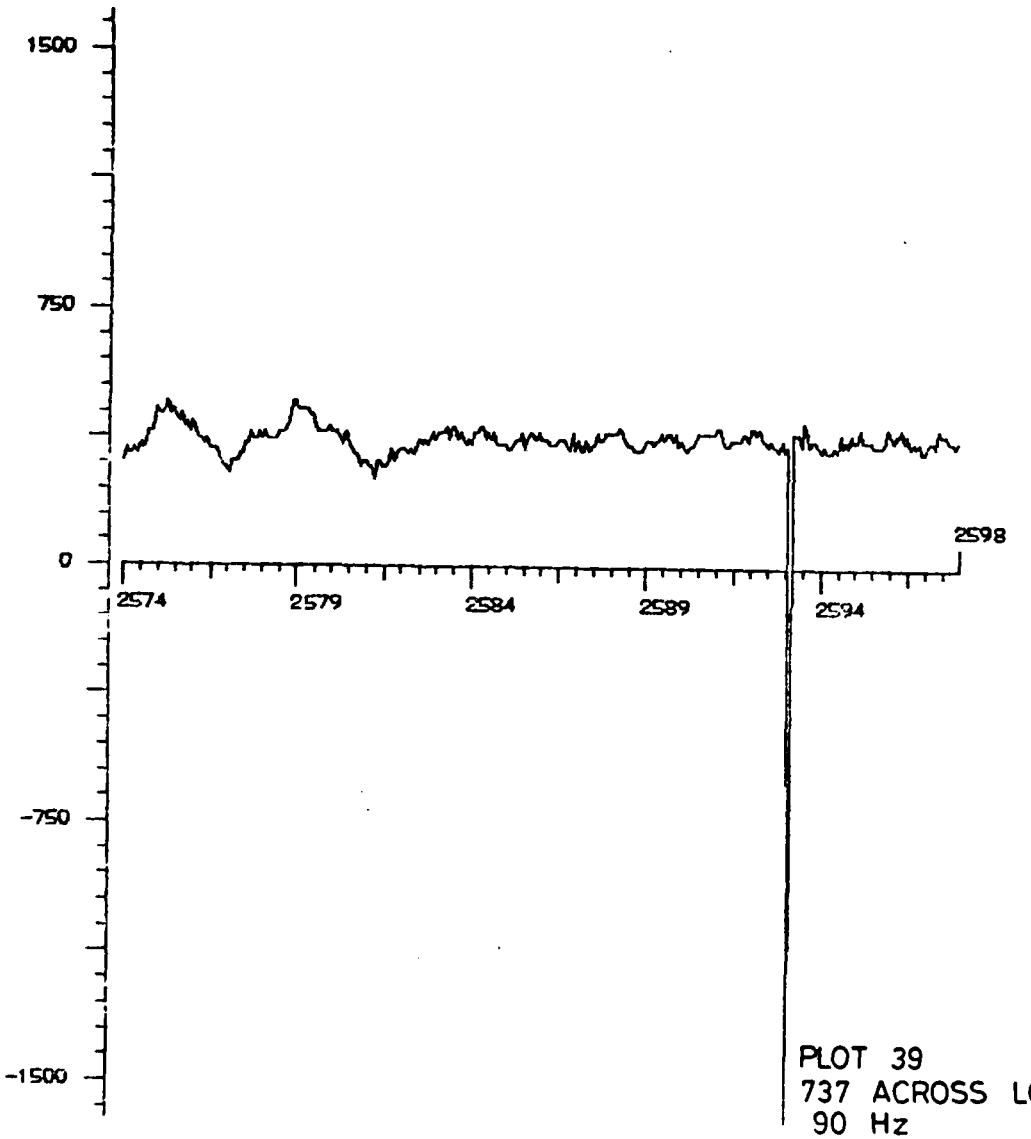

9/19/12 737
TO 05 THRESHOLD

GRAPH B12

WAIT

PARAMETER=1
SAMPLE RATE=16
DISC 3=RICETAP5-200-3
Y SCALE= $_{10}$-2 C5/1
X SCALE=200/200

PLOT 39
737 ACROSS LOCALISER TO 05 (PART 2)
90 Hz

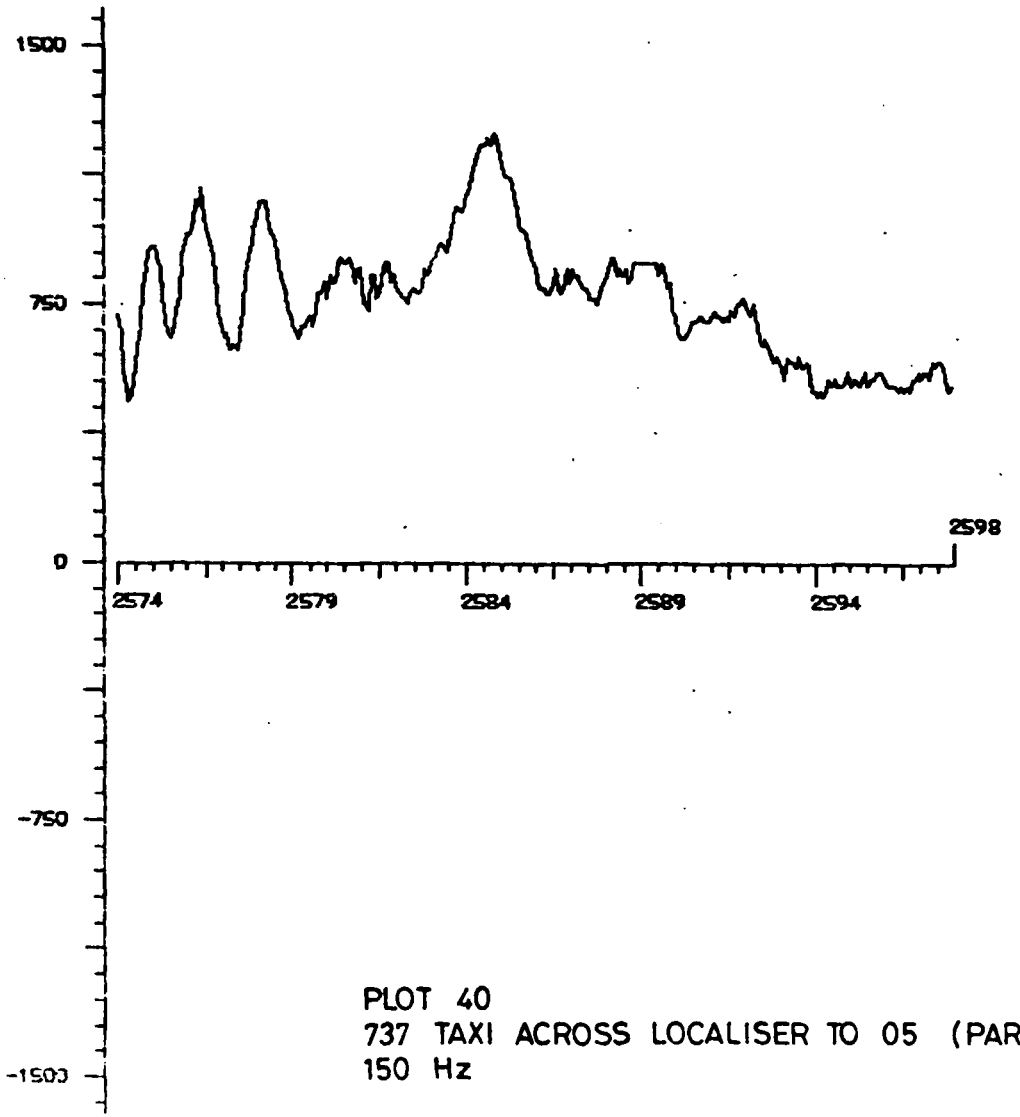

9/19/12 737
TO 05 THRESHOLD

GRAPH B13

WAIT

PARAMETER=2
SAMPLE RATE=16
DISC 3=RICETAP5-200-3
Y SCALE= $_{10}$-2 C5/1
X SCALE=200/200

PLOT 40
737 TAXI ACROSS LOCALISER TO 05 (PART 2)
150 Hz

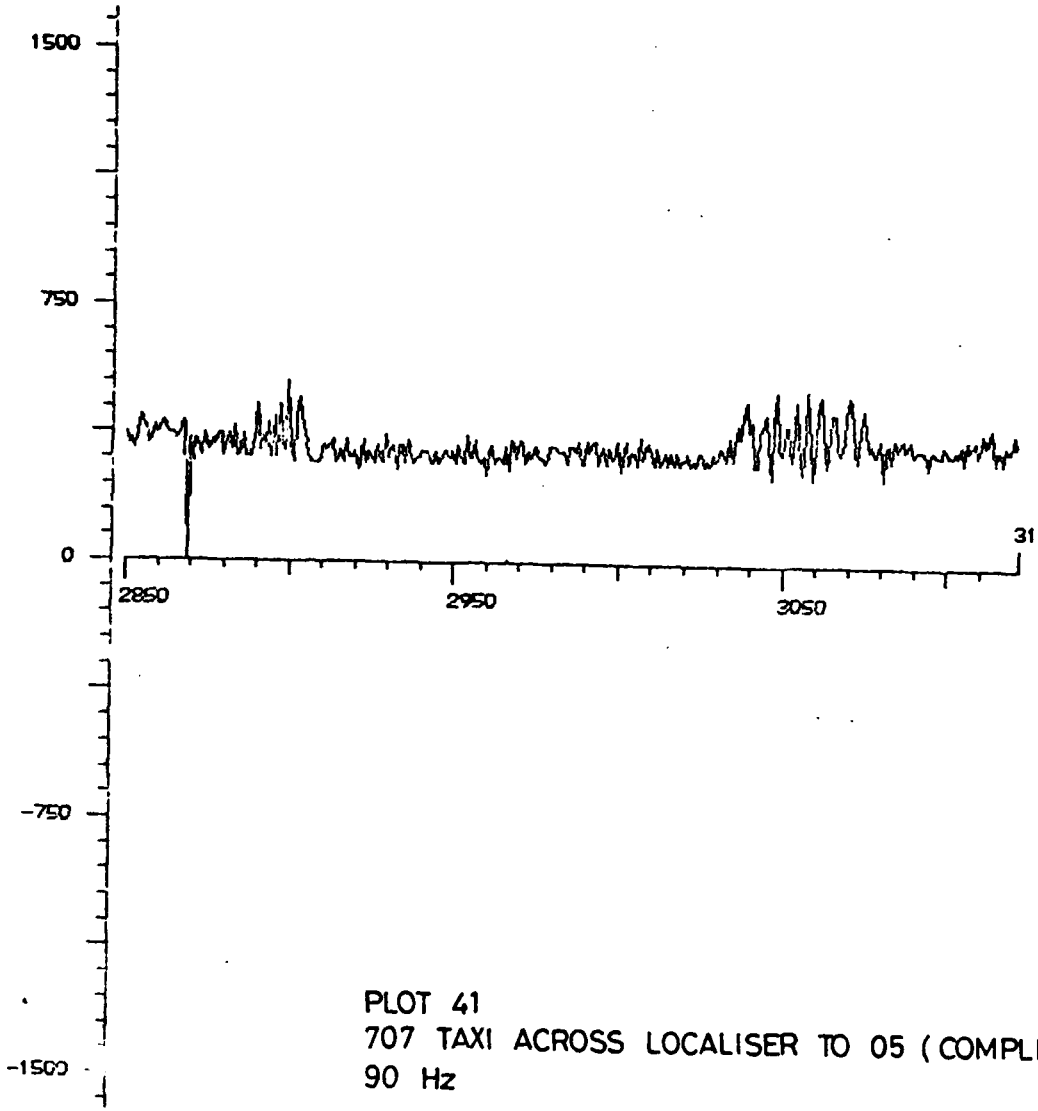

10/19/12 707
TO 05 THRESHOLD
WITH HOLD

GRAPH B14

WAIT

PARAMETER=1
SAMPLE RATE=170
DISC 3=RICETAP5-200-3
Y SCALE= $_{10}$-2 C5/1
X SCALE=200/200

PLOT 41
707 TAXI ACROSS LOCALISER TO 05 (COMPLETE)
90 Hz

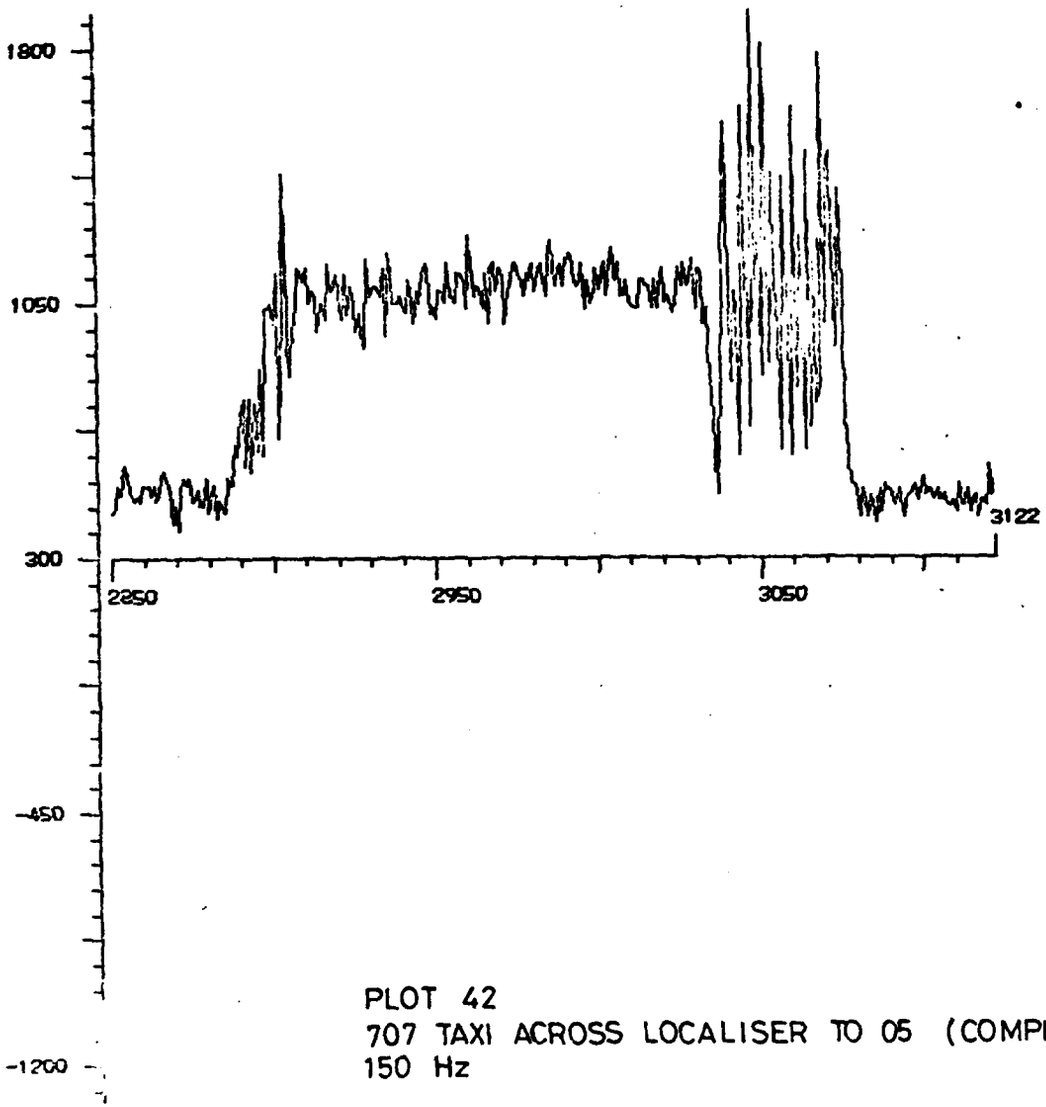

10/19/12 707
TO 05 THRESHOLD
WITH HOLD

GRAPH B15

WAIT

PARAMETER=2
SAMPLE RATE=170
DISC 3=RICETAP5-200-3
Y SCALE= $_{10}$-2 C5/1
X SCALE=200/200

PLOT 42
707 TAXI ACROSS LOCALISER TO 05 (COMPLETE)
150 Hz

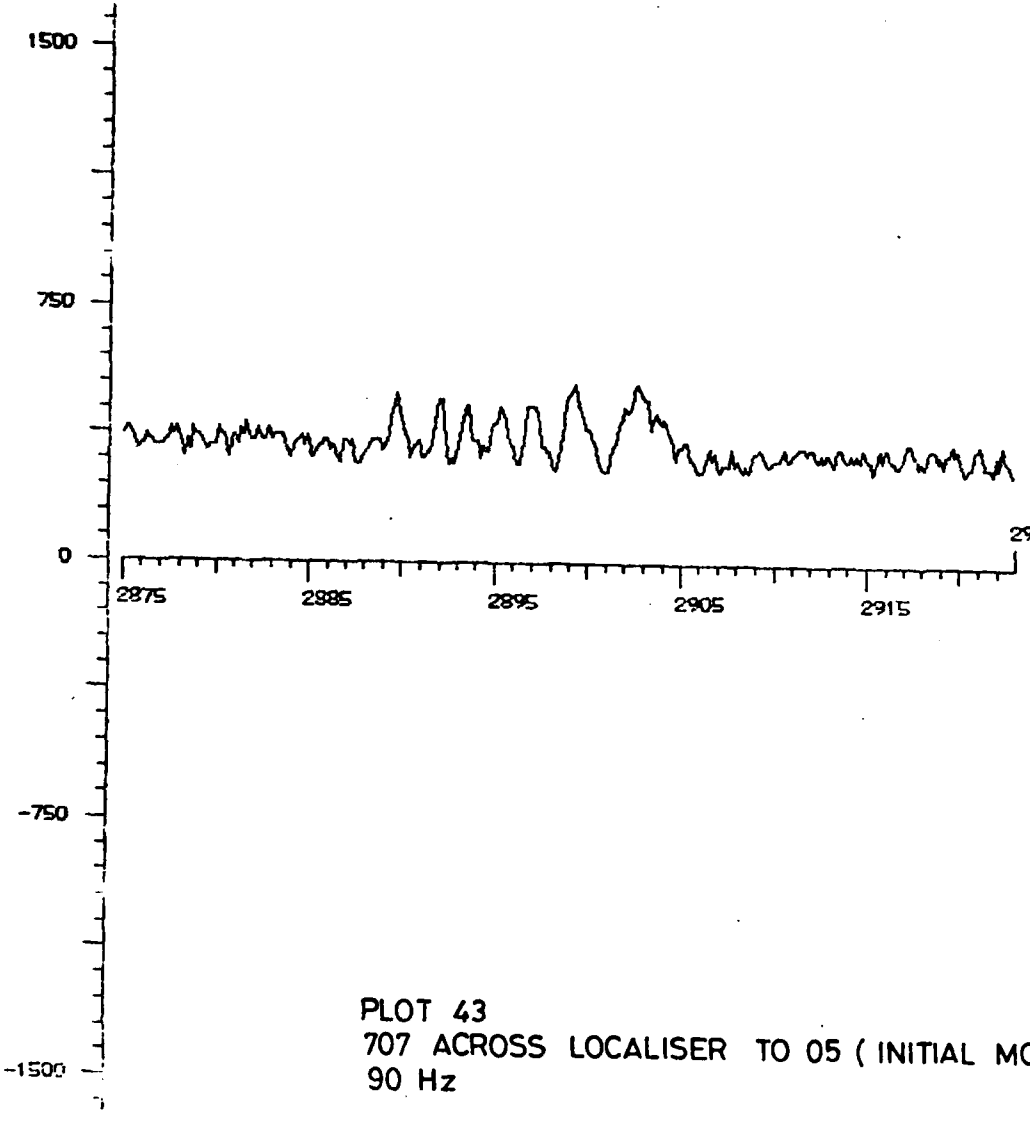

10/19/12 707
TO 05 THRESHOLD
WITH HOLD

GRAPH B16

WAIT

PARAMETER=1
SAMPLE RATE=30
DISC 3=RICETAP5-200-3
Y SCALE= $_{10}$-2 C5/1
X SCALE=200/200

PLOT 43
707 ACROSS LOCALISER TO 05 (INITIAL MOVEMENT)
90 Hz

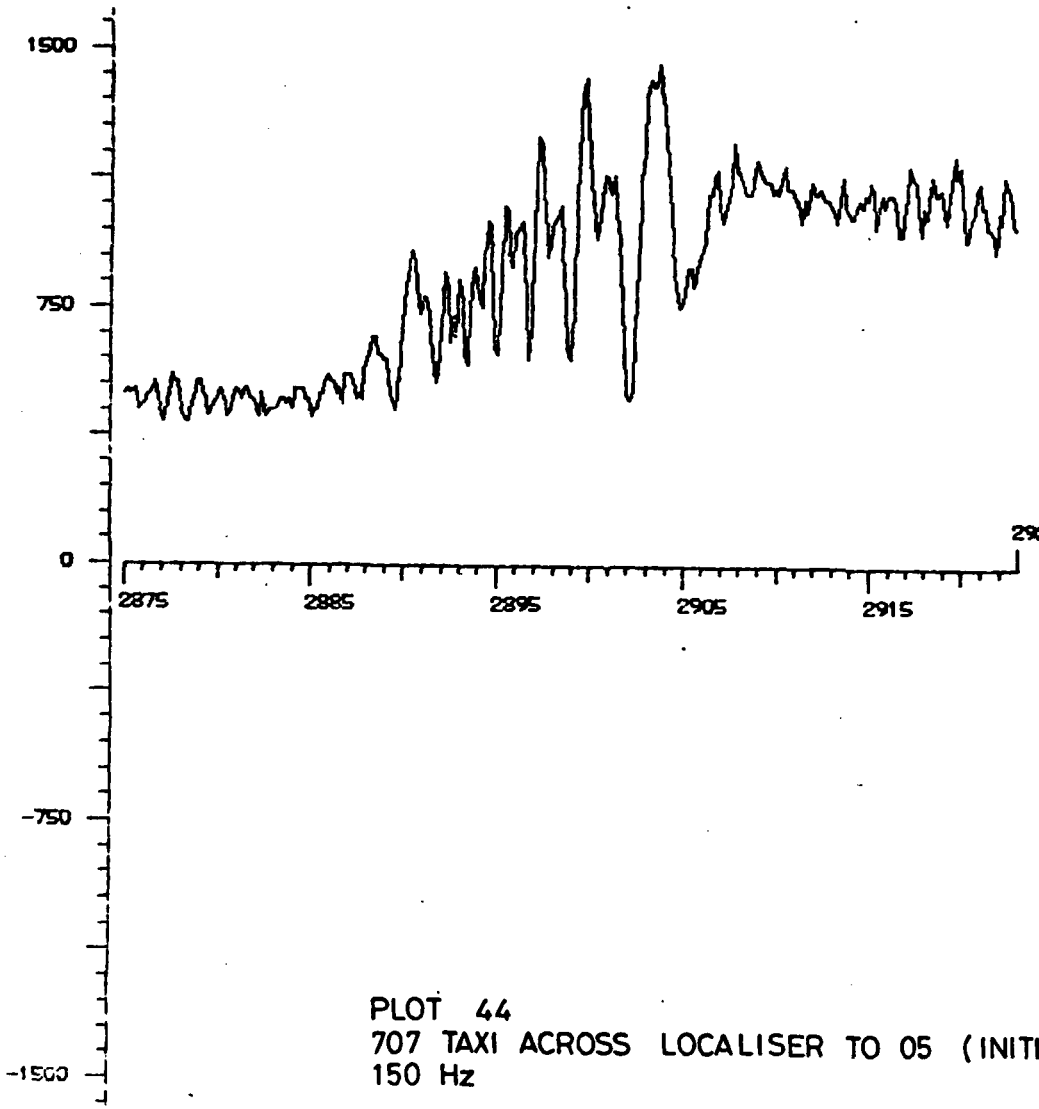

10/19/12 707
TO 05 THRESHOLD
WITH HOLD

GRAPH B17

WAIT

PARAMETER=2
SAMPLE RATE=30
DISC 3=RICETAP5-200-3
Y SCALE= $_{10}$-2 C5/1
X SCALE=200/200

PLOT 44
707 TAXI ACROSS LOCALISER TO 05 (INITIAL MOVEMENT)
150 Hz

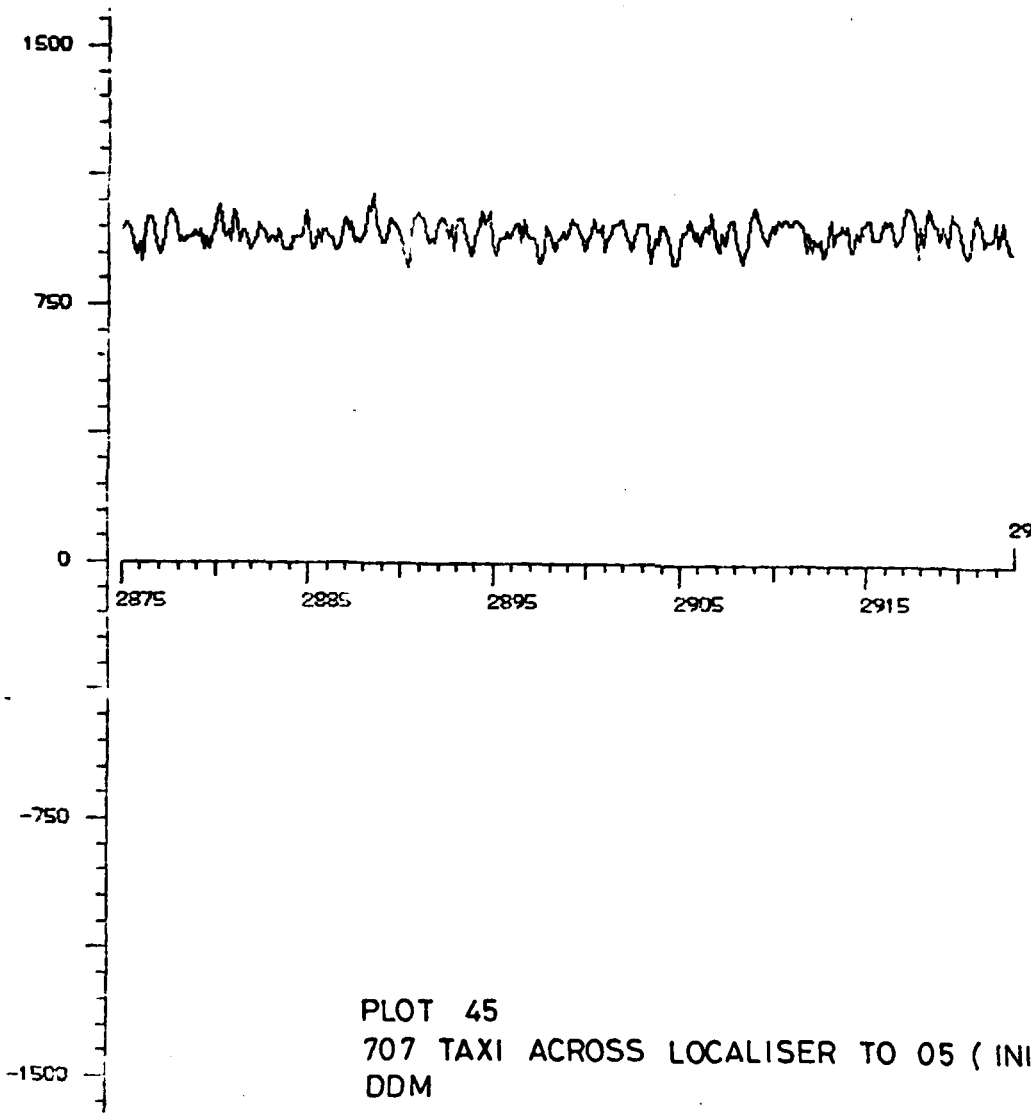

10/19/12 707
TO 05 THRESHOLD
WITH HOLD

GRAPH B18

WAIT

PARAMETER=3
SAMPLE RATE=30
DISC 3=RICETAP5-200-3
Y SCALE= $_{10}$-2 C5/1
X SCALE=200/200

PLOT 45
707 TAXI ACROSS LOCALISER TO 05 (INITIAL MOVEMENT)
DDM

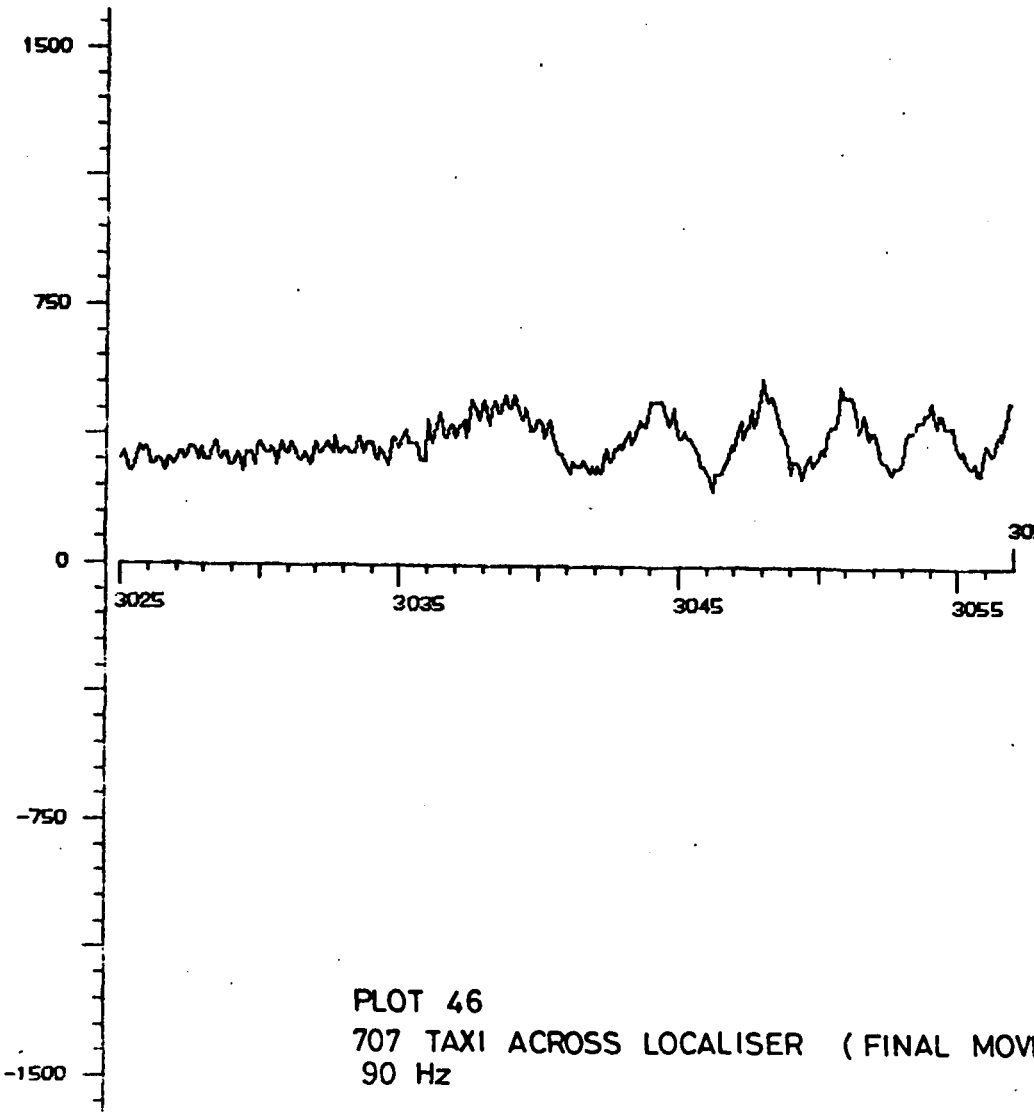

10/19/12 707
TO 05 THRESHOLD
WITH HOLD

GRAPH B19

WAIT

PARAMETER=1
SAMPLE RATE=20
DISC 3=RICETAP5-200-3
Y SCALE= $_{10}$-2 C5/1
X SCALE=200/200

PLOT 46
707 TAXI ACROSS LOCALISER (FINAL MOVE PART1)
90 Hz

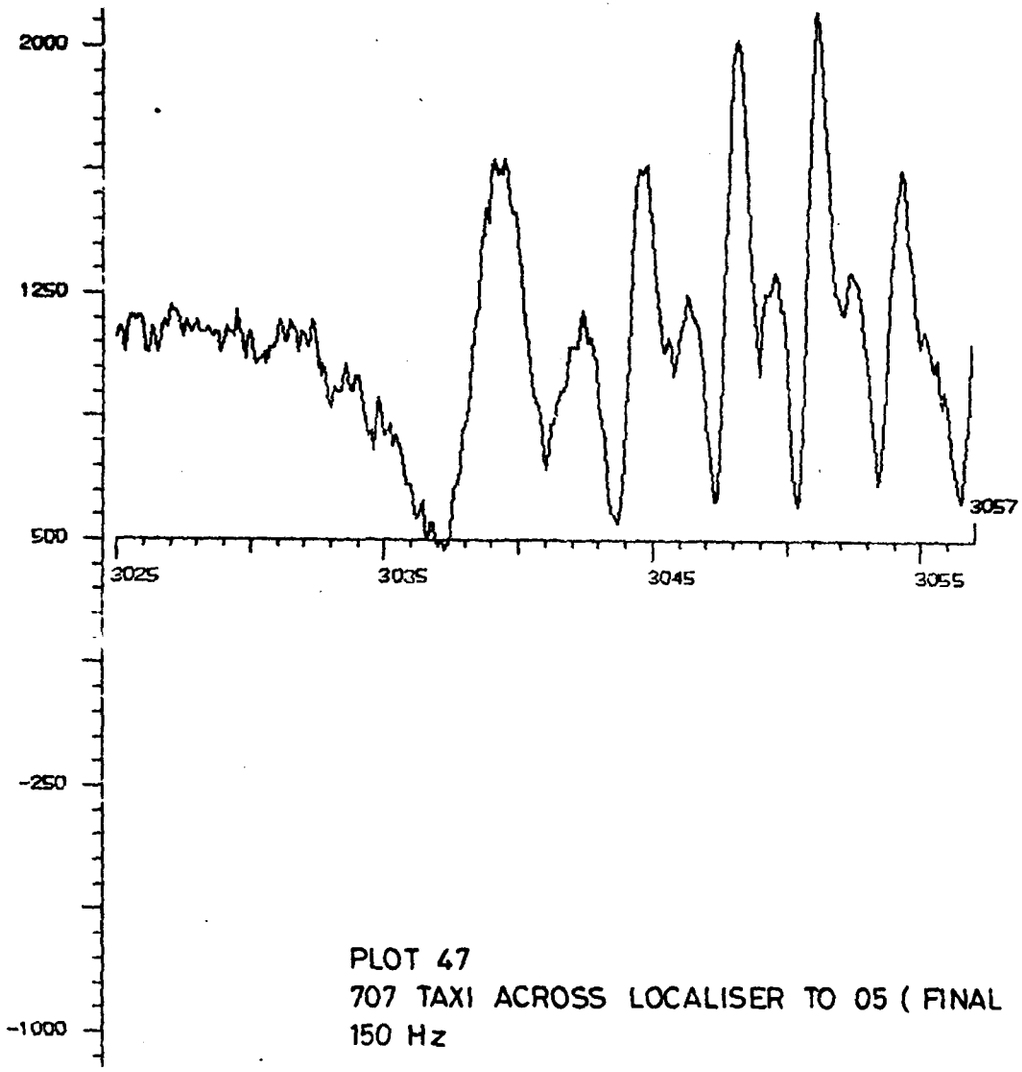

10/19/12 707
TO 05 THRESHOLD
WITH HOLD

GRAPH B20

WAIT

PARAMETER=2
SAMPLE RATE=20
DISC 3=RICETAP5-200-3
Y SCALE= $_{10}$-2 C5/1
X SCALE=200/200

PLOT 47
707 TAXI ACROSS LOCALISER TO 05 (FINAL MOVE PART 1)
150 Hz

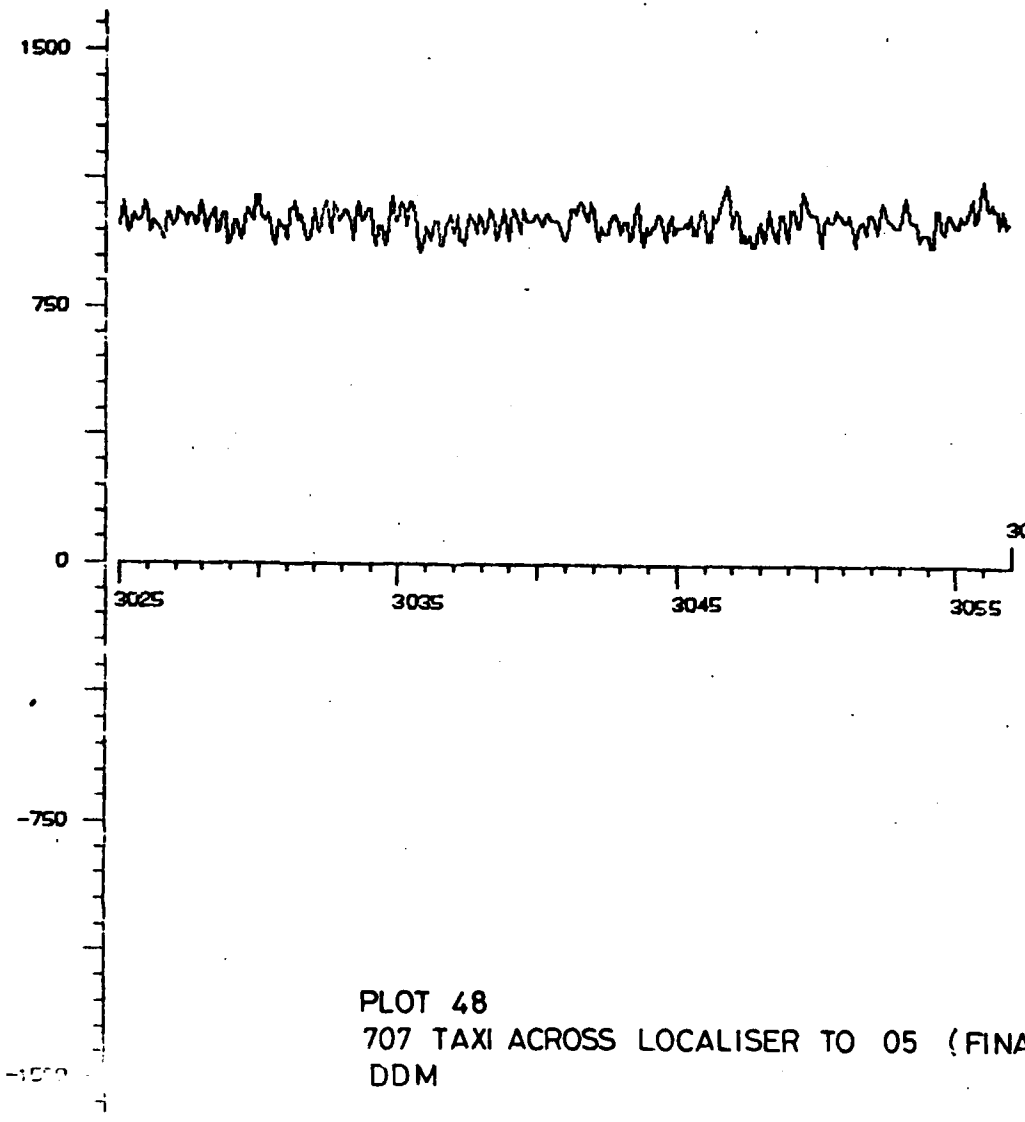

10/19/12 707
TO 05 THRESHOLD
WITH HOLD

GRAPH B21

WAIT

PARAMETER=3
SAMPLE RATE=20
DISC 3=RICETAP5-200-3
Y SCALE= $_{10}$-2 C5/1
X SCALE=200/200

PLOT 48
707 TAXI ACROSS LOCALISER TO 05 (FINAL MOVE PART 1)
DDM

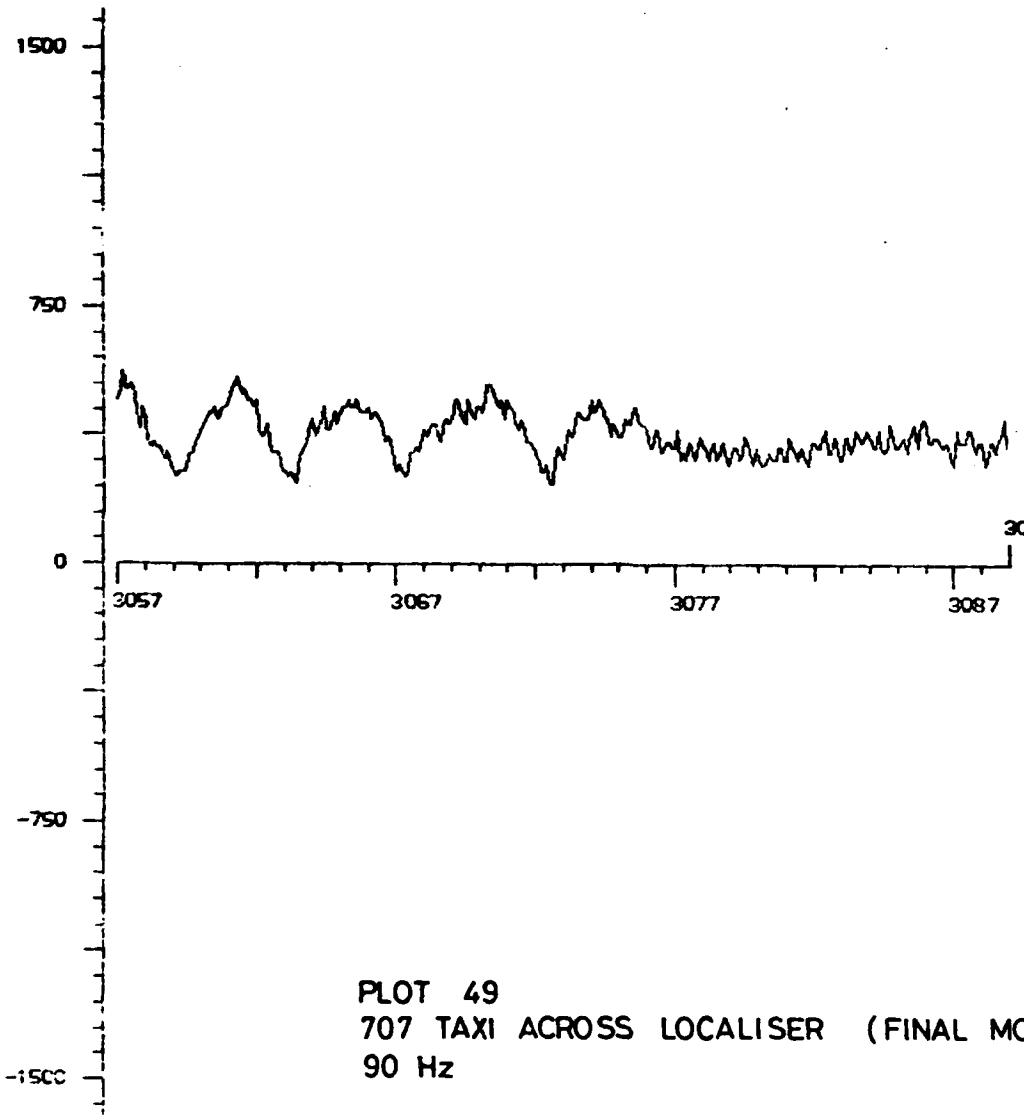

B-95

10/19/12 707
TO 05 THRESHOLD
WITH HOLD

GRAPH B22

WAIT

PARAMETER=1
SAMPLE RATE=20
DISC 3=RICETAP5-200-3
Y SCALE= $_{10}$-2 C5/1
X SCALE=200/200

PLOT 49
707 TAXI ACROSS LOCALISER (FINAL MOVE PART 2)
90 Hz

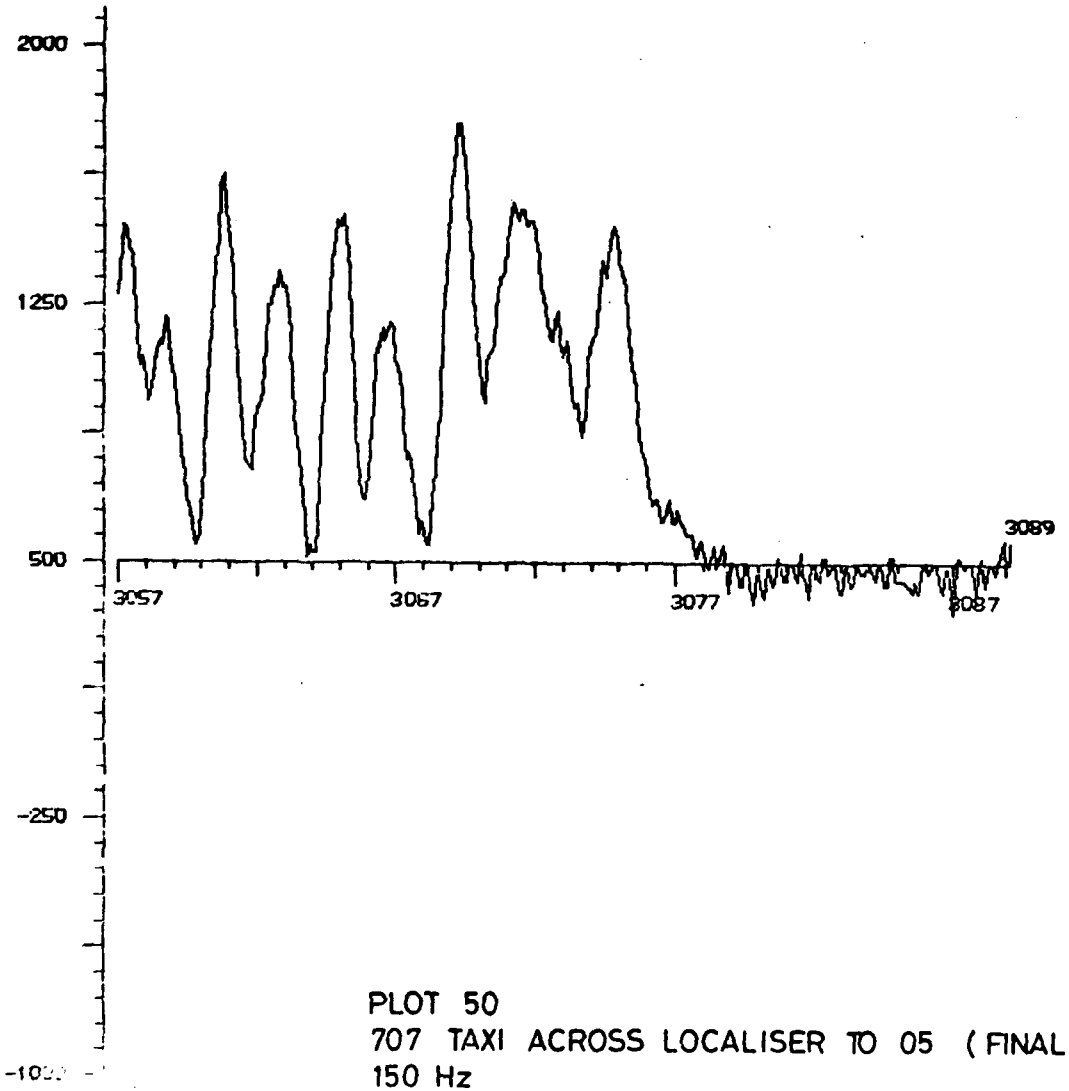

10/19/12 707
TO 05 THRESHOLD
WITH HOLD

GRAPH B23

WAIT

PARAMETER=2
SAMPLE RATE=20
DISC 3=RICETAPS-200-3
Y SCALE= $_{10}$-2 C5/1
X SCALE=200/200

PLOT 50
707 TAXI ACROSS LOCALISER TO 05 (FINAL MOVE PART 2)
150 Hz

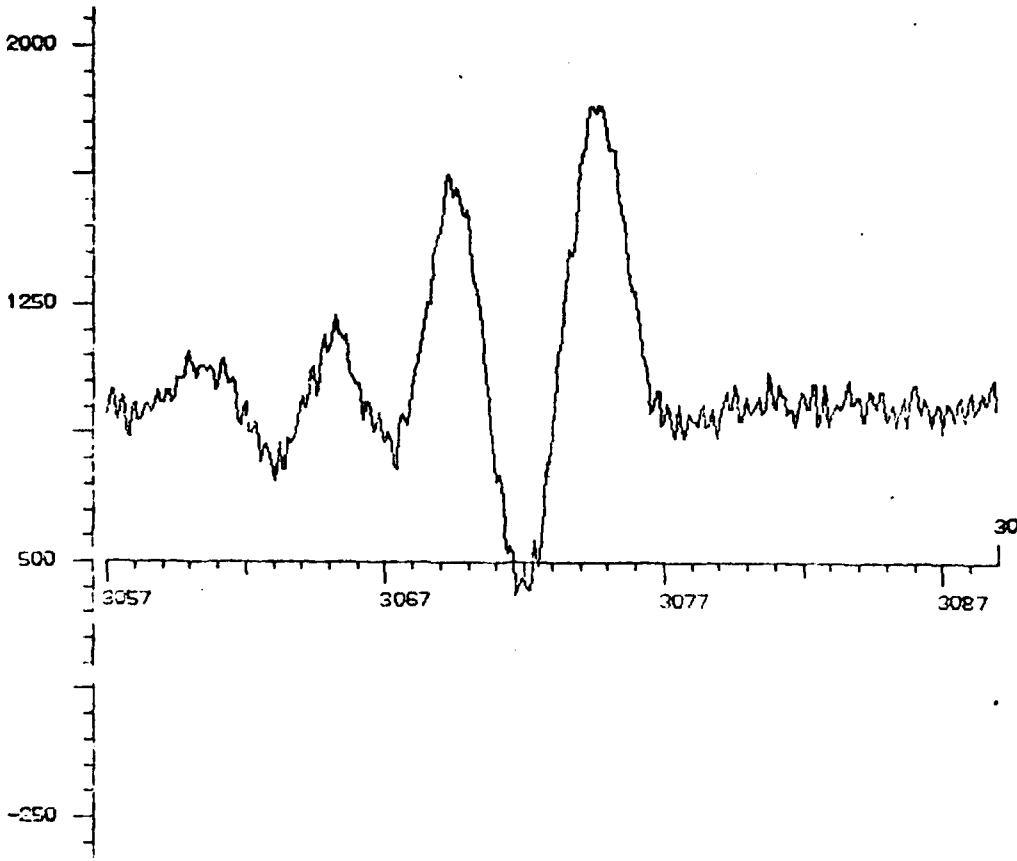

10/19/12 707
TO 05 THRESHOLD
WITH HOLD

GRAPH B24

WAIT

PARAMETER=3
SAMPLE RATE=20
DISC 3=RICETAP5-200-3
Y SCALE= $_{10}$-2 C5/1
X SCALE=200/200

PLOT 51
707 TAXI ACROSS LOCALISER TO 05 (FINAL MOVE PART 2)
DDM

PLOT 52
2872
2910
2932
2956
2994

PLOT 52 CONT' D
2998
3038
3058
3062
3080
3110

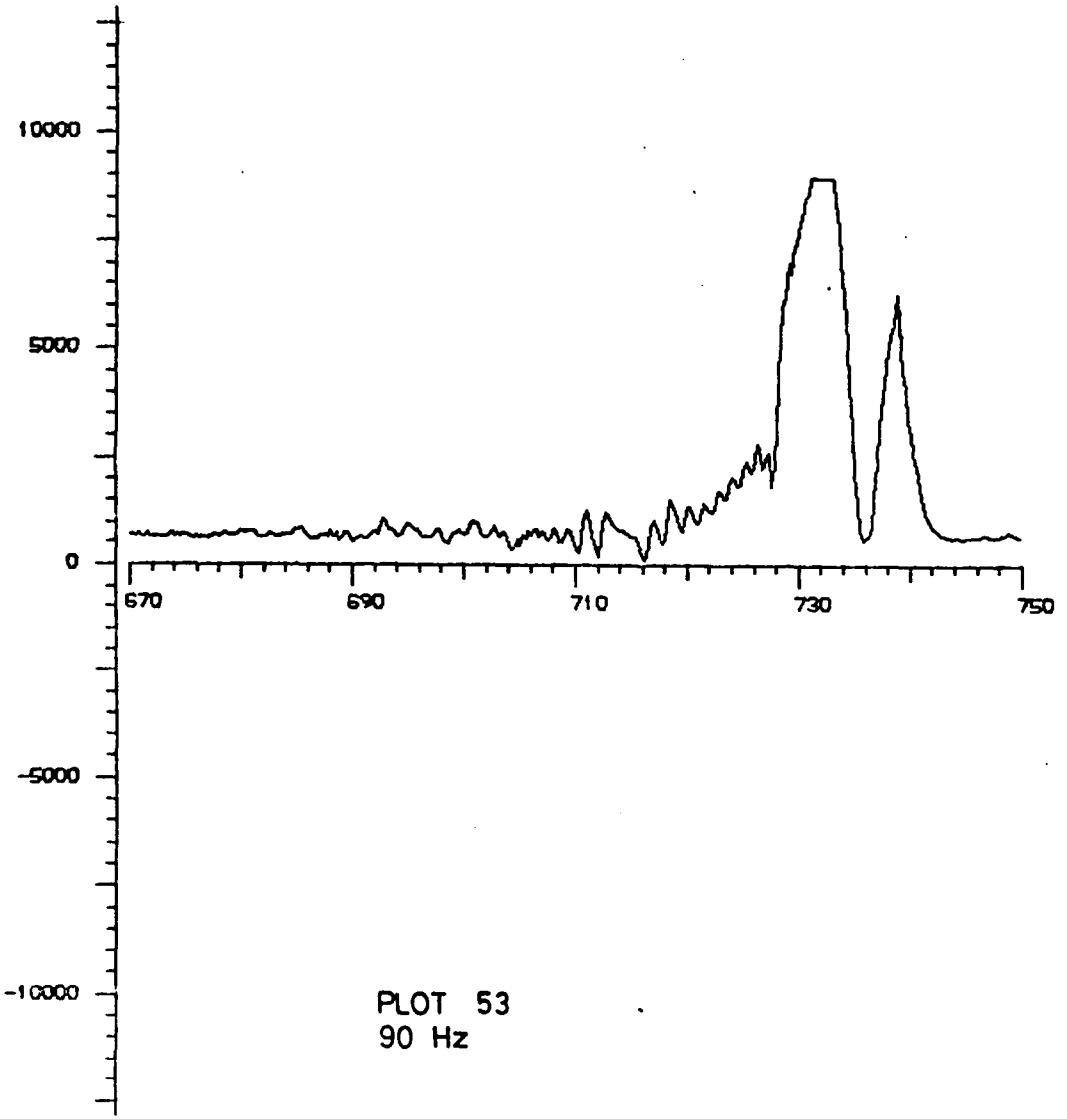

SMALL AIRCRAFT
OVERFLIGHT
3/21/11

GRAPH A1

WAIT

PARAMETER=1
SAMPLE RATE=50
DISC 3=RICETAP4-200-3
Y SCALE= $_{10}$-2 C4/1
X SCALE=200/200

PLOT 53
90 Hz

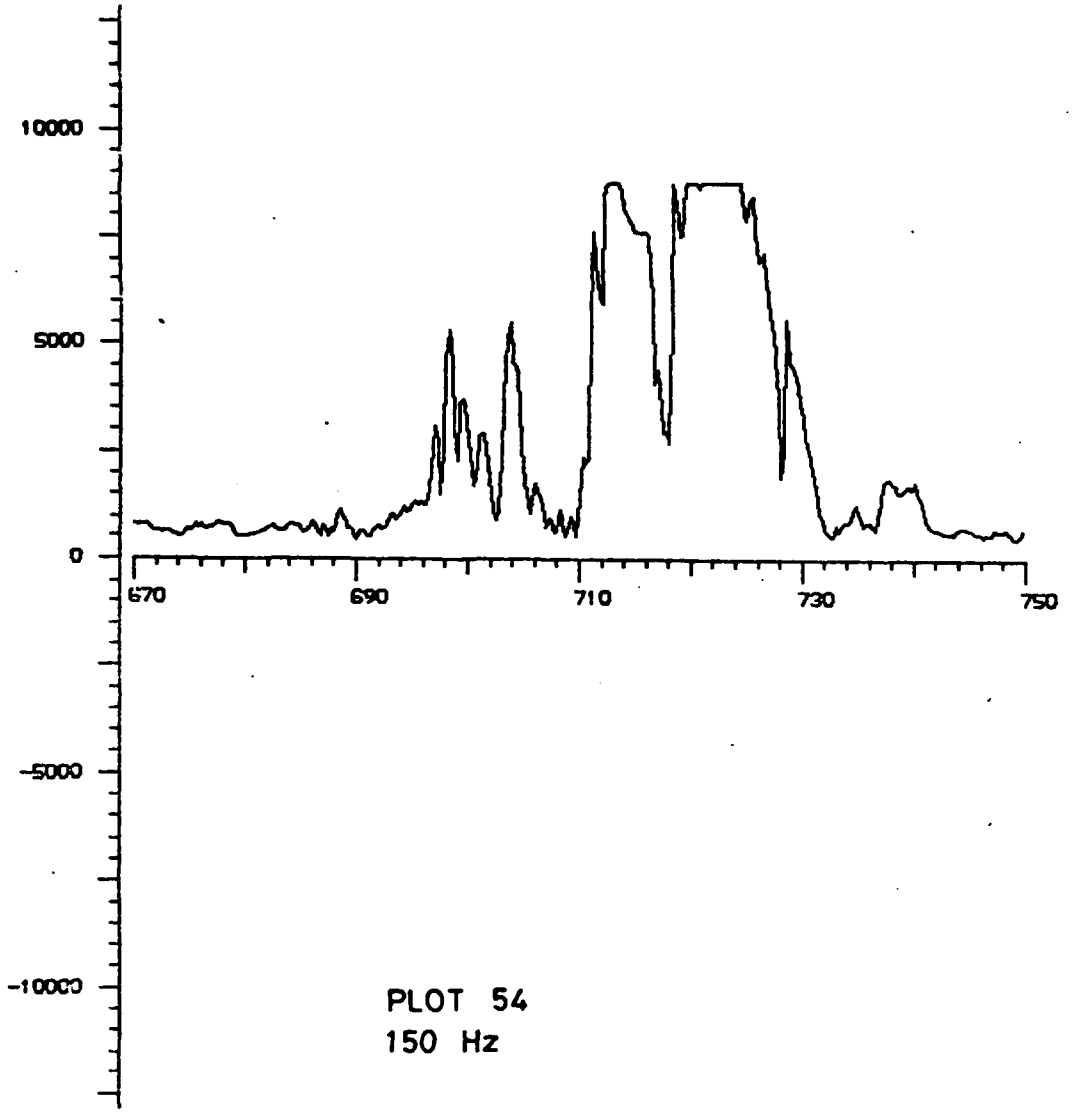

B-101

SMALL AIRCRAFT
OVERFLIGHT
3/21/11

GRAPH A2

WAIT

PARAMETER=2
SAMPLE RATE=50
DISC 3=RICETAP4-200-3
Y SCALE= $_{10}$-2 C4/1
X SCALE=200/200

PLOT 54
150 Hz

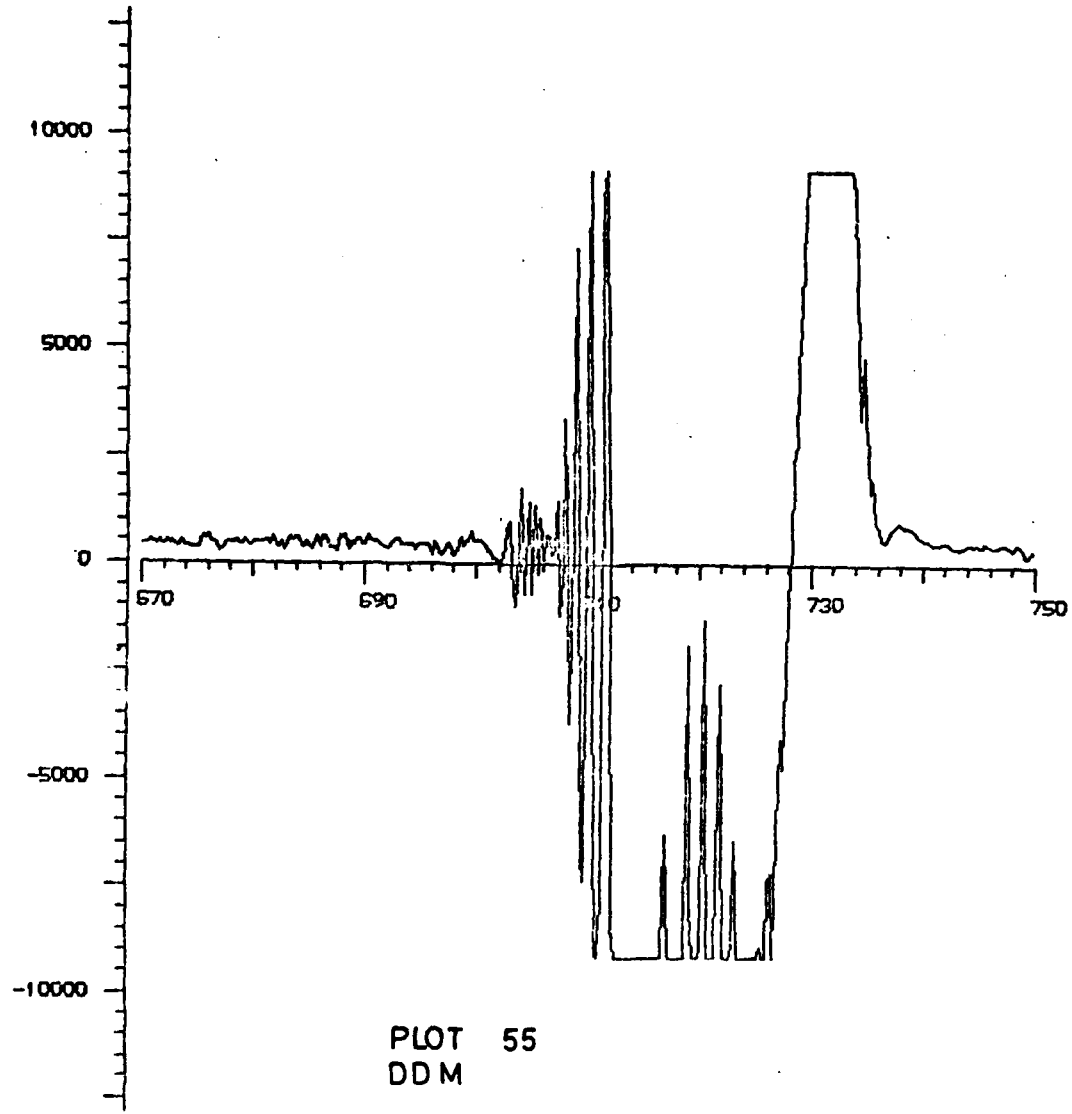

PLOT 55
DDM

SMALL AIRCRAFT
OVERFLIGHT
3/21/11

GRAPH A3

WAIT

PARAMETER=3
SAMPLE RATE=50
DISC 3=RICETAP4-200-3
Y SCALE= $_{10}$-2 C4/1
X SCALE=200/200

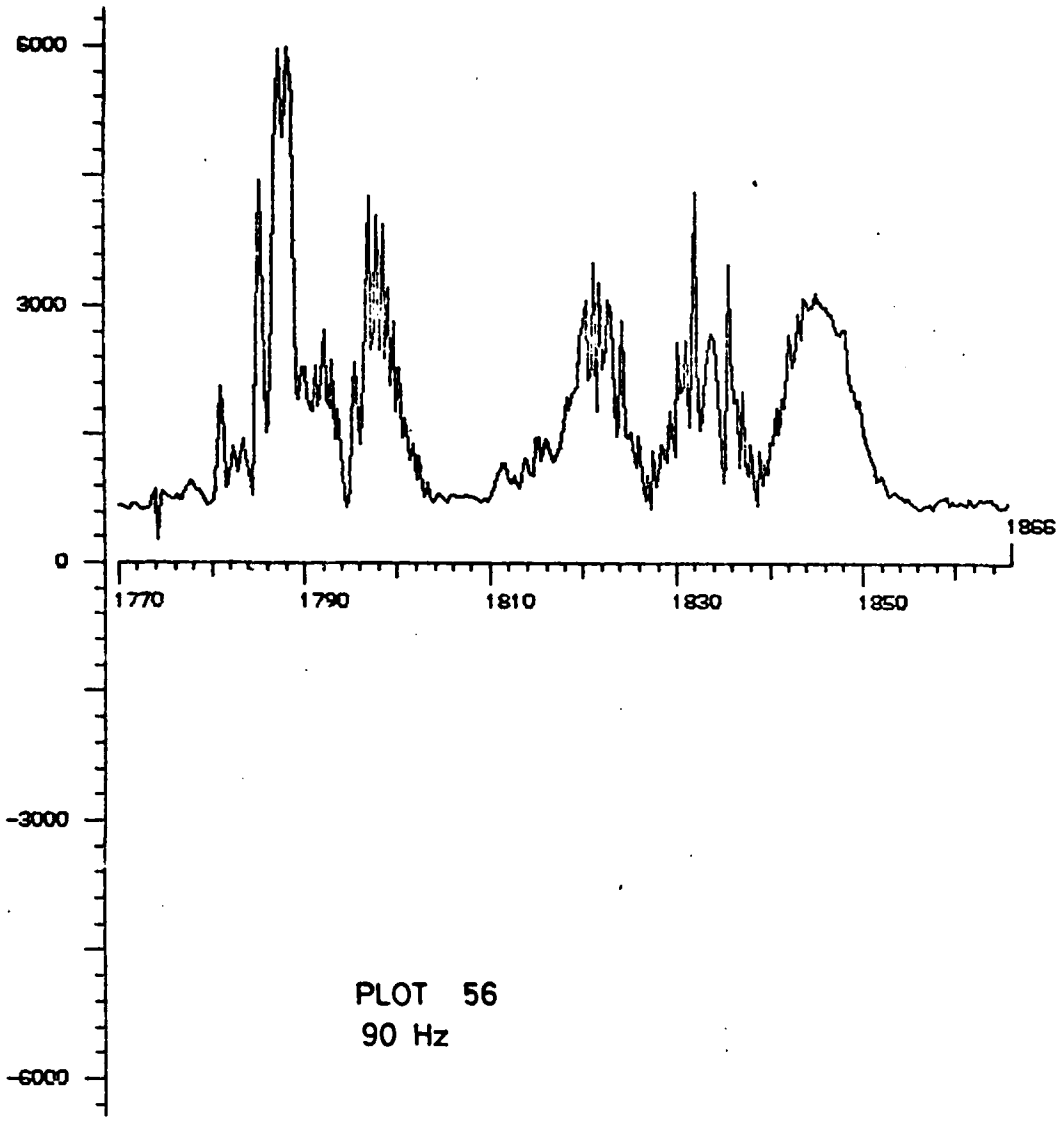

SMALL AIRCRAFT MISSED APPROACH
OVERFLIGHT
5/21/11

GRAPH A4

WAIT

PARAMETER=1
SAMPLE RATE=60
DISC 3=RICETAP4-200-3
Y SCALE= $_{10}$-2 C4/1
X SCALE=200/200

PLOT 56
90 Hz

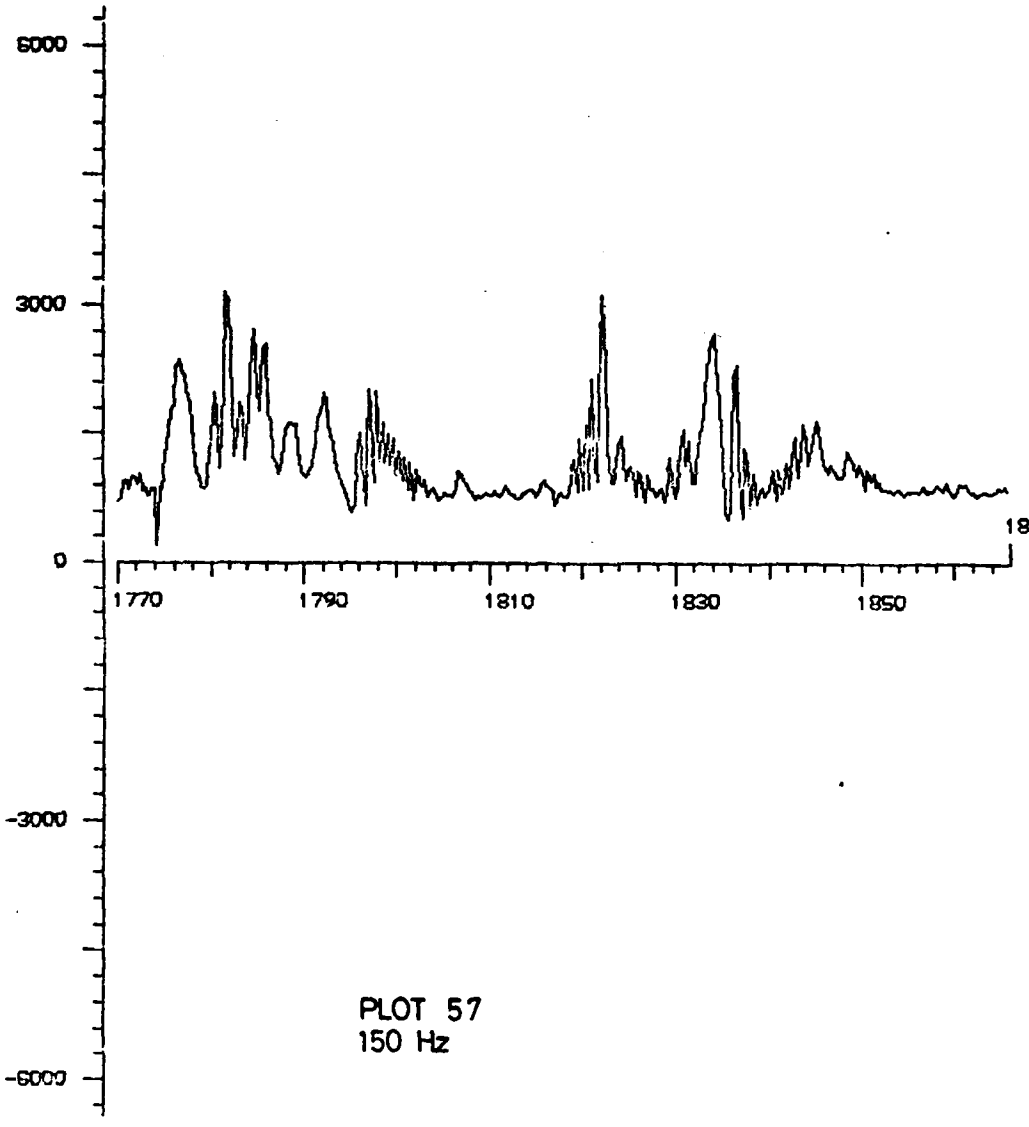

SMALL AIRCRAFT MISSED APPROACH
OVERFLIGHT
6/21/11

GRAPH A5

WAIT

PARAMETER=2
SAMPLE RATE=60
DISC 3=RICETAP4-200-3
Y SCALE= $_{10}$-2 C4/1
X SCALE=200/200

PLOT 57
150 Hz

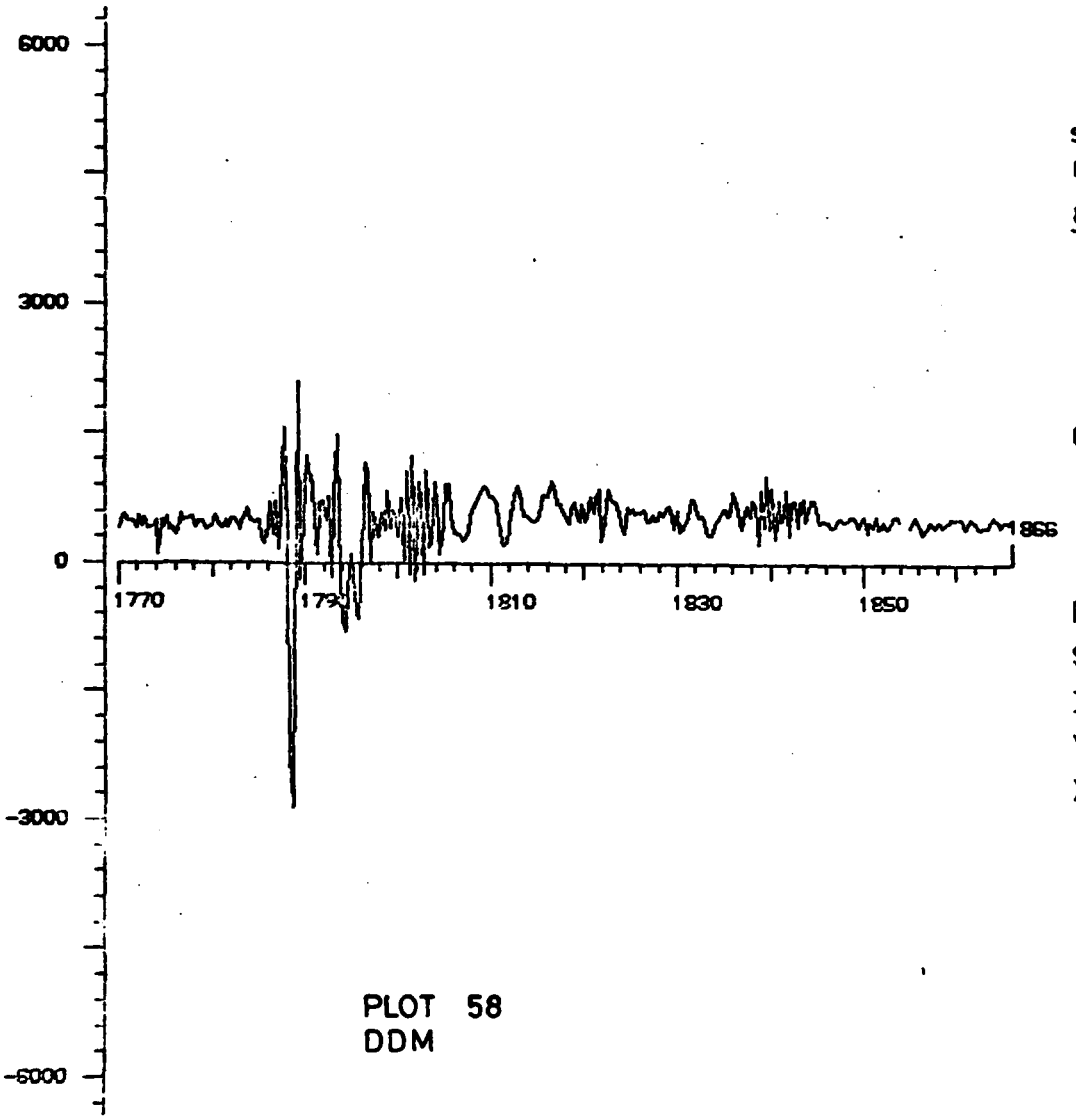

SMALL AIRCRAFT MISSED APPROACH
OVERFLIGHT
5/21/11

GRAPH A6

WAIT

PARAMETER=3
SAMPLE RATE=60
DISC 3=RICETAP4-200-3
Y SCALE= $_{10}$-2 C4/1
X SCALE=200/200

PLOT 58
DDM

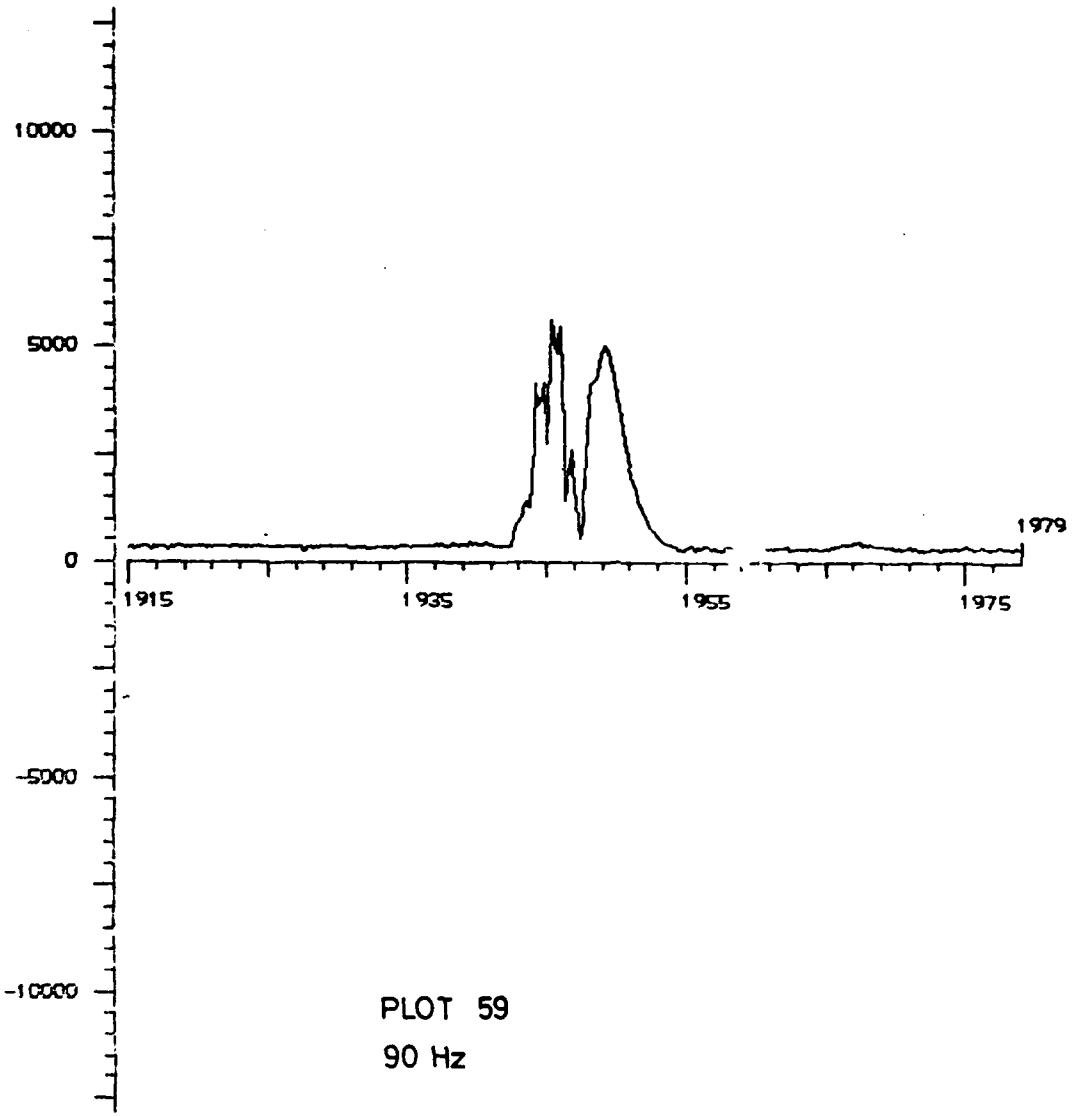

LANDING OVER
LOCALISER
7/19/12

GRAPH A14

WAIT

PARAMETER=1
SAMPLE RATE=40
DISC 2=RICETAP5-200-3
Y SCALE= $_{10}$-2 C5/1
X SCALE=200/200

PLOT 59
90 Hz

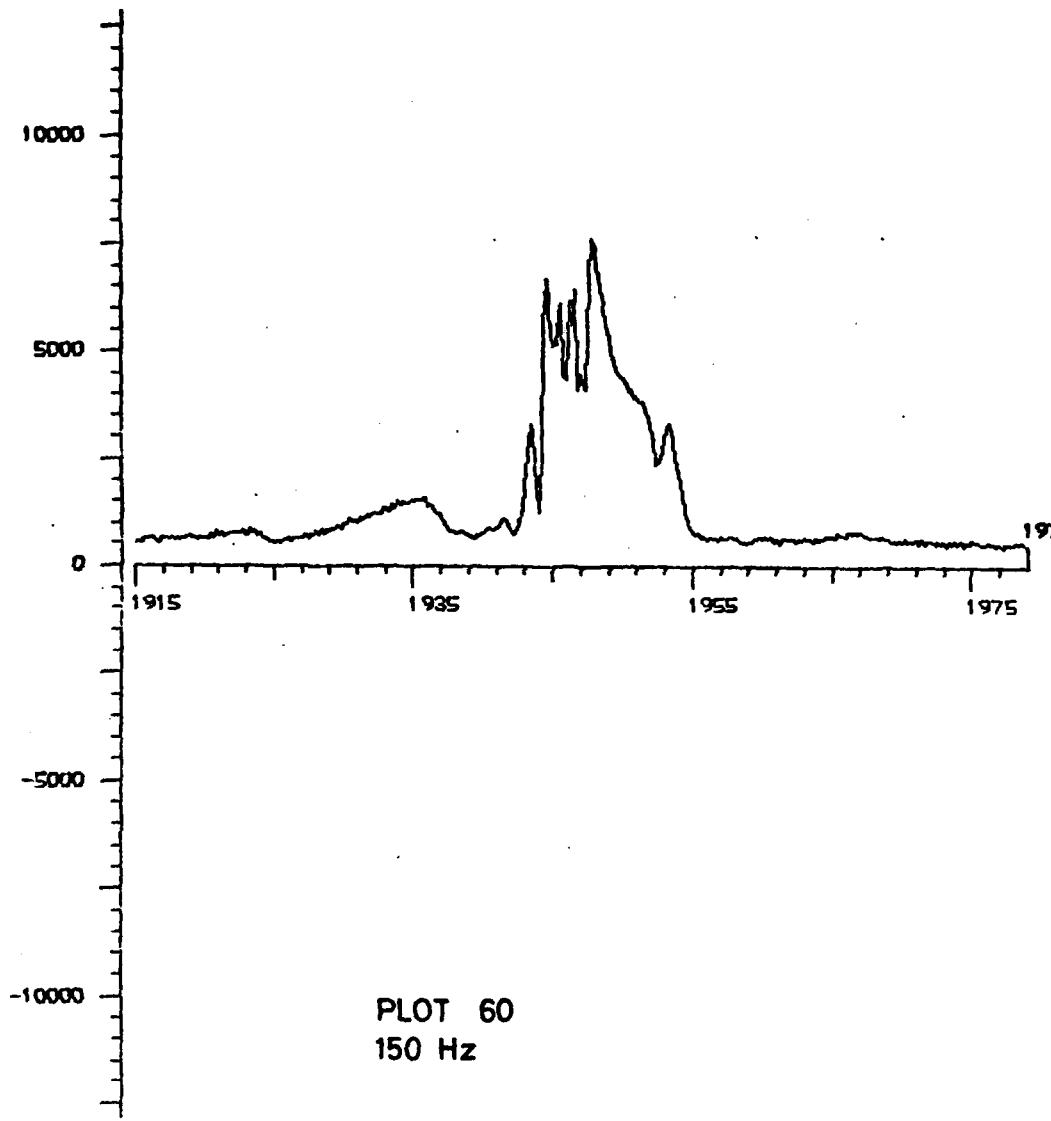

B-107

LANDING OVER
LOCALISER
7/19/12

GRAPH A15

WAIT

PARAMETER=2
SAMPLE RATE=40
DISC 2=RICETAP5-200-3
Y SCALE= $_{10}$-2 C5/1
X SCALE=200/200

PLOT 60
150 Hz

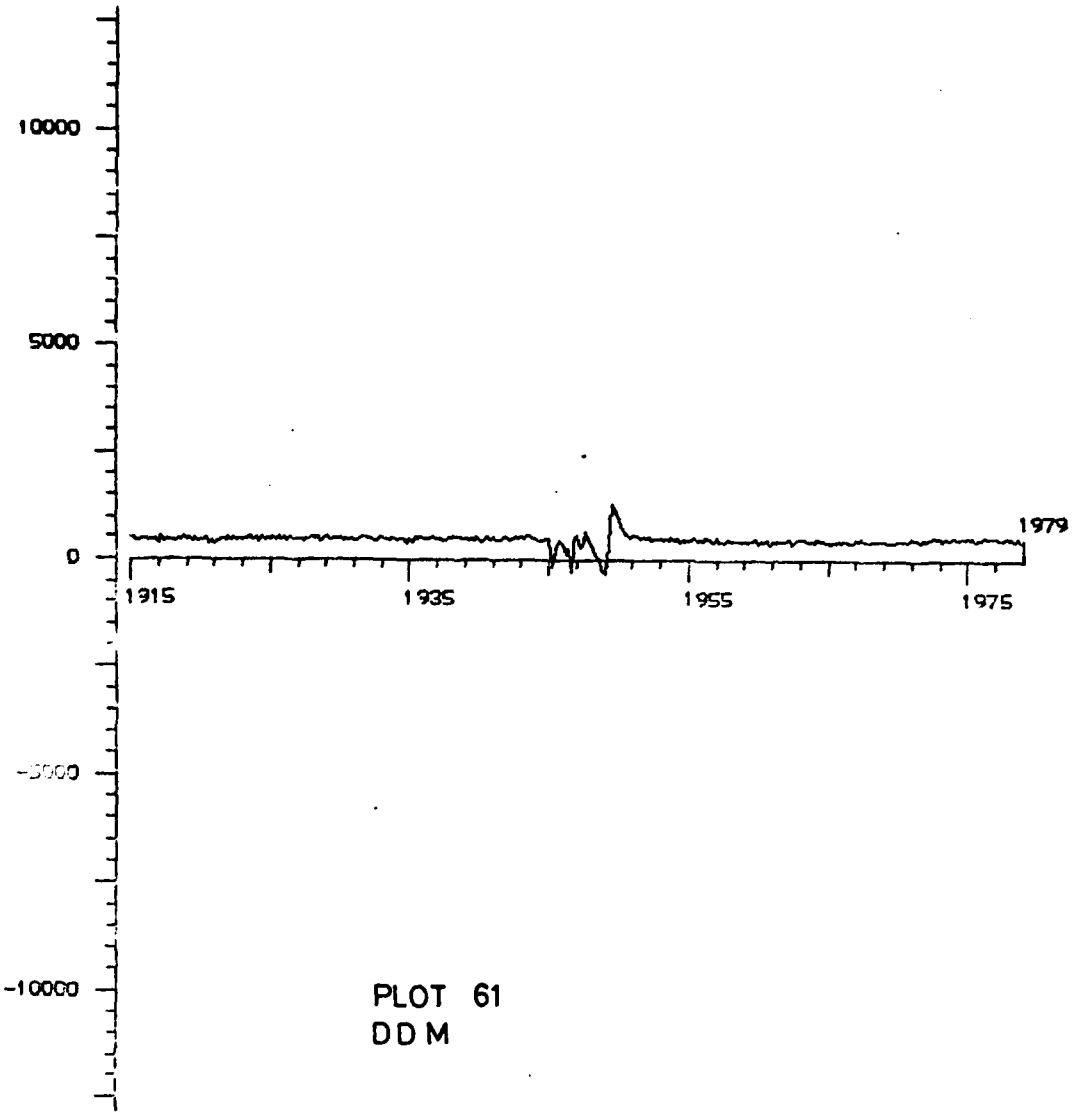

LANDING OVER
LOCALISER
7/19/12

GRAPH A16

WAIT

PARAMETER=3
SAMPLE RATE=40
DISC 2=RICETAP5-200-3
Y SCALE= $_{10}$-2 C5/1
X SCALE=200/200

PLOT 61
DDM

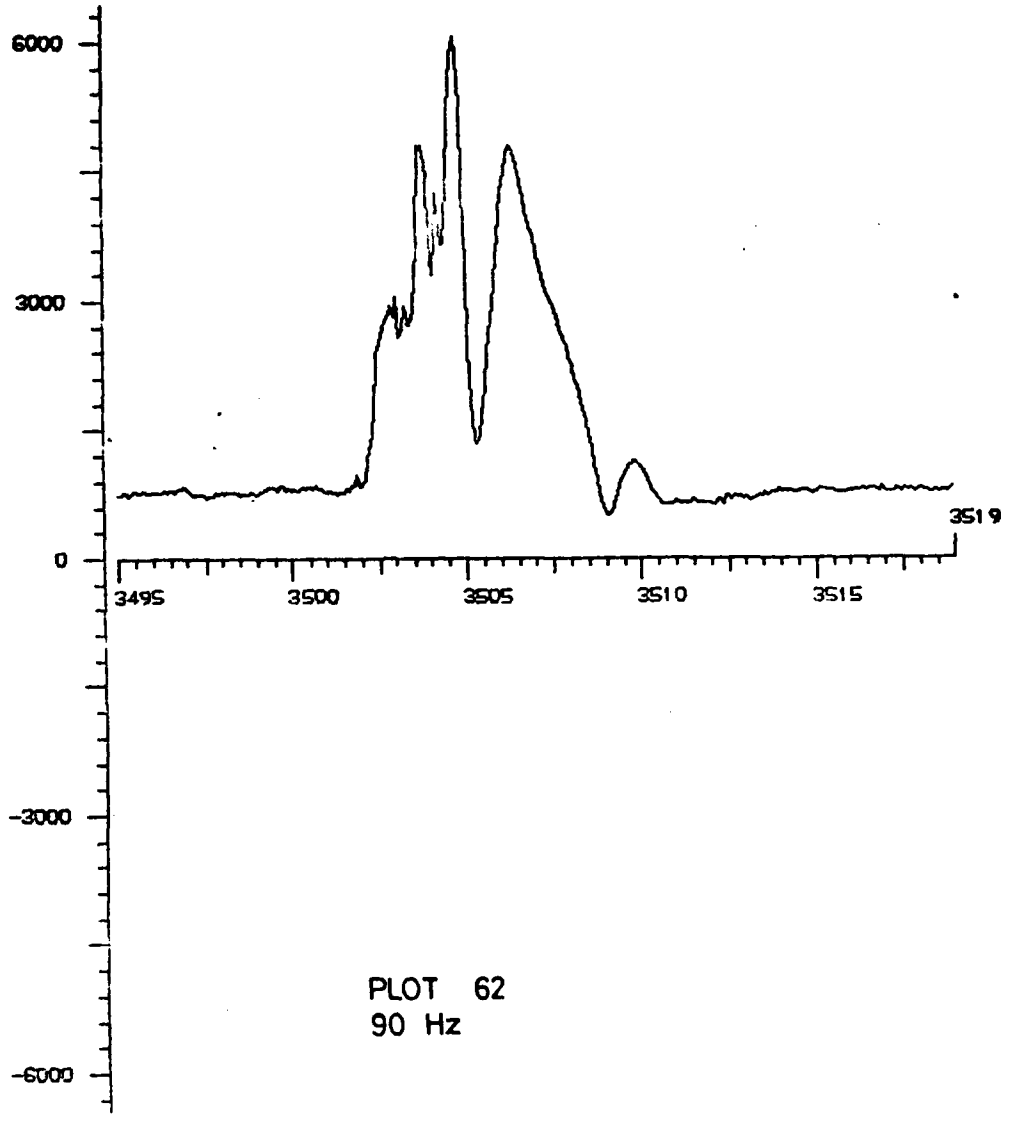

PLOT 62
90 Hz

LANDING OVER
MONITOR
10/21/11

GRAPH A11

WAIT

PARAMETER=1
SAMPLE RATE=16
DISC 3=RICETAP4-200-3
Y SCALE= $_{10}$-2 C4/1
X SCALE=200/200

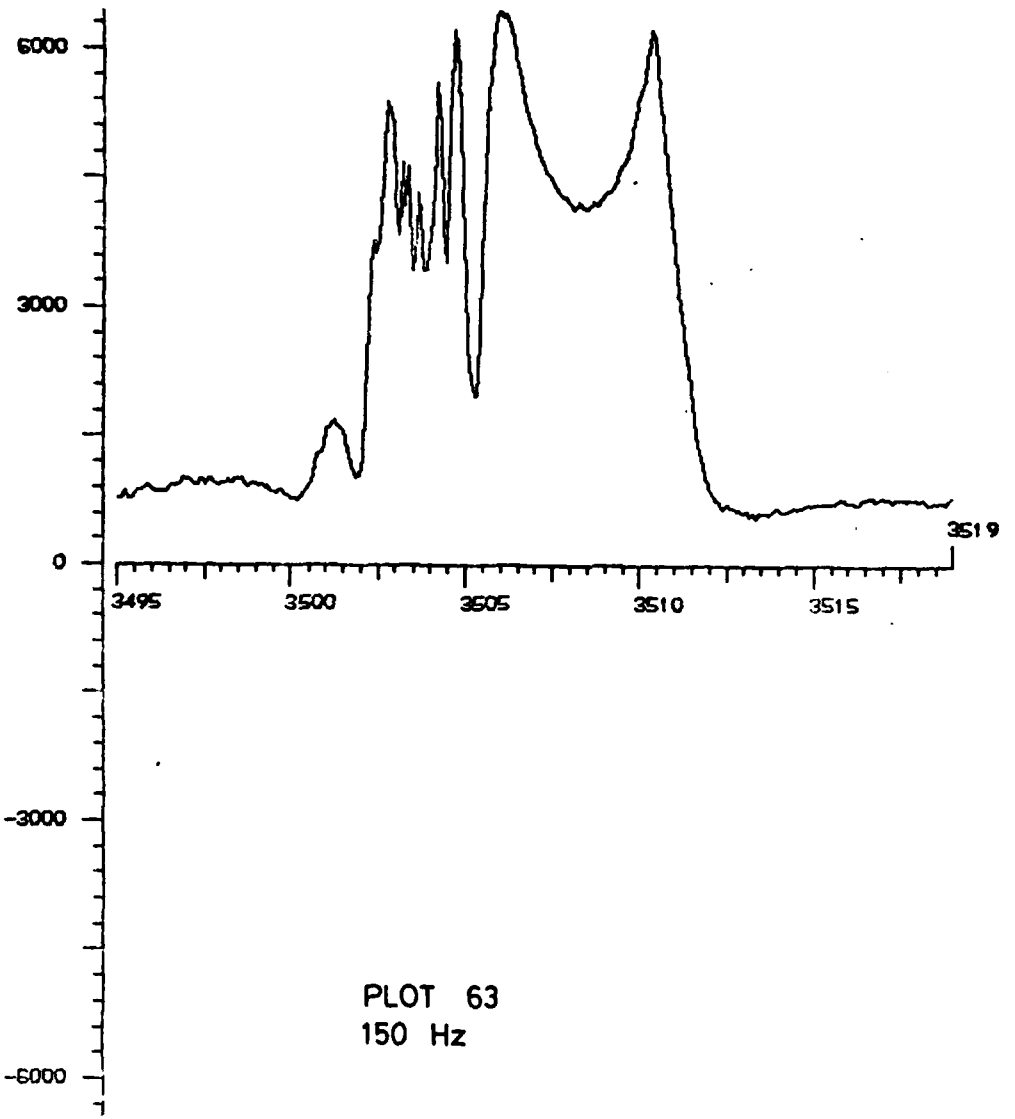

PLOT 63
150 Hz

LANDING OVER
MONITOR
10/21/11

GRAPH A12

WAIT

PARAMETER=2
SAMPLE RATE=16
DISC 3=RICETAP4-200-3
Y SCALE= $_{10}$-2 C4/1
X SCALE=200/200

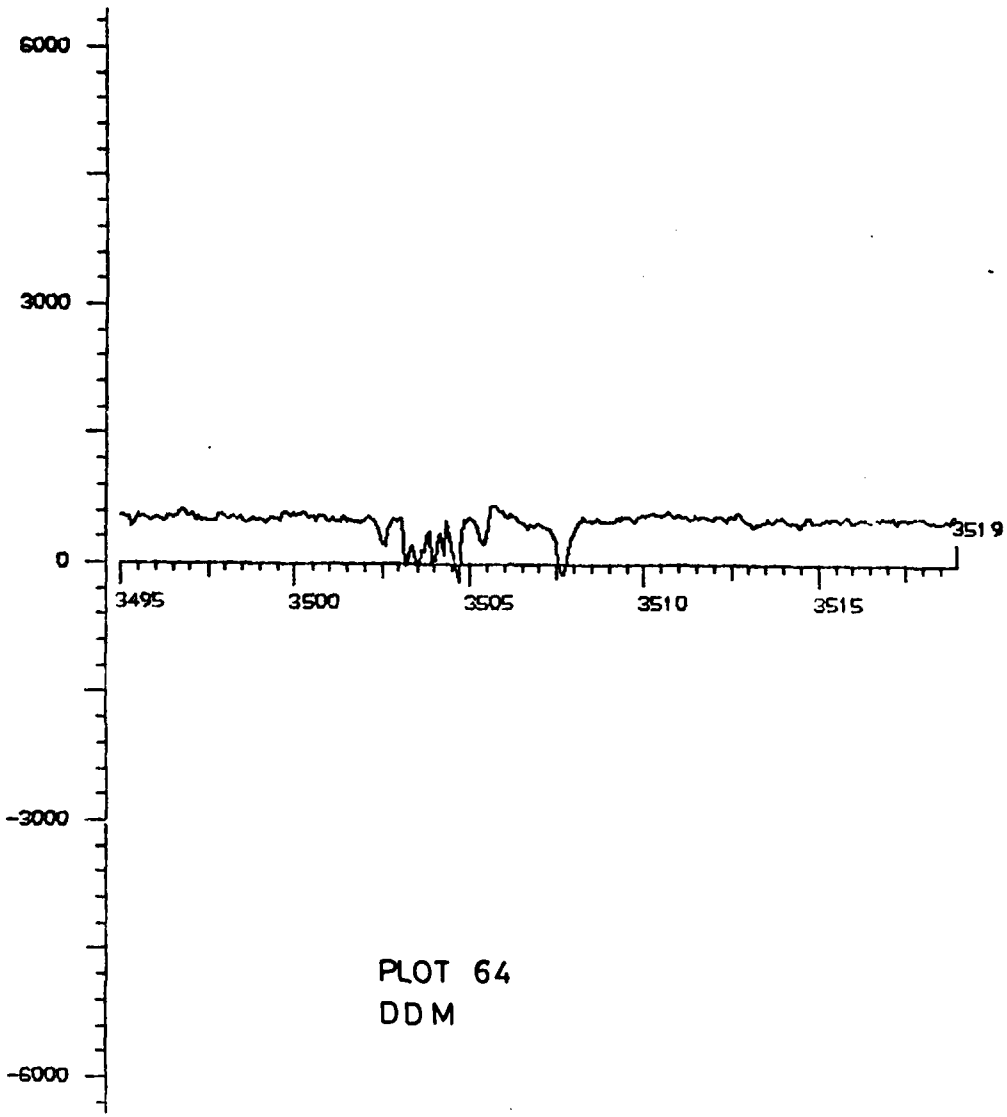

LANDING OVER
MONITOR
10/21/11

GRAPH A13

WAIT

PARAMETER=3
SAMPLE RATE=16
DISC 3=RICETAP4-200-3
Y SCALE= $_{10}$-2 C4/1
X SCALE=200/200

PLOT 64
DDM

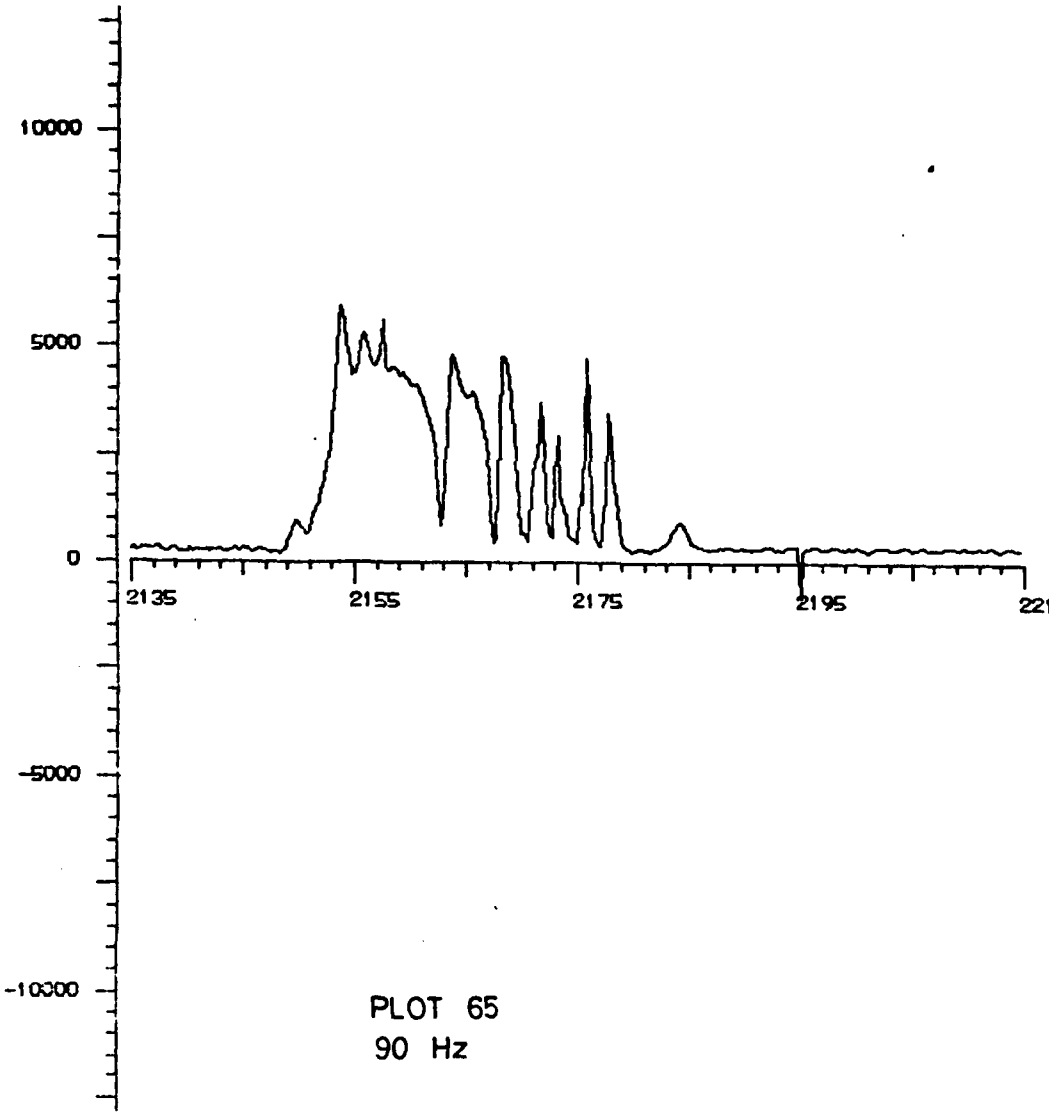

TAKE OFF OVER
MONITOR
7/19/12

GRAPH A17

WAIT

PARAMETER=1
SAMPLE RATE=50
DISC 2=RICETAP5-200-3
Y SCALE= $_{10}$-2 C5/1
X SCALE=200/200

PLOT 65
90 Hz

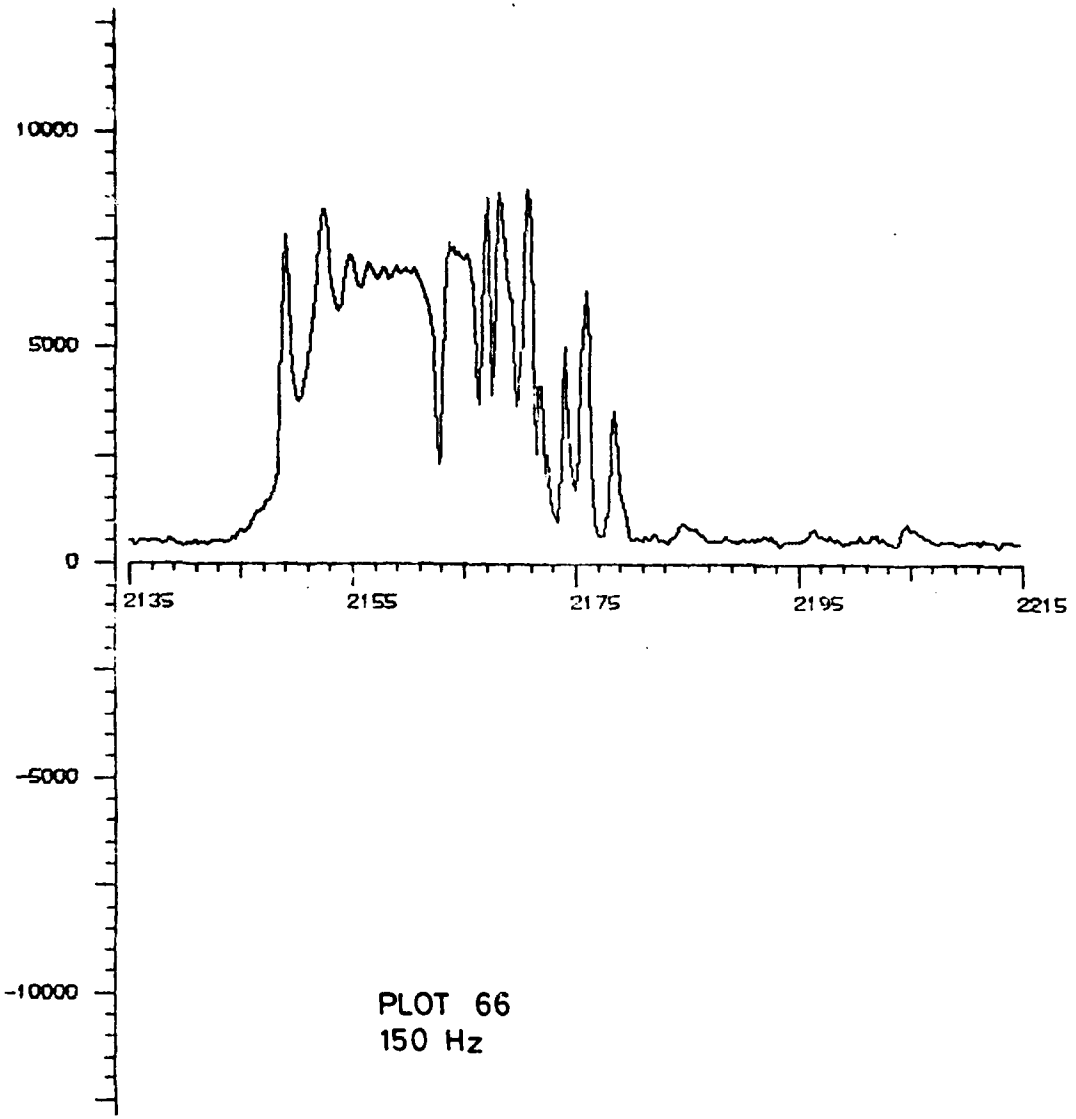

PLOT 66
150 Hz

TAKE OFF OVER
MONITOR
7/19/12

GRAPH A18

WAIT

PARAMETER=2
SAMPLE RATE=50
DISC 2=RICETAP5-200-3
Y SCALE= $_{10}$-2 C5/1
X SCALE=200/200

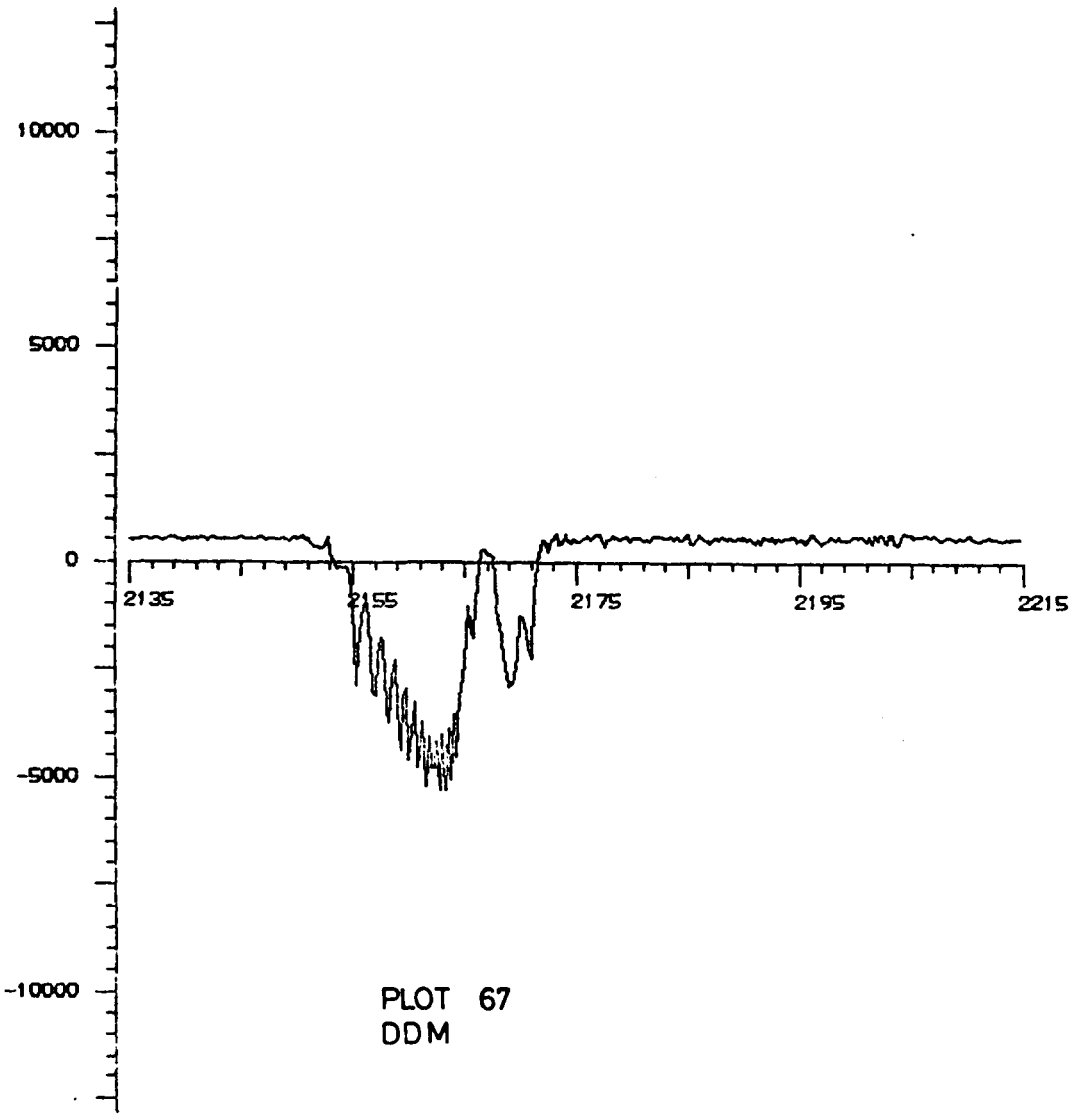

PLOT 67
DDM

TAKE OFF OVER
MONITOR
7/19/12

GRAPH A19

WAIT

PARAMETER=3
SAMPLE RATE=50
DISC 2=RICETAP5-200-3
Y SCALE= $_{10}$-2 C5/1
X SCALE=200/200

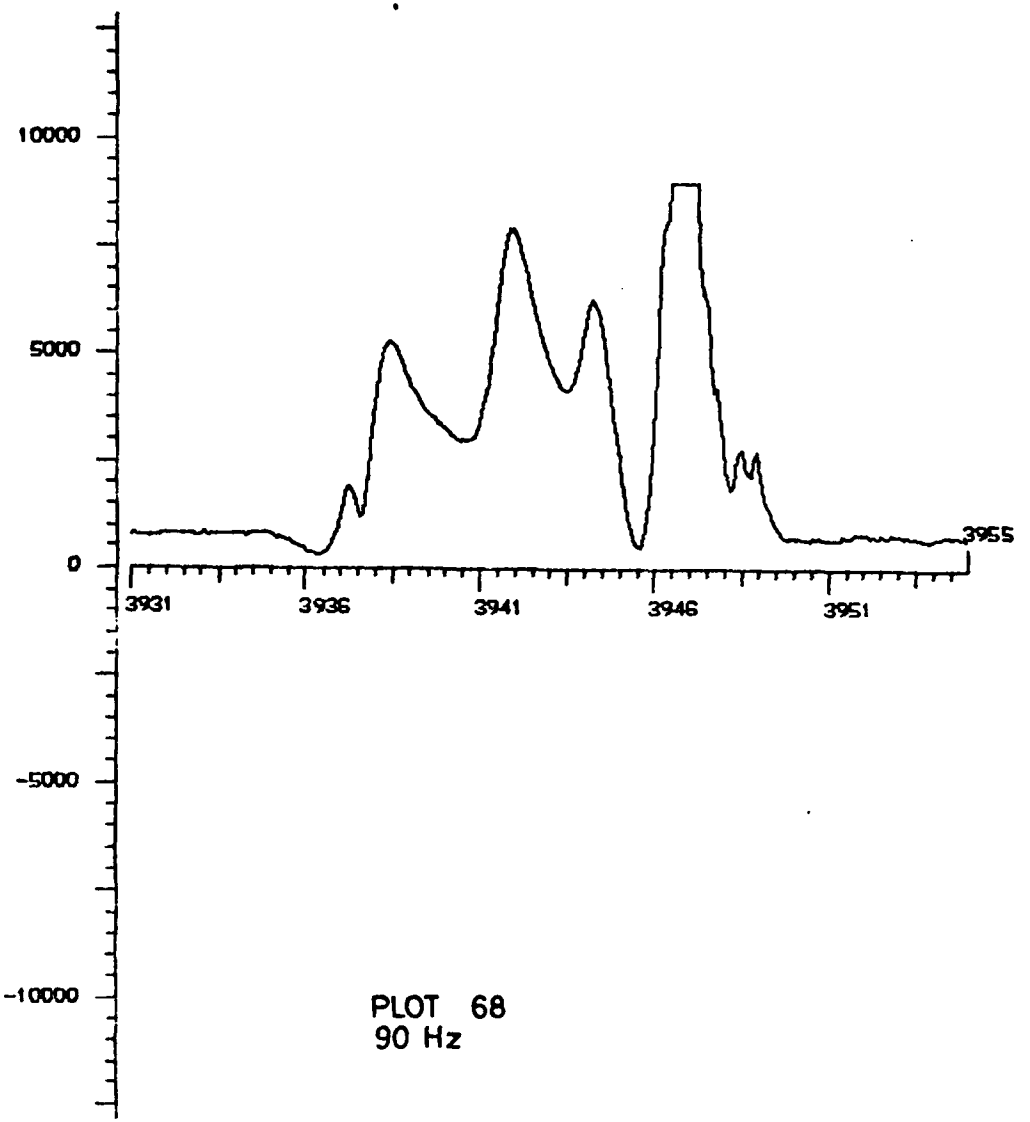

PLOT 68
90 Hz

TAKE OFF OVER
LOCALISER
10/21/11

GRAPH A8

WAIT

PARAMETER=1
SAMPLE RATE=16
DISC 3=RICETAP4-200-3
Y SCALE= $_{10}$-2 C4/1
X SCALE=200/200

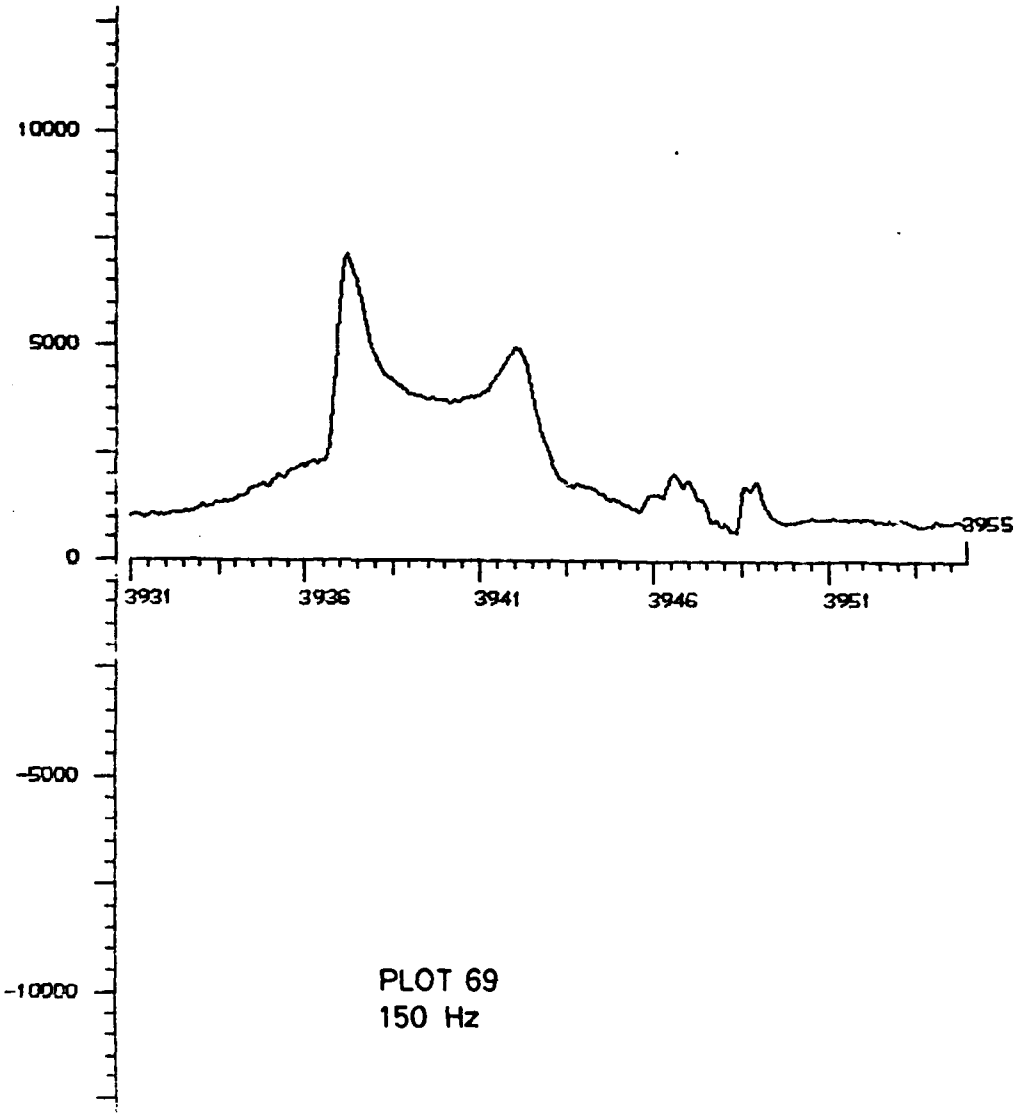

PLOT 69
150 Hz

TAKE OFF OVER
LOCALISER
10/21/11

GRAPH A9

WAIT

PARAMETER=2
SAMPLE RATE=16
DISC 3=RICETAP4-200-3
Y SCALE= $_{10}$-2 C4/1
X SCALE=200/200

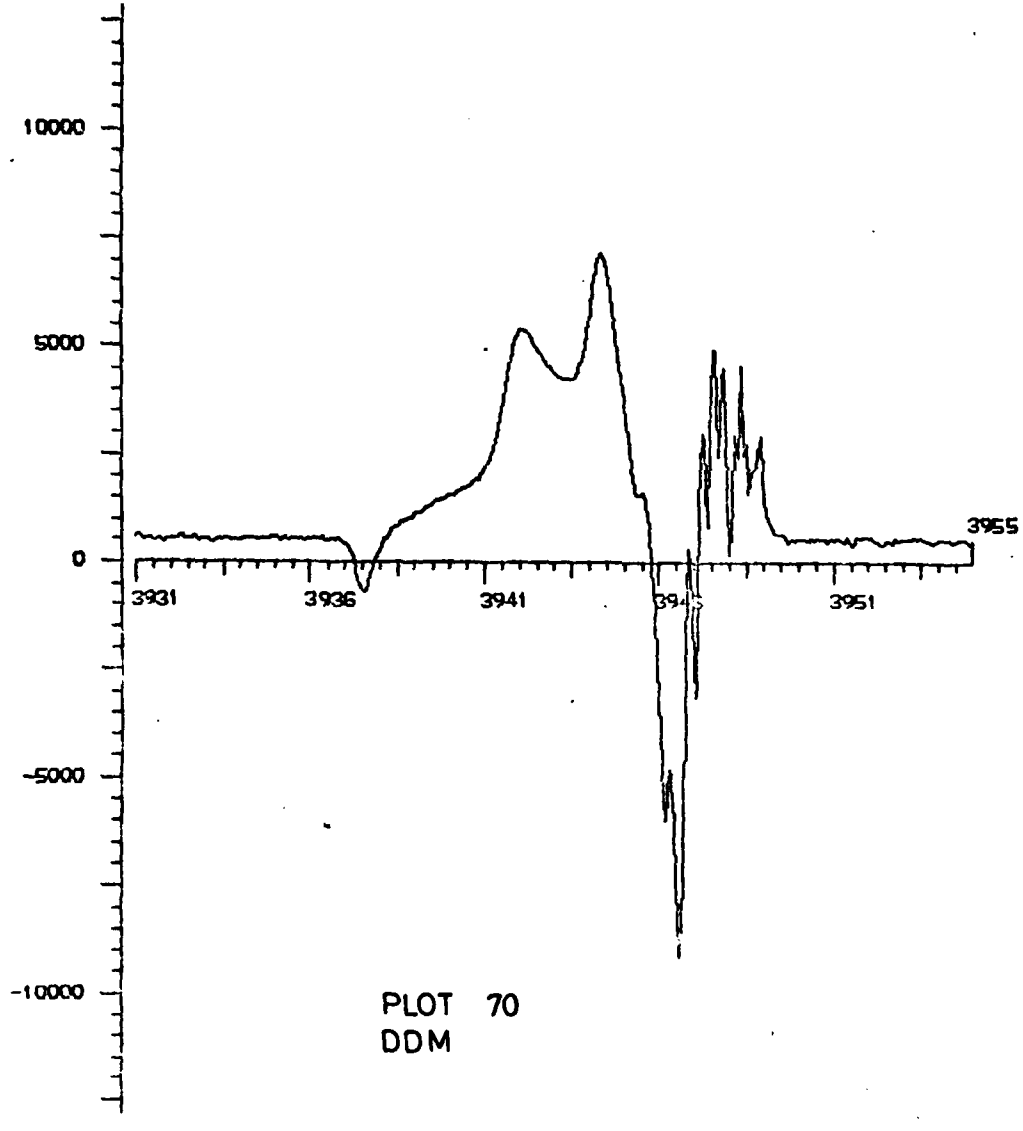

PLOT 70
DDM

TAKE OFF OVER
LOCALISER
10/21/11

GRAPH A10

WAIT

PARAMETER=3
SAMPLE RATE=16
DISC 3=RICETAP4-200-3
Y SCALE= $_{10}$-2 C4/1
X SCALE=200/200

APPENDIX C

BACKGROUND AND STATUS OF PRESENT FAR FIELD MONITOR WORK

C.1 Introduction

Most contemporary far field monitor systems consist of probes that are physically located beyond the near field of the antenna. Processing of the data yields information about the quality of guidance on the glide slope path. The greatest liability of most present far field monitors[1,2] and monitor concepts is their lack of adequate quantity and distribution of probes thus providing insufficient information on which to assess the pattern of ILS guidance. The exceptions to this, to our knowledge, are the study of Heathrow Airport conducted by Marconi[3] and alternate monitor systems[4] such as the Echo system by Plessey.[5] In the Marconi study the analysis was thorough yet limited in scope to local and ground taxiing aircraft. The extent to which the analysis was carried out forms the primary background from which the present study will develop. More will be said of this study later in this report.

The Plessey study considered an echo type monitor in which a large array received ILS echos from approaching aircraft. Since the aircraft, statistically, are expected to fly smoothly along the glide path, the reflected signals from many approaching aircraft will portray the quality of the glide path. This system only provides information when an aircraft is in final approach. Therefore, it cannot be used to direct aircraft to alternate runways or airports until at least one aircraft has sensed the difficulty. Further, since many unacceptable course bends may be of relatively short duration,

such as those due to taxiing or overflying aircraft, a monitor must provide minute by minute information for maximum usefulness. Finally, the signal quality actually achieved was limited, and though not a fundamental difficulty, further improvement might be difficult. Thus, except for a brief review in the body of this report, the echo type monitor will not be considered further.

C.2 ILS Monitor System Types

Limited monitors now exist that can sense the presence of certain time varying, diffracting reflections. In most cases, however, these monitors cannot quantitatively evaluate the magnitude of the resulting guidance perturbation on the approach path, as will be subsequently shown in this report. This problem occurs because there is no simple relationship between the field at a ground location and the field on the approach path. To accurately represent the approach path guidance derogation due to time varying, diffracting reflectors, more than one probe position (typically four to eight) appears to be required. Further, these monitor points should be displaced transversely relatively to runway centerline. A form of signal comparison and processing is required involving both phase and amplitude information to provide an accurate representation.

Although most investigations of far field monitor parameters and techniques have been limited to consideration of very simple monitors[2] there has been one significant investigation for a particular geometry[1]. The specific study referred to is that of monitoring localizer derogation due to taxiing aircraft in the runway environment for Heathrow Airport.

The utilization and requirements for far field monitors can best be understood by considering them in combination with present monitors to provide complete monitoring service. It should be noted that for any installation,

the far field monitor may be used in combination with any present monitor. The primary deficiency of present monitor systems that do not incorporate a far field monitor is the lack of information about events that occur on and beyond the runway. Such events can substantially derogate guidance, and can only be detected by a far field monitor. A far field monitor with sufficient capability to provide complete monitoring would be extremely difficult to design, if possible at all, and would be excessively expensive in production. However, a far field monitor in combination with one or more present monitors could vastly extend the ability to measure events that significantly derogate guidance.

ILS monitor systems are of three basic types and provide varying capabilities for predicting localizer and glide slope guidance quality on the glide path. These monitors, illustrated in Figure C-1 are: integral/aperture, near field and far field. Clearly, a full fledged far field monitor provides the most complete response of the ILS system to effects which could cause derogation to the glide path guidance.

The diagram shows the region of coverage for each type of monitor. In each case, the more comprehensive monitor can, in principal, provide information on all quantities detected by the less comprehensive monitor. Thus, in principle, the far field monitor could detect all sources of derogation, while the integral system monitors transmitter and feedline performance. Because, however, the far field monitor must contend with very difficult geometries, it appears desirable to use it in combination with one of the "close in" (integral, aperture or near field) monitors such that it must only contend with events beyond the transmitter and radiation system.

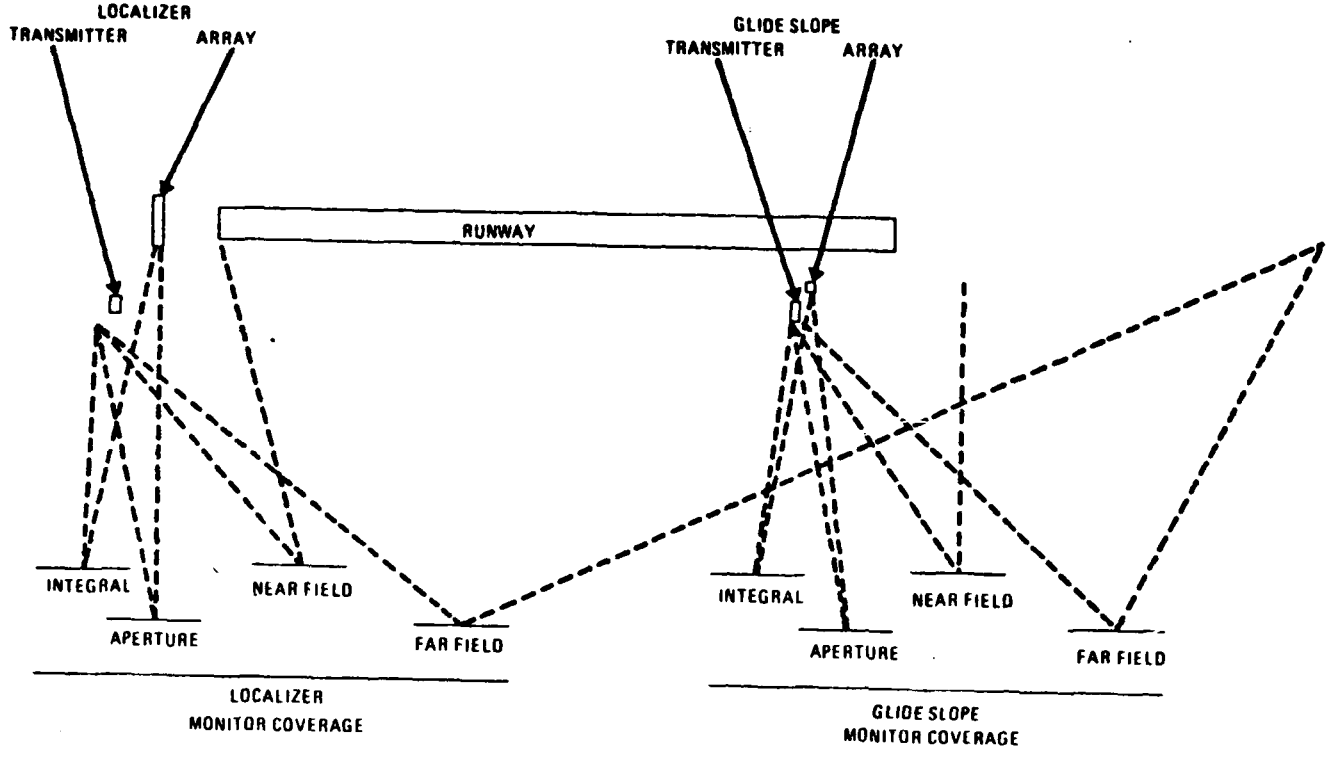

Figure C-1 Regions Potentially Monitored by Each Type System for Both Localizer and Glide Slope

C.2.1 Integral Monitor

The integral monitor is characterized by coupling to the system at any point from the transmitter terminals to the radiation system. It provides information on the integrity of the originally generated signal in the transmitter through the connection point. Its advantage is that it is an integral part of the equipment and once developed it is supplied and installed as a constituent part of the system. To the extent of its coverage (limited to quantities internal to the equipment) it provides maximum reliability and economy.

C.2.2 Aperture Monitor

The aperture monitor provides the transition between integral and near field monitors. It is characterized by pick-up elements which individually couple to a limited number of radiating elements. As such, a single pick-up cannot describe the far field signal at a radiation direction such as course center or the course width point. Such characteristics are available only through the use of a combining network. Typical of the aparture monitors are the pick-up loops or dipoles used with various systems. Aperture monitor systems provide information on actual radiated fields beyond that provided by the integral monitor, but little else. Both integral and aperture monitors require some additional external probes to ensure against a significant physical alteration in the radiation system going undetected, that would cause the radiated guidance to go out of tolerance. This additional monitor can be near to far field.

C.2.3 Near Field Monitor

The near field monitor proves the guidance fields within the near field of the radiation system. Typically, this is within a few hundred feet of the

antenna. Near field monitors have the advantage over integral or aperture monitors in that most major defects of the radiation system from transmitters to antennas can be identified. Near field monitors can also provide some indication of the presence of overflight and nearby taxiing aircraft, although this capability is limited. Near field monitors typically consist of a very limited number of probes which provide course center and width information. This is the most prevelent monitor in use today for both localizer and glide slope. Experimentally, McFarland has shown that analog near field localizer monitors are feasible by using a large number of probes[6]. This monitor is not in general operational use.

C.2.4 Far Field Monitor.

The far field monitor consists of probes in the far field of the system. In principle, the far field monitor is capable of signifying any fault in the ILS system. As a practical matter, present far field monitors consist of a very limited number of probes (typically one or two) located beyond the approach end of the runway and are only used operationally for localizers. This sort of monitor operates on the assumption that any major time varying guidance derogation will alarm the fields at the monitor point. Although there is merit in this type of monitor in that it provides some indication of perturbation in guidance due to time varying, diffracting reflectors, it cannot provide information quantitatively. A sophisticated far field monitor of the type being examined for the present program must be used.

C.3 Requirements and Considerations for Far Field Monitors

Within the context of this program, the far field monitor, in combination with one or more present monitors, is required to provide monitoring capabilities as specified in ICAO, Annex 10, Part 1 and the U.S. Flight Inspection Manual,

FAA Handbook C.P. 82001. The specification requires that the far field monitor sense guidance deviations that are beyond the scope of present monitor systems.

Time invariant deviations in localizer and glide slope guidance arise from fixed perturbations including terrain variations and fixed objects. Time varying deviations such as beam bends can also be illustrated in terms of the geometry of an ILS system and a moving diffracting and/or reflecting object.

C.3.1 Ground Based Sources of Scattering

The ILS system and the scattering object may be regarded initially as two coherent sources, having an amplitude ratio and constant phase difference. Such a system generates a family of hyperbolae with each hyperbola representing a locus of points having a constant path difference between the two foci as seen in Figure C-2. This diagram illustrates a localizer, however, a similar diagram can be constructed for a glide slope array. Successive hyperbolae, drawn at equal increments of path difference, have increasingly spaced intercepts with the course center line as distance increases from the transmitter. If these increments are each one wavelength at the carrier frequency, then the separation of the intercepts is the "wavelength" of a complete cycle of course-line disturbance during which the guidance signal is unbalanced to one side and then the other. The longest "wavelengths" are caused by objects which are closest to the transmitter relative to the observation point.

As illustrated in Figure C-2, the interference pattern of a reradiating object can be illustrated as both beam bend and noise. In between the transmitter and the defracting reflector, the derogation wavelength is very short as shown in Figure C-2. Near the approach direction the wavelength is very

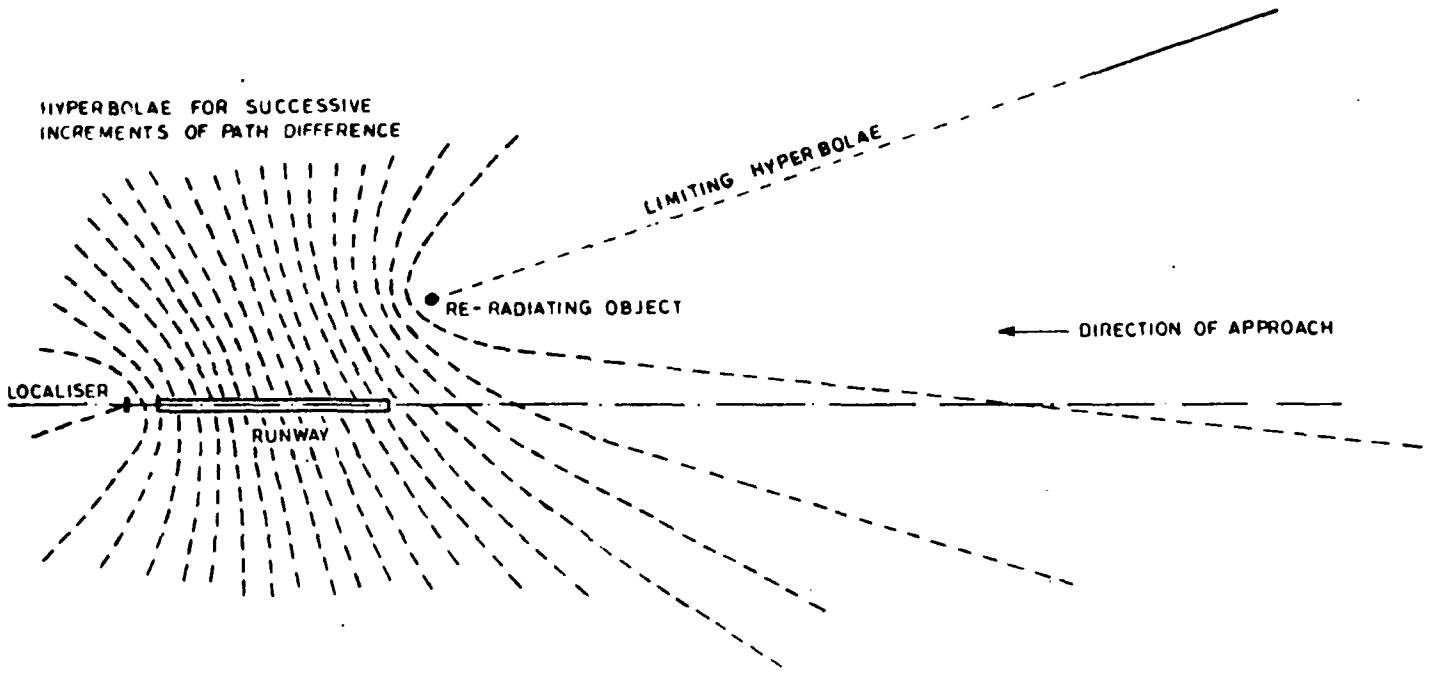

Figure C-2 Hyperbolae of Coherent Interference

long. This is shown quantitatively in Figure C-3 where the interference pattern frequency is shown as a function of the incidence angle between the direct and derogating radiation with plane approach speed as a parameter.

Beam bends can be considered to be the result of reflection or diffraction and can have interference pattern wavelengths of many thousands of feet. Noise occurs in regions where reflected energy is crossing the approach path close to 90 degrees. If only one reflector is involved, the effect would be a sine wave and can involve frequencies as high as 20 to 40 Hz as can be seen by extending the curves in Figure C-3 to 90 degrees. Typically, since several diffracting reflectors or terrain elements are involved in the signal propagation path to a specific location, there will normally be several scattered signals crossing the glide path at each point. A complex or noise-like derogation results.

C.3.2 Effect of Elevated Sources of Reflection

The effect of scattering on ILS monitoring is particularly serious because of the great variety of vertical interference patterns which can be generated. Elevated sources can be the result of reflections or diffractions from the vertical fin of large aircraft or from aircraft in takeoff or landing manuevers. This is illustrated by the next sequence of figures.

Figure C-4 shows the outline drawing of a 747. On the ground, the most prominent source of scattering is the tail because of its height. The effect on the monitor is illustrated in Figure C-5. The broad lobe is the radiation pattern of a localizer at a height of 9 feet. The lower lobe is the result of diffracting/reflections from a 747 tail. Clearly, if the lobe peak amplitudes were equal, the reflected signal would dominate the direct signal both at a ground monitor location and on the glide path. For this reason, even moderate reflections can derogate guidance.

AD-A079 663 WESTINGHOUSE ELECTRIC CORP BALTIMORE MD F/G 17/7
FAR FIELD MONITOR FOR INSTRUMENT LANDING SYSTEMS.(U)
NOV 79 R MORE, J C BRADLEY, B NEWMAN DOT-FA75WA-3689
UNCLASSIFIED FAA-RD-79-70 NL

4 OF 4
AD A079663

END
DATE FILMED
3-80
DDC

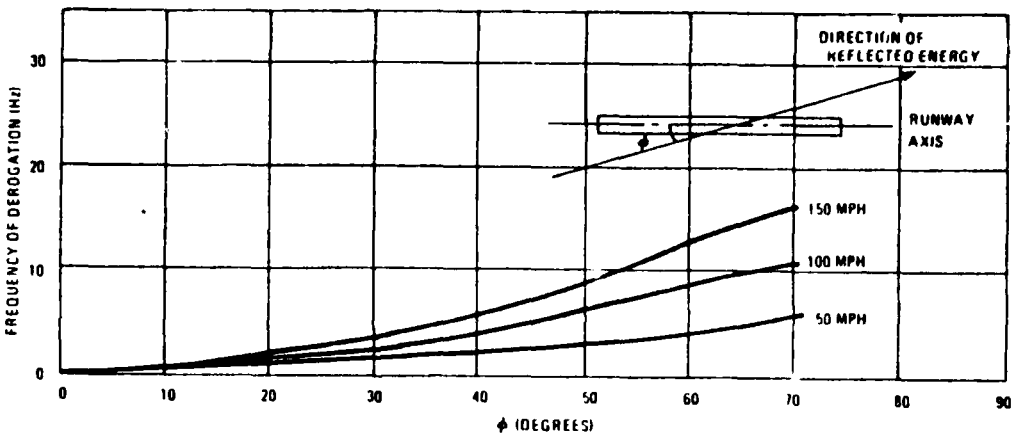

Figure C-3 Oscillatory Frequencies of Localizer Derogation vs Aircraft Landing Speed and Incidence Angle

MAXIMUM TAKEOFF WEIGHT	MAXIMUM LANDING WEIGHT	A	B	C	D	E	F	G	H	J	K	L	M	N	TURN RADIUS
710,000 LB 323,050 KG	564,000 LB 256,620 KG	195'8" 59.64M	231'4" 70.51M	63'5" 19.33M	84'0" 25.60M	104'5" 31.82M	36'2" 11.02M	39'2" 11.96M	69'6" 21.18M	71'1" 23.50M	3'11" 1.19M	5'5" 1.65M	47'0" 14.33M	16'8" 5.08M	156'0" 47.55M

MODELS B, C, F HAVE MAXIMUM TAKEOFF WEIGHT OF 775,000 LB (352,625 KG).

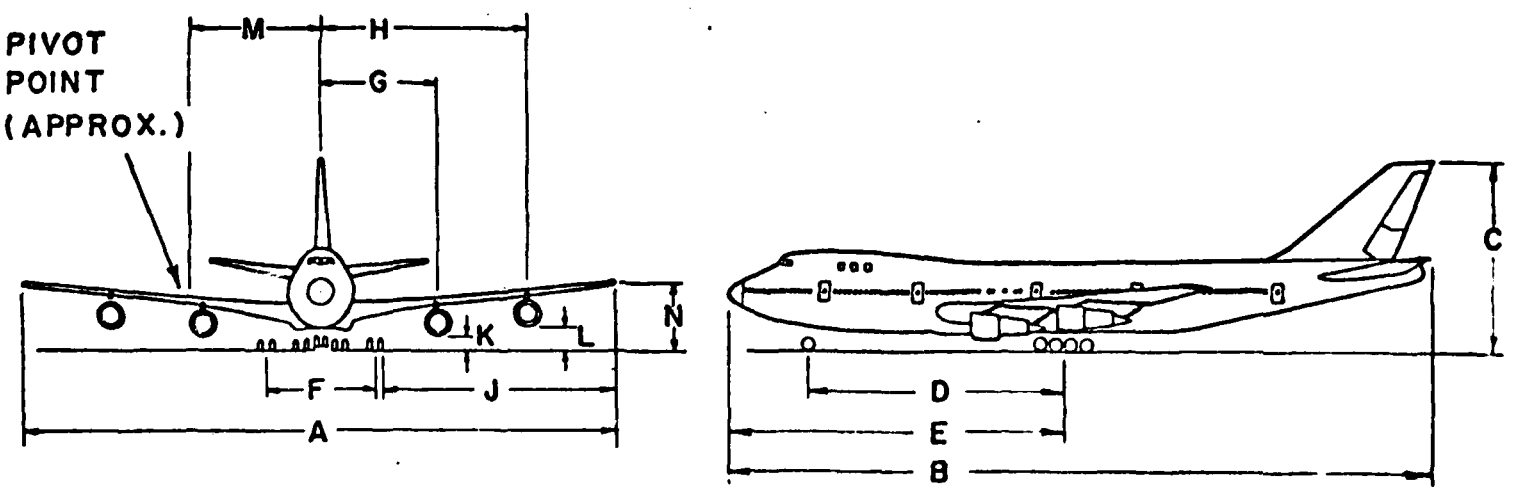

Figure C-4 Outline Drawing of 747

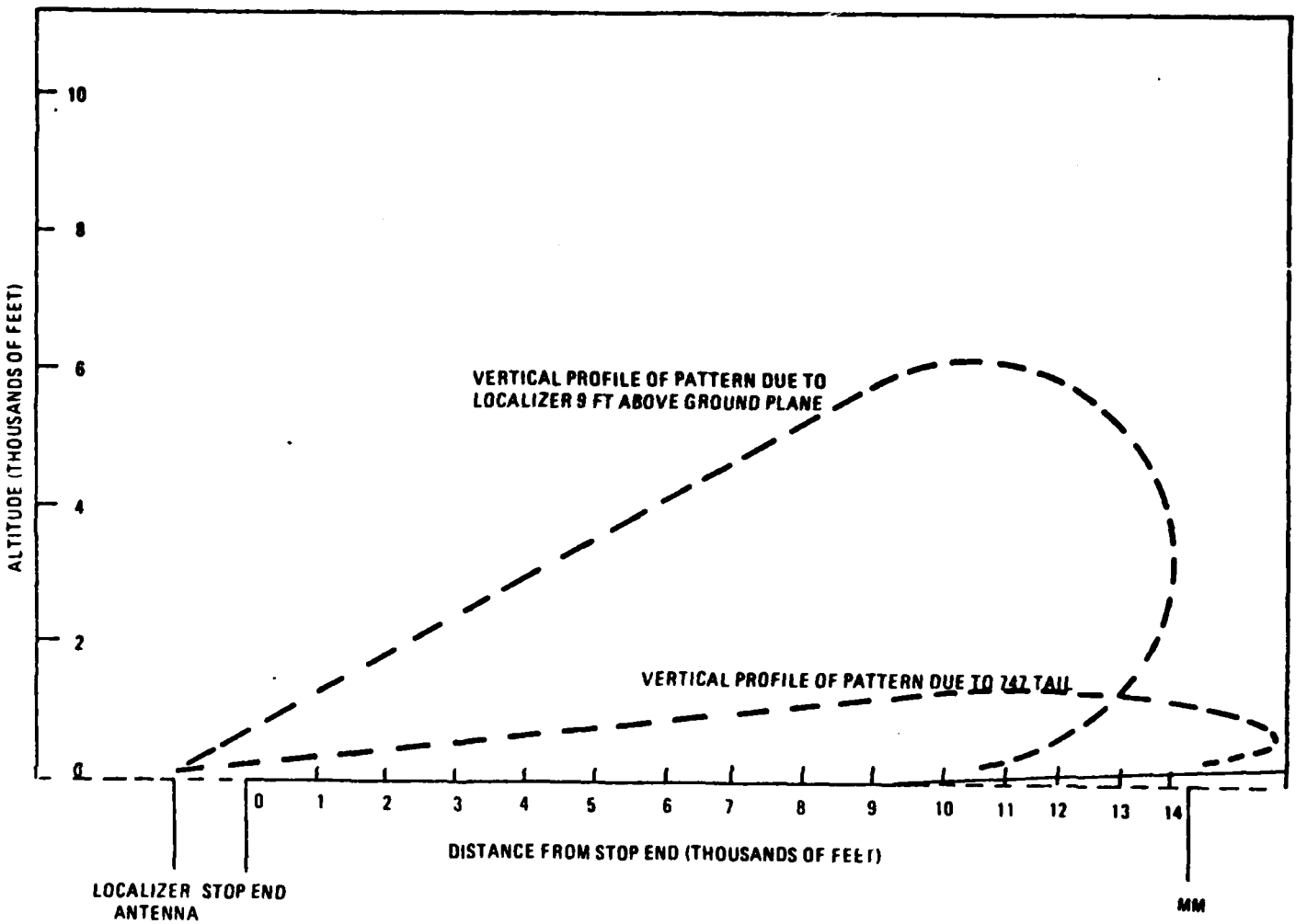

Figure C-5 Vertical Profile of Guidance Lobe of Localizer Signal with 747 Tail Close to the Localizer Antenna

The potential effect on the monitor due to overflying aircraft on takeoff manuevers is illustrated in the next two figures. Figure C-6 illustrates an example takeoff profile for a KC135/707 type aircraft. Assuming that aircraft both in landing and takeoff manuevers move in the same direction down the runway, aircraft landing would arrive from the left of the figure. The localizer would be between the 11,000 and 13,000 foot points. Thus, a lightly loaded aircraft might be high enough when it crosses the localizer antenna to cause little effect while a heavily loaded aircraft might be close enough to the array to seriously derogate the guidance signal. Figure C-7 shows that the reflection interference pattern due to aircraft overflying the localizer can have several lobes in the region between the glide path and any reasonable monitor locations.

The overpowering nature of derogation due to the low lobe posiiton for diffracting reflections from aircraft taking off is illustrated in measurements made by Marconi[3]. Figure C-8 shows the trace of derogation in guidance and flag current. This is one of a series of overflight measurements taken by Marconi at Andrews Airfield, Saling and Stansted Airport. This trace for a 707 aircraft on takeoff illustrates the overpowering effect of overflight derogation on ground-based monitors. Other traces taken for smaller aircraft on takeoff and missed approach manuevers show varying degrees of derogation although all are overpowering.

The significance of this problem is illustrated by studies conducted on the effect of such derogation on landing aircraft at Heathrow Airport, London. It has been stated that interference caused by aircraft taking off and overflying the localizer can be tolerated provided that the landing aircraft is not below approximately 500 feet on the approach. Thus in Category III

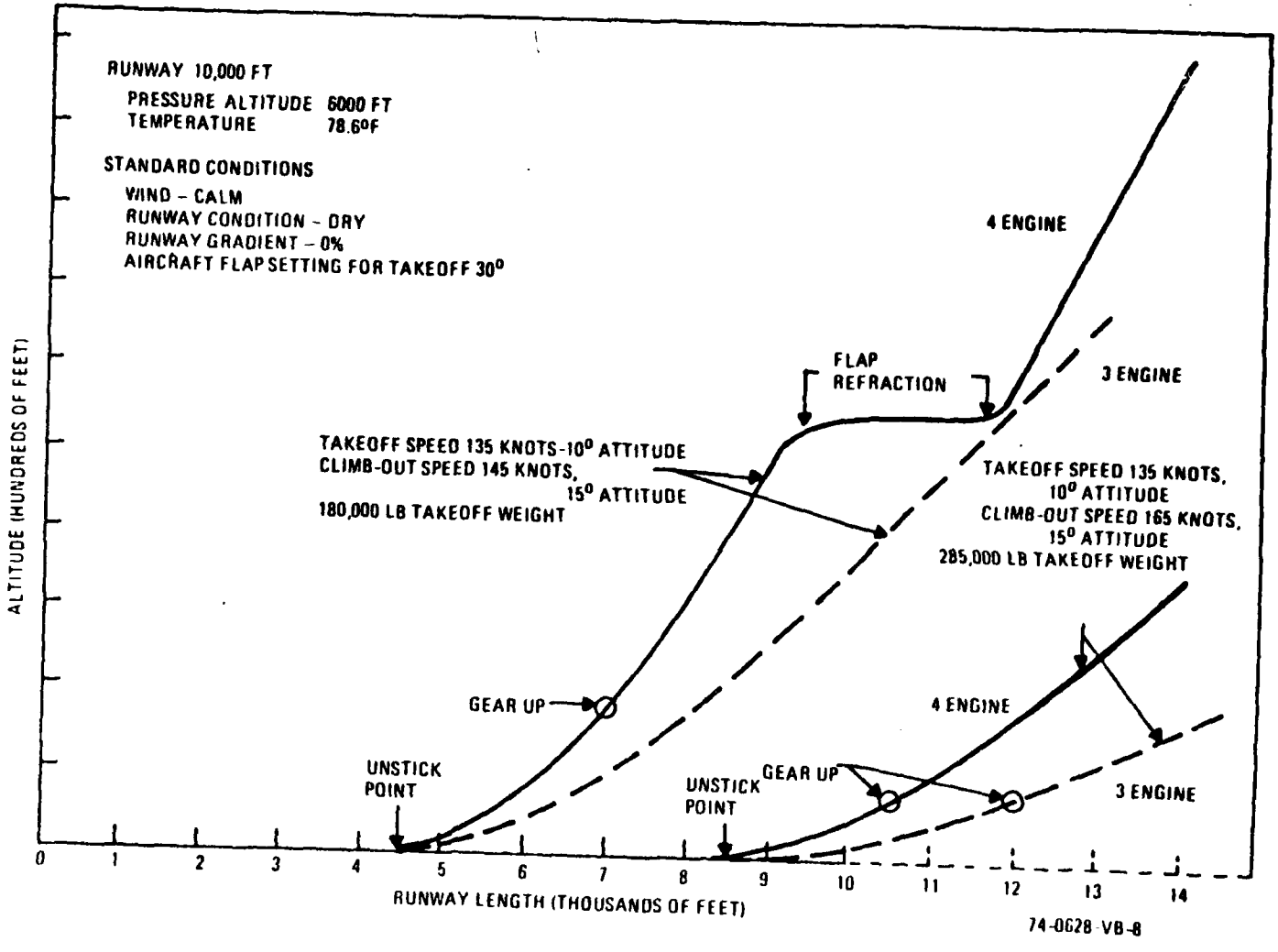

Figure C-6 Examples of Take Off Maneuver Profiles for KG 135/707 Aircraft with Various Load Conditions

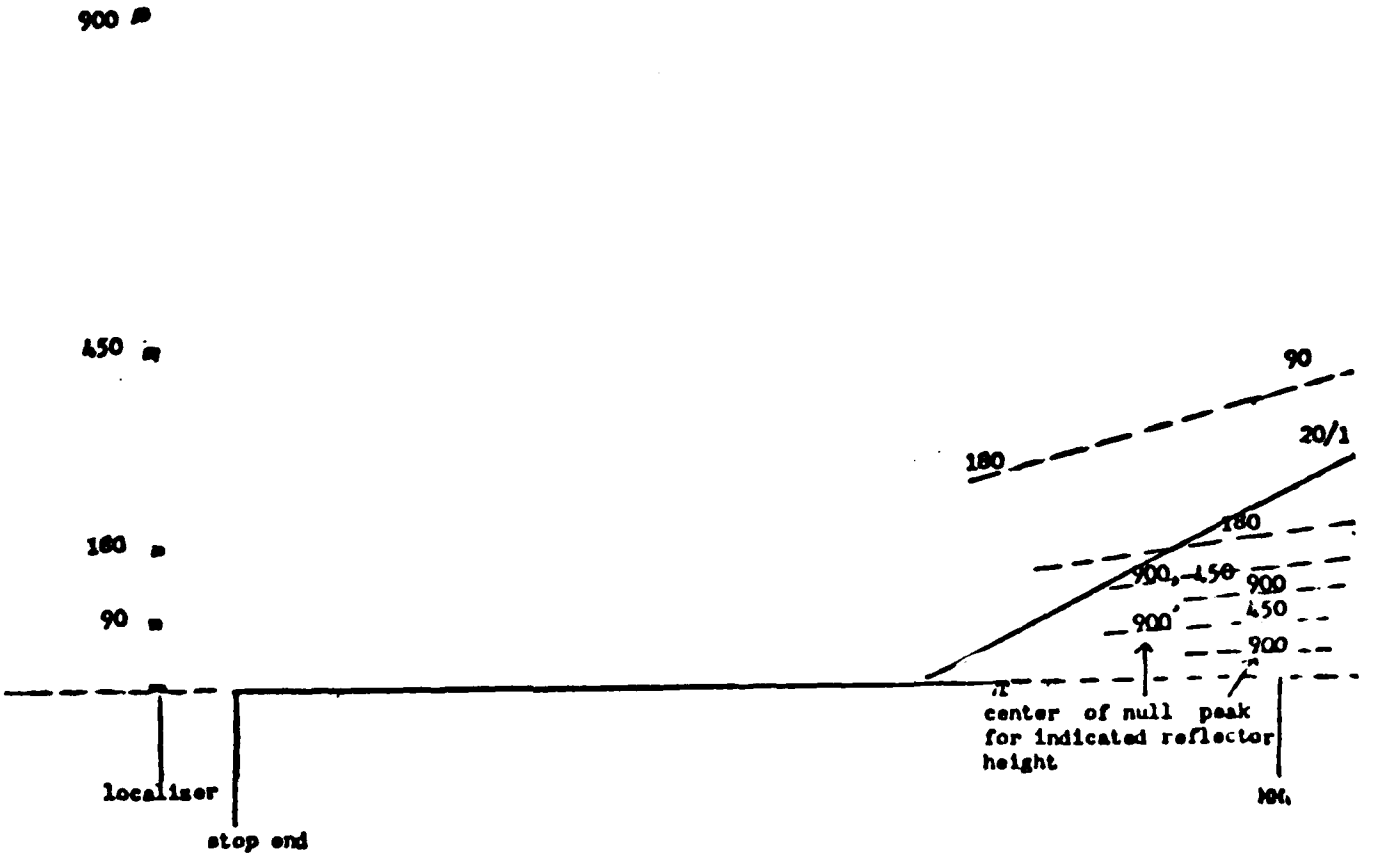

Figure C-7 Diagram showing positions of lobe nulls and maxima due to reflection [illegible]. The reflector height causing the null or maximum is indicated over the line indicating the position of the null or maximum.

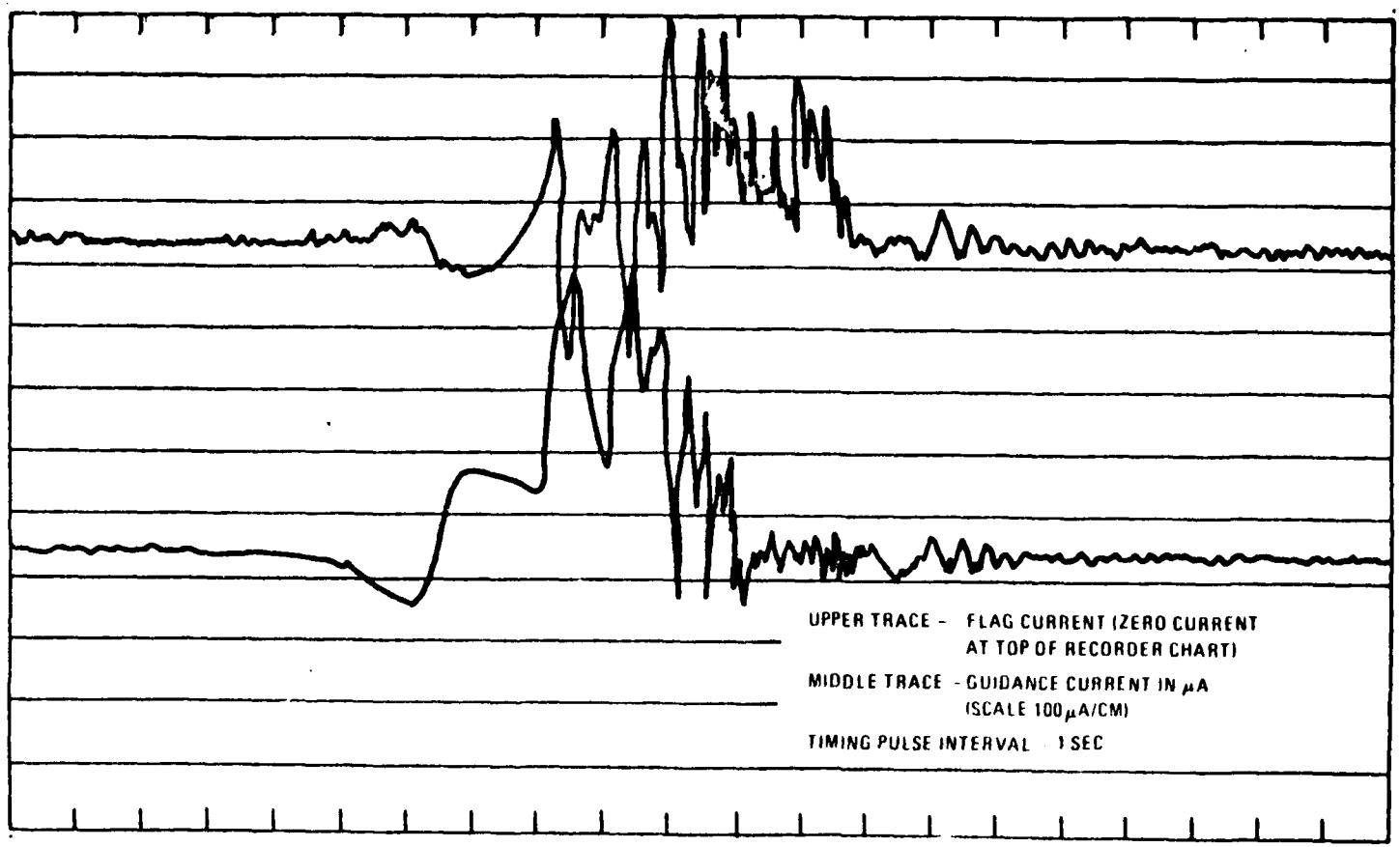

Figure C-8 Overflight Derogation Measured for 140-Foot Offset 12,500 Feet from Localizer for 707 Aircraft in Takcoff Maneuver

weather conditions, procedural arrangements such as those which have been adopted in Category II operations (not permitting aircraft to start a take-off if the approaching aircraft has reached the outer marker) should suffice for many years to come. However, recordings in 1965 indicated that at London Airport (Heathrow) interference of this type occurred with landing aircraft below 600 feet on 2.5 percent of occasions and when below 200 feet on 1 percent of occasions. In 1966 this had built up to interference on 10 percent of occasions with aircraft below 600 feet. It appeared that air traffic control procedures were allowing separation between aircraft to fall below the desired 2 minutes in clear weather and during traffic peaks. However, automatic landing equipment is intended to be used at all times because of its superior "piloting" performance so that the Category III integrity of the ILS is required even in clear weather and during traffic peaks.

The overpowering nature of derogation due to overflying aircraft makes it exceedingly difficult to provide a meaningful relationship between actual glide path values and ground readings. To our best knowledge, no present monitor can cope with this problem.

C.4 Past and Present Far Field Monitor Systems

This section will discuss past and present far field monitors and systems in terms of both localizer and glide slope functions. However, because of the more extensive efforts in the localizer area, most of the discussions and examples will focus on the localizer. In most cases, similar casual relationships can be advanced for both the glide slope and localizer. Two deficiencies of recent localizer monitors, that is the lack of a lateral distribution of sensing elements and the inability to deal with overflight affect also glide slope monitors. They differ, however, in that the glide slope is not affected by aircraft taking off. Also, localizer far field monitors can

be arranged in a line that transversly crosses the localizer guidance plane. This is not possible for glide slope far field monitors since that would require extreme elevations which are not feasible due to obstruction limit requirements.

C.4.1 Localizer Monitor Systems.

For the purpose of this report, far field monitors will be grouped according to:

a) Single probe and limited probe distribution monitors

b) Multiple probe monitors

c) Other monitor concepts

For each class of monitors, discussion will occur on the ability to deal with moving diffracting reflections on the ground, such as taxiing aircraft, and in the air, particularly overflying aircraft. No present monitor system can meet all of these requirements, although, there is a significant range over which present monitor concepts should prove successful.

Extensive studies have been conducted on the utility of localizer far field monitoring and the possibility of developing a truly executive monitor. That no present monitor can fully meet this requirement per ICAO, Annex 10, attests to the great difficulty of the problem. It also suggests the logic underlying the use of far field monitors to satisfy only a portion of these requirements.

C.4.1.1 Single and Limited Distribution Probe Monitors

Although some benefit accrues from a single or limited distribution far field monitor, the benefits are limited. They must be carefully scrutinized since they can both under and over indicate derogation. A probe will under indicate when it is located near a null of the interference pattern resulting

from the direct and reflected energy. This is shown for a localizer geometry in Figure C-9. It illustrates the fact that a series of probes injudiciously placed, can fail to indicate the proper magnitude of the disturbance. The interference pattern is one which might result from a diffracting reflector as suggested by the diagram. Note further that the center RF probe point by itself has no chance of giving a quantitative indication of the derogated field intensity. The information from the row of probe points, combined while preserving phase and amplitude information, can accurately identify the pattern of derogated fields for a variety of interference wavelengths. A multiple probe system is thus required to provide quantitative information on derogated fields sufficiently accurate to generate alarm information.

Although Figure C-9 suggests only ground level sources, time varying reflections can also occur from higher levels than the source antenna, such as the very high tail structure of large transport planes or the moving portion of a large structure such as opening a hanger door.

C.4.1.1.1 AN/GRN 27

The AN/GRN 27 is a present operational system which provides a single probe far field monitor. It is presently used for installation of Category II sites. The single probe monitors the localizer in the far field of the glide slope. A block diagram of the AN/GRN 27 far field monitor is shown in Figure C-10. The single probe is located approximately on the center line of the runway somewhere between the threshold and the middle marker. The monitor provides dual detection channels (i.e. receives/monitors) for redundancy. It provides only a single localizer course radiation peak. As can be seen in Figure C-9, this single location will indicate the presence of derogation unless

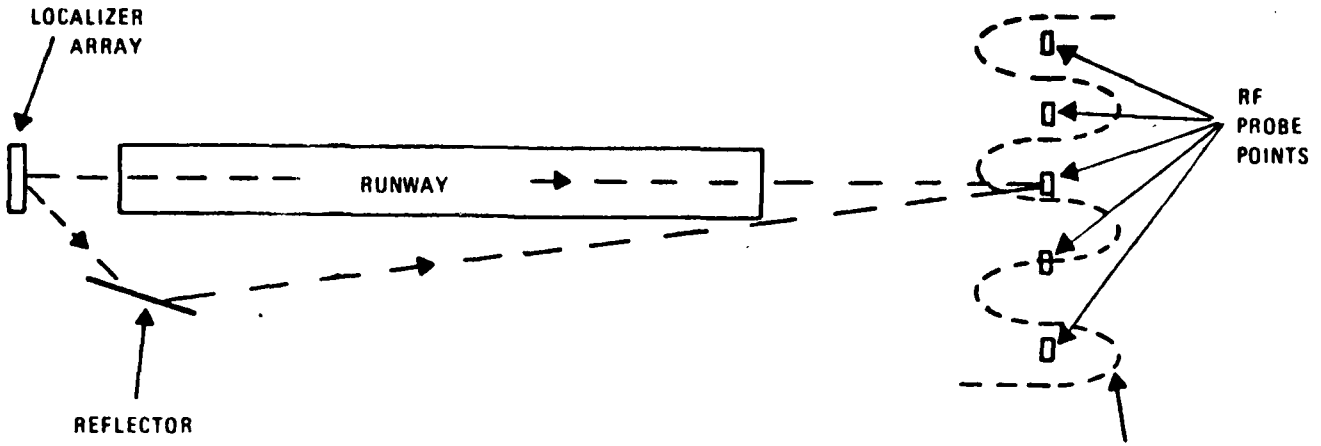

NOTE 1 – NO MONITOR FALLS AT A DEROGATION PATTERN PEAK.

NOTE 2 – IF THE PROCESSING WERE COHERENT THE PEAK OF THE PATTERN COULD BE IDENTIFIED EVEN THOUGH NO PROBE WAS POSITIONED AT A PEAK.

Figure C-9 Illustration of Problem of Identification of Derogation Peak with Simple Monitor

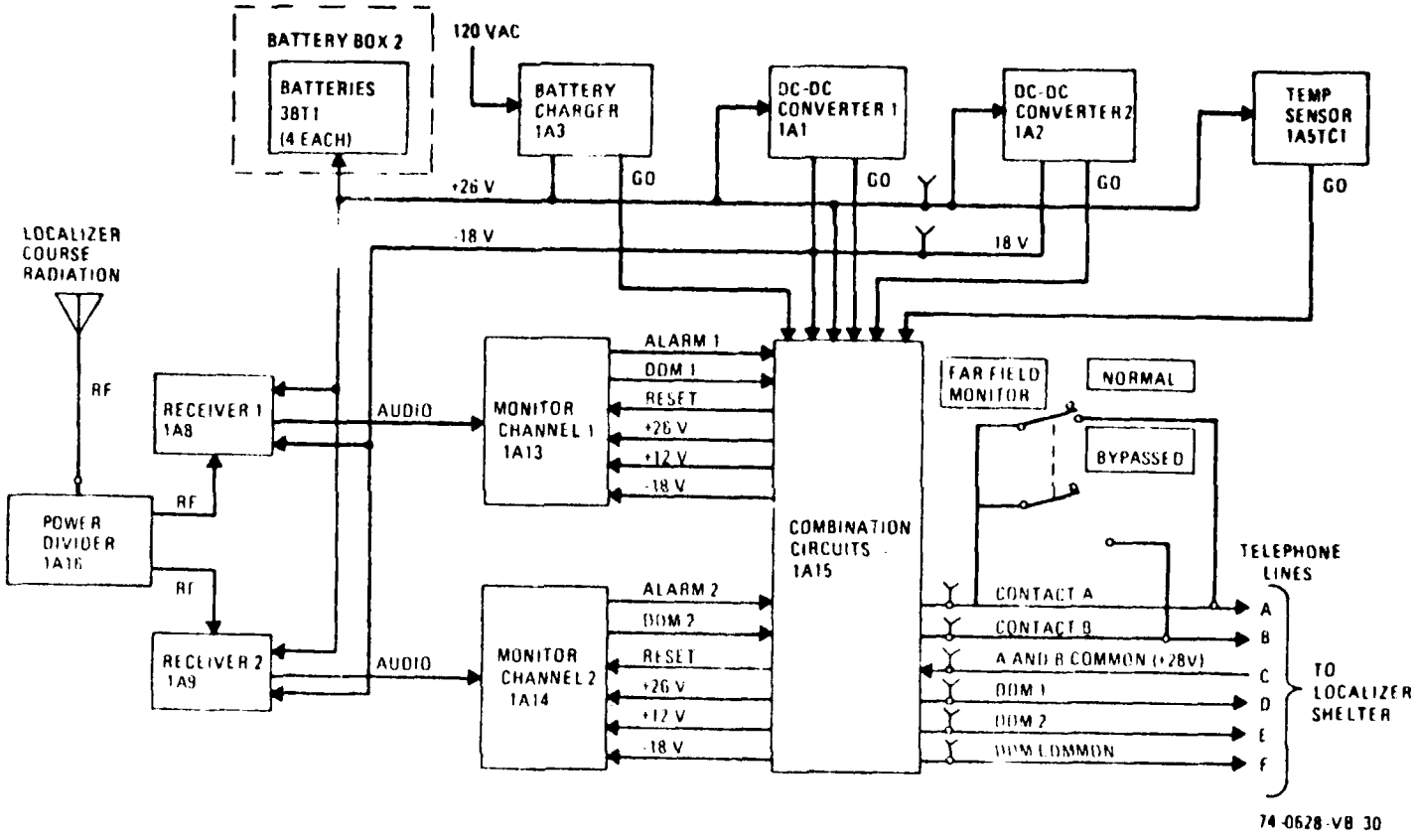

Figure C-10 Far Field Monitor Functional Block Diagram for AN/GRN-27

it happens to be at a null in the derogation interference pattern. Because most moving derogation will cause the interference pattern to oscillate through its extrema, even a single probe monitor will sometimes be indicative of maximum derogation due to vehicles on the ground. It is possible, however, for an aircraft to be taxiing in a direction which does not change the relative phase between direct and reflected energy, so that major derogation can occur without being detected by the monitor. Although such an eventuality is unlikely, constant monitoring of the output might yield an acceptable level of derogation due to ground taxiing aircraft even though guidance was unsatisfactory on the glide path. That is, the ILS system might be derogated beyond specified limits even though the instantaneous monitor reading is acceptable. This, of course, is highly unsatisfactory since it ignores the possibility that alarm conditions still exist, even though further interference maxima have not been detected. It also requires continuous monitoring for interpertation rather than an interpertation based on instantaneous conditions.

C.4.1.1.2 Ohio University Far Field Monitor

Dr. Richard McFarland at Ohio University made use of a far field monitor as a measurement tool in conducting various experiments. The geometry of his monitor, shown in Figure C-11 consists of two probes, one on center line and one to measure the course edge. The monitor was used to measure effects due to other devices that were under test. Included were effects which eminated from the localizer's antenna, such as transmitter and antenna faults. A comparison of calculation and measurement showed that the far field monitor provided a faithful indication. It was not, however, tested for overflying and taxiing aircraft, conditions for which a monitor must work in order to meet the requirements of this program.

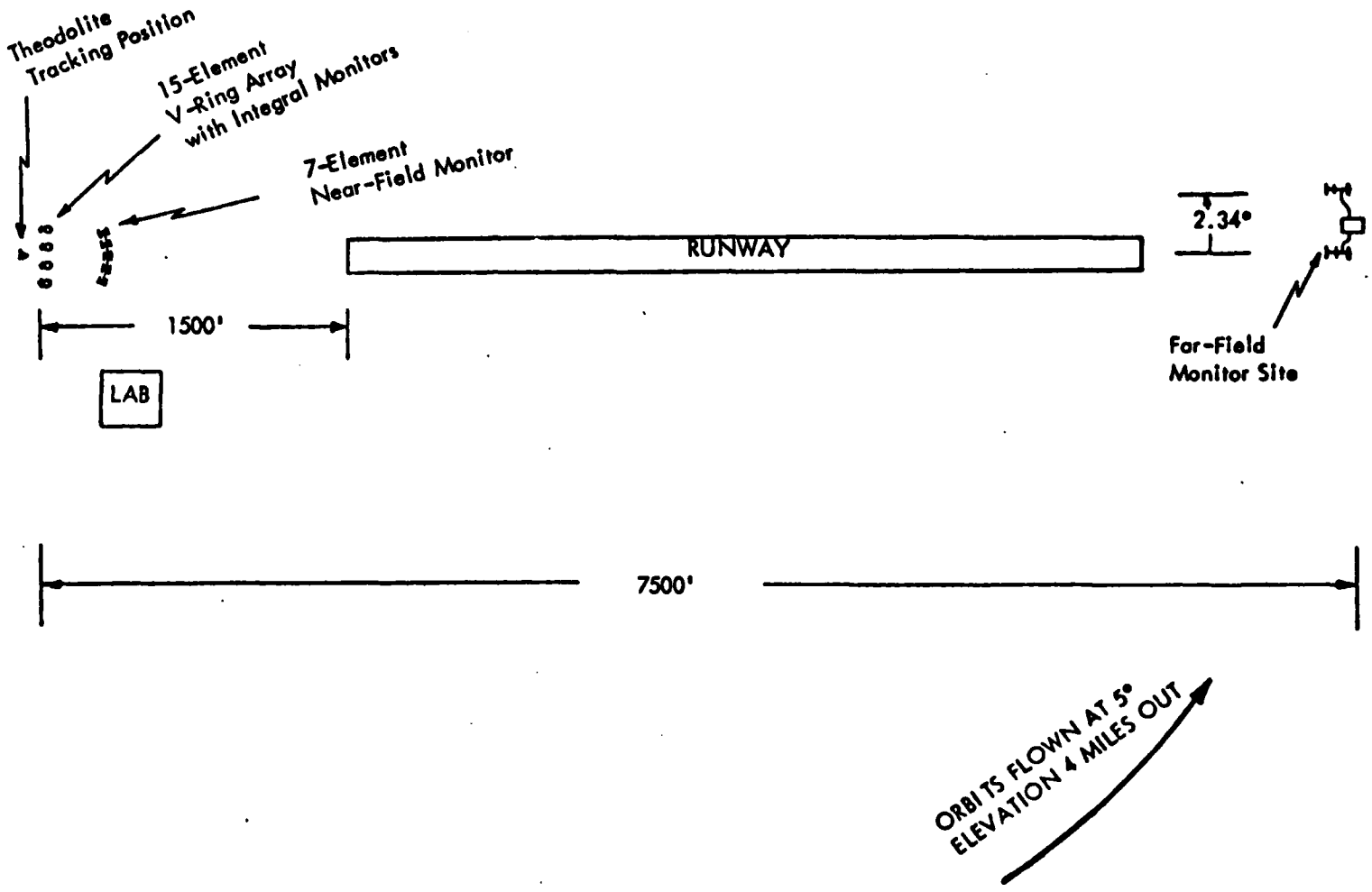

Figure C-11 Geometry of Ohio University Far Field Monitor

C.4.1.1.3 Four Probe Monitor System (NAFEC)

A monitor of four probes in a diamond shape was tested at NAFEC[7]. The system was in a diamond configuration and operated so that it could monitor events such as takeoff and landing of aircraft. The equipment was, in fact, operated such that it would record only when a significant disturbance occurred, as during the takeoff and landing of aircraft.

The geometry of the monitors is shown in Figure C-12. The signals from the four monitors were then recorded on a four channel tape. An example of that tape is shown in Figure C-13. As can be seen, many disturbances were beyond the linear range of the monitor. It can also be seen that the traces for a given event are very similar, except for some phase displacement between channels. Note that the upper two traces, which are for transversely displaced monitors, show a distince phase difference. This illustrates the fact that monitor points must be separated substantially to display the necessary information for adequate monitoring.

It is impossible to tell from the data available for this test if the derogation signal at the monitor is substantially greater than in the glide path. It was stated that as this data was being taken, it would have been instructive to have tests run during which an approaching aircraft monitored the glide path signal as a plane was taking off over the localizer antenna. By recording localizer signals in the air and on the ground, a meaningful comparison could have been made.

The conclusions drawn by this investigation were that insufficient information existed to develop an executive monitor. However, the investigators indicated that with greater effort, an executive monitor may be possible.

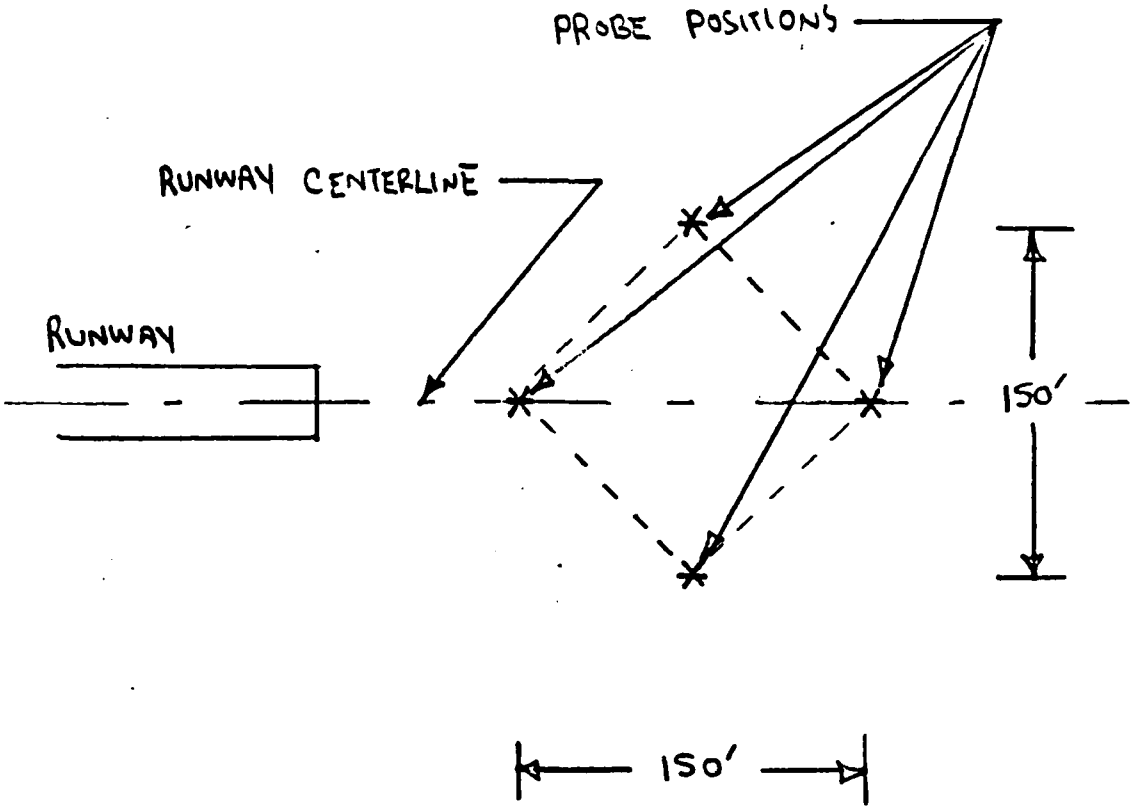

Figure C-12 Distribution of Probes for NAFEC Far Field Monitor

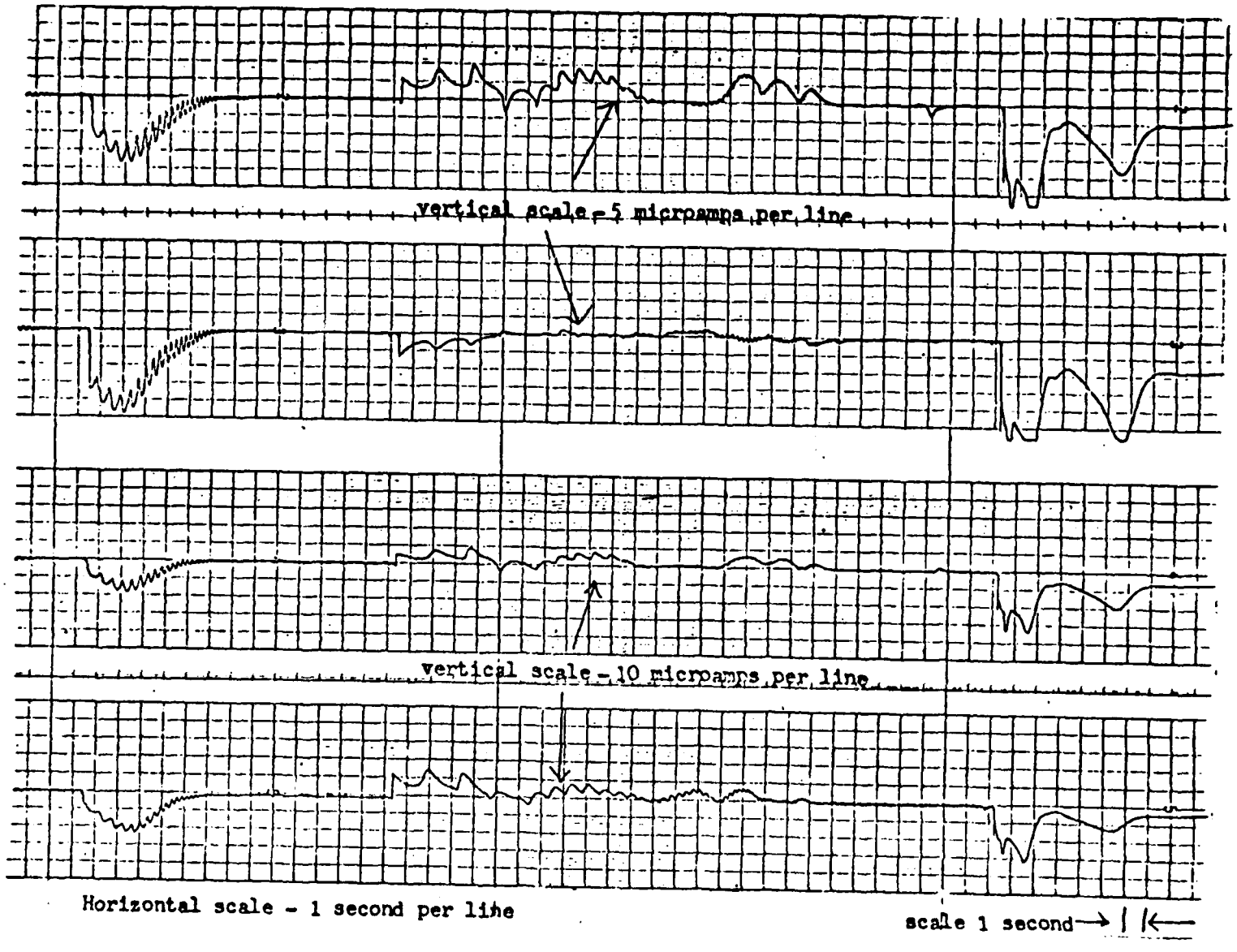

Figure C-13 Overflight Recordings made from Four Element Monitor at NAFEC

C.4.1.2 Multiple Probe Monitor

It has been demonstrated in the previous section that only a monitor with a significant number of monitor points can hope to provide executive monitor capability in compliance with ICAO, Annex 10 requirements. This concept was the basis of a monitor study conducted by Marconi at Heathrow Airport, London[3]. The study was conducted for aircraft on the ground only. The results give no information on monitoring overflying aircraft. The study does, however, lead to a monitor concept capable of handling taxiing aircraft with no restrictions on their movement. It also leads to the concept of a line of transversely distributed monitor locations between the end of the runway and the module marker.

The results of this study are illustrated in terms of the scatter diagrams in Figure C-14 which is an illustration of the performance that can be provided with a system suitably equipped and in which the output of the RF pick-ups are processed at a common point. This diagram is for the localizer system. Although a more detailed analysis of this diagram will be provided later in the report, key points can be illustrated briefly. Each dot on the scatter diagram is due to the scattering from a single object and is a measure of both the disturbance experienced by an aircraft on the approach path and the same disturbance measured by a near optimized ground-based monitor. The dots represent particular scatterers (400) in different locations near the runway area where movable reflectors might typically occur. The diagram shows that most disturbances are either correct alarms or all clear. There are only a small percentage of false or missed alarms. Further, all missed alarms are only mildly outsideof tolerance and all false alarms are close to the correct alarm limit. Thus, there are no cases of alarm failing to occur for grossly

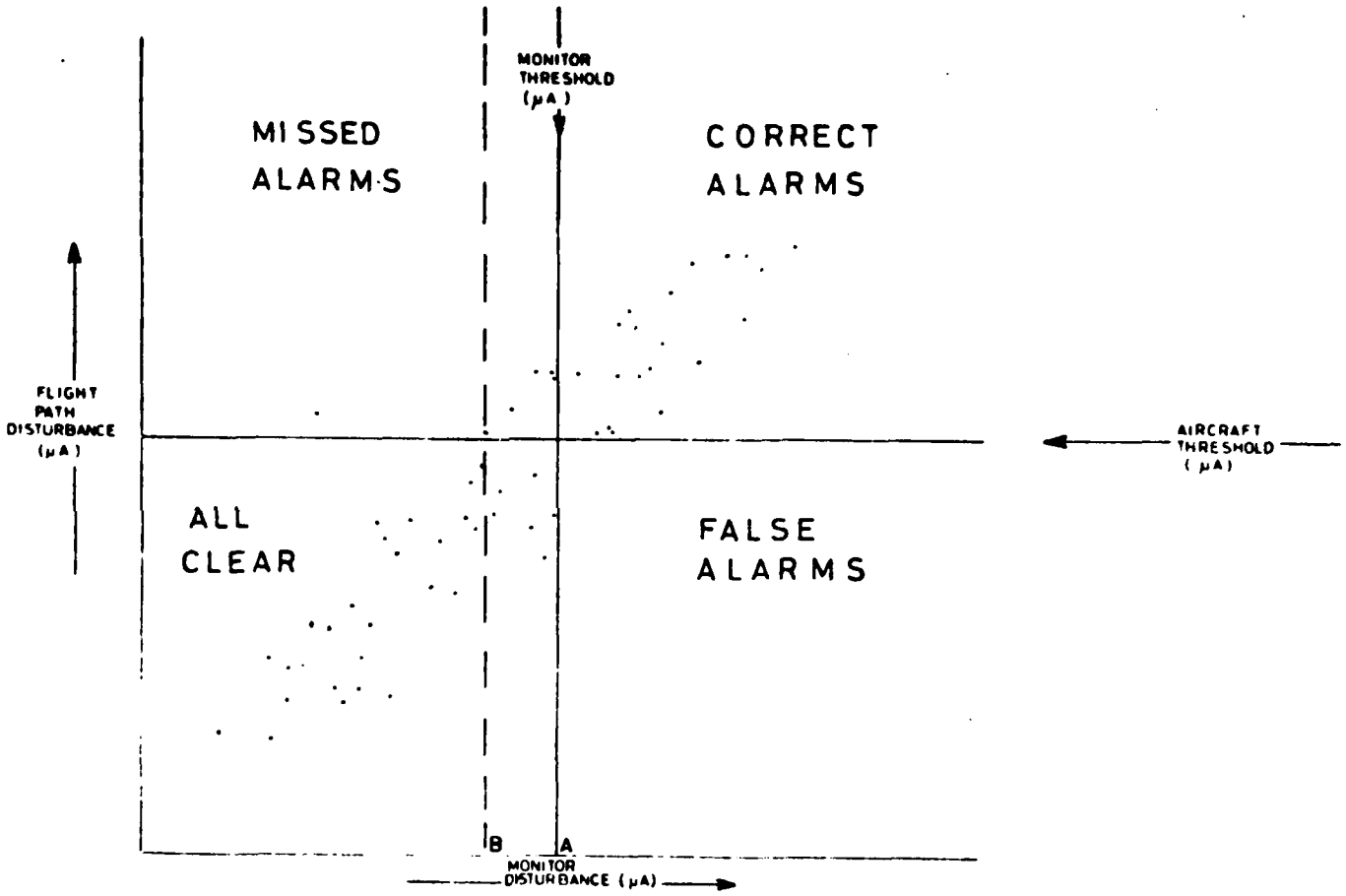

Figure C-14 Scatter Chart Showing Two Thresholds

out of tolerance conditions and no cases of alarms occuring for conditions not close to alarm.

Further, if it is desired that there be no missed alarms, no matter how minor the alarm violation, an alarm level at B rather than A can be established. Note that if the monitor alarms for value B rather than A, the false alarm rate is slightly higher but no missed alarms occur.

The conditions of false alarms occurring for derogation are fewer than alarm limits that exist now in most near field monitors. McFarland, for instance, shows that while a true analog near field monitor would closely approximate far field conditions (for near field causes of derogation) present less sophisticated near field monitors cannot[6]. The present simple two probe monitors can only alarm for "all alarm conditions" by being set to alarm for many conditions in which alarm limits are not even approached.

The false-missed alarm performance of a far field system suggested by the scatter diagram in Figure C-14 is approximately analog in the sense that no false alarm occurs for an actual condition grossly under alarm and no missed alarm occurs for a condition grossly over alarm conditions. Such a close approximation to analog makes it practical to consider a far field monitor system with virtually no missed alarms as suggested by alarm limit B in Figure C-14. (The illustration is for taxiing aircraft only.) The overpowering nature of overflight derogation was also measured by Marconi[3]. The measurement shown in Figure C-15 is the result of an overflying DC 10 at Heathrow Airport making a missed approach maneuver. The data also shows that suitably displaced monitors can provide distinctive information since traces for this test are for monitor points on axis and 100 feet off axis. This suggests the possibility that, for a properly worked out strategy, definite information about the disturbances can be made available.

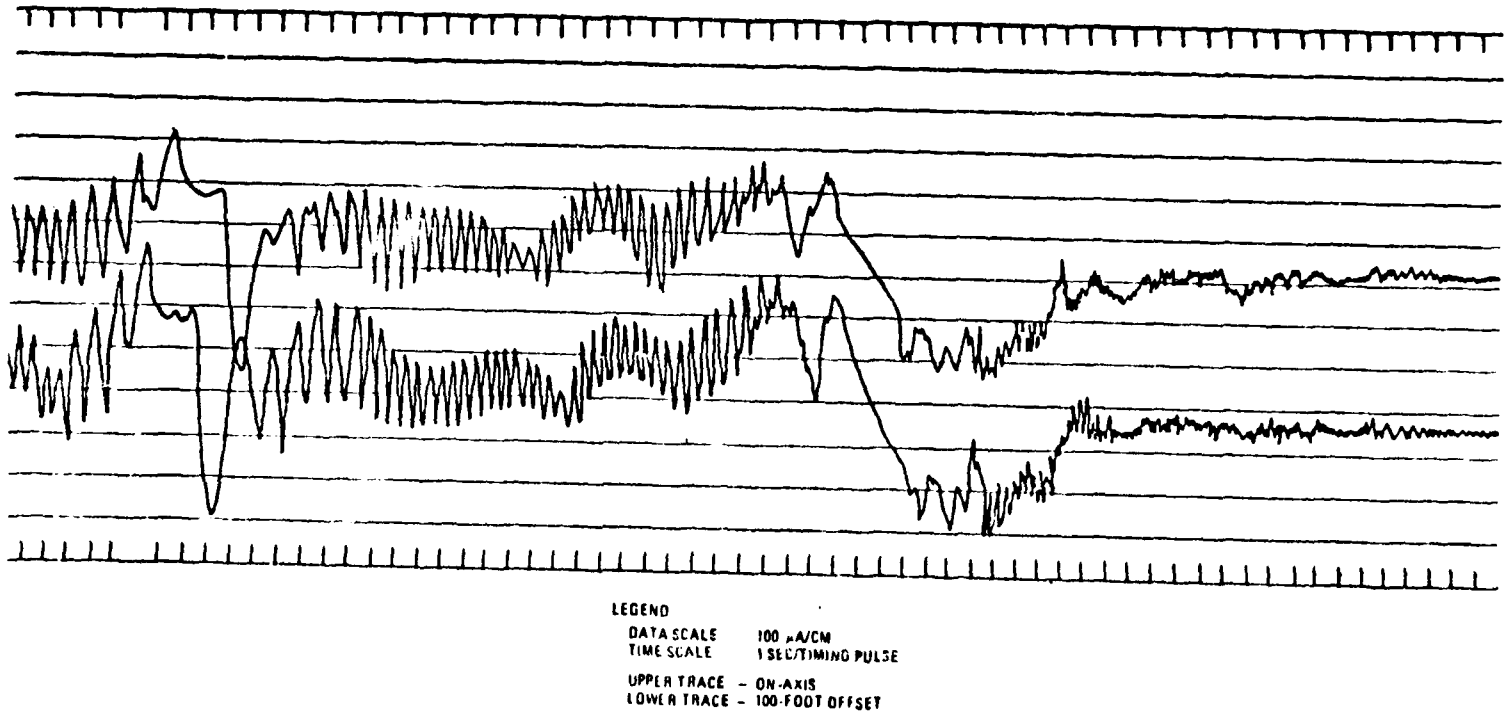

Figure C-15 Monitor Derogation Due to DC-10 Executing a Standard Mist Approach

It is clear that improvement of this monitor is required to fully meet the requirements of this program, specifically including a thinner scatter diagram for all disturbances and an ability to handle overflight disturbances. It is also clear that this study provides a major advance over all other efforts toward implementing a useful far field monitor. It will serve as the basis for our effort.

C.4.1.3 Monitors Utilizing Co-operative Aircraft

Several systems have been examined that require the presence of an aircraft on the glide path before the condition of the guidance can be examined for derogation. Although co-operative systems do allow for a version of real time monitoring, their major drawback is that an ILS would only be shut down after the plane has started its decent. Such systems must take a position subordinate to those that can provide negative information about the ILS before a plane has entered the glide path and hence provide the pilot with an additional measure of safety.

One type of co-operative aircraft system might employ an airborne transmitter that would reradiate the received ILS signal such that ultimate processing would be carried out on the ground[8]. Such a system could only give real time information if a number of ground receivers were employed to effect a triangulation procedure. This scheme would probably be more useful for locating the plane in a gross sense with respect to the airport than for executive landing information.

In a system developed for the FAA[9], a separate transmitter was used to provide a trilateration signal. The position of the aircraft is continously computed and recorded during approach. This type of system could be used to provide warning of unsatisfactory and potentially dangerous aircraft positions

on the glide path. This is accomplished by first generating an integrated superposition of a large number of approach paths and then comparing an individual approach to the mean guidance information.

Another of the specific implementations requiring the presence of an aircraft on the glide slope path is the ILS Echo-Monitoring System[10]. This system uses the reflected localizer signal directly and after establishing the correlation between reflected and airplane received signals allows one to detect derogation of the guidance information on the ground. The correlation of the reflected and directly received signals would require smoothing of the DDM structures that contain the information desired. It is likely that further refinements could be made if individual signatures were generated for each class of aircraft flying each type of approach, but that would require an incoming aircraft to inform the echo-monitor its class type, thereby adding a further complexity.

C.4.2 Glide Slope Monitors

Much less has been written on glide slope far field monitors than on localizer far field monitors. Although there have been explicit programs to solve particular problems[11], very little documented effort has been directed toward a general purpose glide slope monitor. This is perhaps due, in part, to two causes (1) the apparently greater difficulty in conceiving a glide slope far field monitor and (2) the greater ease, in most cases, in preventing glide path derogation during the critical periods of approach in landing maneuvers.

The glide path antenna is sited close to the approach end of the runway. In this regard, the vehicles which might generally be expected to interfere

with the glide slope signal are probably more completely under the controller's surveillance and/or control. Although special situations may occur such that an especially large vehicle on a nearby road could affect glide slope guidances, in general the most significant disturbances are due to planes in line, waiting for takeoff on the taxi-way at the approach end of the runway and planes close to touch-down in final approach. Of these the former are probably the most important. This is not because the aircraft on final approach could not potentially derogate guidance for those behind it, but rather because no other aircraft would be allowed to be in a critical phase of approach when the disturbing aircraft is approaching touch-down. Thus the far field monitor must primarily deal with aircraft taxiing or awaiting takeoff from the appraoch end of the runway and other vehicles which inadvertently occupy critical areas close to the glide slope antenna. Although it is vital to be capable of observing an operationally serious derogation to the glide path guidance, due to decending aircraft, the ground level vehicles suggested above will serve as the initially investigated scatters.

To our knowledge, very little far field monitor work has been carried out and the limited efforts that were conducted were for very special circumstances. For example, one effort used far field monitors to assess the effect of snow on glide slope characteristics.

C.4.2.1 Far Field Monitoring of Snow Effect on Image Glide Path System

A far field monitor was used to evaluate snow cover effects on glide slope performance at Grand Rapids, Michigan. The monitors were mounted at 2.3° and 3.0° in the far field of three ground image type antennas, i.e. sideband reference, null reference and capture effect. The monitors were mounted on the 900 foot tower of Station WZZM-TV of Grand Rapids. The availability

of a TV tower for monitors overcame the over-riding difficulty of glide slope monitoring by providing a monitor position in the glide path. Although this approach was valuable for experimentation, it is not feasible for operational sites since such a monitor would violate obstruction limits. Details of the snow cover experiments that used far field monitor as reference are given in the referenced report[12].

It should be pointed out that in addition to its violation of the obstruction limit, a single probe, or in this case a course center and width monitor, would be unsuitable for complete monitoring for the reasons discussed earlier for the localizer. Where a localized obstruction such as a taxiing aircraft is involved, the interference pattern is that of a quasi-point reflector. Therefore, a multiple position monitor would be absolutely necessary to provide a complete evaluation of the glide path derogation. In the present case, the single location monitors were effective because the cause of derogation was a reasonably uniform perturbation of the ground level. Although the snow thickness was not constant, the relative perturbation at any one location was small and was distributed over a very large area. In this instance, the path deviation for all points is the integrated effect of snow over a large area. Therefore, a single monitor location was effective for this experiment.

C.4.2.2 Glide Slope Monitors Requiring Co-operative Aircraft

Essentially the same principles discussed for localizer monitors applies to the glide slope monitor. Monitors which require co-operative aircraft are effective in providing long term evaluation of guidance but do not provide relative evaluation of derogation unless an aircraft is in approach at the time. Although this is useful information, it does not meet the requirements of this program.

A monitor suggested by McFarland[13] which falls into this category provides the pilot with a glide path reference to a fixed point which can then be compared to the actual glide path guidance. If the two correspond, the pilot then can confidently use the guidance as commissioned. If there is a serious deviation, the pilot would report same and use visual flight rules for landing if visibility permits. Otherwise he would be diverted to an acceptable approach.

This type of co-operative monitor has significant value for regions of high snow frequency (or perhaps other instances such as high variations in ground moisture, if that has significant effect on the near field monitor) since there is presently no effective near zone method of monitoring snow effect on guidance. It would not be suitable, however, for monitoring aircraft reflective perturbation since that probably leads to periodic guidance perturbations in space that could be "in spec" at the point of observation but in a dangerous condition on the glide path.

C.5 Conclusions

With the exception of the Marconi[3] study of Heathrow Airport, contemporary far field monitor systems suffer their greatest shortcoming in their use of limited distribution probes. Specifically, it is felt that beam bends of varying wavelength can only be detected with monitor systems that are physically distributed and contain a number of probe points. Such a monitor system should have the capacity to provide executive monitoring capability without the aid of co-operative aircraft.

Most of the far field monitor work that has been accomplished to date has been carried out for localizer configurations. The single and limited distribution monitors used for localizers can both under and over indicate glide path guidance derogation. Systems such as the AN/GRN 27 allows for

qualitative monitoring but are unable to yield instantaneous information on the extent of time varying derogation due to taxiing and overflying aircraft. The diamond shaped system tested at NAFEC contains the rudiments of a successful approach in that the probes are physically displaced. It did, however, lack the processing that is required to obtain quantitative information. Marconi's study of Heathrow Airport does use a distributed monitor configuration but the placement was longitudinal only with no transverse elements. Their achievements are the most successful to date. Finally, the major deficiency of systems requiring co-operative aircraft is their inability to shut down guidance before a plane has started its decent.

Relatively little effort has been expended on a glide slope far field monitor. This is due to the difficulty in designing a glide slope monitor system and the relative ease in preventing glide slope derogation during critical periods. It should be noted, however, that almost all work accomplished on the localizer problem can be modified to account for the specifics of the glide slope.

As stated above, multi-probe far field monitor systems of the type to be developed for this program should prove adequate to yield quantitative inferences about the quality of guidance on the glide path. Using Marconi's previous studies as a starting point, further development will allow for detection of derogation due to time varying occurances such as taxiing and overflying aircraft. This should result in an executive ability far field monitor system.

C.6 References

1. FAA - E - 21586, "Localizer Monitor Dipole Antenna," Aug. 28, 1970.

2. "Preliminary Instruction Book Monitor, Radio Frequency - (Type MX-9026/GRN-27CV),"

3. The Marconi Company, Research Division, "Investigation into theEffectiveness of a Far Field Monitor," Contract No. KJ/G/7293/CB66(a)2, Final Report, Jan. 1972.

4. A series of articles on ILS monitoring approach in, The Radio and Electronics Engine, Vol. 32, No. 5, pp. 287-356, Nov.; No. 6, 357-362, December 1966; Vol. 33, No.1, pp. 37-54, Jan., 1967.

5. Flounders, J.G., "An Experimental ILS Echo Monitoring System", The Radio and Electronic Engines, Vol. 32, No. 6, pp. 357-362, Dec. 1966.

6. "Instrument Landing System Improvement Program," SRDS Report PD 71-30, Contract FAA69WA-2066, Athens, Ohio, pp. 60-61, Oct. 71.

7. Work carried out by Fred Marshall and associates during 1970-1971 at NAFEC.

8. Jolliffe, S.A.W. et al, "The Character of the Received ILS Signal and its Relation to Monitoring" The Radio and Electronic Engineer, Vol. 32, No. 5, pp. 293-311, Nov. 1966.

9. Westinghouse Electric Corp., Aerospace and Electronic Systems Division, "Performance Monitoring on Final Approach, Touchdown and Rollout," Contract DOT-FA72W-2837, Final Report, Nov. 1975.

10. Flounders, J.G., "An Experimental ILS Echo-Monitoring System," The Radio and Electronic Engineer, Vol. 32, No. 6, pp. 357-362, Dec. 1966.

11. McFarland, R.M., Gorman, J.T., Icharist, T.G., Rice, J. & Wistendage, P.C. "Earth Cause and Contour Effects on Image Glide Paths," Phase III, Report No. 68-60, Contract FA 67WA-1676, SRDS FAA & Aviation Research Group, Dept. of E.E., Ohio University, Athens, Ohio, Sept. 1968.

12. Marehart, J.B., McFarland, R.M., & Hildebrand, D.C. "Snow Effects on Image Glide Path Systems," Report No. FAA-RF-72-85, Contract FA69WA-2061, Mod 6, SRDS, FAA, DOT, by Alumni Buying Center, Dept. of E.E., Ohio University, Athens, Ohio, July 1972.

13. McFarland, R.H., "A Far Field, On-Course Monitor for the ILS Glide Path," Proc. National Aerospace Eelectronics Conference, pp. 339-342, Dayton, Ohio, May 1969.

APPENDIX D

GLOSSARY OF FREQUENTLY USED SYMBOLS

Some effort has been made in this report to systematize the use of symbols contributed by several workers. Various subscripts/superscripts might appear on a symbol and not be included in the list; especially in those latter cases the meaning of the subscript/superscript is made clear from the context in which it is used.

a, width of a scattering screen.

$\vec{a}$, scattered SBO expressed as a 2-component (real) vector.

$\vec{A}$, unscattered or direct SBO expressed as a 2-component (real) vector.

b, height of a scattering screen.

$\vec{b}$, scattered CSB expressed as a 2-component (real) vector.

$\vec{B}$, unscattered or direct CSB expressed as a 2-component (real) vector.

$\vec{C}$, total CSB

CSB, carrier plus side band

DDM, difference in depth of modulation (usually for a direct plus scattered field).

DDM_o, difference in depth of modulation (usually for a direct, unscattered field).

$\overrightarrow{DDM}$, vector DDM with components being DDM and QDDM.

E, scaler field

$\vec{K}$, a complex 2-vector; re-radiated signal at receiver is K times the illuminating signal at the scatterer.

$\vec{n}$,	unit vector.
QDDM	quadrature component of DDM; it is the non-zero component of S x C/C.
$\vec{r}$, $\vec{R}$,	position vectors in 3-space.
SBO	side band only.
$\vec{v}$,	position vector in 3-space.
VDDM	modulus (or norm) of vector DDM.
x, y, z	rectangular coordinates.
$\vec{X}$,	position vector in 3-space
α,	incidence angle at a scattering screen.
Δ(DDM)	DDM - DDM_0
φ, ϵ , Ψ,	Euler angles.
$\tilde{\varphi}$,	azimuthal angle.
ξ, η,	screen or aperture coordinates
$\vec{\rho}$,	position vector in 3-space.
$\vec{a} \cdot \vec{b}$	inner product of vectors a and b
$\vec{a} \times \vec{b}$	cross product of 3-vectors a and b
$\|\vec{a}\|$,	modulus (length or norm) of vector a; also "a" is sometimes used in this context.
$(\vec{a})_i$,	$i^{\underline{th}}$ component of vector a.